Polymeric emulsifiers obtained by bacterial transformation from oily wastes in bioreactor

Ignacio Martín Arjol

FACULTAT DE FARMÀCIA
DEPARTAMENT DE MICROBIOLOGIA i PARASITOLOGIA SANITÀRIES
PROGRAMA DE DOCTORAT: BIOTECNOLOGIA

Polymeric emulsifiers obtained by bacterial transformation from oily wastes in bioreactor

IGNACIO MARTÍN ARJOL
2014

FACULTAT DE FARMÀCIA
DEPARTAMENT DE MICROBIOLOGIA i PARASITOLOGIA SANITÀRIES
PROGRAMA DE DOCTORAT: BIOTECNOLOGIA

Polymeric emulsifiers obtained by bacterial transformation from oily wastes in bioreactor

Memòria presentada per **Ignacio Martín Arjol** per optar al títol de doctor per la Universitat de Barcelona

Directora/tutora: Director:

Dra. Maria Àngels Manresa i Presas Dr. Joan Llorens Llacuna

Doctorand:

IGNACIO MARTÍN ARJOL
2014

Departament de Microbiologia i Parasitologia Sanitàries
Facultat de Farmàcia
Av. Joan XXIII s/n
08028 Barcelona
Tel.: 934 024 496

Dra. Maria Àngels Manresa i Presas, Professora Titular del Departament de Microbiologia i Parasitologia Sanitàries, Facultat de Farmàcia, i el **Dr. Joan Llorens Llacuna**, Professor Catedràtic del Departament d'Enginyeria Química, Facultat de Química, ambdós, de la Universitat de Barcelona,

INFORMEN:

Que la memòria titulada "Polymeric emulsifiers obtained by bacterial transformation from oily wastes in bioreactor", presentada per IGNACIO MARTÍN ARJOL per a optar al títol de Doctor per la Universitat de Barcelona, ha estat realitzat sota la nostre direcció en el Departament de Microbiologia i Parasitologia Sanitàries, i considerant-la finalitzada, autoritzem la seva presentació per a ser jutjada pel tribunal corresponent.

I, perquè així consti, signem la present en Barcelona, el dia 30 de Gener de 2014,

Dra. Maria Àngels Manresa i Presas

Dr. Joan Llorens Llacuna

If I have ever made any valuable discoveries,
it has been due more to pay attention,
than to any other talent.

Sir Isaac Newton

Si una persona es perseverante, aunque sea dura de entendimiento,
se hará inteligente; y aunque sea débil, se transformará en fuerte.

Leonardo da Vinci

Index

List of Figures

List of Tables

Nomenclature

(10*R*)-HOSA: 10(*R*)-hydroxystearic acid, 10(*R*)-hydroxy-octadecanoic acid.
(10*S*)-HOME: 10(*S*)-hydroxy-8(*E*)-octadecenoic acid.
(10*S*)-HPOME: 10(*S*)-hydroperoxy-8(*E*)-octadecenoic acid.
(7*S*,10*S*)-DiHOME: 7,10(*S*,*S*)-dihydroxy-8(*E*)-octadecenoic acid.
$(k_L)_M$: liquid-phase mass-transfer coefficient in culture media, [$m \cdot s^{-1}$].
$(k_L)_W$: liquid-phase mass-transfer coefficient in water, [$m \cdot s^{-1}$].
10-KSA: 10-ketostearic acid, 10-keto-octadecanoic acid.
42A2 LOX: lipoxygenase from *Pseudomonas aeruginosa* 42A2.
A: pre-exponential factor, [Pa·s].
A_i: area of peaks in a HPLC chromatogram, [—].
AV_i: acid value of i, [mg KOH·g $sample^{-1}$].
BSA: *bis*(trimethylsilyl)acetamide.
C*: dissolved oxygen concentration in the equilibrium, [% saturation].
CCO: coconut oil.
C_i: concentracion of i, [C-mol·l^{-1}].
$C_{O2}(t)$: dissolved oxygen concentration at time t, [% saturation].
C_{O2}: dissolved oxygen concentration, [% saturation].
d: external diameter of the wetted-wall column, [m].
Da: Dalton, [Da].
dCi: differential concentration of i, [C-mol i·l^{-1}].
DHB: 2,5-dihydroxybenzoic acid.
$D_{O2\text{-}H2O}$: diffusivity coefficient of oxygen in water, [$m^2 \cdot s^{-1}$].
DSC: differential scanning calorimetry.
dt: differential of time, [h].
E_a: activation energy, [kJ·mol^{-1}].
ESI: electrospray ionization.
EST: estolide.
EtOH: pure ethanol.
FAEE: fatty acid ethyl ester.
FTIR: Fourier transform infrared spectroscopy.
g: gravity, 9.81, [$m \cdot s^{-2}$].
h: height of the wetted-wall column, [m].
HFA: hydroxy-fatty acid.
HPLC: high preassure liquid chromatography.
i.d.: inner diameter, [cm].
k: (10*S*)-HOME first order kinetic constant, [s^{-1}].
K_i: inhibition constant, [C-mol·l^{-1}].
k_La: volumetric mass transfer coefficient in liquid phase, [h^{-1}].
K_s: saturation constant, [C-mol·l^{-1}].
L: molar flow of the stream in the wetted-wall column, [$mol \cdot s^{-1}$].
LA: linoleic acid, 9,12(*Z*,*Z*)-octadienoic acid.
log P: octanol-water partition coefficient, [—].
LOX: lipoxygenase.
M: (10*S*)-HOME or (10*S*)-HOME ethyl ester in mass spectra.
M': (7*S*,10*S*)-DiHOME ethyl ester in mass spectra.
MALDI: matrix-assisted laser desorption/ionization.
MM_i: molecular mass of the compound i, [g·C-mol^{-1}].
MS: mass spectrometry.
NASA: National Aeronautics and Space Administration.
NMR: nuclear magnetic resonance.
OA: oleic acid, 9(*Z*)-octadecenoic acid.
OUR: oxygen uptake rate, [$mg_{O2} \cdot l^{-1} \cdot h^{-1}$].
PDI: proportional-derivative-integral.

PHA: poly(3-hydroxyalkanoate).
PHB: poly(3-hydroxybutyrate).
PUFA: polyunsaturated fatty acids.
$\mathbf{P_V}$: volumetric productivity of products, [$g \cdot l^{-1} \cdot h^{-1}$ or C-$mol \cdot l^{-1} \cdot h^{-1}$].
$\mathbf{q_{O2}}$: molar flow of oxygen, [$mol \cdot s^{-1}$].
R: ideal gas constant, 8.314, [$J \cdot K^{-1} \cdot mol^{-1}$].
RA: ricinoleic acid, 12-hydroxystearic acid, 12(*R*)-hydroxy-9(*Z*)-octadecenoic acid.
RCF: ratio competitive factor, [—].
S: external surface of the wetted-wall column, [m^2].
S: saturated (10*S*)-HOME in mass spectra.
SBO: soybean oil.
SFO: sunflower oil.
sOUR: specific oxygen uptake rate, [$mg_{O2} \cdot g\ cell^{-1} \cdot h^{-1}$].
T: temperatura, [K].
t: time, [s].
$\mathbf{t_e}$: time of exposure, [s].
TGA: thermal gravimetric analysis.
TOF: time-of-flight.
v/v: volume per volume.
v: volume.
w/v: weight per volume.
WWC: wetted wall column.
X: biomass, [C-$mol \cdot l^{-1}$].
x: molar fraction of oxygen, [—].
$\mathbf{x_1}$: oxygen molar fraction at the outlet of the WWC, [—].
$\mathbf{x_2}$: oxygen molar fraction at the inlet of the WWC, [—].
$\mathbf{x_{eq}}$: molar fraction of oxygen in the equilibrium, [—].
$\mathbf{X_{st}}$: biomass at the stationary phase, [g $cell \cdot l^{-1}$].

$\boldsymbol{\psi}$: ratio between liquid-phase mass-transfer coefficients, [—].
$\boldsymbol{\aleph_i}$: redox number of i, [—].
$\boldsymbol{\Delta_i}$: increment of the variable i, [—].
$\mathbf{Y_{(10S)\text{-}HOME/(10S)\text{-}HPOME}}$: yield of (10*S*)-HOME on (10*S*)-HPOME, [C-mol (10*S*)-HOME·C-mol (10*S*)-HPOME $^{-1}$].
$\mathbf{Y_{(10S)\text{-}HOME/OA}}$: yield of (10*S*)-HOME on OA, [C-mol (10*S*)-HOME·C-mol OA^{-1}].
$\mathbf{Y_{(10S)\text{-}HPOME/OA}}$: yield of (10*S*)-HPOME on OA, [C-mol (10*S*)-HPOME·C-mol OA^{-1}].
$\mathbf{Y_{(7S10S)\text{-}DiHOME/(10S)\text{-}HPOME}}$: yield of (7*S*,10*S*)-DiHOME on (10S)-HPOME, [C-mol (7*S*,10*S*)-DiHOME·C-mol (10S)-$HPOME^{-1}$].
$\mathbf{Y_{CO2/(10S)\text{-}HPOME}}$: yield of CO_2 on (10*S*)-HPOME, [C-mol CO_2·C-mol (10*S*)-$HPOME^{-1}$].
$\mathbf{Y_{CO2/OA}}$: yield of CO_2 on OA, [C-mol CO_2·C-mol OA^{-1}].
$\mathbf{Y_{NO3/OA}}$: yield of N on OA, [C-mol N·C-mol OA^{-1}].
$\mathbf{Y_{O2/(10S)\text{-}HPOME}}$: yield O_2 on (10*S*)-HPOME, [C-mol O_2·C-mol (10*S*)-$HPOME^{-1}$].
$\mathbf{Y_{O2/OA}}$: yield of O_2 on OA, [C-mol O_2·C-mol OA^{-1}].
$\mathbf{Y_{X/OA}}$: yield of X on OA, [C-mol X·C-mol OA^{-1}].
$\boldsymbol{\eta}$: reaction yield, [%].
$\boldsymbol{\eta'}$: dynamic or absolute viscosity, [Pa·s].
$\boldsymbol{\mu}$: specific growth rate, [h^{-1}].
$\boldsymbol{\mu'}$: viscosity of water, [$kg \cdot m^{-1} \cdot s^{-1}$].
$\boldsymbol{\mu_i}$: specific growth rate expressed as a kinetic model in the semireaction i, [h^{-1}].

μ_{max}:	maximum specific growth rate, [h^{-1}].
ν:	kinematic viscosity, [cSt or $mm^2 \cdot s^{-1}$].
π':	interfacial preassure, [$N \cdot m^{-1}$].
ρ:	density of water, [$kg \cdot m^{-3}$].
ρ_W:	molar density of water, [$mol \cdot m^{-3}$].

1. Introduction

1.1 Lipid biotechnology

Lipid biotechnology covers the microbial production and biotechnological transformation of lipids and lipid-soluble compounds. Storage lipids in the form of triacylglycerols and their different fatty acid types are the main targets for biotechnological product development. To minor extent, phospholipids, sphingolipids, glycolipids, sterols and carotenoids, as well as, other lipid-soluble compounds are utilized for the production of bioactive molecules for cosmetics, nutrition and pharmaceuticals [1].

About 80% of the oil and fats produced worldwide are vegetable oils and the rest are from animal origin, with a declining tendency. About one quarter of global production come from soybean, palm, rapeseed and sunflower oils. Oleic acid (OA) from sunflower oil (SFO); linoleic acid (LA) from soybean oil (SBO); LA from linseed oil; erucic acid from rapeseed oil; and, ricinoleic acid (RA) from castor oil are the most important oils for bio/chemical transformations offering, in addition to the carboxy group, one or more insaturations, Table 1.1. Coconut (CCO) and palm kernel oil, lauric and mystiric acid, are very important in the production of surfactants [2].

Table 1.1. Fatty acid composition (w %) of common feedstock oils and fats[a].

Fatty acid[b]	CO	PO	SBO	SFO	COO	CSO	CCO	CF	BT
C6:0							1		
C8:0							7		
C10:0							7		
C12:0							47		1
C14:0		1				1	18	1	4
C16:0	4	45	11	6	11	23	9	25	26
C18:0	2	4	4	5	2	2	3	6	20
C20:0									
C22:0				1					
C16:1						1		8	4
C18:1	61	39	23	29	28	17	6	41	28
C18:2	22	11	54	58	58	56	2	18	3
C18:3	10		8	1	1			1	
C20:1	1								
Other									14

[a]**CO**: canola oil; **PO**: palm oil; **SBO**: soybean oil; **SFO**: sunflower oil; **COO**: corn oil; **CSO**: cottonseed oil; **CCO**: coconut oil; **CF**: chicken fat; and, **BT**: beef tallow.
[b]**C6:0**: caproic acid; **C8:0**: caprylic acid; **C10:0**: capric acid; **C12:0**: lauric acid; **C14:0**: mystiric acid; **C16:0**: palmitic acid; **C18:0**: stearic acid; **C20:0**: arachidic acid; **C22:0**: behenic acid; **C16:1**: palmitoleic acid; **C18:1**: oleic acid; **C18:2**: linoleic acid; **C18:3**: linolenic acid; **C20:1**: eicosenoic acid.
Adapted from [3].

New plant oils containing fatty acids with new functionalities such as petroselenic acid (*cis*-6-octadecenoic acid), from *Coriandrum sativum*; calendic acid (*trans*-8,10-*cis*-12-octadecatrienoic acid), from *Calendula officinalis*, α-eleostearic acid (*cis*-9-*trans*-11,13-octadecatrienoic acid) from tung oil (*Vernicia fordii*); santalbic acid (*trans*-11-octadecen-9-ynoic acid) from *Santalum album*; and, vernolic acid ((12*S*,13*R*)-epoxy-

cis-9-octadecenoic acid) from *Vernonia galamensis* are becoming industrial available. The basic oleochemicals are free fatty acids, methyl esters, fatty alcohols and fatty amines, as well as, glycerol as a by-product. Their interesting new industrial applications are the usage as environmentally friendly industrial fluids and lubricants, insulating fluid for electric utilities such as transformers, and additive to asphalt [2].

Modern methods of synthetic organic chemistry including enzymatic and microbial transformations were applied extensively to fatty compounds for the selective functionalization of the alkyl chain. Syntheses of long-chain diacids, ω-hydroxy-fatty acids, and ω-unsaturated-fatty acids as base chemicals derived from vegetable oils were developed. Interesting applications have been recently opened by the epoxidation of double bonds giving the possibility of photochemically initiated cationic curing and access to polyetherpolyols. Enantiomerically pure fatty acids as part of the chiral pool of nature can be used for the synthesis of nonracemic building blocks [2].

1.1.1 Oleic acid transformations by microorganisms

For more than four thousand millions of years ($4 \cdot 10^9$) bacteria have ability of transforming a huge range of substrates, due to the specificity (bond, functional group, substrate, stereo-, regio-, enantio-) of their enzymes, for obtaining energy and feed to grow. The mankind is almost starting to discover such great potentiality and use it for its own purpose; even though improving it. Such kind of reactions that take place in mild conditions in nature would be hardly difficult to carry out in a chemical way or even practically impossible.

OA (*cis*-9-octadecenoic acid) is a common lipid in nature, especially in plant kingdom. Its biotransformation has being studied since decades ago. Piguevskh and Charik were the first in describing a transformation of OA by microorganisms. 10-ketostearic acid (10-KSA), apart from other products, was produced by micro.ovrddot.organisms when olive oil was used [4]. Some years later, Davis *et al*. cited from an article of 1959 the synthesis of 9- and 10-KSA acids from the dehydrogenation of the corresponding hydroxystearic acids [5]. Wallen and collaborators published the single production of 10-hydroxystearic acid (10-HOSA) by a pseudomonad cultivated with OA as substrate [6]; and, in 1965, Schroepfer established the configuration of the hydroxyl group as *R*, (10*R*)-HOSA [7]. Furthermore, Wilde and Dawson presented the biohydrogenation of OA to stearic acid (octadecanoic acid; SA) by rumen microorganisms from sheeps [8]; and in the same year, Ogata and co-workers synthetized α-ketoglutaric acid (2-oxopentanedioic acid) from OA by *Micrococcus sp.* [9].

In 1970's, OA became more relevant and diverse types of microorganisms were used for its modification. Fungi, like *Blakeslea trispora* and *Torulopsis sp*. were used for synthetizing caretenoids and lipids [10], and obtaining 17-L-hydroxyoleic acid [11], respectively. Aerobic and anaerobic bacteria from different sources (sheep rumen, human intestine or soil, inter alia) were cultivated to biohydrogenate or [12-14] degradate [15] OA and synthetize hydroxystearic acid [16, 17]. Moreover, enzymatic transformations started to take place with the hydration of the double bond [18], isomerization [19], dehydrogenation [20] and hydroxylation [21] of OA.

In the following decade, efforts were also focused on transforming OA into (10*R*)-HOSA and/or its corresponding oxo acid, 10-oxooctadecanoic acid, by different genus of bacteria: *Corynebacterium* [22]; *Rhodococcus* [23]; *Norcadia* [24, 25]. Moreover, this biotransformation was used as a model in the experimental adipocere formation, the fat hydrolysis of human corpses [26-28]. It was carried out by microorganisms as *Micrococcus luteus* or *Flavobacterium meningosepticum*.

Two milestones were the biotransformation of OA into RA by *Bacillus pumilus* [29] and a soil bacterium strain, BMD I 20 [30], in significant amounts and the biotransformation of OA into a new biosurfactant, a dihydroxylated compound, by *Pseudomonas aeruginosa* 42A2 [31]. Finally, different new brand products were obtained from OA: diacids, as azelaic (nonanedioic acid) and pimelic (heptanedioic acid) acids by *Micrococcus sp*. [32], and *cis*-9-1,18-octadecenedioic acid by *Candida tropicalis* [33, 34]; and, a double unsaturated fatty acid by the action of a desaturase of *Tetrahymena thermophila* [35].

In 1990's the conversion of OA into (10*R*)-HOSA [36-44], 10-oxostearic acid [45] and 10-ketostearic acid [46-50] were the most studied bioreactions. This OA hydration reaction and others previously described were continuously used as model of adipocere formation [51, 52].

Some other new compounds were produced by biotransformation of OA, Figure 1.1: α,ω-dicarboxilic acids [53] and 3(*R*)-hydroxy-9(*Z*)-octadecenedioic acid [54, 55] by *C. tropicalis* and *C. tropicalis* M25, respectively; hydroxy-fatty acid (HFA) intermediates for the production of lactones as (*R*)-γ-dodecalactone by several species of yeasts [56-59]; diverse fattyamides by some *Bacillus* species [60, 61]; sophorose lipids by *Candida bombolica* ATCC 22214 [62]; oligosaccharide lipids and biosurfactants by *Tsukamurella sp* DSM 44370 [63]; and, poly(3-hydroxyalkanoates) (PHA) by *Alcaligenes eutrophus*, *P. putida* and *P. mendocina* 0806 [64-67] and poly(3-hydroxybutyrates) (PHB) by some strains of *Alcaligenes* [68-70] an one of *Aeromonas hydrophila* [71].

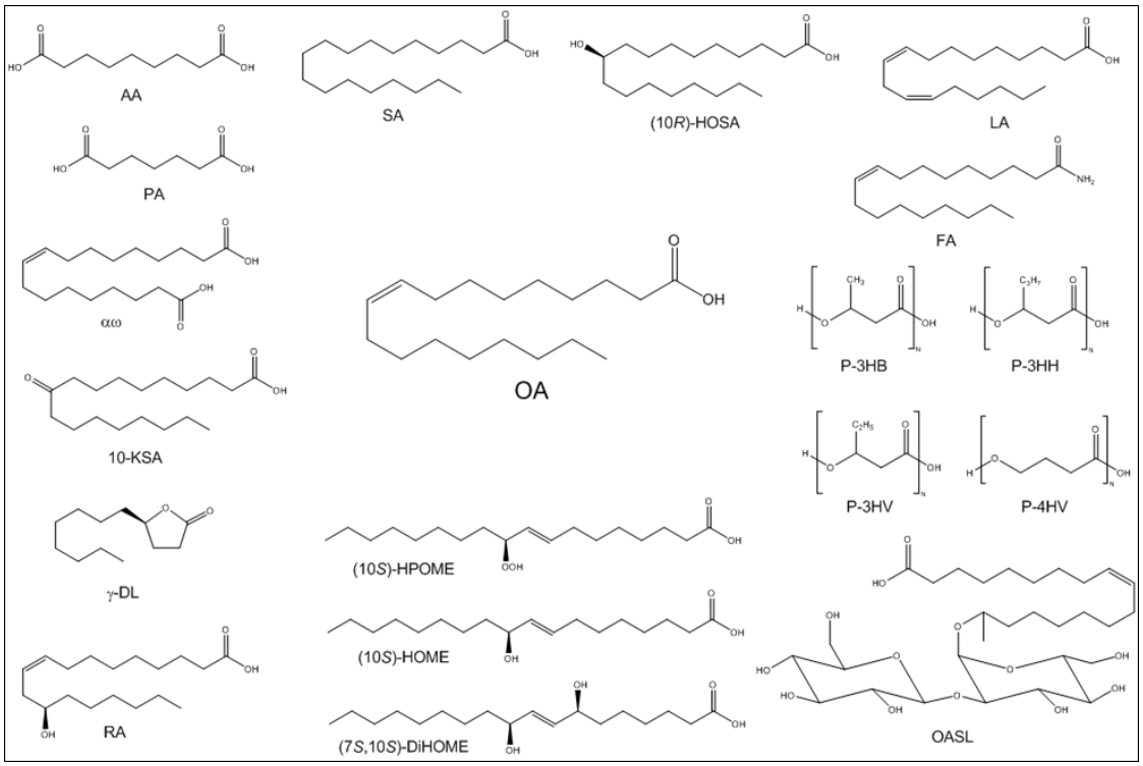

Figure 1.1. The most important biotransformated products obtained from oleic acid. **OA**: oleic acid; **AA**: azelaic or nonanedioic acid; **SA**: stearic acid; **(10*R*)-HOSA**: 10(*R*)-hydroxy-octadecanoic acid; **LA**: linoleic acid; **FA**: fatty amide, 9(*Z*)-octadecenamide; **P-3HB**: poly-3-hydroxybutyrate; **P-3HH**: poly-3-hydroxyhexanoate; **P-3HV**: poly-3-hydroxyvalerate; **P-4HV**: poly-4-hydroxyvalerate; **OASL**: oleic acid sophorolipid; **(10*S*)-HPOME**: 10(*S*)-hydroperoxy-8(*E*)-octadecenoic acid; **(10*S*)-HOME**: 10(*S*)-hydroperoxy-8(*E*)-octadecenoic acid; **(7*S*,10*S*)-DiHOME**: 7,10(S,S)-hydroperoxy-8(*E*)-octadecenoic acid; **RA**: ricinoleic acid; **γ-DL**: γ-dodecalactone; **10-KSA**: 10-keto-octadecanoic acid; **α,ω**: 9(*Z*)-octadecenedioic acid; **PA**: pimelic or heptanedioic acid.

Some other uncommon HFAs were produced: 15-, 16-, 17-hydroxy-9-octadecenoic acids by *B. pumilus* [72]; 3-hydroxy-9(*Z*)-ocradecenoic acid by *Alcaligenes sp.* 5-18 [73]; 4-oxo-dodecanoic acid by *M. luteus* BL0-3 [74]; 7-hydroxy-16-oxo-9(*Z*)-octadecenoic and 7-hydroxy-17-oxo-9(*Z*)-octadecenoic acids by *Bacillus* strain NRRL BD-447 [75, 76] and dihydrosterculic acid (*cis*-9,10-epoxy-nonadecanoic acid) *by Lactobacillus plantarum* [77].

On the other hand, enzymatic transformation of OA started to gain importance and it was reflected on the number of works published. Enzymatic reactions were focused on Δ6-desaturase to produce γ-linolenic acid [78] and Δ12-desaturase to obtain linoleic acid [79, 80]; on ω-hydroxylases from *Vicia sativa* to synthetize 18-hydroxy-9(*Z*)-octadecenoic acid [81, 82]; on hydroperoxidases [83, 84] and peroxygenases [85] to finally obtain 9,10-epoxy-octadecanoic acid; on oleate 6-hydroxylase to form 6-hydroxy-9(*Z*)-octadecenoic acid [86]; and, on lipoxygenases [87].

Finally, Hou and co-workers improved the production of 7,10(*S*,*S*)-dihydroxy-8(*E*)-octadecenoic acid ((7*S*,10*S*)-DiHOME) up to the 60% [88]; one year later, they

postulated that 10(*S*)-hydroxy-8(*E*)-octadecenoic acid ((10*S*)-HOME) was an intermediate in the synthesis of the dihydroxylated compound by *P aeruginosa* PR3 [89]; moreover, determined the total configuration of (7*S*,10*S*)-DiHOME [90].

Since 2000 to nowadays the hydration of OA into (10*R*)-HOSA and its dehydration to 10-KSA were still the most significant bioreaction [91-93]. These reactions were produced by bacteria as *P. aeruginosa* [94], *Sphingobacterium thalpophilum* [95], *Acinobacter spp.* or *Enterobacter cloacae* [96, 97], *Stenotrophomonas nitritireducens* [98, 99], *Flavobacterium sp.* DS5 [100] or *Lactococcus lactis* [101]. The hydration of OA was also carried out with oleate hydratases from *S. maltophilia* [102, 103], *Lysinibacillus fusiformis* [104, 105], *Streptococcus pyogenes* M49 [106] or with antigens from *Lactobacillus rhamnosus* LGG, *L. plantarum* ST-III, *L. acidophilus* NCFM and *Bifidobacterium animalis* [107].

Moreover, OA hydration was investigated to produce (*R*)-γ-dodecalactone due to its aromatic properties by some fungi [108-110] and bacteria [111, 112]; even during malt whisky production was reported its synthesis [113] and some alkyl-γ-lactones showed fungicidal properties [114]. Another OA hydration for producing SA was also investigated using ruminal microorganisms [115, 116]. Ruminal bobine microorganisms were capable to isomerize OA to different *trans* isomers as well [117-119].

The compounds that appear in 1990's were continuously produced: α,ω-dicarboxilic acids [120-122]; fatty amides [123, 124]; glycolipids [125] as sophorolipids [126, 127] or mannosylerythritol lipids (MEL) [128-130]; diverse kind of ω-HFA as ω-hydroxynonanoic acid [131] or ω-1 [132-134], ω-2 and ω-3 HFA [135]. Some other rare HFA as 2(*R*)-hydroperoxy-9(*Z*)-octadecenoic acid by enzymes from a marine alga, *Ulva pertusa* [136], 7-hydroxy-8-octadecenoic acid by *P. aeruginosa* 2HS [137, 138], 9-hydroxy-10(*E*)-octadecenoic, 10-hydroxy-8(*E*)-octadecenoic and 11-hydroxy-9(*E*)-octadecenoic acids by *P. sp.* 32T3 [139], 3(*R*)-hydroxy-9(*Z*)-octadecenoic acid by *S. maltophilia* [140], 9(*E*)-octadecenoic acid by *P. putida* S12 [141], 10-hydroxy-12(*Z*)-octadecenoic acid by *S. acidamiphila* [142] were synthetized. Furthermore, the enzymatic synthesis of *cis*-9,10-epoxyoctadecanoic acid from OA, hydrogen peroxide and lipase B from *Candida antarctica* (Novozym 435) was reported [143-145].

Other enzymatic reactions have been described using OA as substrate, especially with desaturases. OA have been modified by Δ5-desaturases [146, 147], Δ12 desaturases to produce LA [148-151] or in combination with Δ6 in *Yarrowia lipolitica* to produce γ-linolenic acid [152, 153] and Δ15 [154, 155]. Moreover, hydroperoxidases, peroxygenases and lipoxygenases have been still used.

OA has been using as an important carbon source in the production of PHAs by *P. mendocina* 0806 [156], *P. putida* [157-160], *P. aeruginosa* [161, 162], *P. corrugate* [163], *P. sp.* [164, 165], *P. aeruginosa* 42A2 [166], *P. guezenni* [167], *Burkholderia sp.* USM [168], *Pichia pastoris* [169]; PHBs by *Erwinia sp.* USMI-20 [170], *Spharotilus natans* and *P. sp.* 0B17 [171], *Ralstonia eutropha* [172], *Cupriavidus necator* H16 [173] or PHB copolymers with 3-hydroxyvalerate by *R. eutropha* [174] or *Bacillus sp.* BA-019 [175], 3-hydroxyhexanoate by *Aeromonas hydrophila* [176], 3-hydroxyvalerate and 4-hydroxybutyrate [177] or 3-hydroxyalkanoates [178].

Finally, Kuo and co-workers modified the aeration system of a bioreactor to reduce foaming during production of (10*S*)-HOME and (7*S*,10*S*)-DiHOME from OA and, thus, the production of these HFAs was increased and control parameters of this biotransformation in bioreactor were optimized [179, 180]. When this bioreaction was fully controlled, Kuo and collaborators screened other *Pseudomonads* with a higher (10*S*)-HOME production rates than *P. aeruginosa* PR3 [181]. Another carbon source with high content in OA was tested for the production of these two HFAs, like safflower oil [182].

1.1.2 *Pseudomonas aeruginosa* 42A2 NCIB 40045

P. aeruginosa very is a versatile bacteria that has colonized many natural and artificial environments. It is well known to perform a wide variety of bioreactions due to it can use a wide range of organic matter as a carbon source, evidencing its resilience ability. Even though, scientists in Renseelaer Polytechnic Institute, founded by NASA, reported that, during spaceflight inside the International Space Station, *P. aeruginosa* seem to adapt to the microgravity and the biofilms formed during spaceflight exhibited a column-and-canopy structure that has not observed on Earth [183]. *P. aeruginosa* is an opportunistic Gram-negative pathogen that typically causes urinary tract, respiratory system and soft tissue infections and a variety of systemic infections, particularly in patients with severe burns [184].

1.1.2.1 Oxidation of oleic acid

Lipoxygenases (LOX) (EC. 1.13.11.12) are a non-heme iron enzymes which catalyzes the dioxygenation of polyunsaturated fatty acids with one or more 1Z,4Z-pentadiene units to hydroperoxy-fatty acids. LOX were only considered a eukaryotic characteristic due to the major presence in mammals, fishes, small marine invertebrates, corals, plants, algae, fungi, mushrooms, yeast [185].

LOXs are considered a versatile biocatalyst because of the different kind of reactions in which are involved. LOX produces hydroperoxy-fatty acids that are further

metabolized into various signaling compounds, such as leukotrienes and lipoxins in animals. Leukotrienes and lipoxins are reported to be involved in the inflammatory cascade, the formation of biological mediators and signaling molecules, the immune response and mobilization of lipids. In plants, green leaf like compounds and jasmonic acids were detected. These compounds are present in the plant defense system against pests, in the synthesis of oxylipins and germination or senescence. In corals, prostaglandin-like compounds and oxylipinds were detected [186]. Prostaglandins are locally acting messenger molecules in inflammatory mediation, act in hormone regulation, cause constriction or dilation in vascular smooth muscle cells and control cell growth.

Despite of the unknown role of bacterial LOX, where are mainly found in Gram-negative bacteria, it is thought that its function is associated to facilitate the dynamic plasticity of bacterial membranes. This might be an advantage for the colonization of a wide range of environments where bacteria have adapted and coped with the interaction of eukaryotes [187]. However, it is reported that bacterial LOX produced hydroperoxide-fatty acids, which are the precursors of HFAs. Some HFAs as 10-hydroxy- and 13-hydroxyoctadecanoic acids and 14-hydroxynonadecanoic acid, are used as precursors of flavored lactones, γ-decanolide, δ-decanolide and γ-nonanolide, respectively [188].

In 1988, *P. aeruginosa* 42A2 was demonstrated to oxidize OA to a new surfactant, a dihydroxy-fatty acid [31]. This dihydroxilated biosurfactant reduces surface tension to 30 $mN \cdot m^{-1}$ at 50ºC. This strain is characteristic because of the lack on the production of rhamnolipids. Afterwards, in 1994 production parameters of (7*S*,10*S*)-DiHOME were optimizated obtaining up to 7 $g \cdot l^{-1}$ of this new compound [189]. The stereochemistry of this product was later identified as (7*S*,10*S*)-DiHOME by Hou and collaborators [190] using *P. aeruginosa* PR3. Later, in 1997 it was proved that strain 42A2 synthesized 10-hydroperoxy-8(E)-octadecenoic acid ((10*S*)-HPOME) and (10*S*)-HOME during production of this new biosurfactant [191]. The biotransformation of OA into these hydroxylated compounds needs a notable quantity of oxygen and this is proportional to the volumetric productivity of the oxidized compounds [192]. These studies were carried out in a stirred tank bioreactor where the production of (10*S*)-HOME was increased tenfold, from 0.65 to 7.4 $g \cdot l^{-1}$. Even, this bioreaction was realized with immobilized non-proliferanting cells of *P. aeruginosa* 42A2 on different carriers, being Celite R633 the support with the highest OA conversion, 50%, in 48 hours [193]; and, with lyophilized non-proliferating cells obtaining poorly conversion yields [194].

In 2004, *P. aeruginosa* 42A2 LOX (42A2 LOX) was isolated and characterized; kinetics studies with different polyunsaturated fatty acids (PUFA) and OA, containing a

double bond in position 9, were assayed, being LA the most preferred by 42A2 LOX [195]. One year later, in 2005 Vidal-Mas and co-workers cloned and overexpressed 42A2 LOX in *E. coli* BL21(DE3). Further kinetic experiments were carried out and confirmed the preference of the recombinant protein for LA [196]. Concurrently, *P. aeruginosa* 42A2 was used for first time to accumulate PHA using agro-industrial oily wastes as substrate [166] and subsequent different studies were performance to understand the effect of the fatty acid used as substrate on final PHA [197] and its physcochemical properties [198, 199].

On the other hand, the synthetic mechanism of (7*S*,10*S*)-DiHOME from OA was still unknown, until Martinez and collaborators discovered that in this reaction are involved to different enzymes, a dioxygenase and a hydroperoxy isomerase [200]. Finally, in 2013 the structure of 42A2 LOX, the first available from a prokaryote organism, was crystallized and studied, suggesting the capacity of this enzyme for extracting and modifying unsaturated phospholipids from eukaryotic membranes; allowing a role in the interaction of *P. aeruginosa* 42A2 with host cells [201]. Ultimately, Hansen and Garreta discussed the biochemical aspects, the biological applications and some characteristics of bacterial LOX from a phylogenetic point of view, proposing the existence a new subfamily of bacterial LOX [187].

Another fatty acid, LA, was used as a carbon source in mineral cultures of *P. aeruginosa* 42A2 obtaining oxylipins with antifungal properties, specially a blend of two trihydroxylated isomers, 9,10(12),13-tihydroxy-11(10)-octadecenoic acid, never described before for the 42A2 strain [202]. To this date no further studies have been carried out with other fatty acids as a carbon source.

1.1.2.2 Modification of oleic acid

In 2003, estolides were detected in the cultures of *P. aeruginosa* 42A2 using OA as a single carbon source. ESTs are polyesters from fatty acids or HFA. ESTs naturally produced resulted a mixture of OA, (10*S*)-HOME and/or (7*S*,10*S*)-DiHOME forming oligomers up to six monomers by means of the action of *P. aeruginosa* 42A2 lipase [203].

Pseudomonas lipases have some advantages than other bacterial lipases in temperature, salt concentration and pH stability or substrate and reaction medium tolerability (organic solvents, ionic liquids, supercritical fluids, solvent-free or biphasic immiscible media) [204-207].

One of the most important reasons for the large number of applications of lipases is that they exhibit substrate, regio-, enantio- and stereospecificity, Table 1.2. Lipases of

Table 1.2. Illustrative list of lipases whose X-ray structures have been determinated along with their specificity. Adapted from [204].

Lipase source		Specificity
Bacterial	*Bacillus thermocatenulatus*	1,3-regiospecific
	Burkholderia glumae (Pseudomonas glumae)	Non-specific
	Burkholderia cepacia (Pseudomonas cepacia)	Non-specific
	Bacillus subtilis	–
	Chromobacterium viscosum	Non-specific
	Pseudomonas fluorescens	Non-specific
Fungal	*Aspergillus niger*	1,3-regiospecific
	Candida rugosa (Candida cylindracea)	Non-specific
	Candida antarctica A	*trans*-specific
	Candida antarctica B	1,3-regiospecific
	Geotrichum candidum	*cis*-Δ^9
	Mucor javanicus	1,3-regiospecific
	Penicillium camembertii (Penicillium cyclopeum)	1,3-regiospecific
	Penicillium expansum	–
	Rhizomucor miehei (Mucor miehei)	1,3-regiospecific
	Rhizopus delemar	1,3-regiospecific
	Rhizopus oryzae	1,3-regiospecific
	Rhizopus niveus	1,3-regiospecific
	Thermomyces lanuginose (Humicola lanuginosa)	1,3-regiospecific
	Yarrowia lipolytica	1,3-regiospecific
Plant	*Brassica napus* (rapeseed)	1,3-regiospecific
Animal	*Canis lupus familiaris* (dogs)	–
	Equus caballus (equine)	–
	Porcine pancreatic lipase	1,3-regiospecific
	Human pancreatic lipase	1,3-regiospecific
	Sus scrofa (wild bear)	–

microbial origin, mainly bacterial and fungal, represent the most widely used class of enzymes in biotechnological applications (food, detergent, oil and fat, pharmaceutical, textile and leather, cosmetic and paper industries [205]) and organic chemistry [208].

It was found out that *P. aeruginosa* 42A2 produces two extracellular lipases, named LipA and LipC [209]. Both lipases reveal a high similarity each other; but, a substantial difference in the temperature optimum was reported. LipA showed a mesophilic activity, with an optimal temperature of 30ºC; meanwhile, LipC evidences a psicrophilic range of activity, between 4 and 20ºC [209]. Both lipases displayed a maximum activity with medium-chain fatty acids, specifically with caproic (hexanoic acid) and caprylic (octanoic acid) acids; however, LipC also showed a good activity towards long-fatty acids. In addition, LipC is a versatile enzyme due to its capability to tolerate high concentrations of ions and heavy metals, but result less thermo-stable than its homologus LipA [209].

Later, Cesarini and co-workers developed a rational system design to modify specific residues on the enzyme structure of LipC to improve its thermal stability. After a screening of more than 3000 mutants, only the clone D2_H8 evidenced a 7-fold increased thermostability compared with LipC wildtype. Its operational range of temperature was extended to 30ºC [210].

1.2 Bioreactors in biotechnology

Traditionally, microbiologists have played the dominant role in bioreaction development, with collaboration of experts from disciplines as biochemistry, genetics and chemical engineering. Whereas fermentation processes have been used since prehistoric days for producing cheese, bread, wine or beer, is in the last half century when the major breakthrough has taken place by means of technology [211].

A bioreactor is considered a system in which a biological conversion occurs through the action of enzymes, microorganisms or animal, fungal or plants cells. Specifically bioreactors are design for influencing in the metabolic networks to obtain a high yield, productivity and reproducibility of the desired product. Under these conditions a high selectivity is expected, especially when complex molecules as antibiotics, steroids, vitamins, proteins and certain sugars and organic acids are wanted [211]. Conversion rates must also be in mind with bioreactors; especially, in systems where biomass growth is important and depletion times of the reactants can take days. A bioreactor should not be considered as an isolated unit, but as an operational unit with upstream and downstream units within an overall process.

Bioreactions can be carried out in a three different ways: i) processes that products are secreted to the culture media: primary and secondary metabolites; ii) processes that produce biomass; and, iii) processes that biotransform a susbtrates previously added to the culture media [211].

Most bioreactors fall into one of the following categories: unstirred or stirred vessels, bubble columns, airlift reactors, membrane reactors, fluidized or packed beds. Bioreactor types differ primarily with mode of agitation and aeration. Depending on the operational mode, bioreactors can operate in batch, fed-batch or semibatch, repetead fed-batch or cyclic fed-batch, repeated batch or cyclic batch and continuous mode. In some other classifications, another type of operational mode is included, perfusion cell culture. Perfusion mode is a variant of a continuous system with a cell retention device; but this technique is still in its infancy and it is not completely considered an operational mode itself [212]. The most important kind of bioreactor used in the laboratory and industry is the stirred tank bioreactor.

1.2.1 Batch bioreactor

Shaken bioreactors are used as fermentation systems since the beginning of the last century. Probably the first submerged fermentation in a shake flask was realised by Kluyver and Perquin in 1933 [213]. Nowadays shaken bioreactors are employed for a considerable variety of bioreactions. Most common is the use of conventional conical Erlenmeyer flasks with a volume from 25 ml up to 6 l. Baffled-shake flasks are mainly

used to reach higher oxygen transfer rates and enhancing mixing capacities at equivalent shaking frequencies compared to unbaffled flasks. The popularity of shake flasks as bioreactors is the simplicity of the system which enables the performance of a large number of parallel fermentations in small scale and are mainly used for screening and early bioreaction or bioprocess development in industry and academic research [214].

Batch bioreaction systems provide some disadvantages: i) lower productivity levels due to time for filling, heating, sterilizing, cooling, emptying and cleaning the reactor; ii) increased focus on instrumentation due to frequent sterilization; iii) greater expense incurred in preparing several subcultures for inoculation; iv) higher costs for labor and/or process control for this non-stationary process; v) larger industrial hygiene risks due to potential contact with pathogenic microorganisms or toxins.

In contrast the advantages include: i) reduced risk of contamination or cell mutation, due to a relatively brief growth period; ii) lower capital investment when compared to continuous processes for the same bioreactor volume; iii) more flexibility with varying product/biological systems; iv) higher raw material conversion levels, resulting from a controlled growth period.

Outside the food and beverage industries, fermentation processes were initially associated with organic acids (acetic, citric, gluconic, itaconic or lactic acid) and solvents (acetone or butanol), and, later with the production of low-volume, high-added-value products, such as vitamins, antibiotics or vaccines. More recently, there has been a trend to high-volume, low-added-value products such as single-cell protein and fuels. The deciding factor as to whether such processes are economically feasible is the capital cost of the single-purpose equipment required.

1.3 Aeration systems

In aerobic bioprocesses in any type of bioreactor, there are four basic factors that may limit the final performance of the process: mixing, oxygen, carbon dioxide and heat transfers [214]. Transfer of oxygen from a gaseous phase to a liquid one is key issue in many biotechnological processes, especially in microbial cultures due to oxygen is a key component in microbial metabolism, as well as, it could be a co-substrate in bioreactions.

Enhancing microbial production represents an economic challenge for bioindustry. High cell density reactors imply controlling the interactions between microbial behaviour and transfer phenomena, since gas transfer eventually becomes a limiting factor [215]. This bottleneck is especially significant in large-scale bioreactors, bubble columns.

Depending on the mode of introducing the air or oxygen into the culture media, one division of bioreactors could be established: bubble columns, air-lift reactors and stirred tank bioreactors [214]. Stirred tank bioreactors are the most widely used bioreactor type to cultivate suspension cells, mainly due to the broad experience gain from microbial fermentation and chemical engineering fields over the last century and their relative easy design, operation and scale-up.

Aeration of cell cultures bioreactors is usually performed by bubble aeration, bubble-free aeration or indirect aeration [216]. Bubble aeration delivers large quantities of oxygen into the culture medium. Ascending or bursting bubbles in bubble aeration may damage shear stress sensitive cells. This fact leads to reduce cell viability and increase foam formation.

Foaming is produced by i) aeration, ii) medium composition, iii) cell growth, iv) metabolite formation, v) surface-active substance formation or even by vi) vessel geometry [217]. Some amount of foaming during fermentation is acceptable, but excessive foaming requires some type of control action: i) addition of chemical antifoams, ii) installation of foam breakers, iii) reduce working culture volume, iv) connection with other vessels or v) reducing aeration and agitation. All these actions affect bioreaction yields and rate conversions negatively. New aeration systems and configurations have being developed to reduce foam formation during cultivation processes in stirred tank bioreactors: i) membranes, ii) ceramic and iii) metallic spargers and iv) non-dispersive devices based on absorption as surface aeration. The final decision depends on the mineral medium, microorganism and/or operator of the bioreactor.

1.4 Predictive microbiology

Biotechnology uses cellular systems to produce biomolecules that benefit society. The main challenge of biotechnology is the understanding of how cellular mechanisms result in functional responses. Through evolution, cellular systems have been optimized to overcome obstacles to survive including their purposeful reprogramming.

Accordingly, a major obstacle limiting biotechnology applications is the complexity of the cellular systems with the biomolecules involved in these systems (proteins, DNA, RNA, lipids, etc.) and the large number of interactions between them [218]. These interactions are organized into vast complex networks which sense and execute cellular programs, biochemical networks, important for proliferation and survival. Computer simulations and modelling can be valuable tools for investigating such biochemical reaction networks that make up living systems [219].

1.4.1 Process modelling

Microbial modelling allows the description and prediction of microbial behaviours under specific environmental conditions [220]. Sensor technologies are rarely found that can provide real-time assessment of many intra- and extracellular activities. Those currently available tend to suffer from high complexity, insufficient accuracy, risk of contamination or insufficient robustness, which makes process states very difficult to characterize [212].

Despite all those difficulties, process modelling and simulation techniques have gained enormous popularity because it facilitates process optimization. These set of tools give the possibility of exploring alternative routes and hypothetical changes of existing or new processes *in-silico*, before experimentation. This enables tedious experimentation to be directed and focused on speeding up bioprocess development [221].

Process modelling can also be used to develop and evaluate process control strategies to ensure stability and desired efficiency over production characteristics as product quality, as well as, reducing manufacturing costs, risks and time [212, 221].

1.4.2 Mathematical models and types

Although process modelling and simulations tools have been available for many years, the first software programs dedicated for bioprocessing showed up in the mid-1990s. Today, several commercial programs, often with powerful graphic features, include advanced neural networks and fuzzy logic technologies and data analysis features to manipulate data sets for identifying inaccurate or corrupted data points [212].

An investigation of a bioreactor performance and its cell growth behaviour might be almost carried out in an empirical manner. Thereby, bioreactor should be studied under all possible operational conditions and the obtained results expressed as series of correlations, which could be used to hopefully estimated future operational conditions from a given new set of reaction parameters. Although this practice could be rather convenient, has many disadvantages as little real understanding of the process and a routine and long-time consuming way of proceeding [222].

On the other hand, in a modelling exercise, it is necessary to determine all important parameters of a reactor and their effect on the reaction and mathematically defined them for incorporating in the mathematical model. Later, a basic group of experiments should be carried out to obtain different sets of experimental data, for confirming or rejecting the initial proposed mathematical model, by means of modelling and

simulation tools. The task of formulating mathematical equations is a positive factor that forces the clear formulation of basic concepts of the bioreaction [222].

Differences between the experimental and *in-silico* data may be used to further redefine and/or refine the model until good agreement is achieved. Once the model is established, it can be used to predict performances under different initial reaction conditions and design, optimize and control a process. At the end of the modelling exercise, a huge understanding of the process has been gained and the experimental time considerably reduced.

Mathematical models, which describe the living cells cycle, have to represent the dynamic nature of the bioreaction, as general as possible and more complex as a consequence, less empirical and maybe reflecting the biochemistry of the microorganism in the bioreactor. On the basis of these conditions, the model should be set up based on a compromise between the detailed description of the bioreaction and the use to limited parameters to easily estimate and control it [223].

Mathematical models are *in-silico* tools that can be used to describe the past and future performance of biotechnological processes. They can be applied to processes operating at many different levels: from the action of an enzyme within a cell, to the growth of that cell in commercial bioreactor [224]. Mathematical models develop in the field of biotechnology are classified according to their scope in four areas: i) catalyst, kinetic models (KM) describing at molecular level the prediction of a reaction selectivity; ii) reaction, KM describing the mechanism and basic reaction rates based on inputs as concentration profiles or reaction media conditions as pH or temperature; iii) reactor, KM describing reaction kinetics incorporating macroscopic mass, energy and momentum balances; and, iv) process, models for the overall performance of the process, which include the interactions between operational units [221].

Moreover, various types and classifications of models are possible. Depending on mathematical modelling problems, they can be classified: by mathematical structure as deterministic or empirical; by complexity as simple or complex; by spatial resolution as nano, micro or macro; by temporal response as dynamic or steady-state; and, by purpose of application as design, analysis, control or optimization [221].

Another way to classify mathematical models was proposed by different authors. Roberts classified mathematical models by the microbiological event, bacterial behaviour over time, into kinetic and probabilistic models [225]. Roels and Kossen divided them depending on the modelling approach to the bioreaction as empirical and mechanistic [226]; and, Whiting and Buchanan by the number of variables considered in the mathematical expression as primary, secondary and tertiary [227].

The last and most accepted classification of mathematical models is based on cell growth as structured or unstructured and segregated or non-segregated models [228]. A structured model attempts to describe intracellular processes in structural and physiological senses. However, cell behaviour is not completely understood, so a structured model in not applicable to the most bioreactions studied. Thus, the global relationships between cells and culture conditions are described with unstructured models. Segregated models consider different stages of the cell cycle in a precise moment of the culture without structuring the cell composition. Figure 1.2 shows the differences between these kinds of models.

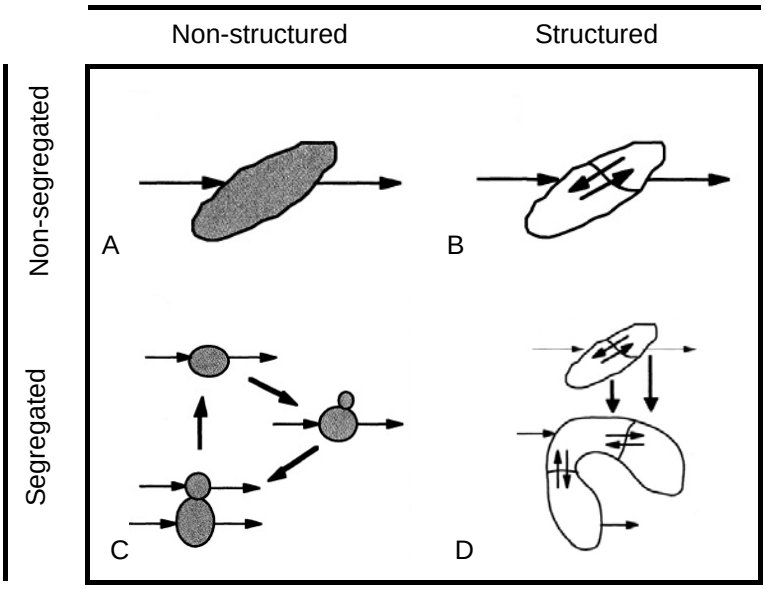

Figure 1.2. Mathematical models. **A**: total cell biomass, **B**: cell parts, **C**: biomass parts and **D**: biomass and cell parts. Adapted from [222].

1.5 Estolides

Nowadays estolides (EST) are defined as a class of polymeric molecules containing an unsaturated bond or hydroxyl group bonded to a carboxyl moiety of another acyl group. In 1920, Grund and co-workers were the first to coin the term *estolides* to define a mixture of esters of higher alcohols and acids produced from the oxidation, with air, of pentatriacontane, an hydrocarbon of 35 carbons [229]. Grund was also the first to use castor oil, the main source of RA (12-hydroxystearic acid) to obtain esters, ESTs, with a molecular weight above 3000 Da and describe the technical properties of this product [230]. Later, Bauer explore the possibility to use unsaturated fatty acids, α- and β-eleostearic acids [231], polyhydroxy acids, two different dihydroxystearic acids [232], and, OA [233] to chemically produce ESTs.

In the following two decades, ESTs became an interesting group of chemicals. They were used, with lactones, lactides and esters, as a source of HFAs [234]; and, their first

applications as demulsifying agents [235], resinous compounds [236], highly elastic products [237], lubricants or additive agents in lubricants [238], plastizicers [239] or antifoamers [240] were developed.

Between 1950 and 1970 efforts were focused on searching new properties and applications of ESTs as: gelled products [241], stabilizers and emulsifying agents [242], surface-active compounds [243], improved lubricating greases [244-246], and, intermediates in polyurethane synthesis [247]. Moreover, first's exhaustive studies of the reaction conditions on EST synthesis were carried out using 12-hydroxy-octadecanoic acid [248] and castor oil [249-251] as raw materials or including their thermal decomposition was studied [252]. Ten years later appeared the first publication using an spectroscopic technique, NMR, to determine the presence of ESTs [253].

In the following twenty years, no great advances were achieved in the synthesis of ESTs. Their synthesis from *n*-decane [254] or heated soybean oil [255] and the production of triglyceride-ESTs were the most important breakthroughs. Even ESTs applications seemed stagnant as emulsifiers [256], lubricants [257-259], antiwears [260] or plastiziers [261].

1.5.1 Estolides in nature

EST natural sources are mainly focused in the vegetal kingdom in minuscule quantities amounts. ESTs were found in the epicuticular wax of differents species of genus *Juniperus* [262, 263], *Pinus* [264-267], *Picea* [268] or *Coniferae* [269] and in the wax leaf of some conifers and allied orders [270-272]. There are also found in the cutin of plants [272], in oat kernels [273] and in oils of certain plants and fungi [274] and, even were detected in stored wheat flour, causing rancidity [275]. ESTs are rarely found in animal kingdom, but there are minute amounts in woolwax [276], beewax, sperm whale [277], in the defensive lipids from the glandular hairs of a caterpillar, *Pieris rapae* [278] and in human meibomian gland secretions [279, 280].

It is well know that HFA are suitable substrates for the synthesis of ESTs and can be found in high concentrations in seed oils of several plants: *Euphoibiaceae*, *Brassicaceae*, *Cruciferae*, *Limmanthaceae*, *Compositae*, *Lesquerella* cited in [281] and *Umbelliferae* [282].

1.5.2 Chemical synthesis

As stated before, in 1991 chemical synthesis of ESTs started to gain relevance. Robert Kleiman was the promoter in this field; but, Terry A. Isbell and Steve Cermak are being the reference in chemical synthesis of ESTs using seed oils from plants as substrates.

The first works were carried out using meadowfoam fatty acids (mainly C20:1 60.7%, positional and geometrical isomers), oleic acid (C18:1 n-9 90.4%) and sunflower oil (C18:1 n-9 72.6%) with inorganic strong acids, as perchloric, sulphuric, or even clays as catalyst at temperatures of 250ºC [283]. Such high temperatures produced undesirable products from branching, isomerization or lactonization reactions [284]. For avoiding these unwanted products and increasing EST yield (28%), reactions took place under an atmosphere of nitrogen [285]. It was in 1997 when reactions with OA were carried out using sulphuric acid as catalyst, at lower temperatures (55ºC) and reaction times were reduced to six hours achieving yields of 75% [286].

Later, EST 2-ethylhexyl esters were synthesized from meadow and cramble oils (erucic acid; C22:1 n-9 57.5%) to improve the lubricant properties of ESTs [287]. Pour points and kinematic viscosity values were enhanced compared with normal ESTs. Apart from that, the possibility of using saturated substrates or hydrogenated ESTs was explored for obtaining better lubricating properties [288, 289]. Another innovation was the use of lesquerella oil (C20:1 hydroxy 55.4%) [290]; coconut oil (C12:0 48.3%) [291]; cuphea oil (C10:0 65.6%) [292]; tallow (C18:1 n-9 43.3%) [293]; and, coriander oil (petroselenic acid; C18:1 n-12 73.5%) [282] as substrates for synthetizing a new brand of vegetal oil-based lubricants with superior cold temperature performance than those synthetized before.

Finally, a new class ESTs are being produced recently: sulfo-ESTs, epoxidized-ESTs and sulfirized-ESTs. Sulfo-ESTs are compounds with surfactants properties which are presented a in high efficiency formulations of laundry detergents [294, 295]. Expoxidized- [296] and sulfurized-ESTs have antiwear, lubricant and plasticizing properties [297]. Apart from that, two new ways of producing ESTs have appeared in scene offering unknown possibilities: the use of microwaves [298] and cross metathesis [299, 300].

1.5.3 Enzymatic synthesis

Although Okamura and co-workers accidentally synthesized ESTs using a *Geotrichum cadidum* lipase during the hydrolysis of castor oil [301], Yamaguchi and collaborators were the pioneers in producing ESTs from castor oil using lipases [302]. Later, they reported the importance of controlling the amount of water present in the reaction media and showed the advantage of immobilizing the lipases; the reaction yield was improved, and the product obtained reached acid values (AV) of 40 [303-305].

Since RA ESTs applications arose, different strategies have been proved: (i) improving the immobilizing carriers [305, 306]; (ii) encapsulating lipases in a reverse

micelle [307]; and (iii) from 1997 to 2009, optimized reaction conditions in a bioreactor to increase the quality and quantity of ESTs production were reported [308-311]. Likewise, molecular sieves have been employed to adsorb water released during polycondensation in order to shift thermodynamic balance [312]. Several other methods, such as air drying [308], nitrogen bubbling, vacuum pressure, or a combination of these two, have also been employed [313].

Recently, organic apolar solvents have started to be used as part of the reaction media in enzymatic reactions [314]; even, in ESTs synthesis [281]. However, organic solvents reduce synthetic stability of enzymes and mass transfer rates when substrates are not totally solubilized; hence, solvent-free systems have gain attention in the synthesis of ESTs due to they allow higher volumetric production than organic media, enzymes are easily separated from products and unreacted substrates. Furthermore, the absence of solvents makes the processes environmentally friendly [315].

1.5.3.1 Selectivity of lipases

Lipases, triacylglycerol acylhydrolases (EC 3.1.1.3) are ubiquitous enzymes of considerable significance industrial potential; especially, in modern organic chemistry for production of chiral building blocks [206]. Lipases have been used for modification of fats and other kind of lipids by hydrolysis, esterification, transesterification or interestification. The utility of lipases is directly related with their ability to discriminate between particular fatty acids.

Table 1.3. Lipases specificity over different *cis*/*trans* double bonds.

Positional specificity	Substrate	Cite
cis-4	all *cis*-**4**,7,10,13,16,19-docohexaenoic acid	[316]
cis-5	all *cis*-**5**,8,11,14,17-eicosapentaenoic acid	[317]
cis-6	*cis*-**6**-octadecenoic acid	[317]
	all *cis*-**6**,9,12,15-octadecatetraenoic acid	
	all *cis*-**6**,9,12-octadecatrienoic acid	
cis-8	all *cis*-8,11,14-eicosatrienoic acid	[318]
cis-9	*cis*-**9**-octadecenoic acid	[318]
	all *cis*-**9**,12,15-octadecenoic acid	
cis-11	all *cis*-9,**11**-octadecadienoic acid	[319]
	cis-**11**-eicosenoic acid	[320]
cis-12	all *cis*-9,**12**-octadecadienoic acid	[321]
cis-13	*cis*-**13**-docosenoic acid	[320]
cis-15	all *cis*-9,12,**15**-octadecatrienoic acid	[321]
trans-2	–	[322]
trans-3	*trans*-**3**-hexadecenoic acid	[323]
	trans-**3**-octadecenoic acid	
	trans-**3**-*cis*-9,12-octadecatrienoic acid	
trans-6	*trans*-**6**-octadecenoic acid	[316]
trans-9	*trans*-**9**-octadecenoic acid	[321]
trans-10	*trans*-**10**,cis-12-octadecadienoic acid	[324]
trans-12	all *trans*-9,**12**-octadecadienoic acid	[321]
trans-15	all *trans*-9,12,**15**-octadecatrienoic acid	[321]

There have been several works studying the selectivity of lipases towards unsaturated fatty acids having different positions of *cis*/*trans* double bonds summed up in the Table 1.3. The source of lipases used in these studies was very varied, from microorganisms, fungus specifically (*Candida antarctica*, *Candida cylindracea*, *Geotrichum candidum, Mucor miehei*, *Rhizopus arrhizus*, *Rhizomucor miehei*), to higher plants (*Brassica napus*, *Carica papaya*) through animals (porcine and human pancreatic lipases).

1.6 Fatty acid ethyl esters

Fatty acid ethyl esters (FAEE) are versatile group of compounds found in very different fields due to the number of carbons and instaurations and the presence of other functional groups along the fatty acid chain.

Since 1981, a huge number of references, articles and reviews, has been published about FAEE as non-oxidative metabolites of ethanol intake [325, 326]. Long-chain FAEE (mainly ethyl palmitate, stearate, oleate, linoleate and arachidonate) have been described as toxic metabolites because of their negative effect on intestinal epithelial barrier [327]; on pancreas [328]; oral tissues [329]; immune system [330]; on mononuclear cells [331]; myocardial tissue [332]; platelets [333]; hepatic cells [334]; on skeletal muscles [335]; atherosclerosis [336]; on erythrocyte morphology and stability [337]; and, brain [338]. Furthermore, FAEE have been described as biomarkers of ethanol intake in hair [339] and skin surface lipids [340] on adult people for drug analyses [341] or in forensic medicine [342]; and, in meconium of newborns to determine alcohol consumption during maternal pregnancy [343].

In contrast, volatile FAEE are odorants in important alcoholic beverages like wine [344, 345], cider [346], whisky [347, 348], white rum [349] and vodka [350]. Depending on the liquor, short- (C2-C5), medium-chain (C6-C12) FAEE or both are found in different proportions.

ω-3 FAEE, particularly ethyl esters from eicosapentanoic and docohexaenoic acids, the two main PUFAs, have been extensively prescribed as dietary supplements in order to reduce cardiovascular risk [351], hypertriglyceridemia [352-354], inflammation of atherosclerotic plaques [355] and were evidenced to improve arterial stiffness in obese people [356]. Recent studies indicate that ω-3 PUFAs show serious potential as tumor sensitizing agents, improving drug delivery effectiveness in cancer treatment [357] and play an important role in the prevention of certain types of cancer [358, 359], such as breast [360-362] and colorectal cancers [363-365]. Moreover, ω-3 PUFAs have been show evidence of beneficial health effects in bone metabolism [366], joint

pain/swelling [367], brain function during aging [368] and psychiatric conditions (e.g. depression or bipolar disorder) [369, 370].

The main source of ω-3 PUFAs and FAEEs is fish oil (e.g. mackerel, herring, sardines, salmon or tuna oil); even though, can be acquired from other sources as microalgae, krill oil or plants [371]. Different methods have been used to enrich fish oil to obtain highly purified ω-3 PUFAs and FAEEs oil. Ionic liquids containing aromatic rings [372], molecular distillation [373], supercritical carbon dioxide fractioning [374], urea complexation followed by high-vacuum rectification [375], silver-ion membranes [376] and supercritical fluid extraction of FAEEs in aqueous silver nitrate solutions [377] were used.

Finally, ω-3, ω-6, ω-7 and ω-9 FAEEs have been described a novel bioactivity against oral pathogens [378, 379].

1.6.1 Enzymatic synthesis

Production of FAEEs by lipases is clearly oriented to biodiesel. Biodiesel is an alternative energy source to conventional fuel. It combines environmental friendliness with biodegradability, low toxicity and renewability. Different kinds of feed-stokes can be used for biodiesel production. The choice of the source depends largely on the country and its climate [380] and also economics [381]. Thus, feed-stokes can be divided in three groups: i) virgin oils as soybean, rapeseed, canola, palm, corn, sunflower, cottonseed, peanut and coconut oil; ii) animals fats as beef tallow, chicken fat; and, iii) aquatic plants as algae and microalgae or *Chlorella vulgaris* which can produce 39% (w/w) of biomass rich in OA [382].

Enzymatic production of biodiesel is focused in the versatile activity of lipases, which facilitates the simultaneous catalysis of triglycerides and fatty acids by transesterification or esterification [383]. Moreover, enzymatic process can be operated at relatively low temperatures and atmospheric pressure, reducing energy consumption [384]. Considerable efforts have been made to increase bioreaction yields and different reaction medium have been assayed: the use of a co-solvent, *tert*-butanol blended with ethanol or methanol, with the aim of reducing oil viscosity and dissolving glycerol byproduct [385]; a salt-solution-based reaction system for maintaining an acceptable concentration of the alcohol [386]; supercritical carbon dioxide for enhancing mass transfer [387]; ionic liquids as reaction solvents as an alternative to volatile, toxic and flammable organic solvents [384]; or, solvent-free systems [281].

2. Objectives

This project was supported by the Ministerio de Economía y Competitividad (CICYT, project CTQ2010-21183-C02-01) of Spain and by the IV Pla de Recerca de Catalunya, Generalitat de Catalunya (grant 2009SGR819) and the PhD-Student was a grateful recipient of an APIF-fellowship from the University of Barcelona.

The objectives of this work are:

1. The optimization of hydroxy-fatty acids production from oleic acid in bioreactor:
    a. Designing a new aeration system for increasing *trans*-hydroxy-fatty acid production.
    b. Modelling the oxidation of oleic acid by *Pseudomonas aeruginosa* 42A2 in bioreactor.
2. Synthesis of a new family of estolides and other derivates, ethyl esters, from *trans*-hydroxy-fatty acids:
    a. Explorining different strategies for enzymatic synthesis of these compounds.
    b. Developing analytical and structural determination methods for detecting these products.

3. Material and Methods

3.1 Microorganism and culture conditions

3.1.1 Microorganism

The microorganism used in this work was *Pseudomonas aeruginosa* 42A2, a gramnegative bacillus isolated from an aqueous sample contaminated with oily wastes. Initially it was registered as *Pseudomonas sp.* 42A2 NCIMB 40045 in the *National Collections of Industrial and Marine Bacteria Ltd, Aberdeen, UK*. Lately, it was identified as *Pseudomonas aeruginosa* by means of the ribosomic RNA sequencing of the 16S gene (reference AJ309500, Genbank). A hundred per cent homology was obtained with *Pseudomonas aeruginosa* PA01 16SrRNA gene [388]. The strain was preserved frozen, -80ºC, in cryobilles (AES CHEMUNEX S.A., Terrassa, Spain).

3.1.2 Culture media

The culture media used was a mineral media (MM1) composed of ($g \cdot l^{-1}$): $CaCl_2$ (0,01), $NaNO_3$ (3,5), K_2HPO_4 (2,0), KH_2PO_4 (1,0), KCl (0,1), $MgSO_4 \cdot 7H_2O$ (0,5), $FeSO_4 \cdot 7H_2O$ (0,012) and 0,05 $ml \cdot l^{-1}$ of trace elements solution. Salt solutions were prepared hundred fold more concentrated than the final concentration indicated above. They were separately sterilized in an autoclaved (1 atm, 30 min, 121 ºC) for avoiding salt precipitation. Trace elements solution had the following composition ($g \cdot 100\ ml^{-1}$): H_3BO_3 (0,148), $CuSO_4 \cdot 5H_2O$ (0,196), $MnSO_4 \cdot H_2O$ (0,154), $Na_2MoO_4 \cdot 2H_2O$ (0,015), $ZnSO_4 \cdot 7H_2O$ (0,307). These were dissolved in distilled water and the solution was sterilized by filtration.

Technical grade oleic acid (OA), 90% (Sigma-Aldrich Chemie GmbH, Steinheim, Germany) was used as carbon source in this work. 20 $g \cdot l^{-1}$ of OA, 2% (v/v), were needed for the pre-inoculum and part of the bioreactor culture media preparations. In the bioreactor experiments, OA initial concentration was 10, 15 and 20 $g \cdot l^{-1}$ (1, 1.5 and 2% (v/v), respectively), as stated in the text.

3.1.3 Inoculum

Inoculum preparation differed for baffled shake flasks or bioreactor cultures. In the baffle-shake flasks (Anorsa, Barcelona, España), pre-inoculum was prepared from a 24 h solid nutritive TSA (Trypticase Soy Agar; Pronadisa, Barcelona, España) culture of *P. aeruginosa* 42A2 at 30ºC. Biomass was resuspended in 5 ml of NaCl sterilized solution (0.9% w/v; Panreac Química S.A., Castellar del Vallès, España). Suspension was adjusted to an optical density of 2.0±0.2 at 540 nm. Optical density was measured with a PharmaSpec UV-1700 series spectrophotometer (Shimadzu, Kyoto, Japan). Baffled shake flasks with 200 ml of culture media were inoculated with a 4ml-bacterial suspension, 2% (v/v).

In the bioreactor experiments, inoculum was obtained from the biomass generated in overnight cultures in 1l-baffled-shake flasks. Cultures were incubated for 18 h at 30ºC in an orbital shaker. Inoculum was obtained from 400 ml of culture media. Cells were harvested by centrifugation (14,700×g for 30 min at 4ºC; Centrikon T-124, Kontron, Madrid, Spain) and resuspended with NaCl 0.9% (w/v) at 2% (v/v) to an optical density of 2.0±0.2 at 540 nm prior to inoculation into the bioreactor. A 40 ml bacterial suspension was inoculated per two liters of culture media, 2% (v/v).

3.1.4 Baffled shake flasks

1l-baffled-shake flasks, with a working volume of 200 ml, were covered with hydrophobic cotton. Prior to use, baffled shake flasks were sterilized with 180 ml of distilled water in autoclave (1 atm, 30 min, 121 ºC; Darlab K-400, Rubilabor, Rubi, Spain). Then, mineral salts, carbon source and inoculum were added. Flasks were incubated at a temperature of 30ºC in an orbital shaker, 150 rpm, during 18 h.

Preparation of part of the culture media used in the bioreactor cultivations was obtained from cultures with 2l-baffled-shake flasks covered with hydrophobic cotton. The final working volume was 500 ml. Baffled shake flasks were sterilized previously with 450 ml of distilled water in autoclave (1 atm, 30 min, 121 ºC). After that, mineral salts, carbon source and inocula were added. Baffled shake flasks were incubated at 30ºC during 48 h in an orbital shaker, 150 rpm.

3.2 Bioreactor

Bioreactor, with the volume of distilled water needed for a final working volume of two liters, was sterilized with dissolved oxygen and pH probes; the last one, previously calibrated with the pH 7 and 9 buffer solution from Mettler Toledo (Urdof, Switzerland). After introducing in the reaction vessel the culture media from the 2l-baffled-shake flasks (two thirds of the working volume), mineral salts and carbon source were added; set points were established in the control unit. Then, one stream of the culture media was pumped through the wetted wall column (WWC) to proceed the calibration of the dissolved oxygen probe. Finally, the inoculum was aseptically added to the reaction media through one of the reaction tank ports.

All experiments were carried out at 30ºC. Temperature was automatically maintained by means of the control unit. Likewise, pH was maintained at 7.00±0.01 with the addition of 2M NaOH and HCl solutions (Panreac Química S.A., Castellar del Vallès, Spain). The basic and acidic solutions were aseptically supplied with two peristaltic pumps controlled by of the control unit of the bioreactor. Volumetric air flow was set up between 2.5 and 7.5 $l \cdot min^{-1}$. Dissolved oxygen was measured with its

corresponding probe and set up at 30%; this value was kept constant through the stirring speed and air flow control by the control unit. Air flow was enriched with pure oxygen (Carburos Metálicos, Barcelona, España) when needed.

3.2.1 Biostat® B 2 L bioreactor

A Biostat® B 2 L bioreactor system (Sartorius Stedim, Melsungen, Germany) was used for producing hydroxy-fatty acid (HFA) by *P. aeruginosa* 42A2. It is a compact reaction systems equipped by a stirred tank reactor and a supplied control unit which ensures the automation of the process.

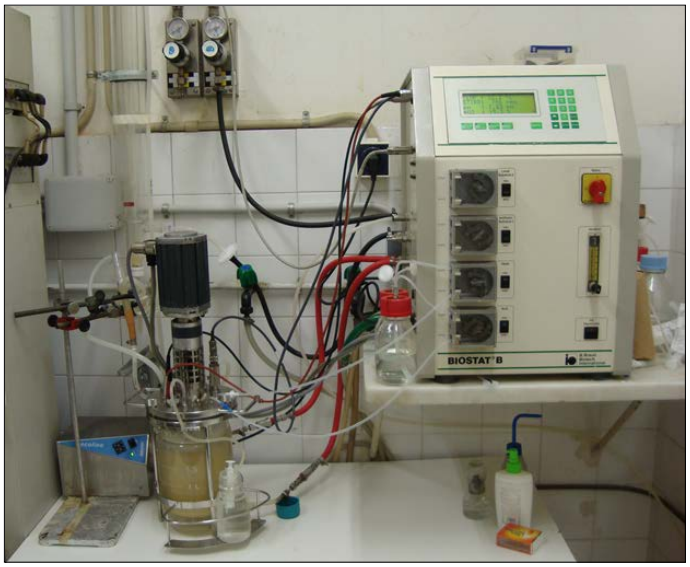

Figure 3.1. Biostat® B 2 L bioreactor.

3.2.1.1 Control unit

The control unit contains the thermostate system, which allows the water flow through the jacket of the culture vessel, and all installations required for power supply, the supply of cooling water, pressurized air and oxygen and waste water removal.

The upper front panel contains the operating terminal of the control system and in the lower front panel includes the main control switch, the fill-thermostate switch, a flowmeter for the control of the air supply and four peristaltic pumps. On the left side of the control unit all conectors for the supplies of the culture vessel are integrated: thermostate, cooling water, air, exhaust cooler, mains supply, power supply to stirring motor and sockets for electrodes and peripheral units.

Thermostatting system includes a 600W electric heater. The operational temperature range is 0-60ºC. Stirring system includes a 180 W electronic motor. Two Rushton impellers were mounted to the stirrer shaft. Operational range is 50-1200 rpm. Air flow is regulated by an electrovalve and, at the same time, it is controlled for the

set-point values. The Microbiology laboratory has an air compressor which supplies the needed air to the reaction system. Control unit has a mixing gas system for enriching the air flow when needed. In the outlet gas stream there is an air filter (Ø 50 mm, 0.2 μm; Millex®-FG, Bedford, USA) for supplying sterilized air to the WWC. Air flow range is 2.5-7.5 $l \cdot min^{-1}$ and was enriched with oxygen (Carburos Metalicos, Barcelona, Spain) when needed.

3.2.1.2 Culture vessel

Culture vessel is a jacketed stirred tank of 2l working volume. It was made of borosilacate glass and the standard stirrer driven vessel have a height:diameter ratio of about 2:1. The vessel has four integrated side entry ports in the head space for acces to the interior culture vessel. The top-plate is connected to the upper flanged ring of the glass vessel with knurled screws. The top-plate contains several ports for assembly of electrodes and accessories. In addition four tubing connectors are welded into the top plate. The culture vessel is mounted into a supporting frame. Two handles allow easy transport. The holder of the storage bottles for addition solutions are welded to the bottom support. The vessel has an internal concave bottom section; this design was proven in fermentations of microorganisms and animal cells. All parts in contact with the medium were made of stainless steel 1.4571 and the O-rings consist of EPDM (ethylene-propylene diene monomer).

Biostat® B used in this work has: a temperature probe Pt-100/200-4 (Sartorius Stedim, Melsungen, Germany); a 405-DPAS-SC-K8S/200 pH electrode from Mettler Toledo GmbH (Urdof, Switzerland); a dissolved oxygen probe 12/200 model 82 (Mettler Toledo GmbH, Urdof, Switzerland); and, level and foam probe are conductive electrodes model 884446/1 (Sartorius Stedim, Melsungen, Germany).

3.2.1.3 Control systems

Biostat® B bioreactor possesses different PDI (proportional-derivative-integral) control systems which are integrated in the control unit. Operating data were entered at the functional keyboard of the operator terminal in the upper front panel of the control unit. The integrated software offers all functions necessary for fermentor operation such as measurement and control of the parameters, the calibration of electrodes and the integrated pumps and the signal transfer from/to peripheral equipment.

Standard measurement and control functions were temperature, stirring speed, pH-value, dissolved oxygen, foam, level, air flow and volumetric flow of two different substrates. After power down, the system automatically restarts with the settings

before. If the interrupt takes longer than an adjustable failtime, the system proceeds as switching off by the main switch.

Moreover, a computer was connected to the control unit in which MFCS/win 2.0 software (Sartorius Stedim, Melsungen, Germany) was installed. This computer program allowed controlling the fermentor. It was used to save experimental data of the controlled variables and visualize online their values.

3.2.2 Aeration system

A non-dispersative aeration system was design to avoid the foam formation. The aeration was accomplished adapting a WWC. The design of the WWC was projected according to a mathematical model in which the objective variable was the time of exposure, t_e, of the Penetration Theory of Higbie [389]. For a given t_e, the liquid-phase mass-transfer coefficient in water, $(k_L)_W$, could be calculated using Equation 1:

$$(k_L)_W = 2\sqrt{\frac{D_{O2-H2O}}{\pi \cdot t_e}} \quad (1)$$

where the diffusion coefficient of oxygen (O_2) in water (H_2O), $D_{O2\text{-}H2O}$, is calculated according to the following expression, obtained from experimental data [390]:

$$D_{O2-H2O} = 1.14 \cdot 10^{-5} + 3.95 \cdot 10^{-7}(T - 273) + 3.59 \cdot 10^{-9}(T - 273)^2 \quad (2)$$

according to the findings of Llorens and coworkers [391], $(k_L)_W$ should be corrected because of the presence of a biosurfactant, (7S,10S)-DiHOME, in the culture media by:

$$(k_L)_M = \psi \cdot (k_L)_W \quad (3)$$

where ψ is the ratio between liquid-phase mass-transfer coefficients [391] and gets the value of 0.41 for an interfacial pressure (π') greater than 0.016 $N \cdot m^{-1}$ [391]. π' is the difference between the surface tension of water, 0.072 $N \cdot m^{-1}$, and the one of the culture media with biosurfactant, 0.030 $N \cdot m^{-1}$ [392].

From a mass balance in a dilute absorption system, the contact surface between the gas and liquid phases is given by:

$$S = \frac{L}{(k_L)_M \cdot \rho_W} \int_{x_1}^{x_2} \frac{dx}{x_{eq} - x} \quad (4)$$

where x_{eq} is the molar fraction of oxygen in the equilibrium, x_1 is molar fraction of

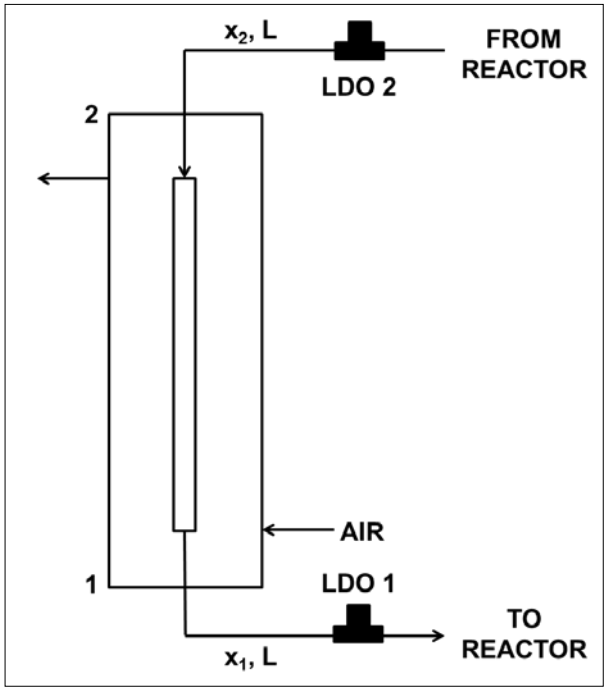

Figure 3.2. Scheme of the wetted wall column. **L**: molar flow of the stream through WWC. **LDO i**: Luminescent dissolvent oxygen probe in the position i of the WWC. $\mathbf{x_i}$: molar fraction of oxygen in position i of the stream L.

oxygen in the stream of culture media saturated of oxygen that leaves the WWC; and, x_2 is the stream that enters in the column and leaves the batch reactor, Figure 3.2. It was considered the assumption that all supplied oxygen in the WWC is consumed in the reactor, thus from a mass balance:

$$x_1 = \frac{q_{O2}}{L} + x_2 \tag{5}$$

where q_{O2} is oxygen requirements of bacteria and L is the molar flow of the stream that is oxygenated in the WWC. Integrating Equation 4 as a logarithmic mean, the following expression is obtained:

$$S = \frac{L}{(k_L)_M \cdot \rho_W} \frac{x_1 - x_2}{\frac{(x_{eq} - x_1) - (x_{eq} - x_2)}{\ln \frac{x_{eq} - x_1}{x_{eq} - x_2}}} \tag{6}$$

in which S is the outside surface of a 15 mm-outside-diameter cylinder. The mathematical process ends with the calculation of the height of the cylinder from the obtained t_e and $(k_L)_M$ throughout the following formulas [393], to ensure that the outside surface is large enough:

$$t_e = \frac{2}{3} h \cdot \sqrt[3]{\frac{3 \cdot \pi^2 \cdot d^2 \cdot \mu' \cdot \rho_W{}^2}{\rho \cdot L^2 \cdot g}} \tag{7}$$

$$(k_L)_W = \sqrt[6]{\left[\frac{6 \cdot D_{O2-H2O}}{\pi \cdot h}\right]^3 \left[\frac{L}{\rho_W \cdot \pi \cdot d}\right]^2 \left[\frac{\rho \cdot g}{3 \cdot \mu'}\right]} \quad (8)$$

3.2.3 $k_L a$ determination

Volumetric mass transfer coefficient ($k_L a$) was determinated using static gassing out method. Reactor vessel was filled with two liters of distilled water; then the vessel was fluxed with pure nitrogen (Carburos Metalicos, Barcelona, Spain) until all oxygen was displaced from the media. At that point stirring, peristaltic pump (Ecoline VC380; Ismatec, Badalona, Spain) and air flow were connected. Dissolved oxygen concentration was measured with the probe described in section 3.2.1.2 and data were recorded by MFCS/win 2.0 software, section 3.2.1.3, for its ulterior processing. The increase in dissolved oxygen concentration ($C_{O2}(t)$) is given by:

$$\frac{dC_{O2}}{dt} = k_L a \cdot \left(C^* - C_{O2}(t)\right) \quad (9)$$

where C* is the dissolved oxygen concentration in the equilibrium at working temperatute, 30ºC. Integrating Equation 9 the following expression is obtained, Equation 10:

$$\ln\left(C^* - C_{O2}(t)\right) = -k_L a \cdot \Delta t \quad (10)$$

$k_L a$ is the slope of a line when $\ln\left(C^* - C_{O2}(t)\right)$ is represented versus Δt, Equation 10.

3.3 Growth measure and production parameters

3.3.1 Biomass determination

Biomass ($g \cdot l^{-1}$) was determined gravimetrically as dried weight (X). An aliquot 5 ml, of the culture was withdrawn aseptically and centrifuged at 8000 rpm for 15 min. Afterwards, supernatant was discarded and biomass was washed with Milli-Q water or with a mixture of Milli-Q water:*n*-hexane (9:1) to remove residual carbon source. The cells were centrifuged again, resuspended in 2 ml of Milli-Q water and dried at 100ºC for 24 h in preweighed tubes.

Concurrently, protein content was determined following the modified Lowry's method from Bio-Rad (Bio-Rad *DC* Protein Assay, El Prat de Llobregat, España). Samples were analysed over a 96-well plate (Sterilin Limited, Newport, UK) to calculate their absorbance with a plate reader (Bio-Tek Instruments Inc. ELx800, Winoosky, USA). This plate reader was connected to a computer in which a computer programme (Bio-Tek Instruments Inc., Winoosky, USA) allows the display and/or storage of the

experimental data. Protein quantitative determination was calculated using a calibration curve with bovine albumin supplied in the same kit.

3.3.2 Nitrate ion determination

Residual nitrogen source determination was carried out by quantification of nitrate ion concentration in the culture samples supernatant. After centrifuging the culture media aliquots, supernatants were analysed with QUANTOFIX® Nitrate-Nitrite test strips (Mancherey-Nagel GmbH & Co. KG., Düren, Germany). Nitrate concentration range was 10-500 $mg \cdot l^{-1}$. When was needed, dilutions of the supernatant samples were done with Milli-Q water.

3.3.3 Phosphate ion determination

Residual nitrogen source determination was carried out by quantification of phosphate ion concentration in the culture samples supernatant. After centrifuging the culture media samples, supernatants were analysed with QUANTOFIX® Phosphate test strips (Mancherey-Nagel GmbH & Co. KG., Düren, Germany). Phosphate concentration range was 3-100 $mg \cdot l^{-1}$. When was needed, dilutions of the supernatant samples were done with Milli-Q water.

3.3.4 Hydroxy-fatty acids quantification

A 2ml-supernatant sample was acidified with concentrated HCl until pH-value was 2. Then, two liquid organic extractions were carried out with 1ml of ethyl acetate (Fisher Scientific UK, Loughborough, UK). Phases were mixed through a REAX top 541 test tube shaker (Heidolph, Schwabach, Germany) and separated by centrifugation at 10,000 rpm for 3 min. Organic phase was separated by means of a Pipetman Classic P1000 adjustable-pipette (Gibson, Middelton, USA).

Quantitative analysis of OA, (10S)-HPOME, (10S)-HOME and (7S,10S)-DiHOME was carried out by liquid chromatography in a Shimadzu LC-9A Chromatograph (Kyoto, Japan). Samples were injected into the HPLC with a Sedex 55 light-scattering detector (Sedere, Alfortville Cedex, France) equipped with a Tracer Excel 120 C8 5μm column (150×4.6 mm) (Teknokroma, Sant Cugat del Vallès, Spain). Optimal separation was achieved with an elution gradient using A, acetonitrile (Fischer Scientific UK, Loughborough, UK) (0.1%, v/v acetic acid), and B, water (0.1%, v/v acetic acid), at a flow rate of 1 $ml \cdot min^{-1}$. The gradient (time (min), %B) used was as follows: (0, 70), (10, 0), (15, 0), (20, 70), and (25, 70). The injection volume was 20 μl. A known homemade standard of each HFA and substrate was used to identify the retention times and to quantify the samples over a calibration curve. LabSolutions LCsolution (Shimadzu, Kyoto, Japón) was employed to manipulated chromatogram methods.

3.3.5 Yield coefficients determination

The oxidation of OA into (10*S*)-HOME and (7*S*,10*S*)-DiHOME by *P. aeruginosa* 42A2 could be described by two semireactions in series:

$$OA + O_2 + NO_3^- \longrightarrow X + (10S) - HPOME + CO_2 \quad (11a)$$

$$(10S) - HPOME + O_2 \xrightarrow{X=cte} (10S) - HOME + (7S,10S) - DiHOME + CO_2 \quad (11b)$$

in which (10*S*)-HPOME is considered an intermediate of the global process:

$$OA + O_2 + NO_3^- \longrightarrow$$

$$\longrightarrow X + (10S) - HPOME + (10S) - HOME + (7S,10S) - DiHOME + CO_2 \quad (12)$$

From the experimental set of data, the following yields , $Y_{X/OA}$, $Y_{(10S)\text{-}HPOME/OA}$, $Y_{(10S)\text{-}HOME/(10S)\text{-}HPOME}$ and $Y_{(7S10S)\text{-}DiHOME/(10S)\text{-}HPOME}$, were determinated using the Equation 11 as first order regression fitting:

$$\Delta C_i / MM_i = Y_{i/z} \Delta C_z / MM_z \quad (13)$$

where z is OA or (10*S*)-HPOME. Yield of CO_2 on OA, $Y_{CO2/OA}$, for the first semireaction, and the yield of CO_2 on (10*S*)-HPOME, $Y_{CO2/(10S)\text{-}HPOME}$; for the second one, were calculated from a C-mol macroscopic mass balance [394], Equation 14.

$$\sum Y_{i/z} = 1 \quad (14)$$

and yield coefficients of O_2 on substrate for each semireaction, $Y_{O2/OA}$ and $Y_{O2/(10S)\text{-}HPOME}$, were calculated from a redox balance for each semireaction, where א is the redox number of each compound:

$$\sum Y_{i/z} \cdot \aleph_i = 0 \quad (15)$$

Yield coefficient of NO_3^- on OA, $Y_{NO3/OA}$, was determinated from a nitrogen macroscopic mass balance [394], where the molecular formula of biomass is $CH_{1.78}O_{0.54}N_{0.21}P_{0.022}$.

$$Y_{NO_3/OA} = 0.21 \cdot Y_{X/OA} \quad (16)$$

later, all the yield coefficients were refined by fitting with the simulation software, section 3.4.1.

Finally, volumetric productivity (P_V) for each product (j) was calculated in g basis and C-mol basis, Equation 17:

$$(P_V)_j = \frac{\Delta C_j}{MM_j \cdot \Delta t} \quad (17)$$

3.3.6 Specific oxygen uptake rate

Specific oxygen uptake rate (sOUR) was determinated by means of two luminescent dissolved oxygen probes (LDO 10103; Hach Lange, Alella, Spain) connected a digital two channel multi meter (HQ40D; Hach Lange, Alella, Spain). Data were recorded in a USB memory in intervals of 1 min during whole batch process. Oxygen probes were installed in tubings that connected WWC and bioreactor vessel to determine dissolved oxygen concentration at the entrance and exit of the WWC, Figure 3.2. Probes measured dissolved oxygen concentration in $mg_{O2} \cdot l^{-1}$. sOUR was calculated as follows:

$$sOUR = \frac{OUR}{X_{st}} \quad (18)$$

where X_{st} is the biomass in the stationary phase and OUR is calculated with Equation 19.

$$OUR = \frac{(C_{O2})_1 - (C_{O2})_2}{\Delta t} \quad (19)$$

where $(C_{O2})i$ are the oxygen concentrations measured by LDO probes in the corresponding position of the WWC, Figure 3.2.

3.4 Modelling the hydroxy-fatty acids production

3.4.1 Kinetic parameters determination procedure

Different kinetic models were used to correlate the substrate concentration with microbial growth rate, μ versus S, with or without substrate inhibition and product formation. AQUASIM® (Swiss Federal Institute for Environmental Science and Technology, Dübendorf, Switzerland), a simulation software program, was used to determine the kinetic constants through the simulation of the experimental sets of data. AQUASIM® uses simplex minimization algorithm for minimizing the sum of the squares of the weighted deviations between experimental data and calculated model results, χ^2. All data used with AQUASIM were expressed in C-molar basis.

3.4.2 Mathematical model

From the first semireaction, Equation 11a, the variation of X, OA and (10*S*)-HPOME concentrations with time could be described by the following expressions, respectively:

$$\frac{dC_X}{dt} = \mu_1 \cdot C_X \tag{20}$$

$$\frac{dC_{OA}}{dt} = -\frac{1}{Y_{X/OA}} \cdot \mu_1 \cdot C_X \tag{21}$$

$$\frac{dC_{(10S)-HPOME}}{dt} = \frac{1}{Y_{X/(10S)-HPOME}} \cdot \mu_1 \cdot C_X \tag{22}$$

and for the second semireaction, Equation 11b, where (10*S*)-HPOME is the substrate for the production of (10*S*)-HOME and (7*S*,10*S*)-DiHOME the following Equations are stablished:

$$\frac{dC_{(10S)-HOME}}{dt} = k \cdot C_{(10S)-HPOME} \tag{23}$$

$$\frac{dC_{(7S,10S)-DiHOME}}{dt} = \frac{1}{Y_{(10S)-HPOME/(7S,10S)-DiHOME}} \cdot \mu_2 \cdot C_X \tag{24}$$

and combining Equation 19, 20 and 21 could be obtained the variation of concentration of the hidroperoxide compound with time over the whole process:

$$\frac{dC_{(10S)-HPOME}}{dt} = \frac{1}{Y_{X/(10S)-HPOME}} \cdot \mu_1 \cdot C_X - k \cdot C_{(10S)-HPOME} - \\ - \frac{1}{Y_{(10S)-HPOME/(7S,10S)-DiHOME}} \cdot \mu_2 \cdot C_X \tag{25}$$

where μ_1 and μ_2 are the different kinetic models, Table 3.1, and the subindex refers to the corresponding semireaction of the process.

Table 3.1. Kinetic models.

Without substrate inhibition		**With substrate inhibition**	
Monod	$\mu = \mu_{max}\frac{S}{KS+S}$	Aiba-Edward	$\mu = \mu_{max}\frac{S}{K_S+S}\cdot e^{-S/K_i}$
Tessier	$\mu = \mu_{max}\left(1-e^{-S/K_S}\right)$	Haldane	$\mu = \mu_{max}\frac{S}{K_S+S+\frac{S^2}{K_i}}$
Contois	$\mu = \mu_{max}\frac{S}{BX+S}$	Yano-Koga	$\mu = \mu_{max}\frac{S}{K_S+S+\frac{S^3}{K_i{}^2}}$
Mosser	$\mu = \mu_{max}\left(1+K_S S^{-\lambda}\right)^{-1}$		

3.5 Estolide production

3.5.1 Monomer purification

At the end of cultivation, the culture was centrifuged (14,700×g for 30 min at 4ºC), the supernatant was acidified to pH 2.0 with 37% HCl (Panreac, Castellar del Vallès, Spain), and two extractions were performed with a half volume of ethyl acetate (Fisher Scientific UK, Loughborough, UK). The organic phase was dried over an anhydrous sodium sulfate filter (Panreac, Castellar del Vallès, Spain), and the solvent of the combined extracts was evaporated with a rotary evaporator (Bücchi, Postfach, Switzerland), resulting in a yellow oil. Organic extracts were kept in vials at 4ºC under nitrogen to prevent further oxidation. The (10S)-HOME and (7S,10S)-DiHOME were purified by flash-chromatography in a glass column (50 cm long, 3 cm i.d.) filled with silica gel 60 (0.040–0.063 mm, Merck, Madrid, Spain). The mobile phase used was formed by *n*-hexane:diethyl ether:methanol (80:20:7; v:v:v) and a stream of nitrogen (Carburos Metalicos, Barcelona, Spain) was applied to obtain the purified products. The purified products were kept at 4ºC under nitrogen, as stated above.

3.5.2 Estolide production from in (10*S*)-HOME in *n*-hexane

3.5.2.1 Measurement of the reaction yield

The reactions were monitored by titration to determine the acid value (AV) of the samples. After evaporating the organic solvent, a 30-mg aliquot of the reaction mixture was dissolved in 8 ml of absolute ethanol and diethyl ether (1:1 *v/v*). Titration was carried out with 0.05 M KOH, using phenolphthalein as the indicator. All samples were analysed in triplicate. The AV and the reaction yield were calculated as follows, Equation 26:

$$\eta(\%) = \frac{(AV_{substrate} - AV_{product})}{AV_{substrate}} \cdot 100 \qquad (26)$$

3.5.2.2 Effect of the enzyme concentration

Different quantities of Novozym 435, 0.3 to 1.5 g, were assayed in order to obtain the optimal amount of enzyme with 0.6 g of (10*S*)-HOME in 20 ml of *n*-hexane in a 100 ml Erlenmeyer flask during 48 h at 50ºC. A rotator evaporator system was used to achieve an efficient degree of contact between the enzyme and the substrate, and the required temperature. All the reactions were carried out at atmospheric pressure. The reaction extension was calculated with the Equation 26 as stated above. A control was assayed in order to confirm that this reaction does not occur spontaneously.

3.5.2.3 Effect of the substrate/enzyme ratio

0.5 g of Novozym 435 was used to study the polymerisation with different amounts of (10*S*)-HOME, 0.25-1.0 g. Enzymatic reaction was carried out in the same conditions as described in section 3.5.2.2, including a control. The yield reaction was calculated using Equation 25.

3.5.2.4 Reusability of the enzyme

Biocatalytic reaction was carried out with 0.5 g of organic substrate, (10*S*)-HOME, which was added to 0.5 g of enzyme. Reaction conditions were the same as in section 3.5.2.2. After each cycle, the enzyme was removed from the reaction medium by filtration and rinsed with *n*-hexane several times. Finally, the solvent was evaporated under a stream of air at room temperature. Product was analyzed and the stability of the enzyme was determined as reaction yield, Equation 26.

3.5.2.5 Screening of other lipases for estolides formation

100 mg of *C. rugosa* lipase, lipase A from *R. oryzae,* Lipozyme RM IM, Lipozyme TL IM and Novozym 435 were assayed with 0.6 g of (10*S*)-HOME in 20 ml of *n*-hexane or *iso*-octane in a 100 ml Erlenmeyer flask during 48 h at 50 ºC. A rotator evaporator was used to attain the mixing degree and to control the necessary temperature. The polymerisation reactions were carried out at atmospheric pressure and the reaction yield was calculated with Equation 26.

3.5.3 Estolide production from (10*S*)-HOME and (7*S*,10*S*)-DiHOME in a solvent-free media

3.5.3.1 Measurement of the reaction yield

The reaction yield was calculated as the consumption of the substrate by normal phase High Pressure Liquid Chromatography (HPLC). Normal-phase HPLC analyses were performed on a Thermo Separations Spectra System AS1000 autosampler/injector (Fremont, USA) with a P2000 binary gradient pump from Thermo Separation Products (Fremont, USA) coupled to an Alltech ELSD 500 evaporative light scattering detector (Alltech Associates, Deerfield, USA). The chromatographic separation was carried out using a Dynamax Microsorb 60-8Si (250 mm x 4.6 mm, 8 μm particle size) from Rainin Instrument Co. (Woburn, MA, USA). A 15-min run time was used to determine the conversion of the reaction. Mobile phase was composed of *n*-hexane:acetone (50:50) at a flow rate of 1 ml·min^{-1}. The ELSD drift tube was set at 56 ºC with the nebulizer set at 20 psi N_2, providing a flow rate of 2.0 standard liters per minute. The yield of the reaction was calculated using Equation 27:

$$\eta(\%) = \frac{(A_{substrate0} - A_{substrate\,t})}{A_{substrate0}} \cdot 100 \quad (27)$$

3.5.3.2 Enzymatic reaction conditions

Three different lipases (Novozym 435, Lipozyme RM IM and Lipozyme TL IM) were employed to synthesize estolides from (10*S*)-HOME and (7*S*,10*S*)-DiHOME. Reaction was carried out in a 15 ml batch reactor magnetically stirred, 500 rpm. Reaction medium temperature, 80ºC, was kept constant using a J-Kem Scientific temperature controller (St. Louis, MO, USA). 3 g of (10*S*)-HOME or (7*S*,10*S*)-DiHOME) reacted with 0.36 g of lipase (12% w/w) during 168 h. Enzymatic reactions took place under vacuum, 1.6 kPa of absolute pressure. Yield was calculated using Equation 27.

3.5.4 Estolide production from saturated (10*S*)-HOME in a solvent free-media

3.5.4.1 Measurement of the reaction yield

Reaction yield was calculated as stated in section 3.5.3.1, Equation 27.

3.5.4.2 Hydrogenation of (10*S*)-HOME

Previous to the hydrogenation reaction, the hydroxyl group on carbon 10 was protected with BSA (*bis*(trimethylsilyl)acetamide; Sigma-Aldrich, St. Louis, MO, USA). 15 g of (10*S*)-HOME reacted with 20 mL of BSA in presence of 10 ml of THF in a round flask magnetically stirred, 300 rpm, for 10 h. Temperature was set at 40ºC and was kept constant using a J-Kem Scientific temperature controller (St. Louis, MO, USA). At the end of the reaction, THF was removed by evaporation in a rotary evaporator (Bücchi, Postfach, Switzerland), obtaining a dark-yellow oil.

Hydrogenation was performed by combining the dark-yellow oil with 1 g of Pd-C (Sigma-Aldrich, St. Louis, MO, USA) and 75 ml of ethyl acetate into a 100 ml stainless steel pressure reactor (Pressure Product Industries, Warminser, PA, USA). The reactor was charged to 200 psi with hydrogen. A temperature of 40ºC was maintained and the reaction was mixed, 300 rpm, for 5 h until consumption of hydrogen ceased. The reaction mixture was cooled to room temperature and the vented to atmospheric pressure. The product was separated from catalyst by vacuum filtration through Celite and #50 Whatman filter paper. Ethyl acetate was removed with a rotary evaporator.

Reduced (10*S*)-HOME reacted with 1M HCl solution for extracting protecting group, TMS (trimethylsilyl), in the presence of THF as a solvent in a 200 ml round flask magnetically stirred, 300 rpm for 7 h. A temperature of 0ºC was kept constant by means of ice in the outside part of the round flask. THF was evaporated with a rotary evaporator. The excess of BSA was eliminated from the reduced (10*S*)-HOME by

distillation Kugelrohr under vacuum, 30 Pa of absolute pressure, at 100ºC for 6 h. The hydrogenated (10*S*)-HOME synthesis was confirmed by NMR.

3.5.4.3 Enzymatic synthesis

A 15 ml batch reactor magnetically stirred, 500 rpm, was used to synthesize enzymatically estolides from saturated (10*S*)-HOME. A temperature of 80ºC was kept constant using a J-Kem Scientific temperature controller (St. Louis, MO, USA). 2 g of saturated (10*S*)-HOME reacted with 0.24 g of Novozym 435 during 168 h. Chemical reaction was carried out under vacuum, 1.6 kPa of absolute pressure. Reaction yield was calculated using Equation 27.

3.5.4.4 Chemical synthesis

Reaction was carried out in a 15 ml batch reactor magnetically stirred, 500 rpm. A J-Kem Scientific temperature controller (St. Louis, MO, USA) was used to maintain the temperature reaction at 80ºC. 2 g of saturated (10*S*)-HOME reacted during 168 h. Vacuum, 1.6 kPa of absolute pressure, was applied during the entire reaction. Yield was determinated with Equation 27.

3.6 Ethyl esters production

3.6.1 Ethyl esters production from (10*S*)-HOME and (7*S*,10*S*)-DiHOME in chloroform

3.6.1.1 Measurement of the reaction yield

Reaction yield was determinated as stated in section 3.5.2.1, Equation 26.

3.6.1.2 Effect of the enzyme concentration

To obtain the optimal amount of enzyme required for the esterification, 0.1 to 0.5 g of Novozym 435 were assayed with 0.5 g of (10*S*)-HOME or 0.5 g of (7*S*,10*S*)-DiHOME in 19.6 ml of trichloromethane and 0.4 ml of ethanol (EtOH). The reactions were performed in 100 ml Erlenmeyer flasks for 12 h at 50ºC. A rotator evaporator system was used to achieve an efficient degree of contact between the enzyme and substrates, and for maintaining the required temperature. All the reactions were carried out at atmospheric pressure. The reaction extension was calculated with Equation 25, as stated above. A control without enzyme was also tested to confirm that this reaction did not occur spontaneously.

3.6.1.3 Effect of substrate/enzyme ratio

To study the esterification with different amounts of (10*S*)-HOME or (7*S*,10*S*)-DiHOME (0.1-0.3 g), 0.1 g of Novozym 435 was used. Enzymatic reactions were

conducted in the same conditions as described in section 3.6.1.2, including a control without enzyme. The reaction yield was calculated using Equation 26.

3.6.1.4 Reusability of the enzyme

Reusability of the biocatalyst was assessed with 0.15 g of (10*S*)-HOME and 0.1 g of enzyme or 0.1 g of (7*S*,10*S*)-DiHOME with 0.1 g of Novozym 435 in 19.6 ml of trichloromethane and 0.4 ml of EtOH. Reaction conditions were the same as described in section 3.6.1.2. After each cycle, the enzyme was removed from the reaction medium by filtration and rinsed with trichloromethane several times. Finally, the solvent was evaporated under a stream of air at room temperature. The product was analysed and the stability of the enzyme determined using Equation 26.

3.6.2 Ethyl esters production from (10*S*)-HOME and (7*S*,10*S*)-DiHOME in a solvent-free media

3.6.2.1 Measurement of the reaction yield

Reaction yield was calculated as stated in section 3.5.3.1, Equation 27.

3.6.2.2 Effect of *trans*-hydroxy-fatty acid/ethanol ratio

Esterification reactions took place in a 15 ml batch reactor magnetically stirred, 200 rpm. Reaction medium temperature, 50ºC, was kept constant using a J-Kem Scientific temperature controller (St. Louis, MO, USA). Different molar ratios of pure EtOH and one mol of each HFA were tested, separately; 1 g of (10*S*)-HOME or (7*S*,10*S*)-DiHOME), with 0.12 g of Novozym 435 during 24 h. All the reactions were carried out at atmospheric pressure. The extent of product formation for the reaction was calculated using Equation 27.

3.6.2.3 Effect of the enzyme concentration

Different quantities of Novozym 435, 0.001 to 0.18 g, were assayed in order to obtain the optimal enzyme amount in the esterification reactions with a molar ratio of each HFA to EtOH of 1:3. Esterifications were carried out under the same conditions as stated in section 3.6.2.2. The reaction yield was calculated with Equation 27. All the reactions were carried out at atmospheric pressure. A control without enzyme was assayed in order to confirm that this reaction does not occur spontaneously.

3.6.2.4 Reusability of the enzyme

Reusability of the biocatalyst was carried out using the optimal conditions found in the previous set of experiments: a molar ratio of HFA to EtOH of 1:3 and 0.06 g of Novozym 435 when (10*S*)-HOME was used as co-substrate and 0.10 g with (7*S*,10*S*)-DiHOME. Reaction conditions were the same as described in section 3.6.2.2. After

each cycle, the enzyme was removed from the reaction medium by filtration and rinsed with *n*-hexane several times. In the set of experiments with (7*S*,10*S*)-DiHOME, after the fifth cycle the enzyme was rinsed with pure EtOH. Finally, the solvent was evaporated under a stream of air at room temperature until the enzyme reached a stable weight. Product was analyzed and the stability of the enzyme was determined based on reaction yield, Equation 27.

3.7 Structural determination techniques

3.7.1 Fourier transform infrared spectroscopy

Infrared spectra were obtained using a Nicolet iZ10 FT-IR module with a smart endurance single bounce diamond ATR cell. Spectra over the 4000-650 cm^{-1} range were obtained by the co-addition of 32 scans with a resolution of 4 cm^{-1}. Spectral manipulations, such as baseline adjustment, smoothing and normalisation, were performed with the OMNIC software package (Thermo Scientific, Karlsruhe, Germany).

3.7.2 Nuclear magnetic resonance

Two different nuclear magnetic resonance (NMR) spectrometers were used in this work:

- A Varian NMSSytems 400 MHz spectrometer. ^{1}H and ^{13}C NMR experiments were recorded at 25ºC with a direct detection probe ASW. Fifty milligrams of each sample were dissolved in 0.7 ml of 99.8% $CDCl_3$. Chemical shifts are expressed in ppm using tetramethylsilane as the internal standard for ^{1}H, while $CDCl_3$ was used as the internal standard in the ^{13}C experiments. Thirty-two scans were used in the ^{1}H experiments and 2000 scans in the ^{13}C experiments. ^{1}H-^{1}H gradient correlated spectroscopic (gCOSY) and ^{1}H-^{13}C gradient heteronuclear single quantum coherence spectroscopic (gHSQC) measurements were also performed in the same conditions.
- A Bruker (Karlsruhe, Germany) Avance 500 spectrometer. ^{1}H and ^{13}C NMR experiments were recorded using a 5 mm BBI probe with an absolute frequency of 500.11 MHz for ^{1}H and 125.76 MHz for ^{13}C. COSY (correlation spectroscopy), HSQC (heteronuclear single quantum correlation), and HMBC (heteronuclear multiple bond correlation) two-dimensional spectra were also collected. Fifty milligrams of each sample were dissolved in 5 ml of 99.8 % $CDCl_3$ (Cambridge Isotope Laboratories Inc. Andover, MA, USA). Chemical shifts are expressed in ppm using the same organic solvent as internal standard. 16 scans were used in ^{1}H experiments, whereas 1024 scans were used in ^{13}C experiments.

3.7.3 MALDI-time-of-flight mass spectrometry

MALDI-time of flight mass spectrometry (TOF MS) experiments were performed on a 4800 Plus MALDI TOF/TOF Analyzer (ABSciex — 2010, USA). Samples were recorded in MS Reflector mode selecting positive ion detection. Desorption and ionization were achieved using a Nd-YAG laser (355 nm, 3-7 ns pulse, 200 Hz). Data were registered using 4000 Series Explorer software (ABSciex — 2010, USA). A 2,5-dihydroxybenzoic acid matrix was neutralized with lithium hydroxide (Sigma-Aldrich, St. Louis, MO, USA) as Cvacka and co-workers established [395]. Lithium salt matrix, 10 $mg \cdot ml^{-1}$, was dissolved in a mixture of acetone:trichloromethane (2:1 v:v). 1 μl of the matrix solution was spotted on the target plate until complete evaporation of the organic solvent, afterwards, 1μl of the samples diluted in chloroform, 2.5 $mg \cdot ml^{-1}$, was deposited over the matrix spot and allowed to dry before analysis.

In subsequent analyses with DHB matrix, it was saturated in 1 ml of acetonitrile by sonification. 1 μl of the sample, 2.5 $mg \cdot ml^{-1}$ of chloroform, was mixed with the same volume of the saturated acetonitrile and 1 μl of the final blend was spotted on the target plate until complete evaporation.

3.7.4 Liquid chromatography coupled to mass spectrometry

The chromatographic separation was carried out in a PerkinElmer (USA) Series 200 liquid chromatographer coupled to a PE SCIEX API 150 EX single-quadrupole mass spectrometer (Applied Biosystems, USA). Column used was a Tracer Kromasil 100 C8 column (250 mm x 46 mm, 5 μm) (Teknokroma, Spain). Separation was achieved with a gradient elution using: A: Acetonitrile (0.1 % v/v acetic acid); B: Acetone (0.1 % v/v acetic acid) at a flow rate of 0.5 $ml \cdot min^{-1}$. Gradient (time, % B): (0,35); (25,100); (30,100); (35,35); (40,35). All reported data were acquired with an APCI ionization source in negative mode with the following parameters: vapouriser temperature of 400 ºC, nebuliser current 3 mA, declustering potencial -25 V, focusing potencial -110 V, entrance potencial -10 V and nitrogen as nebuliser and curtain gas with 10 and 12, arbitrary units. The scan data were obtained by scanning from *m/z* 100-2000 amu. In the analysis of estolides from ricinoleic acid, selected ion monitoring (SIM) technique was also used in order to detect high molecular mass olygomers with a better intensity signal. Ions selected were those, which correspond with the different possible olygomers synthesised. All data were registered using Analyst Software v.1.4.2 (Applied Biosystems, USA).

3.7.5 Electrospray ionization mass spectrometry

Mass spectrometry was performed using an Agilent LC/MSD TOF instrument equipped with a dual-nebuliser electrospray ionization source (ESI). Analyses were carried out in the positive ion mode. Samples were dissolved in a mixture of H_2O:CH_3CN (1:1 *v/v*) and infused into the electrospray source via an HPLC Agilent 1100 pump at a flow rate of 200 $\mu l \cdot min^{-1}$. Nitrogen was used as the nebulising gas (15 psi) and drying gas (7.0 $l \cdot min^{-1}$, 325ºC). The capillary and fragmentor voltages were set to 4000 V and 215 V, respectively. Mass range (*m/z*) was scanned from 50 to 1100 Da. The second nebuliser and calibrant delivery system were used to continuously introduce reference compounds for the mass correction using ions with *m/z* 121.0509 (Purine) and 922.0098 (HP-0921).

3.8 Physicochemical techniques

3.8.1 Viscosity determination

A Haake Mars Modular Advanced Rheometer System (Thermo Scientific, Karlsruhe, Germany) was used to determine dynamic or absolute viscosity (η'). Rheometer was connected to a computer for controlling it through a software packge, Haake RheoWin Job Manager (v 4.30.0023; Thermo Scientific, Karlsruhe, Germany). The sample was heated at desired temperature by means of a Haake C25 circulating bath with a Haake F6 controller (Thermo Scientific, Karlsruhe, Germany). The sensor used in those experiments was a 35 mm plate and cone with an angle of 1º with a shaft length of 77 mm (C35/1º Ti L; Thermo Scientific, Karlsruhe, Germany). The lower plate was P35 Ti L (Thermo Scientific, Karlsruhe, Germany). Both are plug and play accessories and were made of titanium. The plate-cone sensor had an inertia moment (I) of $2.93 \cdot 10^{-6}$ $kg \cdot m^2$ and a constant shear stress factor (A) of $8.65 \cdot 10^4$ $Pa \cdot N^{-1} \cdot m^{-1}$; furthermore, the shear rate factor (M) was 50.60 $rad \cdot s^{-1}$. Sensor was calibrated with a viscosity standard (Brookfield, Middleboro, Ma, USA) with a viscosity of 5040 mPa·s at 25ºC.

Dynamic viscosity was measured over four different shear rates and at three different temperatures, when was possible, 20, 40 and 60ºC. Data were visualized with the computer program and were recorded to calculate pre-exponential factor (A) and activation energy (E_a) of the Arrhenius-type relationship. This mathematical expression permits estimate viscosity as a function of temperature, Equation 28.

$$\eta' = A \cdot \exp\left(-\frac{E_a}{R \cdot T}\right) \tag{28}$$

Previous equation can be linearized as Equation 29:

$$\ln(\eta') = \ln(A) - \frac{E_a}{R \cdot T} \quad (29)$$

Finally, dynamic viscosity values at 40ºC were converted to kinematic viscosity through of density, section 3.8.3, with Equation 30, for comparing obtained values with those published in the literature.

$$\upsilon = \frac{\eta'}{\rho} \quad (30)$$

3.8.2 Density determination

Density (ρ) was determinated introducing 10 μl of a substance in a Kimble® microcapillary pipette (Sigma-Aldrich, St. Louis, MO, USA). Microcapillary pipettes were weighted before and after introducing the sample in an Adventure Pro Av114 analytical scale (Ohaus Corp., Pine Brook, NJ, USA).

3.8.3 Differential scanning calorimetry

Differential scanning calorimetry (DSC) experiments were performance in an automatic Mettler Toledo DSC-30 calorimeter (Greinfesse, Switzerland). The data processing software was STAR^e System (Mettler Toledo, Greinfesse, Switzerland). An 8-22 mg sample was weighted in an aluminium pan with a small pinhole in the lid. Thermograms were run at a heating rate of 10.0ºC/min from -100 to 500ºC under a nitrogen purge of 50 ml·min^{-1}. Peaks were identified by peak temperature.

3.8.4 Thermal gravimetric analysis

A Mettler Toledo TGA-SDTA 851e/SF/1100 thermogravimetric analyser was used to run the samples, 18-38 mg, which were disposed in open alumina crucibles. The data processing software was STAR^e System (Mettler Toledo, Greinfesse, Switzerland). Thermograms were run at a heating rate of 10.0ºC/min from 30 to 600ºC under a nitrogen purge of 50 ml·min^{-1}. Mass loss (%) was calculated from TG curves, based on the mass of the original sample.

4. Results and Discussion

4.1 Design of a non-dispersive aeration system

Many industrial processes bioreactors, where the air is introduced in the culture media, are used to growth microorganisms for producing antibiotics, vaccines, steroids, vitamins, proteins, certain sugars and organic acids [396]. In some of these processes foam is normally produced during exponential growth phase. Foam is located at the air-liquid interphase forming a layer or film. Depending on the origin of the foam, it results very unbreakable. Foam can even ruin batch. A ruined batch represents a considerable amount of money and time misspent. A variety of methods are available to combat foam formation: chemical, like silicone based formulations; and physic agents, like mechanical, acoustic and ultrasonic methods [397].

In previous works for producing *trans*-hydroxy-fatty acids (*trans*-HFA) from oleic acid (OA) in bioreactor by *P. aeruginosa* 42A2, an annular metallic sparger was used, producing large quantities of foam [398]. This type of foam is very stable and the mechanical foam-breaker supplied with the bioreaction system resulted useless. Moreover, the addition of some chemical antifoamers inhibited the bacterial growth. Later a ceramic diffuser with a porous diameter of 800 nm was used as sparger [399]. Foam formation was considerably reduced using this microsparger, but was still an uncontrollable bioreaction. Restraining foam formation in a bioreactor is a crucial point for two reasons: it allows the control of the fermentation itself and equipment can be optimized and it therefore minimises production costs [400].

To overcome this problem, a new aeration system was developed to avoid bubble aeration: an adapted wetted-wall column (WWC) based on the Higbie Penetration theory [401]. Higbie Penetration theory is based on the mass transfer of a gas to a liquid phase which is in contact to a gaseous phase. Mass transfer is produced without chemical reaction and takes place into the gas-liquid interphase.

This is the first time that a WWC was used as a non-dispersative aireation method and some considerations and hypothesis had to be assumed to calculate the time of exposure (t_e) of the liquid phase over the surface (S) of the column. The working temperature was 30ºC (303.15 K); the surface tension of the media was 0.030 $N \cdot m^{-1}$ due to the presence of (7*S*,10*S*)-DiHOME in the culture media [402]; x_2, the oxygen molar fraction of the stream that enter in the WWC (section 3.2.2), was supposed to have, as minimum, a 20% of the O_2 concentration in the equilibrium, x_{eq}, at the working temperature; the O_2 concentration in the equilibrium at 30ºC is 7.6 $mg_{O2} \cdot l^{-1}$ [403]; the O_2 requirement data of *P. aeruginosa* 42A2 was considered $1.75 \cdot 10^{-5}$ $mol_{O2} \cdot s^{-1}$ [404]; and, the maximum molar flow (L) of the stream that enters in the WWC was 0.463 $mol \cdot s^{-1}$ (0.5 $l \cdot min^{-1}$), assuming that the stream is a dilute aqueous solution.

With all these assumptions, an S value of 16.4 cm^2 for the contact surface of the WWC was obtained, Equation 6. Considering that the outer diameter of the WWC was of 0.15 cm, a 12 cm height column was obtained with a t_e value of 0.159 s, Equations 1 and 7, with a liquid-phase mass-transfer coefficient for O_2 in the culture media ($(k_L)_M$) value of 21.5 $cm \cdot h^{-1}$ with equation 3. This 12 cm height column was calculated by the mathematical proposed, but in order to minimize the possible deviations and to ensure the proper oxygenation of the media, an 80 cm height column was used. According to this value, a $(k_L)_M$ value of 21.5 $cm \cdot h^{-1}$ is slightly lower than those found in the literature by DeMoyer [405], 22-266 $cm \cdot h^{-1}$, for bubble columns and tanks.

The 80 cm height column represents a WWC surface of 39.8 cm^2 with a $(k_L)_M$ of 8.32 $cm \cdot h^{-1}$ and t_e of 1.06 s. This increment augmented t_e and reduced $(k_L)_M$ compared with the previous situation, because both situations were calculated with the same molar flow (L). A larger L should be achieved to obtain anterior values of $(k_L)_M$ and t_e.

4.1.1 $k_L a$ determination

Volumetric mass transfer coefficient ($k_L a$) determination was performanced according to the static gassing out method [406] in water due to its simplicity and reproducibility, Equation 10. Different water flows and stirring speeds were tested to find out the best situation according to the initial reaction conditions: air flow of 2.5 $l \cdot min^{-1}$, pH 7 and temperature 30ºC. Results are presented in Figure 4.1.

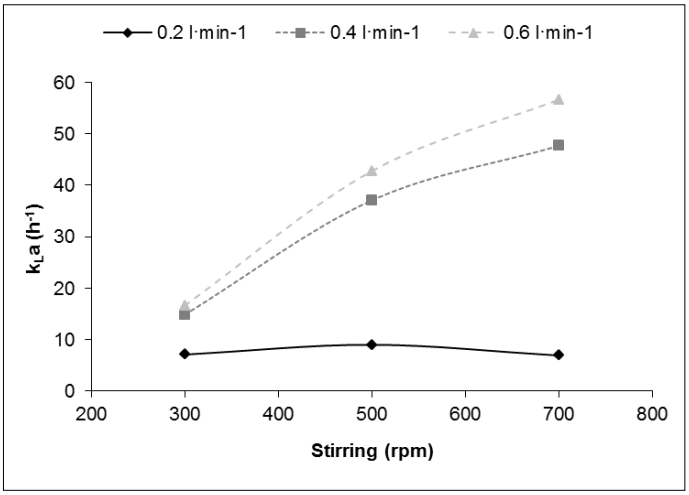

Figure 4.1. $k_L a$ tendency over stirring speed and volumetric flow over wetted wall column. In all experiments air flow was 2.5 $l \cdot min^{-1}$, 30ºC and pH 7.

As can be seen, $k_L a$ has a proportional behaviour with stirring speed and the volumetric water flow that circulated through the WWC. It seems that stirring has no influence on $k_L a$ when water flow was 0.2 $l \cdot min^{-1}$, from 7.1 to 6.9 h^{-1}. However, a big difference can be observed when water flow was 0.4 or 0.6 $l \cdot min^{-1}$; even, close values were obtained between these two situations. Thus, an intermediate solution was chosen: initial volumetric water flow was set 0.5 $l \cdot min^{-1}$, which is the middle value that

peristaltic can provide (0.01-1 l·min^{-1}) and stirring speed of 500 rpm, from previous works is the minimal value for obtaining a good degree of mixing [399]. Hence, an interpolation was needed to work out the k_La value in this situation, 39.9 h^{-1}: water flow 0.5 l·min^{-1} and stirring speed 500 rpm.

A k_La value of 39.9 h^{-1} is lower when is compared to previous findings: 200 h^{-1}, in the production of (10*S*)-HOME by the same bacterial strain in bioreactor aerated with a round metallic sparger [398] or 217 h^{-1} when a 800 nm porus diameter ceramic sparger was used [399] under similar reaction conditions. Such low value could be explained because of the type absorption produced in the WWC. Despite this low value, foaming was completely reduced and a homogeneous culture media was achieved and HFA production rate were increased, as could be observed later. This is the first step in the optimization process of *trans*-HFA in bioreactor.

4.2 Biotransformation kinetics

P. aeruginosa 42A2 produces one hydroperoxide- and two hydroxy-fatty acids when OA used as carbon source in a mineral medium [407, 408]. HFA are interested compounds because of its use in a wide range of industrial products as resins, waxes, nylons, plastics, lubricants, cosmetics, and additives in coatings and paintings [409]. In order to produce these compounds in optimal conditions some processing parameters need to be monitored and controlled [410].

Kinetics of OA conversion by *P. aeruginosa* 42A2 with different initial concentrations of OA, $(C_{OA})_0$, of 10, 15 and 20 g·l^{-1} are illustrated in Figure 4.2 A-F. OA was used as the carbon source for bacterial growth. Bacterial growth, expressed as biomass (X), increased until depletion of nitrates with the exception of 10 g·l^{-1} situation. At that point, bacterial growth entered into the stationary phase when (10*S*)-HPOME concentration reached a maximum. Furthermore, this maximum in concentration practically matches with the total consumption of OA. Afterwards the concentration of (10*S*)-HOME and (7*S*,10*S*)-DiHOME started on increasing considerably while the one of hydroperodixe dimished. This fact evidence that (10*S*)-HPOME is the substrate for the synthesis of (10*S*)-HOME and (7*S*,10*S*)-DiHOME as secondary metabolites [408] and the assumption that the production of hydroxy-fatty acids is performed in two steps, Equations 11a and 11b.

$$OA + O_2 + NO_3^- \longrightarrow X + (10S) - HPOME + CO_2 \quad (11a)$$

$$(10S) - HPOME + O_2 \xrightarrow{X=cte} (10S) - HOME + (7S,10S) - DiHOME + CO_2 \quad (11b)$$

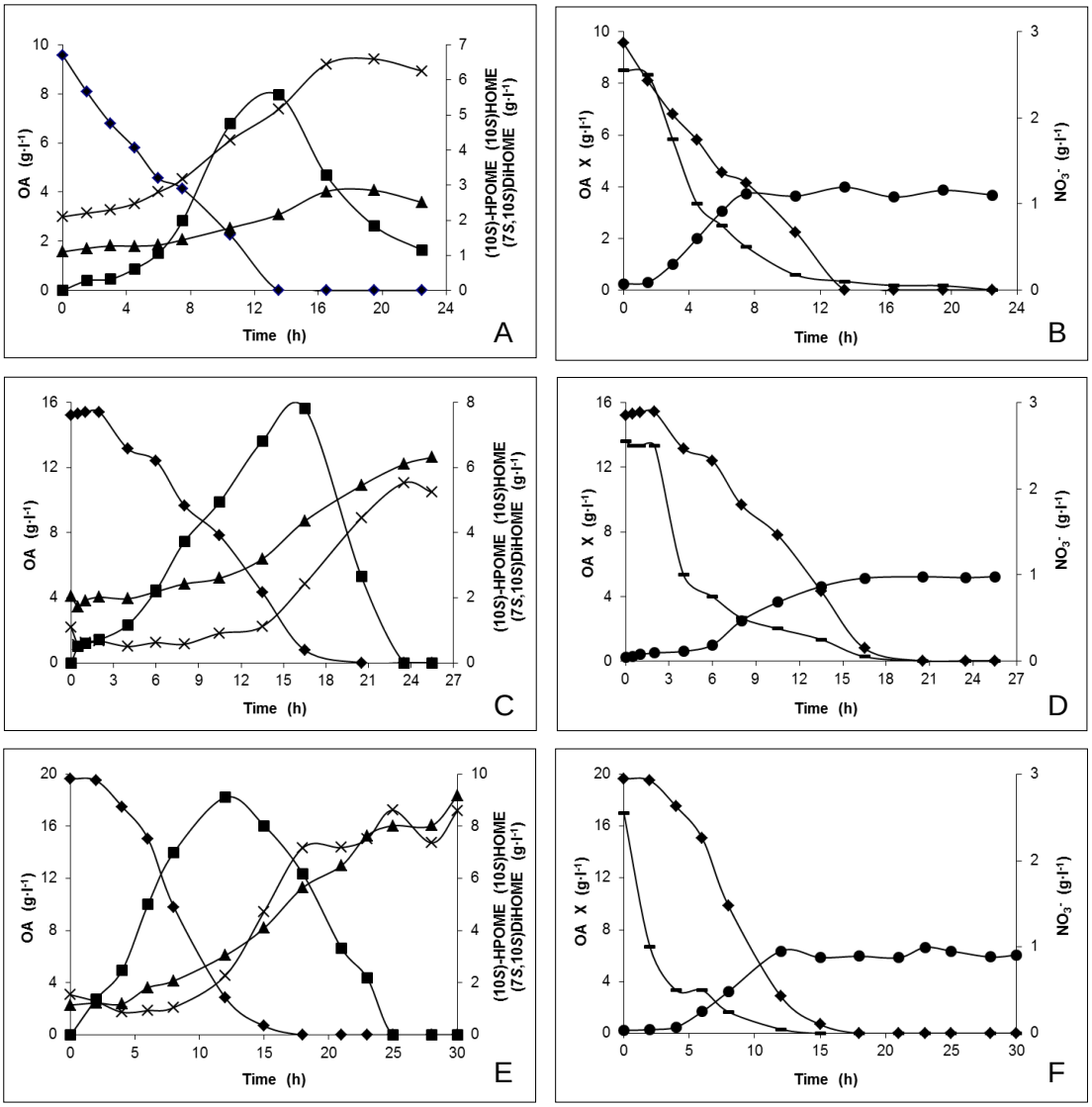

Figure 4.2. Kinetics of OA oxidation by *P. aeruginosa* 42A2 in bioreactor using a WWC as aerator system. **A**, **B**: OA initicial concentration 10 g·l^{-1}. **C**, **D**: OA initicial concentration 15 g·l^{-1}. **E**, **F**: OA initicial concentration 20 g·l^{-1}. **OA**: (♦); **(10*S*)-HPOME**: (■); **(10*S*)-HOME**: (▲); **(7*S*,10*S*)-DiHOME**: (**x**). **NO_3^-** (**–**); **X**: (●). Experimental data are listed in Table A.1.

As can be seen in Figure 4.2 E, a higher production of HFA, around 9 g·l^{-1} of each HFA, was obtained when $(C_{OA})_0$ was 20 g·l^{-1}, despite of observing a longer lag phase. Whereas similar final concentrations of HFA, 6 g·l^{-1}, were reached when $(C_{OA})_0$ was 10 or 15 g·l^{-1}, Figure 4.1 A and C. In all three situations, the biotransformation started with certain concentration of both HFA. As stated before in section 3.2.2, (7*S*,10*S*)-DiHOME is a biosurfactant and it was used for emulsifying initial OA. Initial concentrations of both HFA were taken into account on later calculations.

Few references about production of HFA from OA are in the literature, but less are about the modelling production of them [411]. Product, (10*S*)-HPOME, (10*S*)-HOME and (7*S*,10*S*)-DiHOME, volumetric productivities (P_V) for each batch was calculated by Equation 17, in a g and C-mol basis, Table 4.1.

Table 4.1. Product volumetric productivity for each batch.

$(C_{OA})_0$	(10*S*)-HPOME		(10*S*)-HOME		(7*S*,10*S*)-DiHOME	
$g \cdot l^{-1}$	$g \cdot l^{-1} \cdot h^{-1}$	$C\text{-}mol \cdot l^{-1} \cdot h^{-1}$	$g \cdot l^{-1} \cdot h^{-1}$	$C\text{-}mol \cdot l^{-1} \cdot h^{-1}$	$g \cdot l^{-1} \cdot h^{-1}$	$C\text{-}mol \cdot l^{-1} \cdot h^{-1}$
10	0.413	0.0236	0.146	0.0088	0.338	0.0194
15	0.474	0.0271	0.205	0.0124	0.248	0.0142
20	0.759	0.0435	0.287	0.0173	0.306	0.0175

Experimental data are listed in Table A.1.

As can be seen, (10*S*)-HPOME P_V is proportional to the initial OA concentration, being the last batch which had the highest P_V, 0.749 $g \cdot l^{-1} \cdot h^{-1}$ or 0.0435 $C\text{-}mol \cdot l^{-1} \cdot h^{-1}$. (10*S*)-HOME P_V follows the same pattern as the hydroperoxyl compound due to (10*S*)-HOME production rate, Equation 23, is proportional to the hydroperoxyl concentration according to the mathematical proposed herein. On the other hand, (7*S*,10*S*)-DiHOME P_V does not follow a clear tendency because of the dihydroxyl compound production is caused by an enzymatic system [408]. It seems that (7*S*,10*S*)-DiHOME P_V slightly decreases from 10 to 20 $g \cdot l^{-1}$.

Kuo and Lanser were the first on succeeding to produce (7*S*,10*S*)-DiHOME from OA in bioreactor; although, no details were published of the new designed aerator system. They reached a (7*S*,10*S*)-DiHOME final concentration of 8.9 $g \cdot l^{-1}$ after 96 hours, a P_V of 0.093 $g \cdot l^{-1} \cdot h^{-1}$, with a new aeration system which maintained a dissolved O_2 concentration between 40-60% of the saturation, but they did not avoid or reduce foam formation during the process. However, in the present work, a similar (7*S*,10*S*)-DiHOME final concentration, 9.6 $g \cdot l^{-1}$, was reached after 30 hours avoiding foam formation using a WWC as aeration system. The lesser foam is produced, a better homogeneity of the culture medium is achieved and higher are the production rates.

4.3 Yield coefficients and kinetic constants determination and modelling hydroxy-fatty acid production

There is no work in the literature focused on modelling the bioconversion of OA into HFA. Main efforts are focus on modelling the growth of *Pseudomonas* strains for degrade of benzene compounds [400, 409]; but no mass balances are considered when yield coefficients were calculated.

The different yield coefficients were calculated using Equations 13-16 from the experimental sets of data. They were used as starting point for the simulation with various kinetic models. The initial yield coefficients expressed on C-mol basis are presented in Table 4.2. Yields do not remain constant over the OA initial concentration range studied due to cellular cycle is different in each situation. Thus, modelling of the OA oxidation will be applied at each OA initial concentration.

Table 4.2. Yield coefficients (C-mol basis) obtained from the experimental sets of data and after simulation.

	Experimental data			After simulation		
	C_{OA0} (g·l^{-1})			C_{OA0} (g·l^{-1})		
	10	15	20	10	15	20
Semireaction 1						
$Y_{X/OA}$	0.275	0.198	0.177	0.237	0.199	0.172
$Y_{(10S)\text{-HPOME/OA}}$	0.596	0.423	0.557	0.560	0.411	0.495
$Y_{X/(10S)\text{-HPOME}}$*	0.461	0.445	0.317	0.423	0.485	0.347
$Y_{O2/OA}$	0.187	0.540	0.391	0.295	0.556	0.483
$Y_{CO2/OA}$	0.129	0.389	0.267	0.203	0.391	0.334
$Y_{NO3/OA}$	0.059	0.042	0.038	0.051	0.043	0.037
Semireaction 2						
$Y_{(10S)\text{-HOME/(10S)-HPOME}}$	0.224	0.416	0.243	0.224	0.416	0.243
$Y_{(7S10S)\text{-DiHOME/(10S)-HPOME}}$†	0.434	0.239	0.479	0.450	0.233	0.419
$Y_{O2/(10S)\text{-HPOME}}$	0.459	0.458	0.373	0.437	0.466	0.454
$Y_{CO2/(10S)\text{-HPOME}}$	0.342	0.345	0.279	0.326	0.351	0.339

*Calculated from $Y_{X/OA}$ and $Y_{(10S)\text{-HPOME/OA}}$; †Not fitted with the simulation software.

Seven different kinetic mathematical expressions were found in the literature, Table 3.1. Aiba-Edward, Haldane and Yano-Koga models were chosen to evaluate the possible inhibitory effect of substrates over the bacteria. Other four models, Monod, Tessier, Contois and Mosser, were selected for comparing different mathematical expressions that express bacterial growth.

Coefficient yields obtained from experimental sets of data in addition to the seven kinetic expressions were introduced in the mathematical model proposed, Equation 20-21 and 23-25. Experimental sets of data were used as template for first step in the simulation process of the kinetic constants (μ_{max}, K_S, K_i and k) by AQUASIM® software. Yield coefficients and experimental data were expressed on C-mol basis to obtain consistent and comparable results for the three OA initial concentrations [412].

Table 4.3 shows the results of the simulations. As can be seen, inhibitory constant (K_i) presents large values compared with saturation constant (K_S) in both semireactions and three situations. It evidences that OA and (10*S*)-HPOME have no inhibitory effect over *P. aeruginosa* 42A2 in the first and second semireaction (Equation 11a and 11b), respectively. Within non-inhibitory kinetic models, Contois model presents kinetic constants values which are discordant with Monod, Tessier and Moser models, despite having the lowest χ^2, the best agreement with experimental data. Monod model was the chosen due to its simplicity and agrees with simply enzymatic reactions that occur inside a bacterial cell, even having higher χ^2 than Contois, Tessier or Moser models for modelling the oxidation of OA by *P. aeruginosa* 42A2 in bioreactor. Monod simulations could be observed in Figure A.1.

Table 4.3. Kinetic constant values resulted from simulation of experimental data with seven kinetic mathematical expressions by AQUASIM®.

10 g·l^{-1}	Semireaction 1				Semireaction 2					$Y_{X/OA}$	$Y_{X/(10S)\text{-}HPOME}$	$Y_{(10S)\text{-}HPOME/(7S,10S)\text{-}DIHOME}$	X^2
	μ_{max} (h^{-1})	K_S (C-mol·l^{-1})	K_i (C-mol·l^{-1})	λ	μ_{max} (h^{-1})	K_S (C-mol·l^{-1})	K_i (C-mol·l^{-1})	λ	k (h^{-1})	(C-mol·C-mol^{-1})	(C-mol·C-mol^{-1})	(C-mol·C-mol^{-1})	
MONOD	1.326	3.000	—	—	0.124	0.005	—	—	0.015	0.237	0.423	2.222	7.76
TESSIER	1.244	3.000	—	—	0.116	0.005	—	—	0.015	0.244	0.423	2.173	7.65
CONTOIS	0.263	4.804*	—	—	1.798	20.374*	—	—	0.016	0.252	0.423	2.234	7.16
MOSER	1.379	3.000	—	1.05	0.118	0.005	—	0.80	0.015	0.244	0.423	2.165	7.73
HALDANE	1.326	3.000	96.9	—	0.123	0.055	13.45	—	0.015	0.240	0.423	2.193	7.75
YANO-KOGA	1.320	2.979	104.1	—	0.123	0.005	136.56	—	0.016	0.240	0.423	2.221	7.76
AIBA-EDWARDS	1.332	3.000	169.0	—	0.129	0.005	22.95	—	0.015	0.241	0.423	2.199	7.79
15 g·l^{-1}													
MONOD	0.234	0.400	—	—	0.097	0.005	—	—	0.042	0.199	0.485	4.295	6.46
TESSIER	0.189	0.444	—	—	0.094	0.018	—	—	0.043	0.198	0.485	4.140	6.50
CONTOIS	0.171	1.738*	—	—	0.093	0.001*	—	—	0.043	0.198	0.485	4.122	6.34
MOSER	0.313	0.713	—	0.91	0.095	0.005	—	0.93	0.043	0.198	0.485	4.119	6.23
HALDANE	0.274	0.587	178.8	—	0.094	0.005	48.32	—	0.043	0.198	0.485	4.092	6.36
YANO-KOGA	0.265	0.548	97.8	—	0.096	0.005	173.74	—	0.043	0.198	0.485	4.134	6.34
AIBA-EDWARDS	0.270	0.565	177.3	—	0.098	0.005	44.6	—	0.043	0.198	0.485	4.110	6.25
20 g·l^{-1}													
MONOD	0.510	1.604	—	—	0.120	0.035	—	—	0.033	0.172	0.347	2.388	7.98
TESSIER	0.308	0.988	—	—	0.110	0.058	—	—	0.033	0.172	0.347	2.388	7.89
CONTOIS	0.229	3.190*	—	—	0.113	0.097*	—	—	0.033	0.172	0.347	2.388	8.07
MOSER	0.780	3.000	—	0.88	0.114	0.005	—	1.76	0.033	0.171	0.347	2.388	7.86
HALDANE	0.518	1.634	142.6	—	0.119	0.032	199.5	—	0.033	0.171	0.347	2.388	7.98
YANO-KOGA	0.494	1.522	132.9	—	0.119	0.031	199.5	—	0.033	0.171	0.347	2.388	7.98
AIBA-EDWARDS	0.521	1.638	138.4	—	0.119	0.033	174.1	—	0.032	0.171	0.347	2.388	7.82

* These values correspond to kinetic constant B on Contois mathematical expression.

Table 4.4. Kinetic constants for Monod model.

	Semireaction 1		Semireaction 2		
$(C_{OA})_0$ ($g \cdot l^{-1}$)	μ_{max} (h^{-1})	K_S (C-mol·l^{-1})	μ_{max} (h^{-1})	K_S (C-mol·l^{-1})	k (h^{-1})
10	1.326	3.000	0.124	0.005	0.015
15	0.234	0.400	0.097	0.005	0.042
20	0.510	1.604	0.120	0.035	0.033

Table 4.4 sum up the kinetic constant values for Monod model over the two semireactions. 15 $g \cdot l^{-1}$ situation presents a divergent values when compared with other two. This fact could be due to the slow bacterial growth over the exponential phase, Figure 4.1 D, when it is compared with other two, Figure 4.1 B and F.

Apart from 15 $g \cdot l^{-1}$ situation, a tendency could be appreciated between kinetic constants and OA initial concentration. It seems that when OA initial concentration is increased, maximum specific growth (μ_{max}) decreases as well as K_S for the first semireaction. Stationary phase was reached in 8 h for the 10 $g \cdot l^{-1}$ batch compared with the 12 h for the 20 $g \cdot l^{-1}$; this event could explain this slightly inhibitory effect produced by OA over the studied OA initial concentration range. In the second semi reaction μ_{max} and K_S have a more stable values because (10*S*)-HPOME consumption to produce (10*S*)-HOME and (7*S*,10*S*)-DiHOME occurred along the stationary phase of the bacterial growth. On the other hand, (10*S*)-HOME first order kinetic constant increases due to the higher (10*S*)-HPOME concentration reached when OA initial concentration was increased, as can be seen from the Figures 4.1 A, C and E. To our knowlegde no enzyme was found to the responsible for the production of (10*S*)-HOME from (10*S*)-HPOME; hence, a spontaneous first order reaction was consider as best option to model this transformation.

$Y_{X/OA}$ (yield coefficient of X on OA), $Y_{X/(10S)\text{-HPOME}}$ (yield coefficient of X on (10*S*)-HPOME) and $Y_{(10S)\text{-HPOME}/(7S,10S)\text{-DiHOME}}$ (yield coefficient of (10*S*)-HPOME on (7*S*,10*S*)-HPOME) were refitted during simulation process due to these three yields are part of the mathematical model. From these three coefficient yields and Equations 14-16 were used to recalculated others presented in the Table 4.2.

In the first semireaction could be observed that $Y_{X/OA}$ diminished when OA initial concentration increased; however, approximately is produced the same amount of (10*S*)-HPOME per unit of OA and the amount of O_2 per unit of OA increased as well as CO_2, respectively.

The reduction on the formation of X, biomass, is compensated by an increment of the production of (10*S*)-HPOME. If yield coefficient of (10*S*)-HPOME on X, $Y_{(10S)\text{-HPOME}/X}$, would be calculated, which the inverse of $Y_{X/(10S)\text{-HPOME}}$, (2.169, 2.247 and 3.155 for 10, 15 and 20 $g \cdot l^{-1}$), it could be known which batch is the most efficient, in other

words, the situation with the highest productive biomass: the 20 $g \cdot l^{-1}$ batch in this study. Moreover, this is the reason because μ_{max} is reduced and the possible certain inhibitory of OA is discarded. This metabolic increment is reflected by the O_2 requirements and the CO_2 production.

In the second semireaction, all coefficients remained practically constant over the studied range because the synthesis of HFA from the hydroperoxide is produced over the stationary phase of the bacterial growth. Similarly, O_2 requirements were the same in the three situations because of it as used the bacterial maintenance. The same reasoning could be applied to CO_2.

After applying mass balances and simulation process to the experimental data, oxidation of OA, 20 $g \cdot l^{-1}$, into HFA is defined as follows in a C-mol basis, as example:

$$OA + 0.483O_2 + 0.037NO_3^- \longrightarrow 0.172X + 0.495(10S) - HPOME + 0.334CO_2$$

$$(10S) - HPOME + 0.454O_2 \xrightarrow{X=cte}$$

$$\xrightarrow{X=cte} 0.243(10S) - HOME + 0.419(7S,10S) - DiHOME + 0.339CO_2$$

$$\mu_1 = 0.510\frac{C_{OA}}{1.604 + C_{OA}} \; ; \; \mu_2 = 0.120\frac{C_{(10S)\text{ - HPOME}}}{0.035 + C_{(10S)\text{ - HPOME}}} \; ; \; k = 0.033h^{-1}$$

4.4 Specific oxygen uptake rate

Specific oxygen uptake rate (sOUR) was calculated to determinate *P. aeruginosa* 42A2 oxygen requirements during oxidation of OA into HFAs. Oxygen uptake rate (OUR) could be defined as the quantity of dissolved oxygen consumed by cells per unit of time and volume. OUR was calculated according to Equation 19.

OUR results are presented in Figure A.2. As can be seen OUR increased during first hours of the biotransformation along the biomass, X [413]. Afterwards, OUR stabilized in a value between 260 and 267 $mg_{O2} \cdot l^{-1} \cdot h^{-1}$, with the exception of 15 $g \cdot l^{-1}$ batch which reach a value of 210 $mg_{O2} \cdot l^{-1} \cdot h^{-1}$, Table 4.5. During stationary phase, an oscillation in the OUR values were recorded. This oscillation was caused by the air enrichment with oxygen due to dissolved oxygen concentration in the culture media reached very low values. Moreover, it could be observed that the oscillation intensity was proportional to the OA initial concentration.

Tabla 4.5. Respirometry values during OA oxidation by *P. aeruginosa* 42A2 at each OA initial concentration.

$(C_{OA})_0$ ($g \cdot l^{-1}$)	OUR_{max} ($mg_{O2} \cdot l^{-1} \cdot h^{-1}$)	X_{st} ($g \cdot l^{-1}$)	$sOUR_{max}$ ($mg_{O2} \cdot g^{-1} \cdot h^{-1}$)
10	267	3.71	72.0
15	210	5.19	40.5
20	260	5.89	44.1

$(C_{OA})_0$: OA initial concentration. **(s)OUR**: (specific) oxygen uptake rate. **X_{st}**: biomass in the stationary phase.

As stated before, there is no reference in the literature about respirometry of *P.aeruginosa* 42A2 in the production of HFA; but different OUR values were found for *Pseudomonas* genus. Kronemberger and co-workers obtained an OUR value of 100 $mg_{O2}·l^{-1}·h^{-1}$ in the production of rhamnolipids, a class of biosurfactant, by *P. aeruginosa* from glycerol [413]. In contrast, higher OUR values were obtained using *P. putida* strains in the biosulfuration of dibenzothiophene, 403 $mg_{O2}·l^{-1}·h^{-1}$ [414], and hydroxylation of toluene, 3200 $mg_{O2}·l^{-1}·h^{-1}$ [415]. It seems that bacterial strains need larger quantities of oxygen to metabolised such toxic substrates than fatty acids or glycerol.

sOUR was calculated with Equation 18 for each OA initial concentration using the X concentration in the stationary phase, X_{st}, Table 4.5. Gomez and collaborators using a *P. putida* strain in the biosulfuration of dibenzothiophene obtained an sOUR value of 806 $mg_{O2}·g^{-1}·h^{-1}$ [414] due to the toxic nature of the substrate; however, Kronemberger and coworkers, in the production of rhamnolipids by *P.aeruginosa* determined a sOUR value of 85 $mg_{O2}·g^{-1}·h^{-1}$ [413] similar to the 72 $mg_{O2}·g^{-1}·h^{-1}$ of *P.aeruginosa* 42A2 in the oxidation of OA.

4.5 Estolide production

Estolides are a class of polyesters based on (hydroxy-) fatty acids mainly found in vegetable oils. Those have being produced in a chemical way since early 1990's, but over last ten years an increasing attention has focused on producing them enzymatically with lipases. Estolides are formed by a secondary ester linkage which is more resistant to hydrolysis than those of triglycerides. Such characteristic property offers superior physical properties than vegetable and mineral oils when estolides are used for lubricant applications [397]. Furthermore, estolides have shown promising properties for their use in cosmetics or coatings [416].

A new family of estolides wants to be produced in two different non-conventional reaction media, apolar organic solvent and solvent-free system, to evaluate their properties and their future possible applications.

4.5.1 Estolide production from (10*S*)-HOME in *n*-hexane

(10*S*)-HOME, 10(*S*)-hydroxy-8(*E*)-octadecenoic acid, is an isomer of ricinoleic acid (RA), 12(*R*)-hydroxy-9(*Z*)-octadecenoic acid, with a *trans* double bond and an *S* hydroxyl moiety. Numerous works have been published for producing estolides from RA with lipases, but none with *trans* substrates. The selection of the proper lipase for that goal, as well as, the organic solvent and reaction conditions will be discussed straightforward.

4.5.1.1 Novozym 435 for (10*S*)-HOME esterification: enzyme amount and substrate/enzyme ratio.

In terms of selectivity to a *cis*/*trans* configuration of the double bond in 9-octadecenoic acid isomers, lipases were classified according to a ratio competitive factor (RCF) [417]. This factor describes the selectivity of one single lipase toward two substrates with the same leaving group and to two different acyl groups. Thus, in this study, Novozym 435 (lipase B of *C. antarctica* immobilized in acrylic resin), with an RCF of 0.7, was chosen because it is slightly more active with *trans*-9-octadecenoic isomers, it exhibits versatility and its optimal temperature of enzyme activity is 40–60ºC. *n*-hexane with a log P of 3.5 [418] was chosen for generating compatible new compounds to be in cosmetic or food applications according to the European Directive 2009/32/CE. Log P is a measurement of solvent polarity. Along with the partition coefficient and the enzyme/solvent interaction, log P may determine biocatalytic activity; this activity is low in solvents at log P < 2, moderate at log P between 2 and 4 and high in a polar solvent with log P > 4 [419].

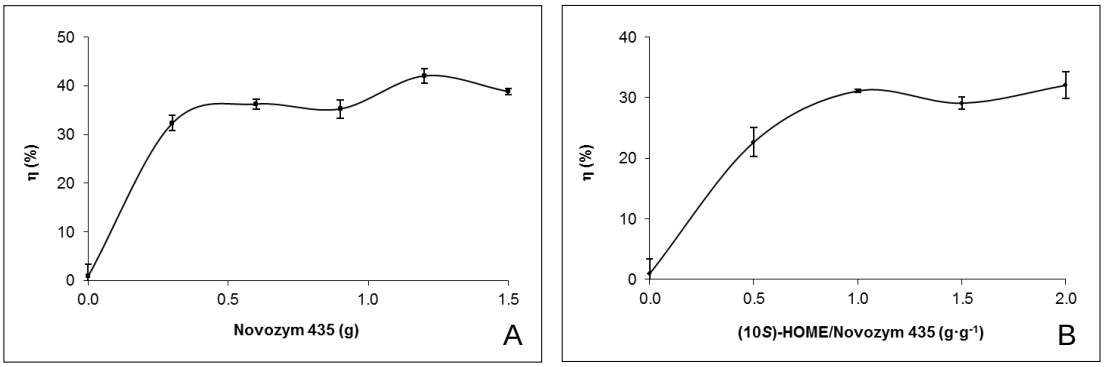

Figure 4.3. Optimization of the enzymatic reaction medium in *n*-hexane. **A**: Yield of the polymerisation with different amounts of enzyme, Novozym 435, in 0.6 g of (10*S*)-HOME at 50ºC during 48 h in *n*-hexane, 20 ml. **B**: Yield of the polymerisation with different amounts of (10*S*)-HOME/Novozym 435 ratio; 0.5 g of Novozym 435 were used in all experiments in 20 ml of *n*-hexane as organic solvent at 50ºC during 48 h. Yield (η (%)) is calculated as percentage of the reduction of AV, Equation 21.

Different amounts of enzyme were tested to establish the optimal amount of biocatalyst for 0.6 g of (10*S*)-HOME. The results are presented in Figure 4.3 A; it could be observed that the reaction yield increased with the amount of enzyme. At values near 0.5 g of enzyme, this yield was 35%, and it increased slightly to 42% at a substrate/enzyme ratio of 1.2 $g \cdot g^{-1}$. Thus, the thermodynamic limit for yield was very similar to this latter value. There are no data in the literature about polymerization with *trans* monomers, although this value is lower than the 58% obtained by Horchani and coworkers when using RA acid to produce estolides in *n*-hexane for 55 h at 55ºC [420]. Bódalo and collaborators obtained a 72% reaction yield when *C. rugosa* was immobilized in Lewatit Monoplus MP64, an anion exchange resin, for 150 h at 40ºC in

a solvent-free system [421]. Various substrate/enzyme ratios were tested to establish the optimal concentration of substrate to be used. As Figure 4.3 B shows, the yield increased up to a ratio of 1, after which the yield remained constant at 30%, indicating that an excess substrate concentration is not effective in enhancing the AV decrease. A similar ratio was found by Langone and co-workers after the conversion of oleic acid/methyl ricinoleate to estolides using Novozym 435 as a biocatalyst in a solvent-free system for 48 h at 80ºC [419].

4.5.1.2 Reusability of the enzyme

The use of enzymes or immobilized enzymes for repeated use may help decrease product cost and make the enzymatic process economically viable. The ability of Novozym 435, to retain its stability during recycling by using fatty acids as substrate was studied by several researchers [419, 422], although it may have drawbacks. Figure 4.4 shows the profile of the polymerization yield during different cycles.

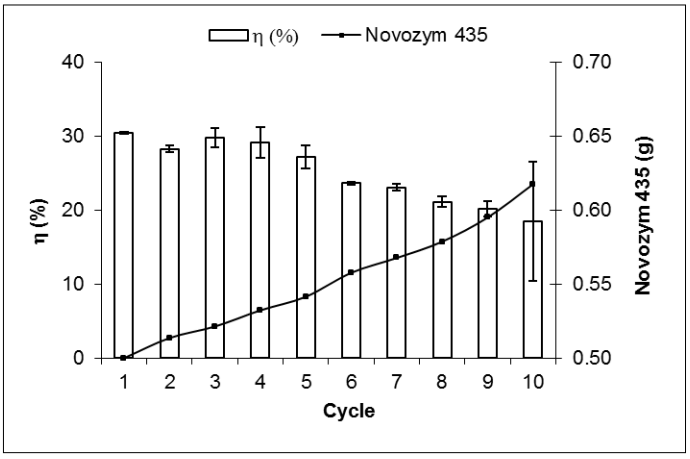

Figure 4.4. Polymerisation yield and enzyme weight at each cycle in *n*-hexane. In all experiments 0.5 g of Novozym 435 and 0.5 g of (10*S*)-HOME were dissolved in 20 ml of *n*-hexane during 48 h at 50ºC. Yield is calculated as percentage of the reduction of AV. Novozym 435: (■); Yield (η (%)): (Bars).

As observed, the synthetic stability of the enzyme decreased throughout the cycles assayed. The yield decreased by 53.3% after ten cycles, from 30.4% to 18.5%, whereas the enzyme weight increased. Although the biocatalyst was rinsed several times with *n*-hexane, a portion of the substrate remained adsorbed on the support due to the poor solubility of the (10*S*)-HOME in *n*-hexane. Langone and co-workers observed a similar reduction in enzyme stability (55%) in the production of estolides from OA and methyl ricinoleate in a solvent-free system when Novozym 435 was used for four batches [419]. In contrast, Radzi and collaborators [422] observed great synthetic stability even after nine cycles (91.9%) during the production of oleyl oleate in *n*-hexane for 1 h, indicating a negligible effect on enzyme stability. This indicates that using an appropriate apolar organic solvent may help maintain enzyme stability and solubilizing the substrate may help so as not to affect enzyme activity.

4.5.1.3 Structural determination of (10*S*)-HOME estolides

A gel-permeation analysis of the polymers has certain difficulties that have been tried to overcome, such as the difficulty of separating different degrees of polymerization properly, especially when the molecular mass of the oligomers analysed does not differ enough. At this juncture, more than one gel permeation column is needed to achieve a good separation, which increases the analysis time and makes this technique tedious and expensive. Alternatively, Bayer and collaborators introduced coordination-ion-spray mass-spectrometry (CIS-MS), in which non-polar compounds or substances with weakly basic or acidic groups are detected, but with poor sensitivity [423]. MALDI time-of-flight (TOF) is ideally suited for polymer analysis because of the simplicity of the mass spectra [424], which show mainly single-charged quasi-molecular ions with little fragmentation when cationization salts are used.

To this end, lipase-formed estolides from (10*S*)-HOME were analysed using RA estolides that were enzymatically produced as a control to confirm the validity of the following structural techniques: MALDI TOF mass spectrometry (MS) and liquid chromatography mass spectrometry.

i. MALDI time-of-flight mass spectrometry

Selecting an appropriate MALDI matrix, cationization salts and sample preparation techniques are critical success factors for obtaining a reliable mass spectrum from which to infer structural information [425]. Previously analysis experiments with RA estolides were carried out using DHB as matrix, showed highly fragmented mass spectra. DHB matrix was unable to stabilize such apolar compounds even with reduced desorption-ionization energy. A 2,5-dihydroxybenzoic acid (DHB) matrix, neutralized with lithium hydroxide (LiOH), was used to analyze RA estolides using the method developed by Cvacka and co-workers in order to analyze wax esters, esters from a fatty acid and a fatty alcohol. Thereafter, the goodness of another matrix will be discus for analysing estolides.

Figure A.3 displays RA estolides, which were enzymatically produced using the method described by Bódalo and coworkers [426], were analysed with lithium DHB salt matrix. A relatively low-intensity peak of *m/z* 305.19 corresponded to the lithium molecular adduct of RA $[RA+^{7}Li]^{+}$ and a peak of *m/z* 287.19, due to the loss of water from the RA lithium adduct, appeared in the left side of the mass spectrum. Three more peaks in the central part of the spectra (585.53, 865.65 and 1145.87 *m/z*) stand out, and these peaks correspond to molecular adducts with lithium of di-estolide, $[2RA-H_2O+^{7}Li]^{+}$; tri-estolide, $[3RA-2H_2O+^{7}Li]^{+}$; and, tetra-estolide, $[4RA-3H_2O+^{7}Li]^{+}$. Finally, a very low-intensity peak, which coincides with the mass of the penta-estolide, [5RA-

$4H_2O+^7Li]^+$, appears in the high-mass field of the spectra, at *m/z* 1426. In contrast to the findings of Hayes and Kelly [427], who used a *trans*-3-indoleacrylic acid matrix with a sodium chloride solution to analyse polyhydric alcohol-poly (ricinoleic acid) species, lithium DHB salt matrix could be used to detect quasi-molecular ions with a molecular weight lower than 500 Da. Other matrices, DHB and α-cyano-4-hydroxycinnamic acid, without cationization salts were tested to detect RA estolides, but highly fragmented mass spectra were obtained, making it tedious and difficult to identify the quasi-molecular ions.

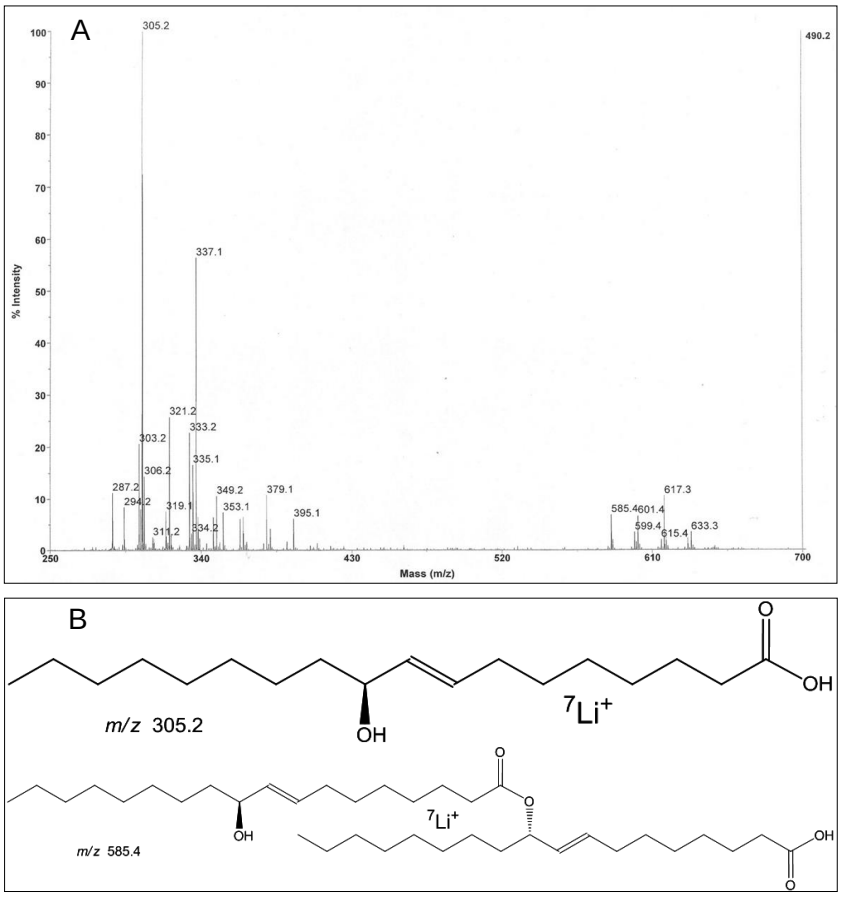

Figure 4.5. MALDI TOF MS analysis of (10*S*)-HOME polymerized in *n*-hexane. **A**: MALDI TOF mass spectrum of (10*S*)-HOME polymerized with Novozym 435 at 50ºC during 48 h; AV of the sample: 127.8 $mg_{KOH} \cdot g_{sample}^{-1}$; DHB matrix was neutralized with LiOH. B: Esctruture of the lithium molecular adducts of the monomer (top) and mono-estolide (bottom).

When a sample of (10*S*)-HOME polymerized with Novozym 435 in *n*-hexane was analysed with an AV of 127.8 $mg_{KOH} \cdot g_{sample}^{-1}$, Figure 4.5 A, two peak groups were found. In the first group, the lithium molecular adduct of the monomer $[M+^7Li]^+$ with *m/z* 305.2 was observed. In the second group, a peak of *m/z* 585.4 was observed, which corresponds to the lithium adduct of the oligomer formed by two units of (10*S*)-HOME $[2M-H_2O+^7Li]^+$. Structures of these compounds could be observed in Figure 4.5 B.

ii. Liquid chromatography coupled to mass spectrometry

Estolides from RA were enzymatically produced using the method described by Bódalo and coworkers [426]. Thus, a sample with an AV of 68 $mg_{KOH} \cdot g_{sample}^{-1}$, were used to confirm the validity of the LC MS technique applied in order to determine the

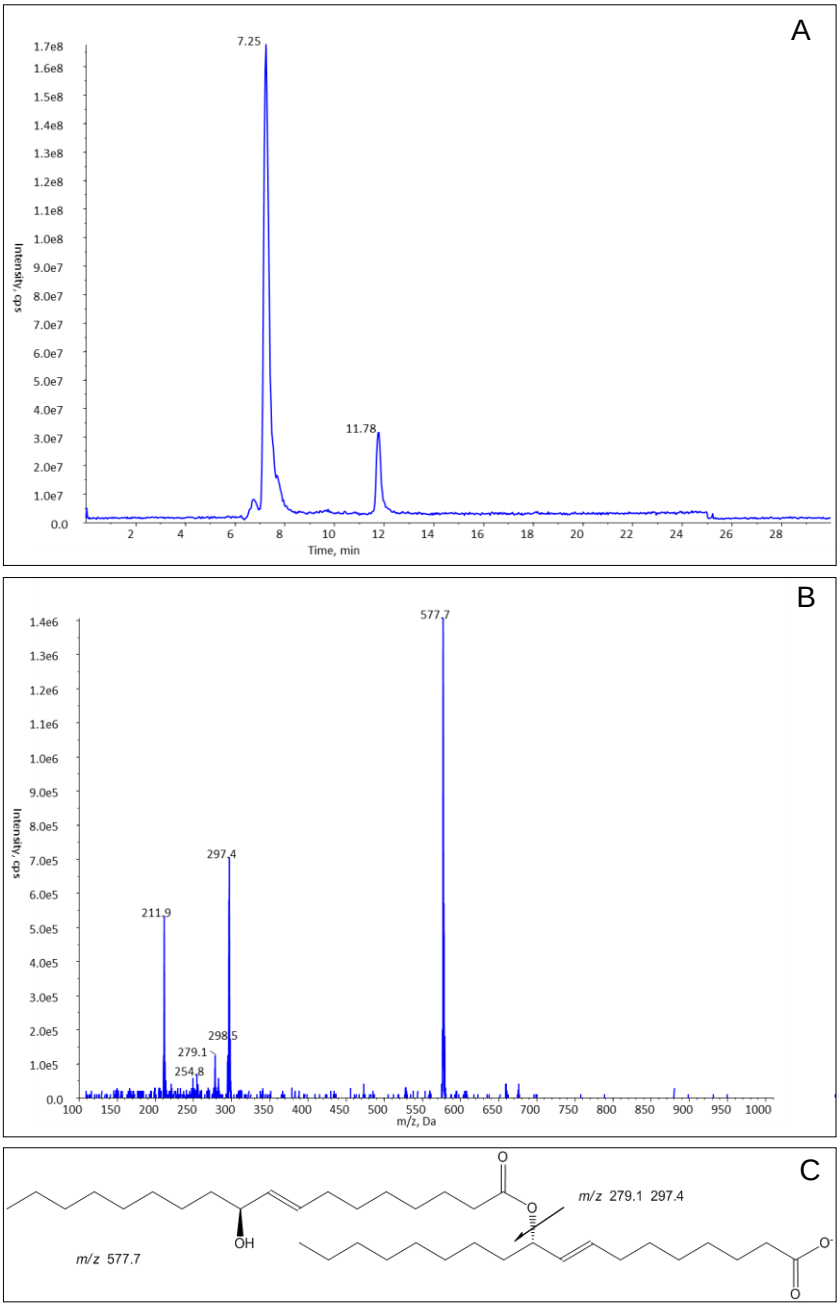

Figure 4.6. LC MS analysis of (10*S*)-HOME polymerized in *n*-hexane. **A**: Full scan chromatogram of (10*S*)-HOME polymerized with Novozym 435 at 50ºC during 48 h; AV of the sample: 127.8 $mg_{KOH} \cdot g_{sample}^{-1}$. **B:** Mass spectrum of the peak of 11.78 min: di-estolide of (10*S*)-HOME. **C**: Structures of the di-estolide of (10*S*)-HOME.

structure of the apolar polymers as polyesters of C18-hydroxyl-fatty acids. The apolar nature and chain length of this kind of compounds forced to use reduced APCI potentials to observe quasi-molecular ions.

In addition, selected ion monitoring (SIM), Figure A.4, was used to detect high molecular mass oligomers with greater intensity. Six ions were selected, *m/z* 298, 578, 858, 1138, 1419 and 1699, that correspond to RA and its oligomers $[2RA-H_2O]^-$, $[3RA-2H_2O]^-$, $[4RA-3H_2O]^-$, $[5RA-4H_2O]^-$ and $[6RA-5H_2O]^-$, respectively. The six-extracted ionsuperimposed chromatogram gives the retention times at which various selected ions are detected. As can be observed, the ion with *m/z* 298 appears at 7.28 min peak corresponds to the unreacted RA; and at the peaks (min) 12.07, 18.70, 24.29, 28.22 and 30.94, an ion with *m/z* 298 appears as a marker of the cleavage of one of the ester bonds in the oligomers synthesized. However, ions with *m/z* 578 (red), 858 (green) and 1138 (grey) are observed at retention times of 12.07, 18.70 and 24.29 min, respectively. Finally, ions with *m/z* 1419 and 1699 (not in the figure) are only detected at retention times of 28.22 and 30.94 min, respectively.

A sample of the same (10*S*)-HOME polymerized in *n*-hexane with Novozym 435 was analyzed, AV of 127.8 $mg_{KOH} \cdot g_{sample}^{-1}$. As seen from Figure 4.6 A, two noticeable peaks at 7.25 and 11.78 min were detected in the full scan chromatogram. The mass spectrum of the 7.25 min peak is shown in Figure A.5, and an ion with *m/z* 297.3 corresponding to the $[M-H]^-$ ion of (10*S*)-HOME can be detected. Likewise, the mass spectrum of the 11.78 min peak shows two main ions, Figure 4.6 B, *m/z* 577.7 and 297.4. The first ion indicates the presence of an oligomer of two units of (10*S*)-HOME, $[2M-H_2O-H]^-$, and the second one represents the cleavage of the ester bond of the same compound, Figure 4.6 C, confirming the results found by MALDI TOF MS.

4.5.1.4 Screening of other lipases for estolides formation

According to the previous results, improvement of the reaction yield must be achieved for *trans*-estolides becoming applicable and atractive. Therefore, diverse lipases and another apolar organic solvent, *iso*-octane, were assayed.

An aliquot of 0.6 g of (10*S*)-HOME was assayed with 100 mg of different lipases in

Table 4.6. Reaction yield, η (%), in the lipase screening with different apolar solvents.

Lipase	RCF	*n*-hexane	*iso*-octane	Specificity
Novozym 435	0.7	11.7	16.0	non-specific
Lipozyme RM IM	1.3	26.4	23.6	*sn*-1,3
Candida rugosa	2.9	16.8	12.5	non-specific
Rhizopus oryzae lipA[a]	3.7-4.1[b]	15.1	13.8	*sn*-1,3
Lipozyme TL IM	–	36.4	32.7	*sn*-1,3

Data are the average of two replicates. **RCF**: ratio competitive factor.
[a] This lipase was kindly donated by Prof. Francisco Valero (Chem. Eng. Dept. UAB, Cerdanyola del Vallès, Spain). [b]From *Rhizopus arrhizus* and *Rhizopus delemar* [417].

both apolar organic solvents, *n*-hexane and *iso*-octane (log P = 4.5 [418]), for 48 h at 50ºC. Table 4.3 summarizes the reaction yields, and the lipases are listed according to their ratio competitive factors (RCF).

It was expected that higher reaction yields would be found with Novozym 435 (11.7%) due to its low RCF (0.7); however, the observed values were lower than those of *C. rugosa* and *R. oryzae* lipases (16.8% and 15.1%, respectively), which both have an RCF higher than 1. On the other hand, Lipozyme RM IM and Lipozyme TL IM had RCF values of 26.4% and 36.4%, respectively. Although the specificity of the assayed lipases was listed with the aim of establishing a correlation with the yield observed, it seems that the non-specific lipases (Novozym 435 and *C. rugosa*) had lower reaction yields than did the *sn*-1,3-specific lipases (Lipozyme RM IM, Lipozyme TL IM and *R. oryzae* lipA) with the exception of lip A from *R. oryzae*. Moreover, it seems that RCF depends on the reaction conditions in which it was defined and they are slightly different from ones presented herein. However, Bódalo found that 1,3-selective lipases are unable to attack secondary alcohols [426]; perhaps, the configuration of the double bond and its relative position to the secondary alcohol had an important effect.

In addition, *iso*-octane, another apolar organic solvent with a higher log P value was tested (4.5). Unlike *n*-hexane, *iso*-octane is not a compatible solvent in food applications; however, estolides produced with this apolar solvent can be used as lubricants in cosmetics, inks or coatings [428]. *Iso*-octane was selected to increase the solubility of the substrate (10*S*)-HOME and, thus, the reaction yield, but no significant differences were observed with *n*-hexane.

It is notable that there is no relationship between the RCF and reaction yield when the enzymatic synthesis proceeds in an aqueous-free solvent. In relation to these results, a future study of the production of estolides with Lipozyme RM IM or Lipozyme TL IM and other reaction media is needed. In such study, there would be an increase in the polymerization conversion to test the physical properties of this new family of *trans*-HFA estolides.

4.5.2 Estolide production from (10*S*)-HOME and (7*S*,10*S*)-DiHOME in a solvent-free media

A few organic solvents can dissolve properly these new *trans*-HFA, but less of those could maintain an appropriate enzymatic stability of lipases. Thus, solvent-free systems for enzymatic synthesis arise as promising alternative to attain higher reaction yields, as well as, making the process environmental friendly and their products are adequate for a wide range of applications, particularly in food industries, where stringent

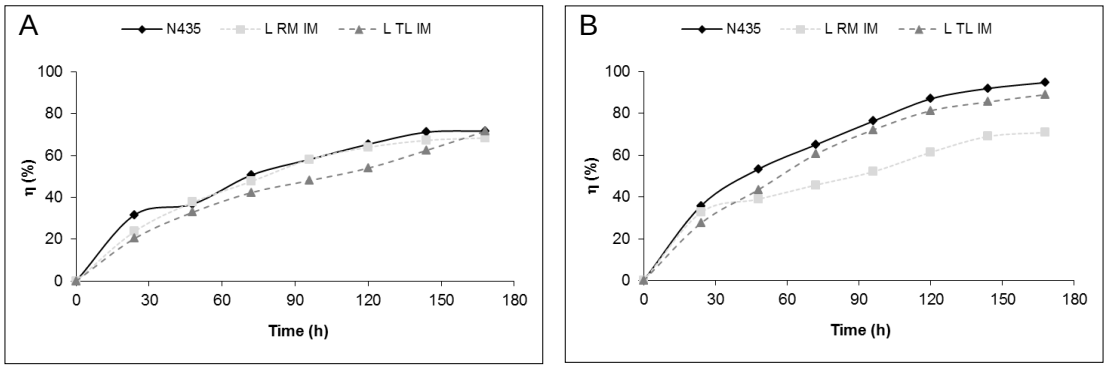

Figure 4.7. Enzymatic estolide production in a solvent-free medium. **A**: Enzymatic estolide production from (10*S*)-HOME with 12% (w/w) of three different lipases and vacuum (total preassure of 1.6 kPa) at 80ºC during 168 h. **B**: Enzymatic estolide production from (7*S*,10*S*)-DiHOME with 12% (*w/w*) of three different lipases and vacuum (total preassure of 1.6 kPa) at 80ºC during 168 h. **N453**: Novozym 435. **L RM IM**: Lipozyme RM IM. **L TL IM**: Lipozyme TL IM.

Table 4.7. Final reaction yield, η (%), in estolide production in a solvent-free medium.

Lipase	RCF	(10*S*)-HOME	(7*S*,10*S*)-DiHOME
Novozym 435	0.7	71.7	94.7
Lipozyme RM IM	1.3	68.4	70.8
Lipozyme TL IM	–	71.6	88.9

regulations exist regarding solvent use [429]. Moreover, the absence of organic solvents in the reaction media avoids compound solubility and enzymatic stability problems.

Two different types of *trans*-estolides are synthesized in a solvent-free system with three lipases Novozym 435, lipase B from *C. antarctica*; Lipozyme RM IM, lipase from *R. miehei*; and Lipozyme TL IM, lipase from *Thermomyces lanuginosus*. Enzymatic reactions were carried with 12% (*w/w*) of lipase, at 80ºC, under vacuum (1.6 kPa absolute preassure) and were magnetically stirred, 500 rpm, following the recommended conditions of Ortega [410].

Time course of the enzymatic reactions were analized by LC for 168 h. Figure 4.7 A shows kinetic reactions for (10*S*)-HOME when was used as substrate. As can be seen, Novozym 435 and Lipozyme RM IM presented comparable tendencies over the entire process; but Lipozyme TL IM with smaller reaction yields, finally reached a similar conversion to the other lipases, Table 4.7. According to the RCF [417], section 4.5.1.4, no clear conclusions could be obtained about selectivity of the lipases tested; however, Novozym 435 presents the highest reaction yield, 71.7%.

Figure 4.7 B shows reaction yields over the polymerization process for the three lipases using (7*S*,10*S*)-DiHOME as substrate. Higher yields were achieved when compared with (10*S*)-HOME ones, Table 4.7. In this polymerization, the highest

reaction yield was for Novozym 435, 94.7%, followed by Lipozyme TL IM, 88.9%, and Lipozyme RM IM, 70.8%.

These results contrast with reaction yields obtained in *n*-hexane in section 4.5.1.2. Greater reaction yields, 71.7%, were obtained in a solvent free-system in the production of estolides from (10*S*)-HOME compared with the previous apolar organic solvent system, 30.0%. Additionally, higher yields were accomplished when (7*S*,10*S*)-DiHOME was the susbtrate, 94.7%, instead of (10*S*)-HOME, 71.7%, maybe caused by the extra hydroxyl group of (7*S*,10*S*)-DiHOME

There are a no works in the literature about estolide production from *trans*-HFA in a solvent-free media due to these kind of substrates are uncommon in nature. But Aguieiras and partners tested these very three enzymes in the production of a mono-estolide from OA and methyl ricinoleate (both with a *cis* unsaturation) being Novozym 435 (6% *w/w*), the enzyme with the highest conversion, 33%, after 48 h at 80ºC [419]. In the same work, reaction yields for Lipozyme RM IM and TL IM were 13 and 14%, respectively. This very reaction was also studied by Horchani and coworkers with an immobilized *Staphylococcus xylosus* lipase. A 65% reaction yield was achieved after 55 h at 55ºC [420], proving the great efficiency of this lipase.

4.5.2.1 MALDI time-of-flight mass spectrometry

As stated before, selecting the appropriate MALDI matrix, cationization salts and sample preparation techniques are critical success factors for obtaining a reliable mass spectrum from which to infer structural information [425] and saving time. Additionally another matrix was tested: DHB matrix saturated in acetonitrile. Price and coworkers used this matrix to analyze liamocins, polyesters of mannitol and C10 polyols lipids, with a reliable accuracy and sensitivity [399]. According to these findings, DHB saturated with acetonitrile was tested to detect oligomers with molecular mass higher than 1000 Da. Estolides were analysed in positive ion mode giving rise to sodium pseudomolecular ions with a good sensitivity; although, monomer sodium adduct could not be detected due to the nature of the matrix, in contrast to the lithium DHB matrix [430].

Prior to analyze *trans*-HFA estolides, RA estolides, which were enzymatically produced using the method described by Bódalo and coworkers [426], were analysed with DHB matrix saturated in acetonitrile. Figure A.6 shows the corresponding MALDI TOF mass spectrum. Different peaks stand out from others: *m/z* 601.5, 881.7, 1162.0, 1443.2 and 1723.5. These ions correspond to the sodium adducts of a mono-estolide, $[2RA\text{-}H_2O+^{23}Na]^+$; di-estolide, $[3RA\text{-}2H_2O+^{23}Na]^+$; tri-estolide, $[4RA\text{-}3H_2O+^{23}Na]^+$; tetra-

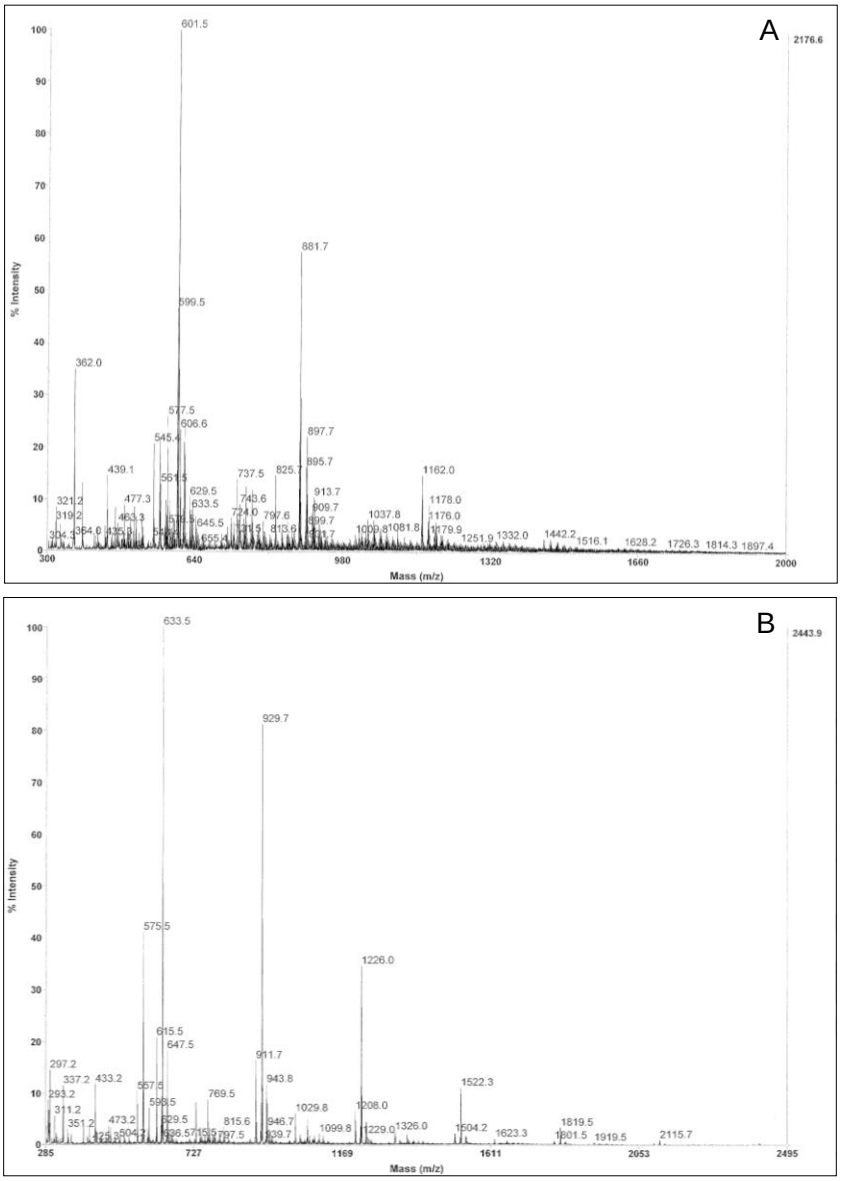

Figure 4.8. MALDI TOF mass spectra with DHB matrix saturated in acetonitrile. **A**: Estolides from (10*S*)-HOME polymerized with Novozym 435 (12% *w/w*) at 80ºC during 168 h and vacuum (total preassure of 1.6 kPa). **B**: Estolides from (7*S*,10*S*)-DiHOME polymerized with Novozym 435 (12% *w/w*) at 80ºC during 168 h and vacuum (total preassure of 1.6 kPa).

estolide, $[5RA\text{-}4H_2O+^{23}Na]^+$; penta-estolide, $[6RA\text{-}5H_2O+^{23}Na]^+$; and hexa-estolide, $[7RA\text{-}6H_2O+^{23}Na]^+$, respectively. A very low signal was observed for the last two peaks.

Figure 4.8 A shows mass spectra of (10*S*)-HOME (M) estolides obtained after polymerization with Novozym 435 in a solvent-free system; mass spectra of other estolides synthetized by Lipozyme RM IM and TL IM are presented in Figure A.7. Different ions stand out from the rest, making possible an easier and faster identification of the olygomers produced. Ions are the following: *m/z* 601.5, $[2M\text{-}H_20+^{23}Na]^+$; 881.7, $[3M\text{-}2H_20+^{23}Na]^+$; 1162.0, $[4M\text{-}3H_20+^{23}Na]^+$; and 1442.2, $[5M\text{-}4H_20+^{23}Na]^+$. The ion *m/z* 1722.4, which refer to a penta-estolide, $[6M'\text{-}5H_20+^{23}Na]^+$, is

not appreciable in the figure 4.8 A; however, it was detected. Figure 4.8 B presents (7*S*,10*S*)-DiHOME (M') estolides synthetized by Novozym 435. As can be seen, up to six pseudomolecular ions were detected. The first one with a *m/z* 633.5, [2M'-H_20+^{23}Na]$^+$, corresponds to a dimer, mono-estolide; lower mass ions were uncapable to detect with this matrix. Moreover, the following ions were also detected *m/z* 929.7, [3M'-2H_20+^{23}Na]$^+$; 1226.0, [4M'-3H_20+^{23}Na]$^+$; 1522.3, [5M'-4H_20+^{23}Na]$^+$; 1819.5, [6M'-5H_20+^{23}Na]$^+$; and, 2115.7, [7M'-6H_20+^{23}Na]$^+$. As could be observed, pseudomolecular ions of (7*S*,10*S*)-DiHOME estolides were detected with higher sensitivity because of they were produced in more quantity than (10*S*)-HOME ones; reaction yields were higher when the dihydroxylated compound was used as substrate, Table 4.7. Mass spectra of other estolides synthetized by Lipozyme RM IM and TL IM are presented in Figure A.8.

4.5.2.2 Nuclear magnetic resonance

NMR analyses were carried out to determine the structure of the estolides synthetized in a solvent-free system. A sample of each compound was analysed by ^{1}H and ^{13}C NMR. Moreover, 2D experiments were used to help in the structural determination. ^{13}C and ^{1}H NMR spectra of (10*S*)-HOME and (7*S*,10*S*)-DiHOME are presented in Figure 4.9 and 4.10 respectively.

Figure 4.9 shows ^{13}C spectra of (10*S*)-HOME and (7*S*,10*S*)-DiHOME estolides. Different common features in both figures will be commented. A signal for an ester carbonyl appears around 173 ppm (C1) [431]; moreover, signal of an acid carbonyl group, 179 ppm, is appreciable in the spectra, indicating a partial conversion of the substrate under reaction conditions, as observed from kinetics. Later, the signal of 24 ppm which matches with C3, corresponds to a methylene carbon. Finally, the terminal methyl carbon (C18) of the chain appears at 14.10 ppm.

trans-double bond in monohydroxylated estolides, Figure 4.9 A, has a chemical shift of 128.65 (C9) and 134.01 (C8) pmm; meanwhile, in the monomer or in the part of estolides molecules non affected by the ester bond is at 131.94 (C8) and 133.13 (C9) ppm. Furthermore, C2 and C10 signals are also modified downfield, from 33.94 to 34.56 ppm, and from 73.27 to 74.79 ppm [432], respectively. Both signals and the ester carbonyl could be considered as key markers in the identification of estolide formation.

In the case of the dihydroxylated estolides, Figure 4.9 B, oleofinic carbons (C8 and C9) appear together as one signal, 129.01 ppm. When they are not affected by the ester linkage have a chemical shift of 133.64 ppm, a higher signal due to both carbons are surrounded by two atoms of oxygen, which is an electronegative element. In this case, both types of C2 signals appear very close each other, around 34.48 ppm.

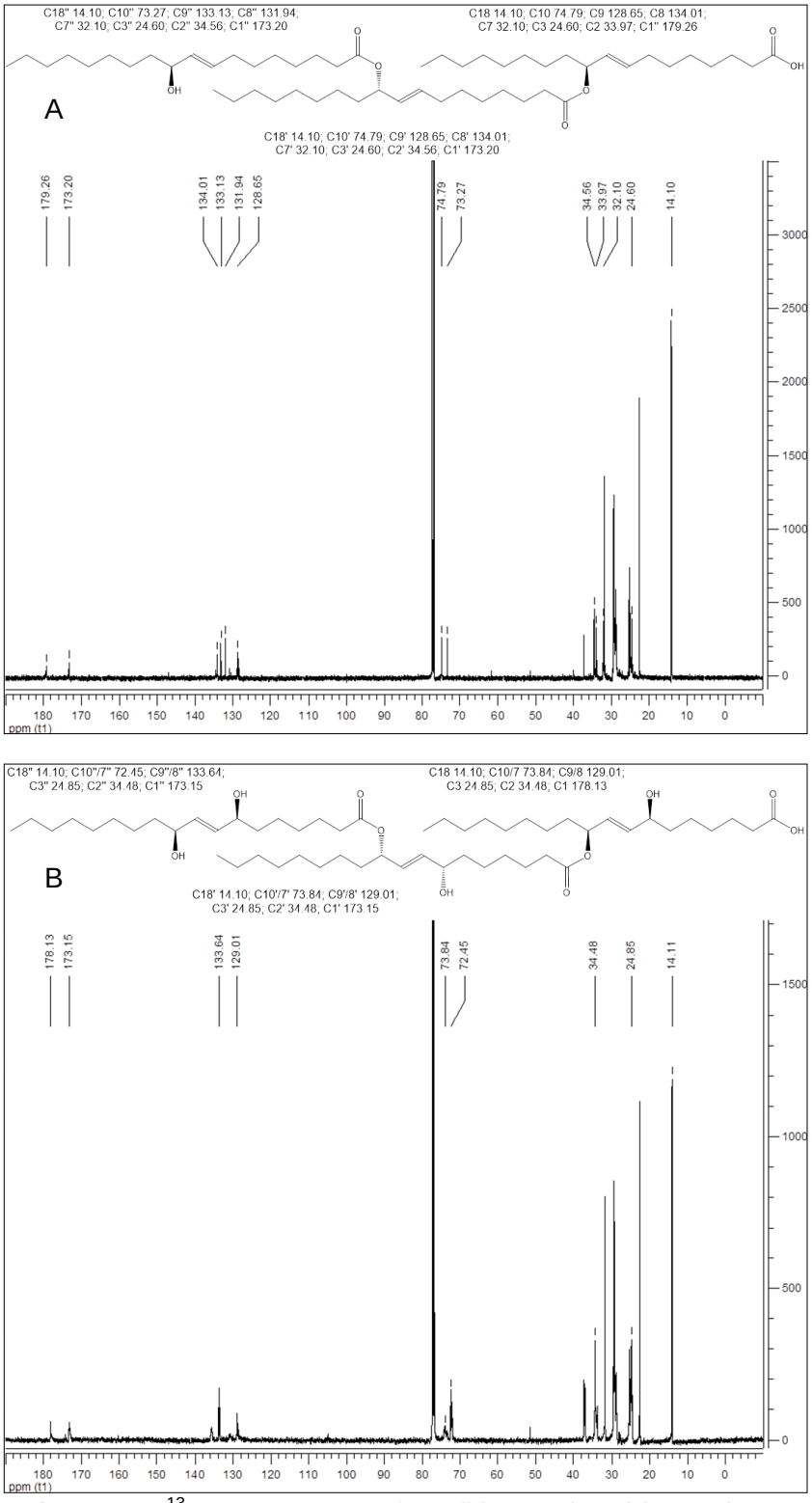

Figure 4.9. ^{13}C NMR spectra of estolides produced in a solvent-free medium. **A**: (10*S*)-HOME estolides produced by with Novozym 435 (12% *w/w*) at 80ºC during 168 h and vacuum (total preassure of 1.6 kPa). **B**: (7*S*,10*S*)-DiHOME estolides produced by Novozym 435 (12% *w/w*) at 80ºC during 168 h and vacuum (total preassure of 1.6 kPa). Chemical shifts are expressed in parts per million. Structure figures depicted in the figures are a guide to understand the different types of carbon present in the estolides.

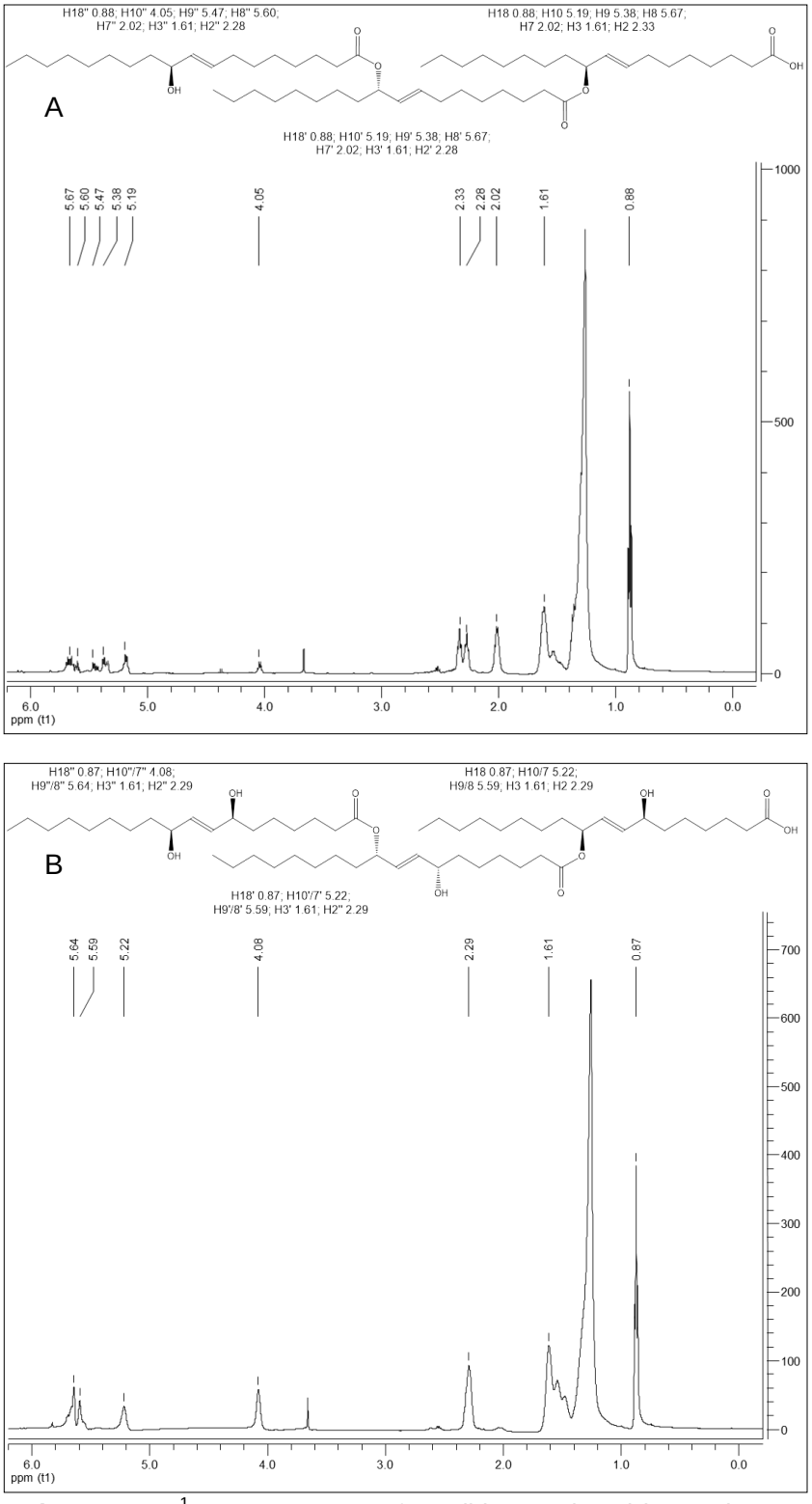

Figure 4.10. ^{1}H NMR spectra of estolides produced in a solvent-free medium. **A**: (10*S*)-HOME estolides produced by with Novozym 435 (12% *w/w*) at 80ºC during 168 h and vacuum (total preassure of 1.6 kPa). **B**: (7*S*,10*S*)-DiHOME estolides produced by Novozym 435 (12% *w/w*) at 80ºC during 168 h and vacuum (total preassure of 1.6 kPa). Chemical shifts are expressed in parts per million. Structure figures depicted in the figures are a guide to understand the different types of proton present in the estolides.

A higher magnetic field would be necessary to identify with more accuracy each kind of C2 signals. Lastly, C7 and C10 signals present the same chemical shift as in the substrate, 72.45 ppm, due to the symmetry of the molecule across the double bond and shifted downfield, 73.84 ppm [432], when they are present in the estolide molecule. Estolide structure presented in the Figure 4.9 B is only a possible representation of the formed *trans*-estolide because of 500 MHz experiments could not precisely if the ester linkage was produced by C7, C10 or both.

Figure 4.10 shows ^{1}H spectra of (10*S*)-HOME and (7*S*,10*S*)-DiHOME estolides. Some common signals will be discuss ahead. The signal of the terminal methyl hydrogens (H18) are at 0.88 ppm and methylene hydrogens H3 and H7 have an downfield chemical shift of 1.61 and 2.02 ppm due to the presence of the carbonyl group and the *trans*-double bond, respectively.

In the case of the monohydroxylated estolides, Figure 4.10 A, oleofinic hydrogens H8 and H9 have a chemical shift of 5.67 and 5.38 ppm, slightly different when they no affected by the ester linkage, 5.60 and 5.47 ppm, respective. Methylene hydrogens in the position 2 (H2) are also affected when are next to a ester carbonyl, 2.28 ppm, or an acid carbonyl 2.33 ppm [433]. Finally, methine hydrogen (H10) experimented a big change from 4.05 ppm when is next to the secondary alcohol to 5.19 ppm. This last signal is considered the most important for the identification of estolides synthesis in 1H NMR spectra.

When (7*S*,10*S*)-DiHOME estolides were analysed the following special features were found out, Figure 4.10 B. *trans*-double bond hydrogens (H8 and H9) appears as one signal, at 5.59 ppm in the polymerized part of the molecules and at 5.64 ppm in the substrate. Methine hydrogens (H7 and H10) are also found as one signal, like oleofinic hydrogens, due to the symmetry of the molecules in that point and by the low magnetic field in which (7*S*,10*S*)-DiHOME samples were analysed. These hydrogens have been downfielded from 4.08 to 5.22 ppm. Finally, H2 signal, 2.29 ppm, is composed by to signals, the acid and ester hydrogens; only observed in 2D experiments.

Similar features can be observed for estolides synthetized by Lipozyme RM IM and Lipozyme TL IM. Their corresponding figures, Figure A.11-14, could be found in the Appendix. Finally, estolide number (EN) could be calculated according to the following formula:

$$EN_{(10S)-HOME} = \frac{H10 + H10'}{H10''} = \frac{i-1}{1} \quad (31a)$$

$$EN_{(7S,10S)-DiHOME} = \frac{H7/10 + H7'/10'}{H7''/10''} = \frac{i-1}{i+1} \quad (31b)$$

where i represents the average number of monomers in the polyester, the degree of polymerization (DP) [434]. EN represents the average oligomeric distribution of the estolide [400]. From the integration of the signals H10+H10', 4.05 ppm, and H10'', 5.19 ppm for monohydroxylated estolides, Figure 4.10 A; and H7/10+H7'/10', 5.22 ppm, and H7''/10'', 4.08 ppm for dihydroxylated polyesters, Figure 4.10 B, and applying the corresponding Equation 31, the EN could be obtained and it is listed in Table 4.8.

Table 4.8. Estolide number (EN) and degree of polymerization (DP) of the different estolides which were enzymatically synthesized.

	(10*S*)-HOME		**(7*S*,10*S*)-DiHOME**	
Lipase	**EN**	**DP**	**EN**	**DP**
Novozym 435	2.00	3	0.67	5
Lipozyme RM IM	1.59	2-3	0.43	2-3
Lipozyme TL IM	1.15	2-3	0.64	4-5

Table 4.8 shows the EN obtained from Equation 31 and the degree of polymerization (DP; i). As can be seen higher values are achieved when dihydroxylated compound was the substrate used. Moreover, Novozyme 435 resulted as the most effective catalyst of the three tested. The results agree with reaction yields previously showed in Table 4.7.

Despite there is no reference in the literature about EN of *trans*-hydroxy-estolides, Isbell and coworkers chemically synthetized estolides from C18:1 monomers from lequerella and castor oils, both rich in HFA, with EN of 0.97 and 1.55 (DP = EN + 1), respectively [435]; very similar values to the ones obtained for (10*S*)-HOME, Table 4.8.

According to these results and MALDI TOF-MS ones, production of estolides in a solvent-free system offers better yields and higher DP than production of estolides in *n*-hexane.

4.5.3 Estolide production from saturated (10*S*)-HOME in a solvent-free media

A hydroxyl moiety in α-position to a double bond becomes a highly nucleophilic reaction group from a chemical point of view and, maybe, an uncommon group for the catalytic centre of lipases because of it could present some steric hindrance. Hence, for reducing double bond selectivity of lipases, a saturated (10*S*)-HOME was produced to improved reaction yields and synthetizing another type of estolides.

Saturated (10*S*)-HOME was chemically synthetized by means of protecting hydroxyl moiety with *bis*(trimethylsilyl)acetamide before catalytic hydrogenation. Previous hydrogenation experiments without such protecting group led to the modification of hydroxyl group apart from reducing the double bond. Finally, trimethylsilyl protecting group was detached from saturated (10*S*)-HOME in acidic conditions. Prior to polymerization all organic solvent traces were removed under vaccum.

4.5.3.1 Enzymatic and chemical synthesis

Saturated (10*S*)-HOME was polymerized chemically and enzymatically to produced estolides. Time course reaction is shown in Figure 4.11.

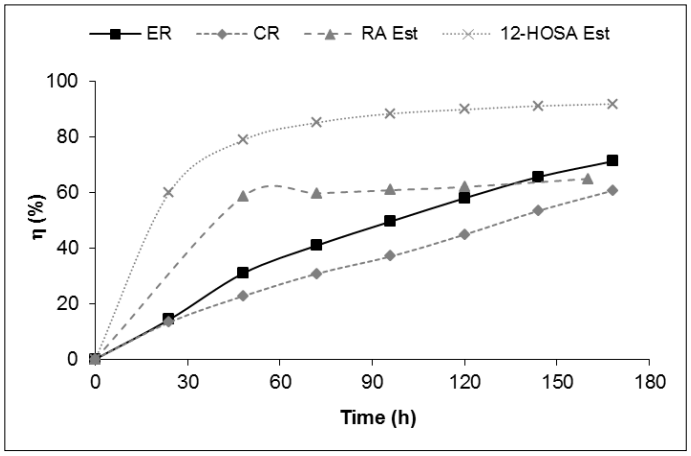

Figure 4.11. Saturated (10*S*)-HOME polymerization. **ER**: Enzymatic reaction, synthesis of estolides from saturated (10*S*)-HOME, 2 g, with Novozym 435 12 % (*w/w*), 0.24 g, at 80ºC, stirred at 500 rpm during 168 h and vacuum, 1.6 kPa of absolute preassure. **CR**: Same reaction conditions as in ER without enzyme. **RA Est**: Estolides from RA, according to [410]. **12-HOSA Est**: estolides synthetized from 12-HOSA, 100 g, at 150ºC stirred at 500 rpm during 96 h.

As can be seen, enzymatic reaction presents a better yield, 71.2%, than chemical one, 60.7%. Enzymatic reactions are known by their versatility and regio-, chemo- and enantioselectivity while operating under mild conditions [409] and here is presented one prove about their performance in front of chemical reactions. Moreover, two additional reactions were added to the Figure 4.11: the enzymatic production of RA estolides with *C. rugosa* [410] and the chemical synthesis of 12-hydroxystearic acid (12-HOSA) estolides under vacuum. As can be seen for RA estolides, despite the fact that reaction yield increased very fast in 48 h, it is not improved after that point, even the final conversion value, 64.9%, is lower than the one for the enzymatic reaction with saturated (10*S*)-HOME. It should also be remembered that RA is a HFA produced by nature and saturated (10*S*)-HOME is a synthetic one and higher yields should be expected for the first one. On the other hand, the production of 12-HOSA estolides has the highest yield after 168 h, 91.9%. The conversion difference with the chemical reaction of saturated (10*S*)-HOME is significant. Both HFA are saturated but differ in the position of the hydroxyl moiety and the stereochemistry of this quiral center: *S* for saturated (10*S*)-HOME and a mixture of both enantiomers for 12-HOSA.

As stated before, it seems that the position of a hydroxyl moiety and its stereochemistry must be taken into account for synthetizing estolides from HFA.

4.5.3.2 MALDI time-of-flight mass spectrometry

According to the good results obtained previously in section 4.5.2.1 with estolides synthetized in a solvent-free system, DHB matrix saturated in acetonitrile was also

used to determine the number of oligomers produced. Must be remembered that ions are sodium adducts with positive charge.

Figure 4.12 displays MALDI TOF MS spectra of saturated (10*S*)-HOME when was polymerized enzymatically, A, and chemically, B. In both mass spectra, some pseudomolecular ions stand out from others. Surprisingly, the ion corresponding to the unreacted saturated (10S)-HOME (S), *m/z* 324.2, have been detected $[S+^{23}Na]^+$, in contrast to previous analyses, section 4.5.2.1. Moreover, ions *m/z* 605.5, $[2S-H_2O+^{23}Na]^+$; 887.8, $[3S-2H_2O+^{23}Na]^+$; 1170.1, $[4S-3H_2O+^{23}Na]^+$; and 1453.4, $[5S-4H_2O+^{23}Na]^+$, which correspond to mono-, di-, tri- and tetra-estolide, respectively, were

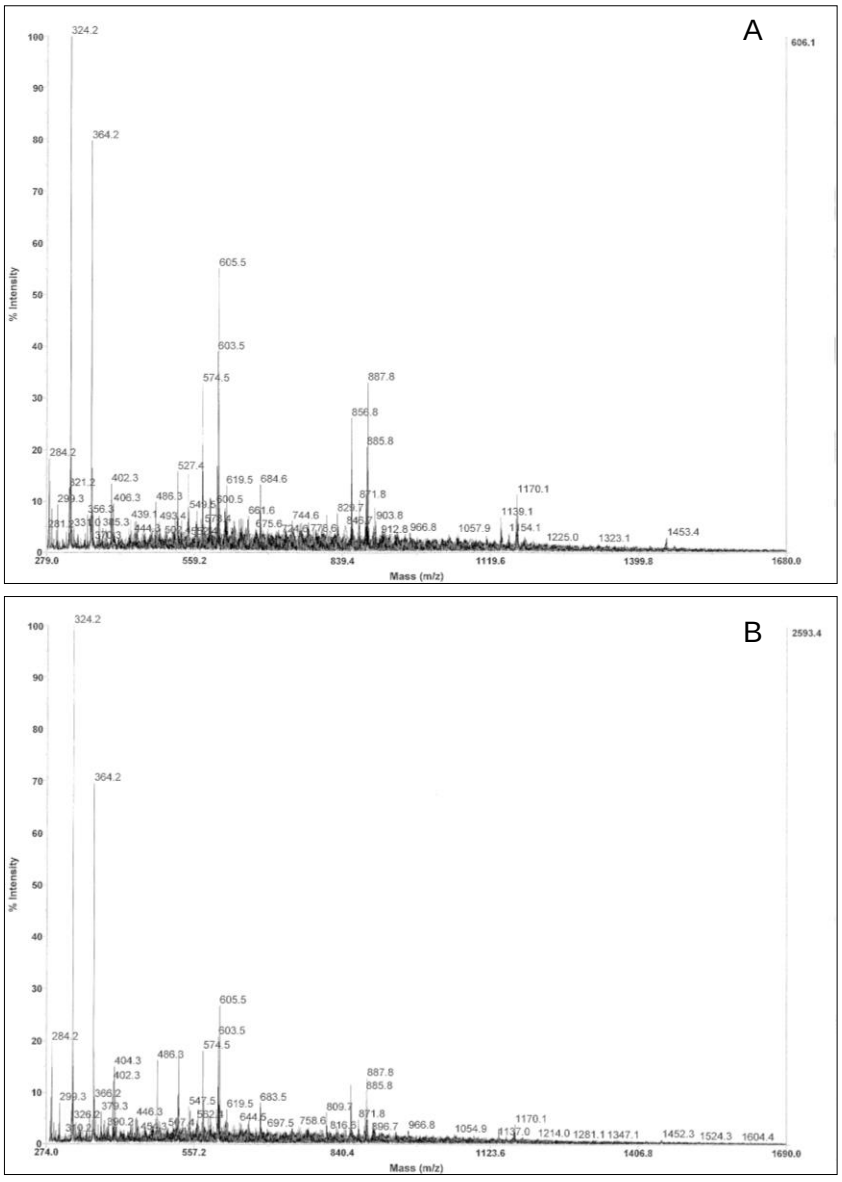

Figure 4.12. MALDI TOF MS analyses of saturated (10*S*)-HOME estolides. **A**: Under enzymatic reaction at 80ºC during 168 h and vacuum (total preassure of 1.6 kPa). **B**: Under chemical reaction at 80ºC during 168 h and vacuum (total preassure of 1.6 kPa). Matrix used was DHB saturated with acetonitrile.

detected. All these adducts were detected in both mass spectra; however, oligomers produced in the enzymatic reaction were detected with higher intensity than the chemical reaction, indicating a higher production of oligomers. As stated before, this signalling increase is proportional to the reaction yield.

4.5.3.3 Magnetic nuclear resonance

For confirming the nature of the oligomers synthetized a sample of each reaction was analized by NMR; additionally, 2D experiments were used to understand all signals in ^{1}H and ^{13}C NMR spectra.

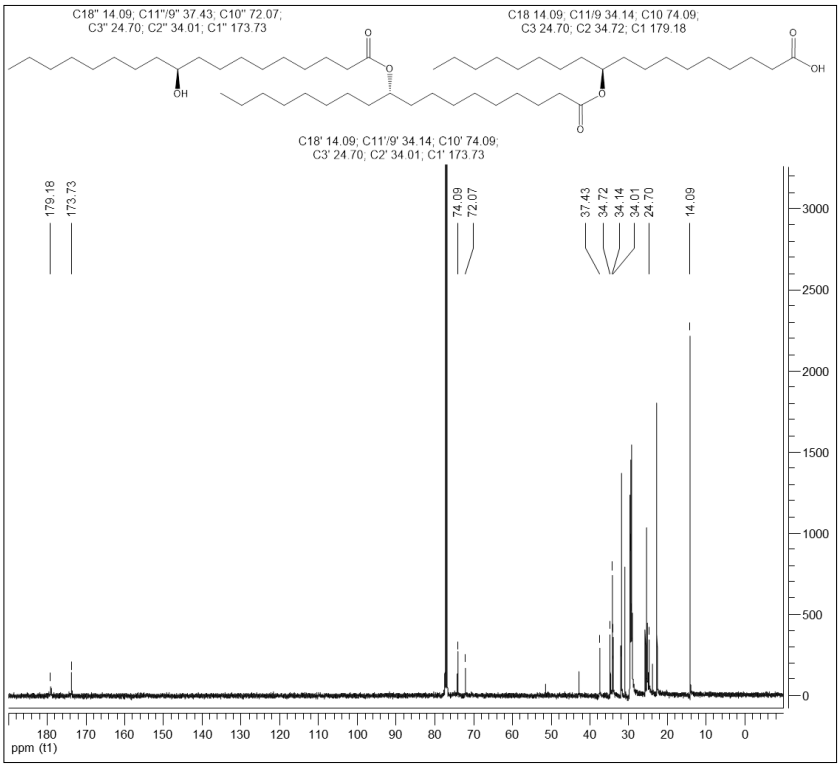

Figure 4.13. ^{13}C NMR spectrum of saturated (10*S*)-HOME estolides under enzymatic reaction at 80ºC during 168 h and vacuum (total preassure of 1.6 kPa). Chemical shifts are expressed in parts per million. Molecule structure depicted in the figure is a guide to understand the different types of carbon present in the estolides.

Figure 4.13 shows ^{13}C spectra of saturated (10*S*)-HOME estolides produce by Novozym 435, 12% (*w/w*) [436]. ^{13}C NMR spectra of estolides produced by chemical reaction could be found in the Appendix, Figure A.16 A, as well as saturated (10*S*)-HOME, Figure A.15. The main difference with polyesters commented in section 4.5.2.2 (solvent-free) is the lack of oleofinic carbon signals around 132 ppm.

However, the presence of an ester carbonyl signal, 179.18 ppm (C1) a methylene carbon (C2) at 34.01 ppm and a methine carbon (C10) at 74.09 ppm [433] confirm the formation of the saturated polyesters. Finally, a new signal of C9/11 methylene carbon

is shifted from 37.43 to 34.14 ppm by the ester bond. Two other carbon signals C3 and C18 become common with *trans*-estolides, 24.70 and 14.09 ppm, respectively.

Figure 4.14 displays ^{1}H spectrum of saturated (10*S*)-HOME estolides produce by Novozym 435, 12% (*w/w*). As stated before, ^{1}H NMR spectra of estolides produced by chemical reaction could be found in the Appendix, Figure A.16 B. Figure 4.13 shows

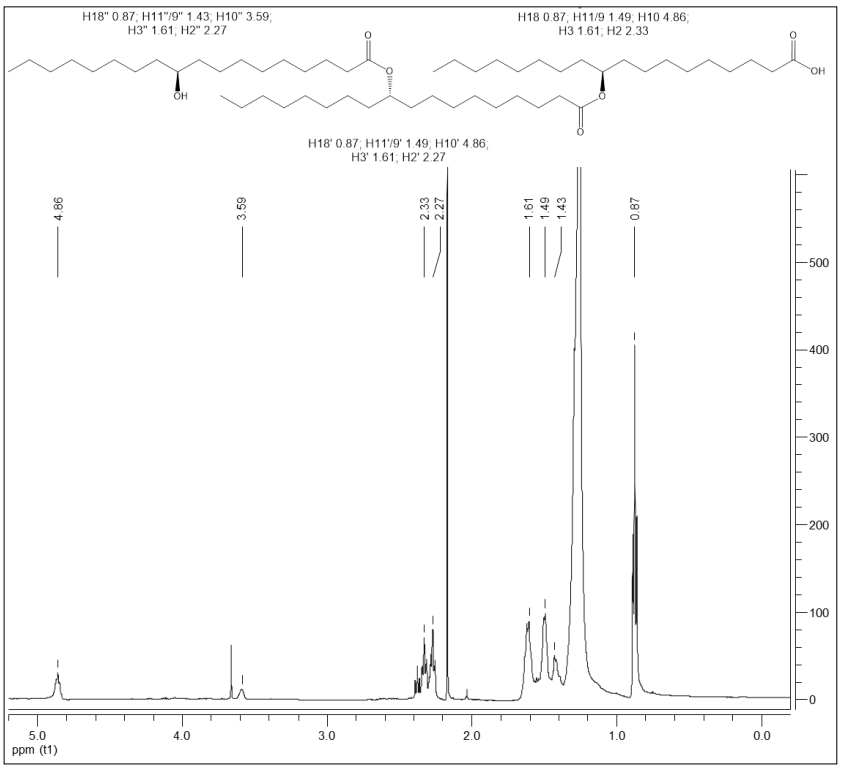

Figure 4.14. ^{1}H NMR spectrum of saturated (10*S*)-HOME estolides under enzymatic reaction conditions at 80ºC during 168 h and vacuum (total preassure of 1.6 kPa). Chemical shifts are expressed in parts per million. Structure molecule depicted in the figure is a guide to understand the different types of hydrogens present in the estolides.

some important signals of an estolide. The methine signal (H10) at 4.86 ppm is indicative of an ester linkage [433]; this signal is downfielded from 3.59 ppm when is closed to an hydroxyl group. The methylene protons in α to the acid group (H2) are shifted from 2.33 to 2.27 ppm when are next to an ester bond [433]. Furthermore, methylene protons that surrounded position 10, H11/9 are shifted from 1.43 to 1.49 by the ester bond formation. As stated previously, NMR analyses with a 500 MHz magnetic field is insufficient to precisely distinguish between 9 and 11 proton signals. Finally, methyl hydrogens at position 18 with a chemical shift of 0.87 ppm and methylene hydrogens in β to the ester group (H3) at 1.61 ppm are shared signals to all the preceding commented estolides. Similar signals were found for saturated (10*S*)-

HOME estolides chemically produced, Figure A.16 B; furthermore all these spectra could be compared with saturated (10*S*)-HOME ones, Figure A.9.

Ultimately, DP could be calculated here from EN and Equation 31a for saturated estolides synthetized chemically and enzymatically. Signals selected for that purpose are at 3.59 ppm for H10'' and 4.86 ppm for H10+H10', Figure 4.14 and A.16 B.

Table 4.9. Estolide number (EN) and degree of polymerization (DP) of the different estolides synthetized.

	Saturated (10*S*)-HOME			
	Chemically		**Enzymatically**	
	EN	**DP**	**EN**	**DP**
	1.95	2-3	2.49	3-4
	(10*S*)-HOME		**(7*S*,10*S*)-DiHOME**	
Lipase	**EN**	**DP**	**EN**	**DP**
Novozym 435	2.00	3	0.67	5
Lipozyme RM IM	1.59	2-3	0.43	2-3
Lipozyme TL IM	1.15	2-3	0.64	4-5

Table 4.9 displays the different values obtained for EN and DP. As can be seen, the enzymatic reaction produced a higher EN, 2.49, than chemical reaction, 1.95. These EN values show that enzymatic reaction has a DP between 3 and 4 monomeric units and chemical reaction between 2 and 3, one oligomer less. EN is proportional to reaction yield. These values are slighty higher than those found out by Cermak and collaborators in the chemical production of an stearic-oleic capped estolide with a 44.5% reaction yield, at 55ºC during 24 h. The DP of this estolide was 0.4, which means that approximately the fifty percent of the product is a mono-estolide [416], due to the low temperature and reaction time.

When these values are compared with previous ones of (10*S*)-HOME, inserted in Table 4.9, no great improvements have been achieved from a synthetic point of view. DP was only augmented in one monomeric unit in the enzymatic reaction, meanwhile chemical one offer the same DP range. On the other hand, DP of saturated (10*S*)-HOME estolides are lower than those obtained for (7*S*,10*S*)-DiHOME estolides produced by Novozym 435 and Lipozyme TL IM; because of, as stated before, EN and DP are totally related with reaction yield.

Finally, EN and DP calculated from ^{1}H NMR spectra confirm results observed from MALDI TOF-MS spectra: enzymatic reaction produced higher mass estolides than chemical reaction under the same synthetic conditions.

4.5.4 Physicochemical properties

A few physicochemical properties of estolides produced from section 4.5.1 to 4.5.3 were analysed in order to determine their viscosity and density (ρ) to compare them against the values of estolides previously published in the literature. Moreover, calorimetric analysis as differential scanning calorimetry (DSC) and thermal gravimetric analysis (TGA) were performanced to find out their characteristic calorimetric parameters.

4.5.4.1 Viscosity determination

This is the first time that estolides from *trans*-HFA are analyzed to determine their viscosity and few references of similar compounds were found in the literature. Estolides analysed in this section were considered as oligomers and not polymers strictly, due to their low DP values. Such simple molecules were determined as Newtonian fluids, because their viscosity remained constant over different shear rates. Dynamic or absolute viscosity (η') determination was run over three different temperatures (20, 40 and 60ºC) when was possible for calculating the pre-exponential factor (A) and activation energy (E_a) of the Arrhenius-type relationship [437]. This equation describes the dependence of viscosity on temperature, where A can be considered as the infinite-temperature viscosity value and E_a indicates the sensibility of a substance to the temperature [438]. Some authors consider that E_a gives much more accurate information to that given by the viscosity index, since this parameter is estimated from kinematic viscosities (ν) at two limiting temperatures 40ºC and 100ºC [439]. Additionally, ρ was determined to compare η' values obtained herein with kinematic viscosities (ν) of other estolides previously published at 40ºC.

In Table 4.10 pre-exponential factor, A, and activation energy, E_a, can be observed. Some of the monomers, (7*S*,10*S*)-DiHOME, 12-HOSA and saturated (10*S*)-HOME, did not melted at 60ºC; thus viscosity parameters could not be calculated. However, the two monohydroxylated compounds, (10*S*)-HOME and RA, present similar A values (9.47 and 2.77 10^{-10} Pa·s) and E_a values (49.9 and 53.3 kJ·mol^{-1}). These small differences between these isomeric HFA are referred to the position and configuration of the hydroxyl moiety, as well as, their double bond.

Estolides synthetized from (10*S*)-HOME present comparable A values; although, entrances (10*S*)-HOME *n*-hexane and (10*S*)-HOME TL IM values are slightly higher. Nevertheless, these discrepancies were not found on E_a values. All them fell on a small range values of 40.8 to 55.1 kJ·mol^{-1}, indicating similar thermal susceptibilities to flow. (10*S*)-HOME estolides values are close to those found for PR estolides, Table 4.10.

Table 4.10. Viscosity analysis parameters from estolides and degree of polymerization (DP).

Sample	$A \cdot 10^{-10}$ (Pa·s)	E_a (kJ·mol^{-1})	ρ (g·ml^{-1})	ν (cSt)	η (%)	DP
(10*S*)-HOME	9.47	49.9	0.96	205	–	1
(7*S*,10*S*)-DiHOME	n.d.	n.d.	0.99	n.d.	–	1
RA	2.77	53.3	0.94	213	–	1
Sat (10*S*)-HOME	n.d.	n.d.	0.93	n.d.	–	1
12-HOSA	n.d.	n.d.	0.95	n.d.	–	1
PR	16.1	50.9	0.98	478	64.9	4-5†
(10*S*)-HOME *n*-hexane	180	40.8	0.96	112	30.0	1-2†
(10*S*)-HOME N435	3.48	55.1	0.97	608	71.7	3
(10*S*)-HOME RM IM	5.79	53.6	0.97	495	68.4	2-3
(10*S*)-HOME TL IM	24.2	49.3	0.97	402	71.6	2-3
(7*S*,10*S*)-DiHOME N435	3.62	59.1	1.00	2510	94.7	5
(7*S*,10*S*)-DiHOME RM IM	0.14	67.7	1.02	3235	70.8	2-3
(7*S*,10*S*)-DiHOME TL IM	1.06	62.7	1.00	3000	88.9	4-5
Sat (10*S*)-HOME ER*	0.050	65.4	0.95	417	71.2	3-4
Sat (10*S*)-HOME CR*	0.007	72.1	0.95	746	60.7	2-3
12-HOSA CR	1080	42.1	0.91	1284	91.9	4-5†

A: Pre-exponential factor. **E_a**: Activation energy. **ρ**: Density. **ν**: kinematic viscosity. **η**: Reaction yield. **DP**: Degree of polymerization. **RA**: Ricinoleic acid 80%. **Sat (10*S*)-HOME**: Saturated (10*S*)-HOME. **12-HOSA**: 12-hydroxystearic acid. **PR**: Polyricinoleic acid estolides. **(10*S*)-HOME *n*-hexane**: (10*S*)-HOME mono-estolide in *n*-hexane. **(10*S*)-HOME N435**: (10*S*)-HOME with Novozym 435 solvent-free. **(10*S*)-HOME RM IM**: (10*S*)-HOME with Lipozyme RM IM solvent-free. **(10*S*)-HOME TL IM**: (10*S*)-HOME with Lipozyme TL IM solvent-free. **(7*S*,10*S*)-DiHOME N435**: (7*S*,10*S*)-DiHOME with Novozym 435 solvent-free. **(7*S*,10*S*)-DiHOME RM IM**: (7*S*,10*S*)-DiHOME with Lipozyme RM IM solvent-free. **(7*S*,10*S*)-DiHOME TL IM**: (7*S*,10*S*)-DiHOME with Lipozyme TL IM solvent-free. **Sat (10*S*)-HOME ER**: Saturated (10*S*)-HOME, enzymatic reaction. **Sat (10*S*)-HOME CR**: Saturated (10*S*)-HOME, chemical reaction. **12-HOSA CR**: 12-HOSA estolides, chemical reaction.
*Obtained at 40 and 60ºC. †Estimated

(7*S*,10*S*)-DiHOME estolides follow the same pattern as (10*S*)-HOME ones, close values for infinite-temperature viscosity and activation energy. On the other hand, A and Ea values for dihydroxylated estolides are higher than monohydrylated ones, indicating that they are more viscous compounds. This tendency is reflected by higher reaction yields and DP, as could be observed for entrance (7*S*,10*S*)-DiHOME N435 to (7*S*,10*S*)-DiHOME TL IM when are compared to (10*S*)-HOME estolide group in Table 4.10.

Finally, saturated estolides were analysed. Saturated (10*S*)-HOME estolides present very low A values (0.050 and 0.007 10^{-10} Pa·s) when compared to 12-HOSA CR estolides ($1080 \cdot 10^{-10}$ Pa·s). No reasoning was found for that situation, because E_a (42.1 kJ·mol^{-1}) is in the same range as the two other saturated estolides (65.4 and 72.1 kJ·mol^{-1}). Moreover, these E_a values are the highest of all compounds listed in Table 4.10, indicating that saturated (10*S*)-HOME estolides are (proportionally to the DP) the compounds which offer the largest resistance to flow. Few references have been found about E_a of HFA, but García-Zapateiro and co-workers determined the E_a values of estolides chemically produced from high-oleic sunflower oil in a range of 36.7-40.5

$kJ \cdot mol^{-1}$ [437]. These values are slightly lower when are compared to those found for (10*S*)-HOME estolides and PR, maybe, caused by the presence of a double bond and hydroxyl moieties.

Furthermore, kinematic viscosity, ν, of the diverse types of produced estolides was calculated. As could be observed, (10*S*)-HOME and RA have similar values because of both are isomeric compounds, 205 and 213 cSt, respectively. (7*S*,10*S*)-DiHOME, RA, 12-HOSA and Sat (10*S*)-HOME viscosities could not be calculated due to at 40ºC still remain solid. Valeri and Meirelles determined an OA viscosity as of 19.7 cSt [440]. Such low value gives an idea the contribution of a *trans* double bond and one single hydroxyl moiety to the viscosity when is compared to the monohydroxylated compounds.

The unsaturated monohydroxylated estolides have ν values between 400 and 500 cSt, with the exception of compound (10*S*)-HOME *n*-hexane, 112 cSt, because its DP is very low; and (10*S*)-HOME N435, 608 cSt. It is abnormally higher when is compared with entrance (10*S*)-HOME TL IM. These values are very similar to that found for ν of PR, 478 cSt, despite of a higher DP. This fact indicates a larger contribution of a *trans* double bond than a *cis* one to viscosity. In any case, all these compound and PR present higher ν when are compared to their corresponding substrates by the polymerization effect. The dihydroxylated estolides have the highest ν of all the compounds listed, 2510-3235 cSt. This was expected since (7*S*,10*S*)-DiHOME remained solid at 40ºC and the higher DP obtained in their polymerization reactions. Viscosity values for the dihydroxylated estolides are six-fold higher, as average, than monohydroxylated ones. This increment is caused by the extra hydroxyl group in position 7 and hydrogen bonds. The most similar compounds found in the literature are oleic-castor and oleic–lesquerella estolides, probably mono-estolides, produced by Cermak and coworkers [441] from *cis*-HFA (RA and 14-hydroxy-11(Z)-eicosenoic acid, respectively), which had a viscosity value of 34.5 and 35.4 cSt, respectively. These low values contrast with previous ones due to the different DP obtained in each, probably to the *cis* configuration of the double bond.

Finally, saturated (10*S*)-HOME estolides (Sat (10*S*)-HOME ER and Sat (10*S*)-HOME CR) have lower viscosity values, 417 and 746 cSt, than 12-HOSA CR, 1284 cSt. This fact is due to 12-HOSA remained solid at 40ºC and its DP higher than Sat (10*S*)-HOME ER and Sat (10*S*)-HOME CR entrances. Furthermore, ν value for Sat (10*S*)-HOME CR polyesters are higher than Sat (10*S*)-HOME ER one, despite of having a lower DP. It is believed that in chemical reaction, some other compounds as by-products could be produced and they would be responsible for this almost two-fold

increase in viscosity value, 746 cSt, respect to entrance Sat (10*S*)-HOME ER, 417 cSt. There were no differences in ν values of saturated (10*S*)-HOME estolides when were compared to unsaturated (10*S*)-HOME ones. It seems that a saturated and *trans*-estolides have the same behaviour from a rheological point of view. Cermak and collaborators hydrogenated oleic-castor and oleic-lesquerella estolides, obtaining a viscosity values of 68.3 and 37.0 cSt, respectively [441]. Viscosity was increased as they previously published [434], because the initial estolides have a *cis* unsaturation.

Finally, it is worthy to remark that depending on the possible future applications of *trans*-estolides different parameters, ν or DP, will be taken into account for optimizing synthetic reaction, apart from the nature of the initial substrate: position and configuration of the hydroxyl moiety and double bond.

4.5.4.2 Calorimetric analyses

Thermal analyses include a family of techniques that, when used together to characterize material properties, will yield information regarding how material will perform under a wide range of temperatures. DSC provides quantitative and qualitative information about physical and chemical changes that involve endothermic or exothermic processes or changes in heat capacity. TGA measures the amount and

Table 4.11. Calorimetric analysis parameters of estolides.

Sample	T_g (ºC)	T_{onset1} (ºC)	ΔH_1 ($J \cdot g^{-1}$)	T_{onset2} (ºC)	ΔH_2 ($J \cdot g^{-1}$)	T_{onset3} (ºC)	ΔH_3 ($J \cdot g^{-1}$)	Residue (%)
(10*S*)-HOME	-60	119	-7.08	196	47.33	315	-161.3	0.35
(7*S*,10*S*)-DiHOME	-49	185	37.79	277	-56.16	366	147.3	1.23
RA	-70	–	–	308	120.67	390	-172.9	0.77
Sat (10*S*)-HOME	-10	–	–	–	–	325	192.1	1.66
12-HOSA	-11	–	–	–	–	327	372.8	0.12
PR	-61	127	-15.74	306	106.95	380	-188.7	1.90
(10*S*)-HOME *n*-hexane	-72	–	–	224	28.90	336	-371.9	0.55
(10*S*)-HOME N435	-63	–	–	213	33.97	323	-174.1	2.27
(10*S*)-HOME RM IM	-64	–	–	217	35.73	322	-174.0	1.57
(10*S*)-HOME TL IM	-66	–	–	218	27.64	338	-252.9	1.73
(7*S*,10*S*)-DiHOME N435	-50	187	34.37	295	-30.18	362	-118.9	1.37
(7*S*,10*S*)-DiHOME RM IM	-49	200	28.22	302	-36.23	370	-105.5	1.12
(7*S*,10*S*)-DiHOME TL IM	-50	201	18.97	300	-37.07	364	-133.5	2.74
Sat (10*S*)-HOME ER*	-18	–	–	–	–	313	206.0	2.07
Sat (10*S*)-HOME CR*	-14	–	–	–	–	324	287.6	2.13
12-HOSA CR	-13	–	–	–	–	323	371.4	0.11

T_g: Glass transition temperature. **T_{onset}**: Initial temperature of ΔH. **ΔH**: Decomposition enthalpy. **RA**: Ricinoleic acid 80%. **Sat (10*S*)-HOME**: Saturated (10*S*)-HOME. **12-HOSA**: 12-hydroxystearic acid. **PR**: Polyricinoleic acid estolides. **(10*S*)-HOME *n*-hexane**: (10*S*)-HOME mono-estolide in *n*-hexane. **(10*S*)-HOME N435**: (10*S*)-HOME with Novozym 435 solvent-free. **(10*S*)-HOME RM IM**: (10*S*)-HOME with Lipozyme RM IM solvent-free. **(10*S*)-HOME TL IM**: (10*S*)-HOME with Lipozyme TL IM solvent-free. **(7*S*,10*S*)-DiHOME N435**: (7*S*,10*S*)-DiHOME with Novozym 435 solvent-free. **(7*S*,10*S*)-DiHOME RM IM**: (7*S*,10*S*)-DiHOME with Lipozyme RM IM solvent-free. **(7*S*,10*S*)-DiHOME TL IM**: (7*S*,10*S*)-DiHOME with Lipozyme TL IM solvent-free. **Sat (10*S*)-HOME ER**: Saturated (10*S*)-HOME, enzymatic reaction. **Sat (10*S*)-HOME CR**: Saturated (10*S*)-HOME, chemical reaction. **12-HOSA CR**: 12-HOSA estolides, chemical reaction.

rate of change in sample weight as a function of time or temperature. Thermal parameters obtained from those techniques can be observed in Table 4.11.

Table 4.11 displays different calorimetric parameters obtained from DSC and TGA curves. T_g, glass transition temperature could be determined for all estolides analyzed in this section, which indicate that this kind of polyesters are amorphous compounds. Melting point is not listed in Table 4.11, due to it could be only detected for (7*S*,10*S*)-DiHOME, 56ºC, hence is the only compound which presents a crystalline structure. This fact could be caused by the hydrogen bonds produced by the two hydroxyl groups and the acid moiety in the *trans*-HFA.

T_g of the monomers seems to present some especial features. As can be seen, monohydroxylated and monounsaturated substrates, (10*S*)-HOME and RA, present the lowest T_g, -60ºC and -70ºC, respectively, which is very similar. Then, it is found out that for (7*S*,10*S*)-DiHOME T_g was -49ºC; and finally monohydroxylated and saturated substrates, saturated (10*S*)-HOME and 12-HOSA, have the highest Tg, -10ºC and -11ºC, respectively. The following T_g tendency could be established: monohydroxylated-saturated, monohydroxylated-monounsaturated and dihydroxylated-monounsaturated, if it were because (7*S*,10*S*)-DiHOME has certain crystalline structure that increments its T_g value.

T_g values for produced estolides do not greatly differ from their substrates T_g with the only exception of PR, -61ºC, which increased regarding to RA, -70ºC. Entrances (10*S*)-HOME *n*-hexane to (10*S*)-HOME TL IM, present slightly lower T_g values, around -65ºC, than their corresponding substrate, (10*S*)-HOME, -60ºC. Similar results are observed for (7*S*,10*S*)-DiHOME N435 to (7*S*,10*S*)-DiHOME TL IM estolides. In this case their T_g practically remains constant, -50ºC, when is compared to (7*S*,10*S*)-DiHOME, -49ºC. Finally, Sat (10*S*)-HOME ER, Sat (10*S*)-HOME CR and 12-HOSA CR saturated estolides have similar T_g values than their substrates, saturated (10*S*)-HOME and 12-HOSA. Estolides Sat (10*S*)-HOME ER and Sat (10*S*)-HOME CR, -18ºC and -14ºC, respectively, have lowered their T_g respecting to saturated (10*S*)-HOME, -10ºC. On the other hand, T_g of 12-HOSA CR compound, -13ºC, is comparable to 12-HOSA, -11ºC.

According to these values, estolides produced in this section could be used as lubricating oils, one of the main applications of estolides [428], as long as the lowest temperature end of the working range will be higher than their T_g. T_g is defined as the temperature in which a compound changes its rigid and brittle state to another soft and malleable, only present in amorphous substances.

Additionally, different decomposition enthalpies (ΔH) and their initial temperature (T_{onset}) of these ΔH were listed in Table 4.11, obtained from DSC curves. *trans*-HFA,

(10*S*)-HOME and (7*S*,10*S*)-DiHOME, present three different ΔH. Two exothermic enthalpy, negative value, and an endothermic one, positive value. In contrast, RA, has two ΔH, one of each type, and saturates substrates, 12-HOSA and saturated (10*S*)-HOME, have an endothermic one, with similar T_{onset}, 327ºC and 325ºC, respectively.

(10*S*)-HOME *n*-hexane to (10*S*)-HOME TL IM estolides, present two ΔH which their T_{onset} is approximately 217ºC (+) and 326ºC (-), but (10*S*)-HOME has three ΔH with the following T_{onset}: 119ºC (-), 196ºC (+) and 315ºC (-). Those estolides lack of the initial exothermic ΔH. On the other hand, PR exhibits an extra initial ΔH respecting RA, 127 ºC (-); however, other two are coincident at 307ºC (+) and 385ºC (-). Regarding to dihydroxylated estolides, (7*S*,10*S*)-DiHOME N435 to (7*S*,10*S*)-DiHOME TL IM polyesters possess three ΔH at 195ºC (+), 300ºC (-) and 365ºC (-) which are very similar to their initial substrate, (7*S*,10*S*)-DiHOME, at 185ºC (+), 277ºC (-) and 366ºC (-). This similarity is not found in monohydroxylated compounds. Finally, saturated estolides, Sat (10*S*)-HOME ER to 12-HOSA CR, show only one ΔH at 320ºC (+) as their substrates, saturated (10*S*)-HOME and 12-HOSA, 326ºC (+). At that point decomposition and compound fusion is produced at the same time, but in other estolides and substrates, decomposition is produced in different stages. In monohydroxylated compounds, with the exception of RA and PR, decomposition is produced in two stages and in dihydroxylated ones, in three.

It is important to note that saturated and dihydroxylated estolides maintain the number and natures of ΔH and their corresponding T_{onset} respect to their substrates; not as monohydroxylated polyesters.

4.6 Ethyl esters production

There is great interest on producing biodiesel from natural sources as vegetable oils or animal fats. Usually, biodiesel, (m)ethyl fatty ethyl esters are produced enzymatically from fatty acids by esterification and/or from triglycerides by transesterification. On the other hand, HFA, mainly RA as castor oil, have not been extensively used to produce their corresponding (m)ethyl esters. Furthermore, some fatty acid ethyl esters (FAEE) have been described as aromatic compounds in fruit and wine [413-415]. In this section, two different *trans*-HFA ethyl esters are enzymatically produced in non-conventional media.

4.6.1 Ethyl esters production from (10*S*)-HOME and (7*S*,10*S*)-DiHOME in chloroform

As stated before, Novozym 435 was chosen due to its ability to react with *trans*-9-octadecenoic acids [417], its versatility, and the optimal temperature range of its activity

(40-60ºC). The poor solubility of (10*S*)-HOME in *n*-hexane negatively affects the production yield of estolides [430], section 4.5.1. Thus, to improve the solubility of (10*S*)-HOME and (7*S*,10*S*)-DiHOME, both were dissolved in chloroform, log P of 1.97, a polar organic solvent that enhances their solubility. Log P provides a measure of the lipophilic versus hydrophilic nature of a compound [442] that could affect biocatalytic activity in the solvent.

4.6.1.1 Effect of the enzyme concentration

Different amounts of the lipase were assayed to determine the optimal quantity that reacted with 0.5 g of (10*S*)-HOME and 0.4 ml of ethanol (oil to ethanol molar ratio of 1:4). Results are presented in Figure 4.15. The reaction yield increased with the amount of enzyme, until a plateau was reached, in the presence of approximately 0.10 g of Novozym 435 and 0.5 g of (10*S*)-HOME, in which a yield of 89.1% was reached. After this point, the reaction yield remained constant, even though when the enzyme amount was increased. Thus, a thermodynamic balance between the limiting substrate, (10*S*)-HOME, and the lipase had been reached at this point. The same pattern was observed when 0.5 g of (7*S*,10*S*)-DiHOME and 0.4 ml of ethanol (oil-to-ethanol molar ratio of 1:4) were reacted with different concentrations of the lipase, Figure 4.15. A conversion rate of 89.9% was achieved in 12 hours at 50ºC using 0.10 g of Novozym 435. At higher enzyme concentrations, no increases in the reaction yield were detected for either *trans*-HFA. At this moment, there are currently no data in the literature about the production of ethyl esters from *trans*-HFA. These yields are slightly higher than the 81.4% obtained by Oliveira and collaborators, who used castor oil, mainly RA, and the same concentration of Novozym 435 used here at 65ºC for 8 hours, with ethanol as solvent (oil-to-ethanol ratio of 1:10) [443].

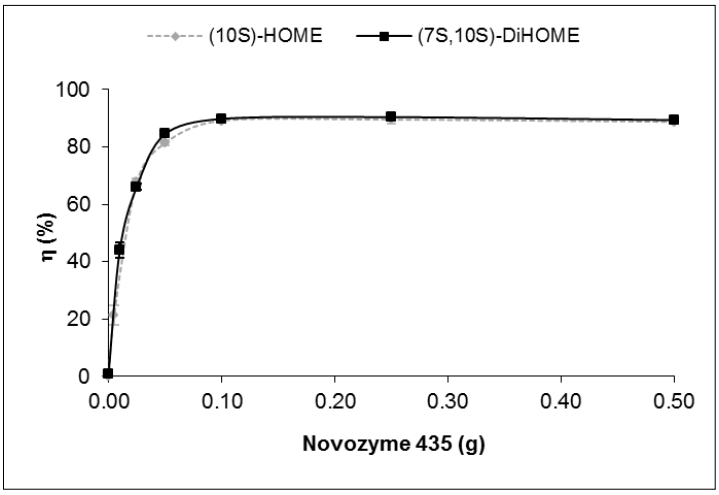

Figure 4.15. Effect of Novozym 435 concentration on ethyl ester production of (10*S*)-HOME, 0.5 g, and (7*S*,10*S*)-DiHOME, 0.5 g, with EtOH, 0.4 ml, at 50ºC during 12 h in 19.6 ml of chloroform.

4.6.1.2 Effect of the substrate/enzyme ratio

Various substrate/enzyme ratios were tested to establish the optimal concentration of *trans*-HFA. Figure 4.16 illustrates the results with (10*S*)-HOME as the substrate. The reaction yield increased with the substrate/enzyme ratio up to the ratio of 1.5 $g \cdot g^{-1}$ (0.15 g of (10*S*)-HOME per 0.10 g of Novozym 435). After that, the yield remained constant at 87.0%. Similar was observed with (7*S*,10*S*)-DiHOME, Figure 4.16; however, the highest reaction yield here was 90.3%, which was obtained with a ratio of 1 $g \cdot g^{-1}$ (0.10 g of (7*S*,10*S*)-DiHOME per 0.10 g of Novozym 435). Afterwards, no further upturn was detected.

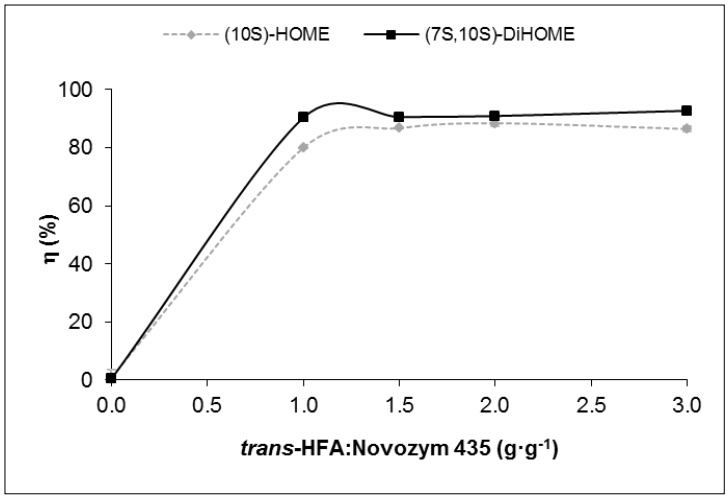

Figure 4.16. Effect of *trans*-HFA:Novozym 435 ratio on the ethyl ester production of (10*S*)-HOME or (7*S*,10*S*)-DiHOME with 0.1 g of lipase and 0.4 ml of EtOH at 50ºC during 12 h in 19.6 ml of chloroform.

4.6.1.3 Resusability of the enzyme

The reusability of Novozym 435 was studied by assessing the *trans*-HFA conversion rates after consecutive batch cycles under optimal reaction conditions. Reuse of the lipase in several reactions reduces reaction costs and makes it an economically feasible process [420], which can operate in batch or continuous regimes. The ability of Novozym 435 to retain its stability during recycling with HFAs as the substrate has already been studied [419, 422].

Figure 4.17 shows the reaction yields in the polymerisation of the two *trans*-HFAs in different cycles, as well as the enzyme weight in each process. The synthetic stability of the enzyme remained constant for fifteen cycles. When (10*S*)-HOME was the substrate, the conversion rate reached 86.1%, on average, while in the assays with (7*S*,10*S*)-DiHOME, the average conversion rate was 90.3%. Differences in enzyme stability between these two *trans*-HFAs were less than 5%, indicating the non-specificity of Novozym 435 for the two *trans*-HFAs as substrates when chloroform was used as solvent. This behaviour differed from that earlier found by Martin-Arjol and coworkers, who observed that Novozym 435 stability decreased by 53.3% in ten cycles

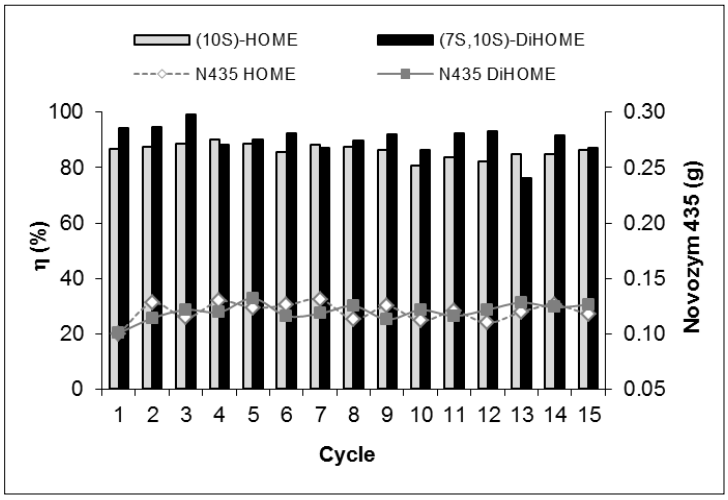

Figure 4.17. Yield of the esterification (bars) and enzyme weight (lines) at each cycle. Optimal reaction conditions were used in all experiments. **HOME**: (10*S*)-HOME; **DiHOME**: (7*S*,10*S*)-DiHOME**; N435 HOME**: Novozym 435 weight when (10*S*)-HOME was used as substrate; and, **N435 DiHOME**: Novozym 435 weight when (7*S*,10*S*)-HOME was used as substrate.

during the synthesis of monoestolides using (10*S*)-HOME as the substrate in *n*-hexane [430], section 4.5.1.2. Langone and collaborators observed a similar reduction in the stability of the same enzyme, 55%, in the production of estolides from OA and methyl ricinoleate after four cycles in a solvent-free system [419]. On the other hand, Radzi and partners noted high synthetic stability even after nine cycles, 91.9%, during the production of oleyl oleate in *n*-hexane [422]. Thus, the nature of the substrates and the organic solvent play an important role in the enzymatic stability of Novozym 435.

4.6.1.4 Structural determination

i. Fourier transform infrared spectroscopy

One sample of each *trans*-HFA ethyl ester obtained in the optimal reaction conditions was analysed to determine the functional groups present in the two new compounds as well as the initial substrates (10*S*)-HOME and (7*S*,10*S*)-DiHOME.

The FTIR spectra of (10*S*)-HOME and its corresponding ethyl ester showed one main difference, Figure A.17: the stretching of the carbonyl gave a peak at 1709 cm^{-1} in the free fatty acid and at 1736 cm^{-1} in the ethyl ester [444]. In the case of the dihydroxy-fatty acid, the band corresponding to the carbonyl stretching in the free fatty acid, 1693 cm^{-1}, was displaced to 1738 cm^{-1} in its ethyl ester, Figure A.17, demonstrating in both cases the formation of an ester linkage. These findings are consistent with the work of Zagonel and coworkers, who monitored soybean oil ethanolysis by FTIR multivariate analysis models [445].

ii. Nuclear magnetic resonance

NMR analyses were carried out to determine the structure of the ethyl esters synthesized. A sample of each compound produced in optimal reaction conditions was analysed by ^{1}H and ^{13}C NMR.

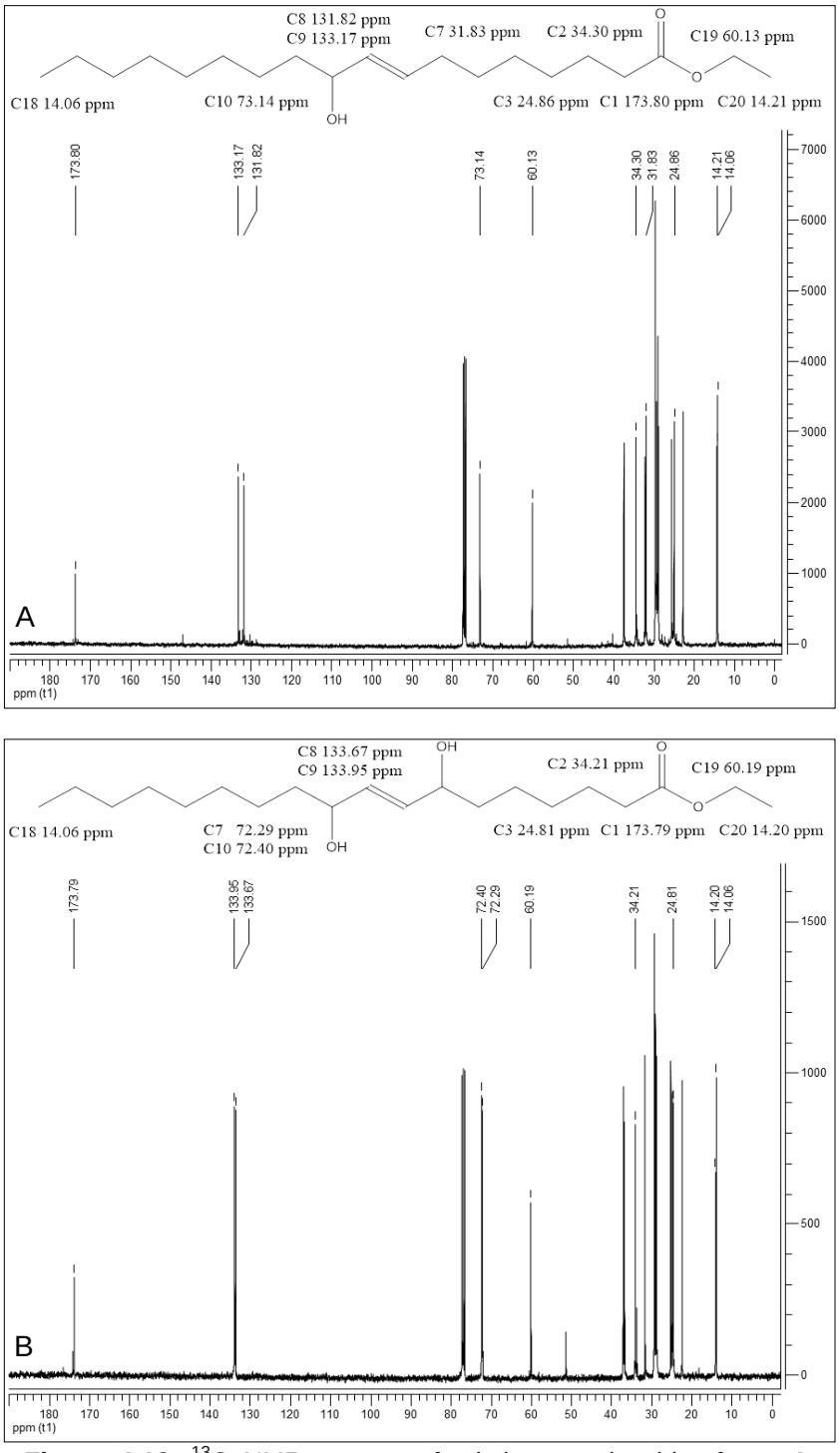

Figure 4.18. ^{13}C NMR spectra of ethyl esters in chloroform. **A**: (10*S*)-HOME ethyl ester. **B**: (7*S*,10*S*)-HOME ethyl ester. Ethyl esters were synthetized in optimal conditions: *trans*-HFA:Novozym 435 ratio of 1.5 and 1 $g \cdot g^{-1}$ for (10*S*)-HOME and (7*S*,10*S*)-DiHOME, respectively; 0.1 g of lipase, 0.4 ml of EtOH, 50ºC and 19.6 ml of chloroform.. Chemical shifts are expressed in parts per million.

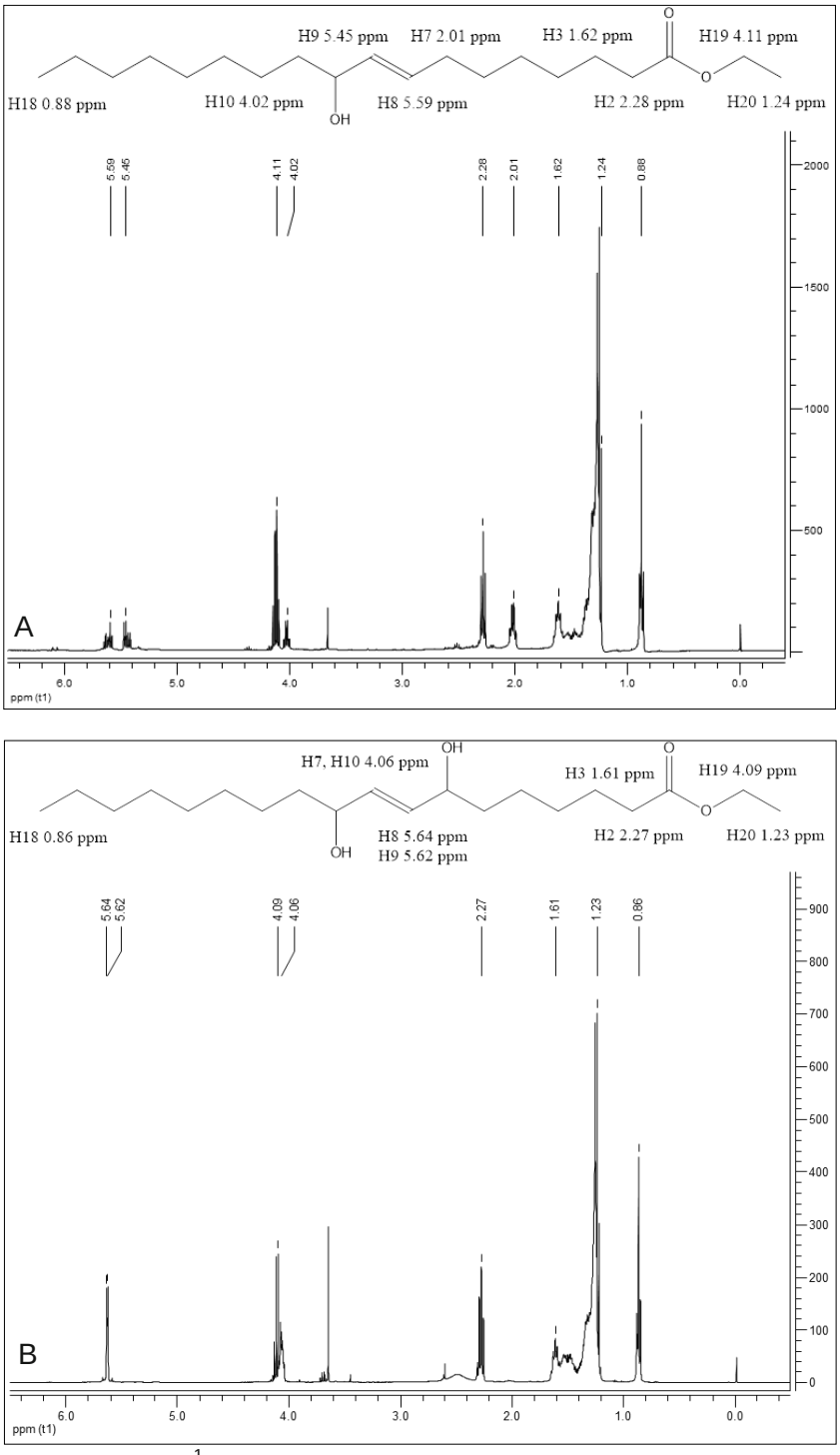

Figure 4.19. ^{1}H NMR spectra of ethyl esters in chloroform. **A**: (10*S*)-HOME ethyl ester. **B**: (7*S*,10*S*)-HOME ethyl ester. Ethyl esters were synthetized in optimal conditions: *trans*-HFA:Novozym 435 ratio of 1.5 and 1 $g \cdot g^{-1}$ for (10*S*)-HOME and (7*S*,10*S*)-DiHOME, respectively; 0.1 g of lipase, 0.4 ml of EtOH, 50ºC and 19.6 ml of chloroform. Chemical shifts are expressed in parts per million.

Figure 4.18 shows the ^{13}C NMR spectra obtained for the two ethyl esters. In both spectra, a double signal of the methylenic carbons appeared at 14.06 and 14.20 ppm. The signal at 14.20 ppm corresponded to the methyl carbon of the ethyl ester side chain (C20) and the one at 14.06 ppm to the methyl carbon of the fatty acid side chain (C18). The signal at 60.16 ppm was due to the methylene carbon of the ethyl ester (C19) [446]. Finally, a signal for an ester carbonyl appeared at 173.80 ppm (C1) [447].

Moreover, no signal corresponding to an acid carbonyl, 179.15 ppm, was appreciable in the spectra, indicating total conversion of the substrates in the optimal reaction conditions. Additionally, the signals at 24.84 and 34.25 ppm represented the methylene carbons of the *trans*-HFA chain at positions 3 and 2, respectively. The ones at 72-73 ppm indicated the methine carbons that bond with hydroxyl moieties (C7 and C10), while the signals at 131-134 ppm represented the olefinic carbons of the *trans* double bond (C8 and C9). Finally, there was a signal at 31.83 ppm only in the monohydroxy ethyl ester spectrum, which corresponded to the methylene carbon at position 7.

In both ^{1}H NMR spectra, Figure 4.19, a sharp quartet appeared at 4.10 ppm. This corresponded to the methylenic hydrogens of the ethyl ester (H19); however, the methyl hydrogens of the same part of the molecule were noticeable at 1.24 ppm (H20) [399], slightly overlapping with the methine hydrogens, 4.04 ppm, of the *trans*-HFA side chain (H7 and H10). These signals confirmed the formation of the *trans*-HFA ethyl esters by Novozym 435 in organic media. Moreover, different types of signals appeared in each ^{1}H NMR spectrum, indicating different compounds.

In the ^{1}H NMR spectrum of the monohydroxy ethyl ester, Figure 4.19 A, the oleofinic hydrogen signals appeared between 5.45 and 5.59 ppm (H9 and H8, respectively). The methine hydrogen close to the hydroxyl group, H10, demonstrated a chemical shift to 4.02 ppm. Other interesting findings included a triplet at 2.28 ppm, which corresponded to the hydrogens next to the carbonyl group (H2); a chemical shift of 1.62 ppm is for the hydrogens at position 3 as a result of the effect of the carbonyl group; and, a signal at 2.01 ppm represents the influence of the *trans* double bond on the hydrogens at position 7. In the ^{1}H NMR spectrum of the dihydroxy ethyl ester, Figure 4.19 B, the hydrogens of the *trans* double bond underwent a chemical shift of 5.63 ppm (H8 and H9). In this case, there were two methine hydrogens, H7 and H10, close to the hydroxyl groups, with a chemical shift of 4.06 ppm. The presence of a hydroxyl moiety at position 7 shifted the signal downfield, from 2.01 to 4.06 ppm. The downfield methylenic signals were the same as stated above, with the exception of the hydrogens at position 7.

iii. Electrospray ionization mass spectrometry

Electrospray ionization mass spectrometry (ESI-MS) was applied to determine the mass of the compounds formed during the enzymatic synthesis. The spectrum of the (10*S*)-HOME ethyl ester is presented in Figure 4.20 A, showing two main ions with *m/z* 121.0509 and 922.0098 corresponding to the two internal references. Other important ion was the one with *m/z* 309.2789, which represented the loss of a water molecule from the (10*S*)-HOME ethyl ester (M), $[M\text{-}H_2O+^{1}H]^+$. In addition to these, a group of low-intensity ions of between 300-400 Daltons (Da) (enlargement) was of great significance. This group included ions with *m/z* of 344.3154 and 349.2718, which corresponded to the molecular adducts of the M with ammonium and sodium cations, $[M+NH_4]^+$ and $[M+^{23}Na]^+$, respectively. These three adducts were consistent with a mass of 326.5159 Da, further confirming the synthesis of a monohydroxy fatty ethyl ester.

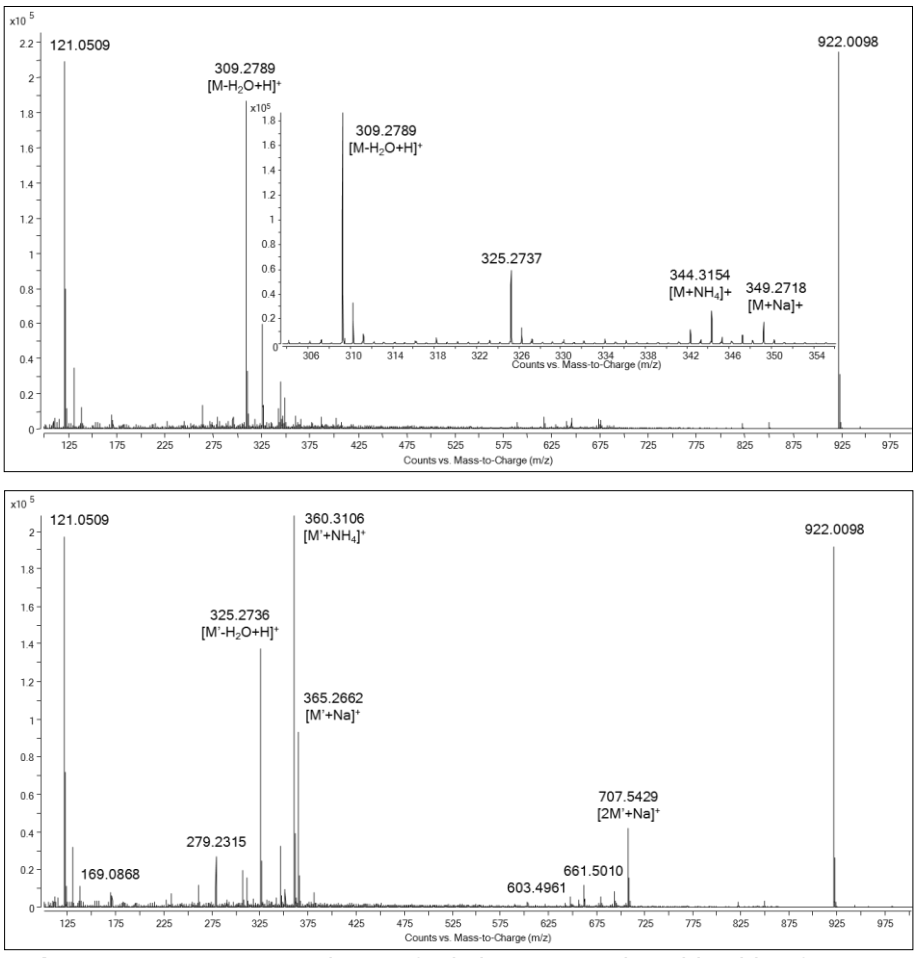

Figure 4.20. ESI MS analyses of ethyl esters produced in chloroform. **A**: Mass spectrum of monohydroxylated ethyl ester. **B**: Mass spectrum of dihydroxylated ethyl ester. Synthesis was carried out under optimal conditions: *trans*-HFA:Novozym 435 ratio of 1.5 and 1 $g \cdot g^{-1}$ for (10*S*)-HOME and (7*S*,10*S*)-DiHOME, respectively; 0.1 g of lipase, 0.4 ml of EtOH, 50ºC and 19.6 ml of chloroform.

As can be observed in Figure 4.20 B, three main ions appeared for the (7*S*,10*S*)-DiHOME ethyl ester. Two of them corresponded to the internal references and the other one, with *m/z* of 360.3106, to the molecular adduct of the (7*S*,10*S*)-DiHOME ethyl ester (M') with an ammonium cation, $[M'+NH_4]^+$. Moreover, two ions with a lower intensity, *m/z* 365.2662 and 707.5429, which represented the sodium molecular adducts of M' and 2M', $[M'+^{23}Na]^+$ and $[2M'+^{23}Na]^+$, respectively, were relevant. Finally, another ion with *m/z* 325.2736 represented the loss of a water molecule from the ethyl ester, $[M'-H_2O+H]^+$. These four molecular adducts confirmed the synthesis of a dihydroxy fatty ethyl ester with a mass of 342.5153 Da.

4.6.2 Ethyl esters production from (10*S*)-HOME and (7*S*,10*S*)-DiHOME in a solvent-free media

According to the previous results obtained in solvent-free media, it was decided to synthetize *trans*-HFA ethyl esters in this non-conventional reaction medium despite the high reaction yields obtained in chloroform.

4.6.2.1 Effect of *trans*-hydroxy-fatty acid/ethanol ratio

Hydroxy-fatty acids, positionally different from RA, were used to synthesize their corresponding ethyl esters in solvent-free media. Different molar ratios of *trans*-HFA to EtOH were assayed to determine the optimal molar ratio to maximize reaction yield with 0.12 g of Novozym 435 at 50ºC during 24 h, Figure 4.21.

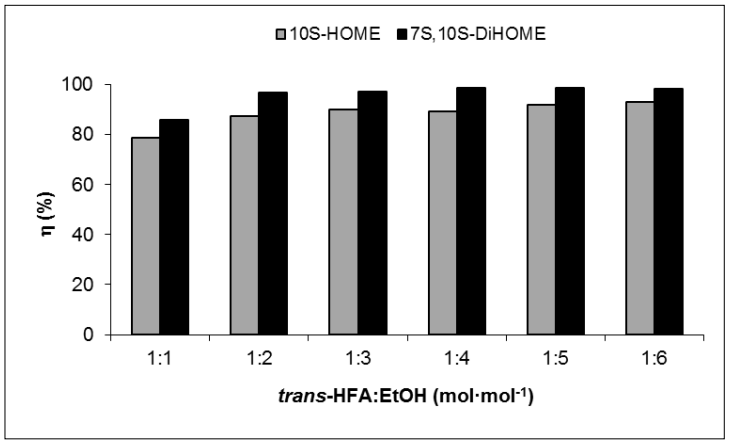

Figure 4.21. Effect of the molar ratio of *trans*-HFA to EtOH on the yield of ethyl esters synthesis with Novozym 435, 0.12 g, at 50ºC during 24 h in a solvent-free medium.

It could be observed in Figure 4.21 that both *trans*-HFA presented the same pattern, reaction yield increased from molar ratio 1:1 to 1:3, then, conversion remained practically constant. The optimal molar ratio was 1:3 (*trans*-HFA/EtOH) considering both the reaction yield and the future possible production costs. There are no data in the literature about the production of *trans*-HFA ethyl esters, although this molar ratio value, *trans*-HFA to EtOH of 1:3, agrees with that found in the production of methyl esters from a vegetable oil (a soybean and rapeseed oil mixture) in a solvent-free

system for 36 h at 30ºC [448] and with the one in the production of fatty acid ethyl esters from camellia oil soapstocks and diethyl carbonate, instead of a short-chain alcohol, for 24 h at 50°C [449], both using Novozym 435.

4.6.2.2 Effect of the enzyme concentration

Different amounts of enzyme were tested to establish the optimal amount of biocatalyst for a *trans*-HFA to EtOH molar ratio of 1:3, Figure 4.22. As observed, higher yields were achieved when (7*S*,10*S*)-DiHOME was used as a substrate, 98%, whereas the 90% of the monohydroxylated compound. However, less quantity of Novozym 435 was needed to reach higher yields with (10*S*)-HOME, 0.06 g, than using the dihydroxylated fatty acid, 0.10 g. The amounts of enzyme needed in each reaction system, 0.06 and 0.10 g, when (10*S*)-HOME and (7*S*,10*S*)-DiHOME were used as substrate, respectively, which represent 8.6 and 14.3% (*w/v*), respectively, were in the same range of Novozym 435 concentration, 10–15% (*w/v*), used in the production of fatty acid ethyl esters from palm oil fatty acids in a solvent-free medium [450].

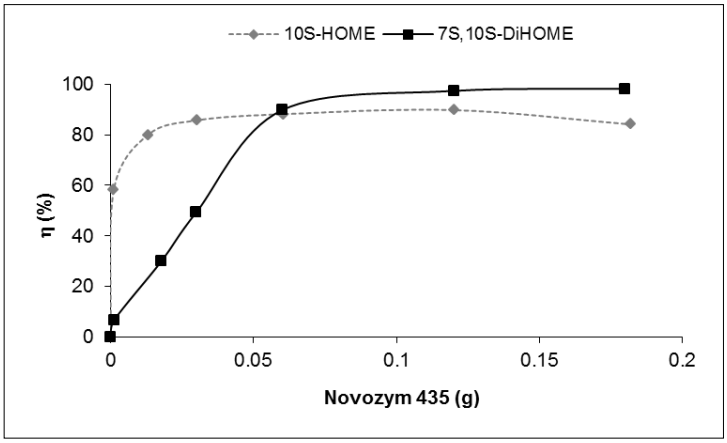

Figure 4.22. Effect of Novozym 435 of the yield of the ethyl esters synthesis with a molar ratio of *trans*-HFA to EtOH of 1:3 at 50ºC during 24 h in a solvent-free medium.

4.6.2.3 Reusability of the enzyme

The synthetic stability of Novozym 435 was studied under the optimal reaction conditions as well as the enzyme weight after each cycle, Figure 4.23. When (10*S*)-HOME was used as substrate, the enzyme synthetic stability remained constant around 79.0% even after ten reaction cycles; and, enzyme weight never exceeded a value of 0.07 g. In contrast, when (7*S*,10*S*)-DiHOME was used, enzyme stability dropped abruptly after the third cycle, reaching a yield of 16.3%. An enzyme stability reduction of 81.4% was detected after five cycles, which occurred with an increase on enzyme weight. After these five trials, the enzyme was rinsed with EtOH to desorb the (7*S*,10*S*)-DiHOME from the Novozym 435 carrier. As a consequence, the enzymatic stability was partially recovered, 37.4%, and within the next five cycles diminished slowly to 19.8%; and, the enzyme weight did not increase as seen in the first five

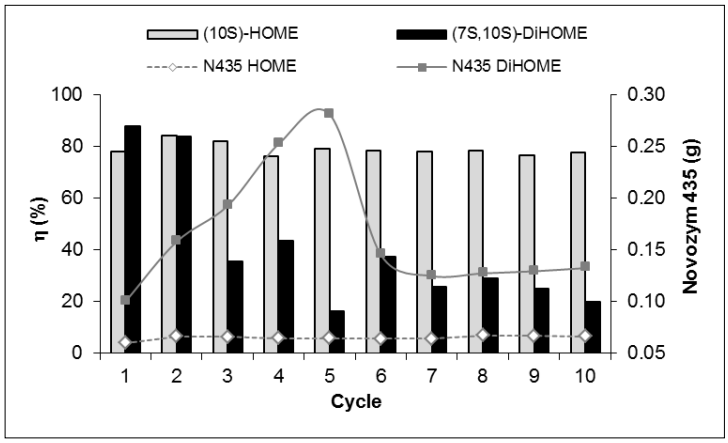

Figure 4.23. Yield of the esterification (bars) and enzyme weight (lines) at each cycle. Optimal reaction conditions were used in all experiments. **HOME**: (10*S*)-HOME. **DiHOME**: (7*S*,10*S*)-DiHOME. **N435 HOME**: Novozym 435 weight when (10*S*)-HOME was used. **N435 DiHOME**: Novozym 435 weight when (7*S*,10*S*)-HOME was used.

cycles. The weight of the enzyme was notably affected by the rinses with EtOH. EtOH removed more quantity of (7*S*,10*S*)-DiHOME than *n*-hexane from the enzyme carrier improving the stability of Novozym 435. This fact indicated that (7*S*,10*S*)-DiHOME was adsorbed on the enzyme carrier compromising the synthetic performance of Novozym 435 under the reaction conditions tested, as it was already demonstrated in the production of estolides from (10*S*)-HOME in *n*-hexane with the same commercial lipase [430], section 4.5.1.2.

4.6.2.4 Structural determination

i. Fourier transformed infrared spectroscopy

One sample of each starting substrate and *trans*-HFA ethyl ester synthesized under optimal reaction conditions was analyzed to determine the functional groups present, Figure A.18. In both cases, FTIR spectra from substrates to their corresponding ethyl esters showed one main difference: the movement of a carbonyl stretch corresponding to the free fatty acid to a carbonyl stretch of an ester bond. In the case of the monohydroxylated compound, a frequency of 1709 cm^{-1} corresponding to the stretching of the carbonyl in an acid moiety moved to a frequency of 1736 cm^{-1} corresponding to the stretching of carbonyl in an ester compound. In the case of the dihydroxyfatty acid, the movement of the carbonyl band shifted from 1693 cm^{-1} to 1738 cm^{-1}. These results agree with the work of Zagonel and co-workers in the ethanolysis of soybean oil [445].

ii. MALDI time-of-flight mass spectrometry

trans-HFA esters synthesized in optimal reaction conditions were analyzed by MALDI-TOF-MS with a DHB lithium matrix to determine the molecular mass of these compounds, Figure 4.24. In the spectrum of (10*S*)-HOME ethyl ester (M), Figure 4.24 A, two groups of ions are noticeable. In the low-mass ion group, an ion of *m/z* 333.2 stands out. This ion corresponds to molecular adduct of M with lithium, $[M+^{7}Li]^{+}$.

The two low-intensity ions of *m/z* 349.2 and 365.2 are important. These are the molecular adducts of M with sodium and potassium, respectively: $[M+^{23}Na]^+$ and $[M+^{39}K]^+$. These three adducts give a molecular mass of M of 326.2 Da. In the second group, there is a high-intensity ion of *m/z* 613.5. This ion is the molecular lithium adduct of a mono-estolide ethyl ester (1M), $[1M+^{7}Li]^+$. Next to this ion, there is a lower-intensity signal of *m/z* 629.5 which

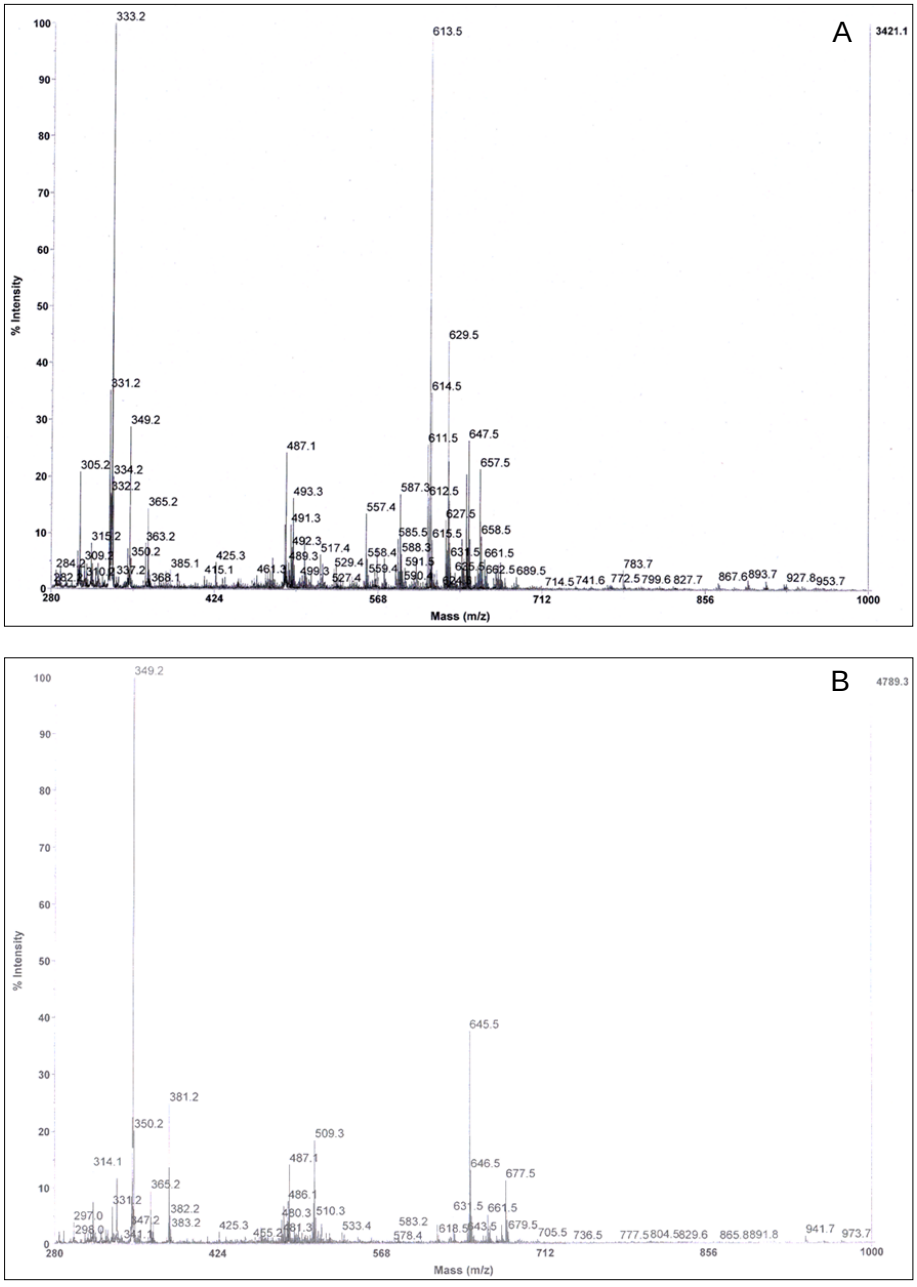

Figure 4.24. MALDI TOF mass spectra of ethyl esters produced in a solvent-free medium. **A**: (10*S*)-HOME ethyl ester. **B**: (7*S*,10*S*)-DiHOME ethyl ester. Ethyl esters were synthesized under optimal conditions: *trans*-HFA:EtOH 1:3 mol·mol^{-1}, 0.06 g of Novozym 435 for (10*S*)-HOME and 0.10 g of Novozym 435 for (7*S*,10*S*)-DiHOME at 50ºC during 24 h.

corresponds to the sodium molecular adduct of 1M, $[1M+^{23}Na]^+$. The molecular mass obtained for the mono-estolide ethyl ester from these two adducts is 606.5 Da. Finally, a very low-intensity ion, *m/z* 893.7, is noticeable. This ion is the lithium adduct of a di-estolide ethyl ester (2M), $[2M+^{7}Li]^+$, with a mass of 886.7 Da.

The (7*S*,10*S*)-DiHOME ethyl ester (M′) spectrum, Figure 4.24 B, shows one main ion of *m/z* 349.2 which corresponds to molecular adduct of M′ with lithium, $[M'+^{7}Li]^+$. Next to it, there are two low-intensity ions of *m/z* 365.2 and 381.2. These two ions represent the molecular adducts of M′ with sodium and potassium, respectively; $[M'+^{23}Na]^+$ and $[M'+^{39}K]^+$. These three adducts give a mass of 342.2 Da for M′. Then, there is another important group ofions in which an *m/z* 645.5 ion stands out. This ion is the molecular adduct of a mono-estolide ethyl ester with lithium, $[1M'+^{7}Li]^+$, and the potassium molecular adduct of 1M′, $[1M'+^{23}Na]^+$, is also noticeable with a mass of 677.5 Da. These two adducts reveal a mass for 1M′ of 638.5 Da. Ultimately, a low-intensity ion of *m/z* 941.7 reveals the formation of a di-estolide ethyl ester, $[2M'+^{7}Li]^+$, with a molecular mass of 934.7 Da.

iii. Nuclear magnetic resonance

As could be observed in (10*S*)-HOME and (7*S*,10*S*)-DiHOME ethyl ester ^{13}C NMR spectra, Figure 4.25 A and B, respectively, a signal for an ester carbonyl appears at 173.76 ppm (C1) [431]; moreover, no signal of an acid carbonyl group, 179.15 ppm, is appreciable in the spectra, indicating a total conversion under the optimal reaction conditions described previously. A double signal of the terminal methyl carbons appeared at 14.00 and 14.15 ppm. The signal of 14.15 ppm corresponds to the methyl carbon of the ethyl ester side chain (C20) and the one at 14.00 ppm to the methyl carbon of the *trans*-HFA side (C18). The signal at 60.10 ppm is due to the methylene carbon of the ethyl ester side (C19); the ones at 72–73 ppm indicate the methine carbons in which the hydroxy groups are bonded (C10 and C7 in the case of dihydroxylated ethyl ester); and the signals at 131–134 ppm represent the olefinic carbons of the *trans* double bond (C8 and C9). Finally, the signals at 34 ppm correspond to the methylene carbon next to the carbonyl moiety in the *trans*-HFA side chain (C2) and the signal of 24 ppm is another methylene on carbon C3.

In (10*S*)-HOME and (7*S*,10*S*)-DiHOME ethyl ester ^{1}H NMR spectra, Figure 4.26 A and B, the signal of the terminal methyl hydrogens are at 0.86 and 1.23 ppm. The downfield signal corresponds to the methyl hydrogens of the ethyl ester side chain (H20) and the other one to the methyl hydrogens of the *trans*-HFA chain (H1). 4.10 ppm represents a downfield methylene hydrogen signal next to ester moiety in the ethyl

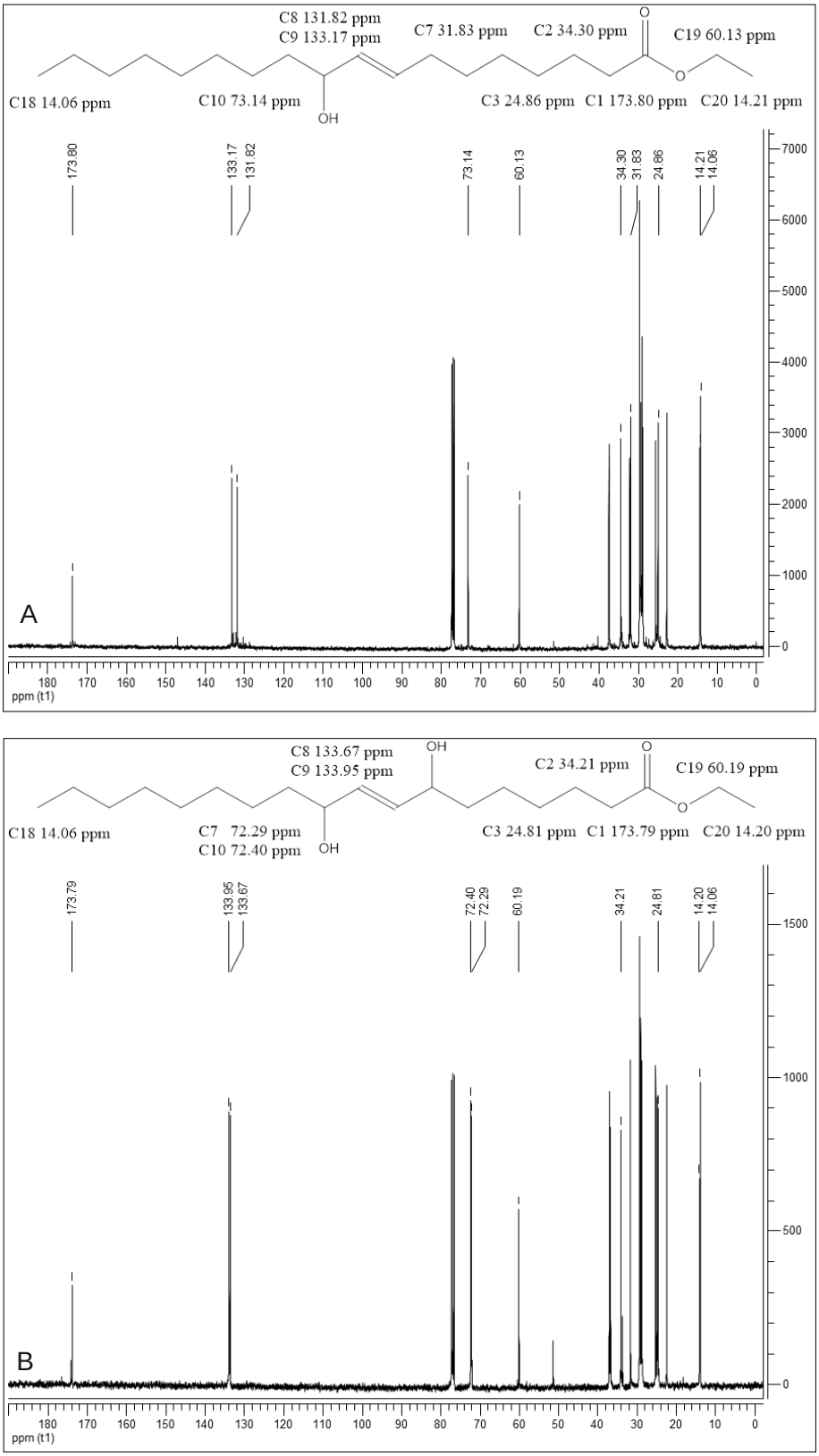

Figure 4.25. ^{13}C NMR spectra of ethyl esters produced in a solvent-free medium. **A**: (10*S*)-HOME ethyl ester. **B**: ^{13}C spectrum of (7*S*,10*S*)-HOME ethyl ester. Ethyl esters were synthesized under optimal conditions: *trans*-HFA:EtOH 1:3 mol·mol^{-1}, 0.06 g of Novozym 435 for (10*S*)-HOME and 0.10 g of Novozym 435 for (7*S*,10*S*)-DiHOME at 50ºC during 24 h. Chemical shifts are expressed in parts per million.

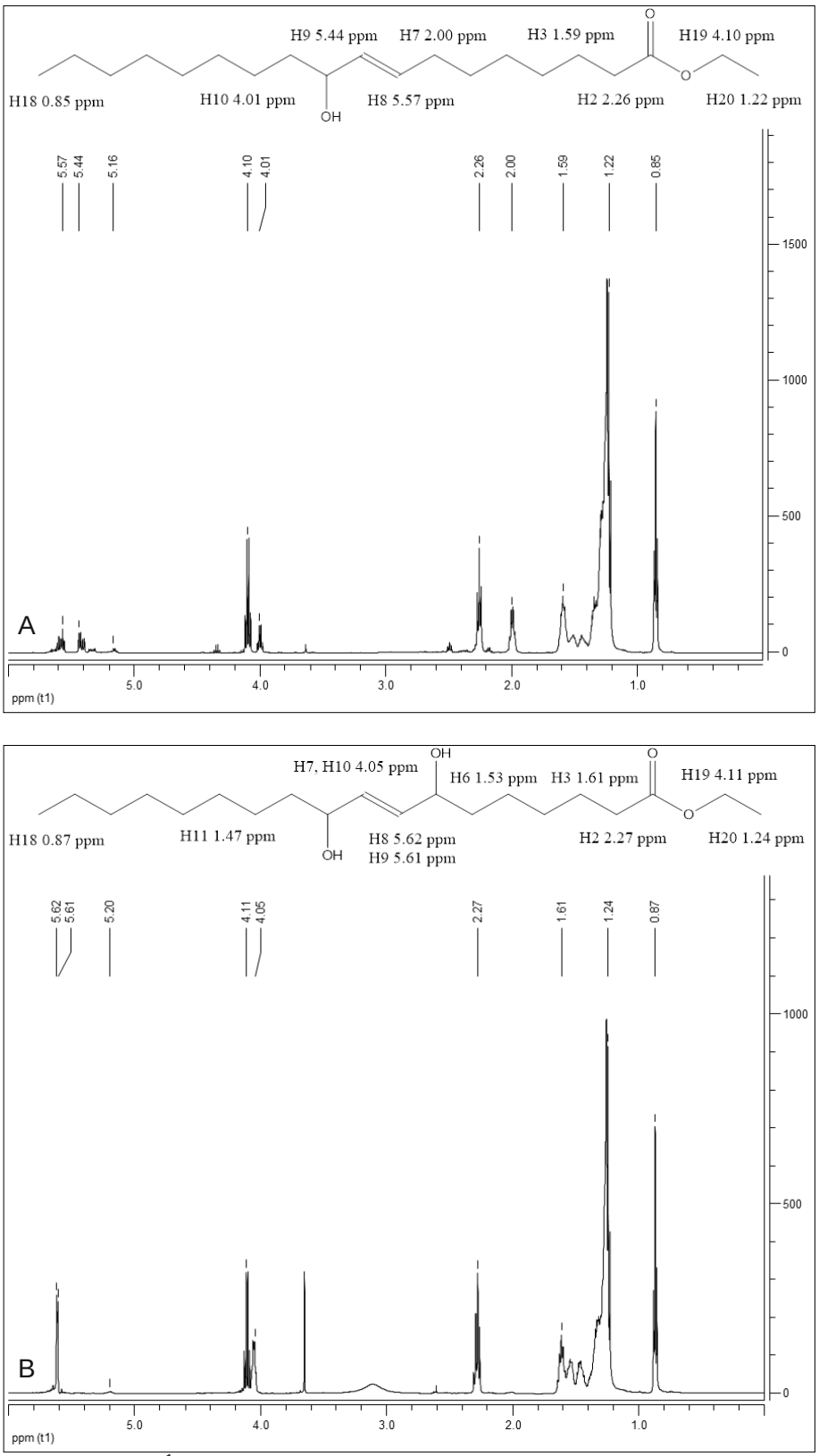

Figure 4.26. ^{1}H NMR spectra of ethyl esters produced in a solvent-free medium. **A**: (10*S*)-HOME ethyl ester. **B**: (7*S*,10*S*)-HOME ethyl ester. Ethyl esters were synthesized under optimal conditions: *trans*-HFA:EtOH 1:3 mol·mol^{-1}, 0.06 g of Novozym 435 for (10*S*)-HOME and 0.10 g of Novozym 435 for (7*S*,10*S*)-DiHOME at 50ºC during 24 h. Chemical shifts are expressed in parts per million. Chemical shifts are expressed in parts per million.

ester side (H19). The methine hydrogens, which are bounded to the same carbon as hydroxyl moiety, have a chemical shift of 4.03 ppm (H10 and H7 in the case of dihydroxylated ethyl ester). In the case of the (10*S*)-HOME ethyl ester, the methylenic hydrogens next to the double bond (H7) appear at 2.00 ppm. Ultimately, the methylene hydrogens H2 and H3 have a chemical shift of 2.26 and 1.60 ppm, respectively. Finally, there is a signal in both ^{1}H NMR spectra which are important. There is a low-intensity quadruplet, 5.18 ppm, in the ^{1}H NMR from the monohydroxylated ethyl ester which corresponds to a methine signal. This methine signal reveals the formation of estolides and is downfielded by the effect of the *trans*-double bond.

The integration of that signal, H10+H10' in the case of the monohydroxylated compounds and H7/10+H7'/10'' for dihydroxylated ones, and compared to non-afected ones let calculate EN [447] using Equation 31a and 31b. EN for the monohydroxylated sample is 0.29. EN indicates that the average formation of estolide ethyl esters is one-third of the sample since an EN value of 1.00 would represent that the whole sample is a mono-estolide. In the case of the dihydroxylated ethyl ester, an EN value of 0.13 was obtained from Equation 31b. This fact reveals that the average formation of estolide ethyl esters is more than one-third of the sample, a 39%; because a EN value of 0.33 would be a for a total mono-estolide sample. The synthesis of mono-estolide ethyl esters confirms the capability of Novozym 435 to synthetize estolides from *trans*-HFA.

4.6.3 Physicochemical properties

trans-FAEE described in section 4.6.1 and 4.6.2 were analysed to determine some of their physicochemical properties as in section 4.5.4.

4.6.3.1 Viscosity determination

trans-HFA ethyl esters were synthetized as alternative aromatic compounds. It must remember that syntheses in a solvent-free medium produced estolides ethyl esters apart from the corresponding ethyl esters. Dynamic or absolute viscosity, η', was determined and Arrhenius-type relationship factors [437] as well, instead of viscosity index. Finally, viscosity values at 40ºC were compared with bibliographic ones [437].

trans-HFA ethyl esters were determined as Newtonian fluids because their viscosity was independent of the shear rate applied. Table 4.12 displays Arrhenius-type parameters A, the infinite-temperature viscosity value, and E_a, the stability of the liquid [438]. A values for ethyl esters ((10*S*)-HOME EE and (7*S*,10*S*)-DiHOME EE), 3490 and 278 10^{-10} Pa·s, are higher than (10*S*)-HOME one, 9.47 10^{-10} Pa·s. Likewise occurs with estolide ethyl esters ((10*S*)-HOME Est EE and (7*S*,10*S*)-DiHOME Est EE), 625 and 7.02 10^{-10} Pa·s. Surprisingly, dihydroxylated esters ((7*S*,10*S*)-DiHOME EE and

Taula 4.12. Viscosity analysis parameters from *trans*-HFA ethyl esters.

Sample	$A \cdot 10^{-10}$ (Pa·s)	E_a (kJ·mol^{-1})	ρ (g·ml^{-1})	ν (cSt)	η (%)	DP
(10*S*)-HOME	9.47	49.9	0.96	205	–	1
(7*S*,10*S*)-DiHOME	–	–	0.99	–	–	1
(10*S*)-HOME EE	3490	29.2	0.94	26	87.0	1
(7*S*,10*S*)-DiHOME EE	278	39.9	1.02	120	90.3	1
(10*S*)-HOME Est EE	625	34.7	0.94	39	90.0	1-2
(7*S*,10*S*)-DiHOME Est EE	7.02	51.2	0.97	240	98.0	1-2

A: Pre-exponential factor. **E_a**: Activation energy. ρ: Density. ν: Kinematic viscosity. η: Reaction yield. **(10*S*)-HOME EE**: (10*S*)-HOME ethyl ester in chloroform. **(7*S*,10*S*)-DiHOME EE**: (7*S*,10*S*)-DiHOME ethyl ester in chloroform. **(10*S*)-HOME Est EE**: (10*S*)-HOME ethyl ester in solvent-free. **(7*S*,10*S*)-DiHOME Est EE**: (7*S*,10*S*)-DiHOME ethyl ester in solvent-free.

(7*S*,10*S*)-DiHOME Est EE) have lower values, 278 and 7.02 10^{-10} Pa·s, than monohydroxylated ones ((10*S*)-HOME EE and ((10*S*)-HOME Est EE) 3490 and 625 10^{-10} Pa·s, despite of having an extra hydroxyl group. On the other hand, E_a values have other pattern. *trans*-ethyl esters ((10*S*)-HOME EE and (7*S*,10*S*)-DiHOME EE) and estolides ethyl esters ((10*S*)-HOME Est EE and (7*S*,10*S*)-DiHOME Est EE) have lower E_a values (29.2, 39.9, 34.7 and 51.2 kJ·mol^{-1}, respectively) than their corresponding substrates. Moreover, ethyl esters have lower E_a values than estolides ethyl esters due to they are simpler molecules and required less energy for flowing.

Kinematic viscosity (ν) values follow the same tendency as E_a. It is broadly know that (m)ethyl esters have lower viscosities values than their corresponding free acids [434]. However, it can be appreciated the difference between mono- and dihydroxylated compounds. Entrance (7*S*,10*S*)-DiHOME EE, 120 cSt, presents a five-fold increment in ν value respected to compound (10*S*)-HOME EE, 26 cSt. Approximately the same increment, six-fold, is observed when ν of the compounds (10*S*)-HOME Est EE, 26 cSt, and (7*S*,10*S*)-DiHOME Est EE, 120 cSt, are compared. As state before, estolide ethyl esters, (10*S*)-HOME Est EE and (7*S*,10*S*)-DiHOME Est EE, present higher ν values because are more complex molecules than ethyl esters, (10*S*)-HOME EE and (7*S*,10*S*)-DiHOME EE.

Different values of ν were found in the literature for biodiesel from castor oil, from 10.75 to 24 cSt [451, 452], slightly low than (10*S*)-HOME ethyl ester enzymatically produced in chloroform, 26 cSt, Table 4.12. Despite of (10*S*)-HOME and RA, the main fatty acid of castor oil, are isomers, the *trans* configuration of the double bond confers higher values of viscosity and the addition of an extra hydroxyl moiety to the molecule, (7*S*,10*S*)-DiHOME EE, sharply increases viscosity values, 120 cSt, affecting the unexplored applications of these new compounds.

Viscosity values of (10*S*)-HOME Est EE and (7*S*,10*S*)-DiHOME Est EE entrances from table 4.12, 39 and 240 cST, respectively, are greater than ones for castor- and lesquerella-2-ethylhexyl estolides, probably mono-estolides, 22 and 15.4 cSt, reported by Cermak and co-workers [441]. They established that 2-ethylhexyl group diminishes viscosity respect to the ethyl group in estolides.

4.6.3.2 Calorimetric analyses

Calorimetric analyses, differential scanning calorimetry (DSC) and thermal gravimetric analysis (TGA), were performanced to determine glass transition temperature (T_g), decomposition enthalpies (ΔH) and residue percentage. As state previously, these thermal analyses were carried out to test the physical and chemical changes of these new compounds, table 4.13.

Taula 4.13. Calorimetric analysis parameters from *trans*-HFA ethyl esters.

Sample	T_g (ºC)	T_{onset1} (ºC)	ΔH_1 ($J \cdot g^{-1}$)	T_{onset2} (ºC)	ΔH_2 ($J \cdot g^{-1}$)	T_{onset3} (ºC)	ΔH_3 ($J \cdot g^{-1}$)	Residue (%)
(10*S*)-HOME	-60	119	-7.08	196	47.33	315	-161.3	0.35
(7*S*,10*S*)-DiHOME	-49	185	37.79	277	-56.16	366	147.3	1.23
(10*S*)-HOME EE	-70	115	-21.64	212	39.44	350	-292.7	0.38
(7*S*,10*S*)-DiHOME EE	-65	114	-6.99	218	40.38	347	-248.9	1.32
(10*S*)-HOME Est EE	-81	93	-21.46	228	38.76	352	-209.3	0.56
(7*S*,10*S*)-DiHOME Est EE	-58	105	-45.84	290	-25.36	365	-181.3	0.93

T_g: Glass transition temperature **T_{onset}**: Initial temperature of ΔH. **ΔH**: Decomposition enthalpy. **(10*S*)-HOME EE**: (10*S*)-HOME ethyl ester in chloroform. **(7*S*,10*S*)-DiHOME EE**: (7*S*,10*S*)-DiHOME ethyl ester in chloroform. **(10*S*)-HOME Est EE**: (10*S*)-HOME ethyl ester in solvent-free. **(7*S*,10*S*)-DiHOME Est EE**: (7*S*,10*S*)-DiHOME ethyl ester in solvent-free.

Table 4.13 shows T_g values of the different ester produced in section 4.6. As could be observed, all ethyl esters and estolides ethyl esters have lower T_g values than their corresponding substrates. Ethyl esters, (10*S*)-HOME EE and (7*S*,10*S*)-DiHOME EE, have lower T_g values, -70 and -65ºC, respectively, than their substrates, (10*S*)-HOME, -60ºC, and (7*S*,10*S*)-DiHOME, -49ºC. Moreover, estolides ethyl esters, (10*S*)-HOME Est EE and (7*S*,10*S*)-DiHOME Est EE, T_g values, -81ºC and -58ºC, are lower than ethyl ester ones, with the exception of entrance (7*S*,10*S*)-DiHOME Est EE, which is abnormally higher. This tendency can be clearly appreciated with monohydroxylated compounds: substrate, -60ºC; (10*S*)-HOME EE, -70ºC; and (10*S*)-HOME Est EE, -81ºC.

Finally, decomposition enthalpies (ΔH) and their initial temperature (T_{onset}) were listed in Table 4.13. In this case, ethyl esters and estolides ethyl esters maintain the three ΔH. Entrance (10*S*)-HOME EE has increases its three T_{onset} (115ºC (-), 212ºC (+) and 350ºC (-)) respecting its substrate, 119ºC (-), 196ºC (+) and 315ºC (-). On the other hand, entrance (7*S*,10*S*)-DiHOME EE has reduced its three T_{onset} (114ºC (-), 218ºC (+), 347ºC (-)) when compared to (7*S*,10*S*)-DiHOME, 185ºC (+), 277ºC (-) and

366ºC (+). Regarding to estolides ethyl esters, no clear tendency is observed on their T_{onset} and ΔH when are compared to their corresponding substrate. Certain variability can be appreciated, even in the sign of the ΔH. However, when compounds are compared within groups, (10*S*)-HOME EE with (7*S*,10*S*)-DiHOME EE and (10*S*)-HOME Est EE with (7*S*,10*S*)-DiHOME Est EE, it can be observed that T_{onset} and ΔH have similar values.

5. Conclusions

The conclusions of this work are:

1. A new non-dispersive aeration system has been designed and implemented successfully, with a k_La of 39.9 h^{-1}, which is lower than traditional bubbling systems.

2. The transformation of oleic acid in *trans*-hydroxy-fatty acids by *P. aeruginosa* 42A2 in bioreactor has been modelled using Monod kinetic model.

3. A new family of estolides from *trans*-hydroxy-fatty acids has been synthesized in *n*-hexane (degree of polymerization: 1-2) and solvent-free media (degree of polymerization: 2-5) with lipases.

4. Saturated (10*S*)-HOME and their corresponding estolides have been enzymatically and chemically produced as an alternative to *trans*-estolides.

5. *trans*-hydroxy-fatty ethyl esters haven been produced in chloroform (degree of polymerization: 1) and in solvent-free media (degree of polymerization: 1-2) with Novozym 435.

6. Liquid chromatography mass spectrometry, MALDI time-of-flight mass spectrometry and nuclear magnetic resonance techniques have been adapted to analyze this two new series of *trans*-esters.

7. These new compounds haven been determined as Newtonian fluids, as well as their amorphous nature.

6. Bibliography

[1] Schörken U, Kempers P. Lipid biotechnology: Industrially relevant production processes. Eur J Lipid Sci Technol 2009;111:627-645.
[2] Metzger JO, Bornscheuer U. Lipids as renewable resources: current state of chemical and biotechnological conversion and diversification. Appl Biochem Biotechnol 2006;71:13-22.
[3] Moser BR. Biodiesel production, properties, and feedstocks. In Vitro Cell Dev-Pl 2009;45:229-266.
[4] Pigulevskh G, Charik N. Decomposition of olive oil under the influence of the vital activity of some micro-organisms; transformation of oleic acid into ketostearic acid. Biochemische Zeitschrift 1928;200.
[5] Davis EN, Wallen LL, Goodwin JC, Rohwedder WK, Rhodes RA. Microbial hydration of *cis*-9-alkenoic acids. Lipids 1969;4:356-362.
[6] Wallen LL, Benedict RG, Jackson RW. The microbiological production of 10-hydroxystearic acid from oleic acid. Archives of Biochemistry and Biophysics 1962;99:249-253.
[7] Schroepfer GJ. Enzymatic Stereospecificity in the Conversion of Oleic Acid to 10-Hydroxystearic Acid. Journal of American Oil Chemical Society 1965;87:1411-1412.
[8] Wilde PF, Dawson RMC. The biohydrogenation of α-linoleic acid and oleic acid by rumen micro-organisms. Biochem J 1966;98:469-475.
[9] Ogata K, Osugi M, Tochikura T. Fatty acid metabolism in microorganisms. II. Production of a-ketoglutaric acid from fatty acids. Agr Biol Chem 1966;30:1024-1029.
[10] Bekhtereva MN, Dedyukhina EO. Oleic acid as a carbon source for the growth of *Blakeslea trispora* and for biosynthesis of carotenoids and lipids. Mikrobiologiya 1970;39:77-81.
[11] Heinz E, Tulloch AP, Spencer JFT. Fermentation of long-chain compounds by *Torulopsis sp*. VII. Hydroxylation of oleic acid by cell-free extracts of a species of *Torulopsis*. BBA-Lipid Lipid Met 1970;202:49-55.
[12] White RW, Kemp P, Dawson RMC. Isolation of rumen bacterium that hydrogenates oleic acid as well as linoleic acid and linolenic acid. Biochem J 1970;116:767-768.
[13] Kepler CR, Tove SB. Induction of biohydrogenation of oleic acid in *Bacillus cereus* by increase in temperature. Biochem Bioph Res Co 1973;52:1434-1439.
[14] Kemp P, White RW, Lander DJ. Hydrogenation of unsaturated fatty acids by five bacterial isolates from the sheep rumen, including a new species. J Gen Microbiol 1975;90:100-114.
[15] Vuillemin N, Leluan G, Bory J. Degradation of oleic acid by various microorganisms. Ann Pharm Fr 1979;37:181-184.
[16] Thomas PJ. Identification of some enteric bacteria which convert oleic acid to hydroxystearic acid in vitro. Gastroenterology 1972;62:430-435.
[17] Mankovskaya NK, Kobilinskaya IF, Maskaev AK, Krasnova SI. Hydroxylation of oleic acid to monohydroxystearic acid for manufacturing lubricants. Sb tr Vses obedin Neftekhim 1973;5:22-26.
[18] Niehaus WG, Kisic A, Torkelson A, Bednarczyk DJ, Schroepfer GJ. Stereospecific hydration of the D9 double bond of oleic acid. JBiol Chem 1970;245:3790-3797.
[19] Mortimer CE, Niehaus WG. Enzymic isomerization of oleic acid to *trans*-D10-octadecenoic acid. Biochem Bioph Res Co 1972;49:1650-1656.
[20] Howling D, Morris LJ, Gurr MI, James AT. Specificity of fatty acid desaturases and hydroxylases. Dehydrogenation and hydroxylation of monoenoic acids. BBA-Lipid Lipid Met 1972;260:10-19.
[21] Mortimer CE, Niehaus WG. Enzymic interconversion of oleic acid, 10-hydroxyoctadecanoic acid, and *trans*-D10-octadecenoic acid. Reaction pathway and stereospecificity. JBiol Chem 1974;249:2833-2842.
[22] Seo CW, Yamada Y, Takada N, Okada H. Hydration of squalene and oleic acid by Corynebacterium sp. S-401. Agr Biol Chem 1981;45:2025-2030.
[23] Litchfield JH, Pierce GE. Microbiological synthesis of hydroxy-fatty acids and keto-fatty acids. US 4582804 A 19860415 1986.
[24] Koritala S, Hosie L, Hou CT, Hesseltine CW, Bagby MO. Microbial conversion of oleic acid to 10-hydroxystearic acid. Appl Biochem Biotechnol 1989;32:299-304.
[25] Koritala S, Hosie L, Bagby MO. Oleic acid conversion to 10-hydroxystearic acid by *Nocardia* species. Proc - World Conf Biotechnol Fats Oils Ind 1989:298-300.
[26] Takatori T, Ishiguro N, Tarao H, Matsumiya H. Microbial production of hydroxy and oxo fatty acids by several microorganisms as a model of adipocere formation. Forensic Sci Int 1986;32:5-11.

[27] Takatori T, Gotouda H, Terazawa K, Mizukami K, Nagao M. The mechanism of experimental adipocere formation: substrate specificity on microbial production of hydroxy and oxo fatty acids. Forensic Sci Int 1987;35:277-281.
[28] Gotouda H, Takatori T, Terazawa K, Nagao M, Tarao H. The mechanism of experimental adipocere formation: hydration and dehydrogenation in microbial synthesis of hydroxy and oxo fatty acids. Forensic Sci Int 1988;37(4):249-257.
[29] Soda K, Kido T. Manufacture of hydroxy unsaturated fatty acids with *Bacillus pumilus*. JP 01051092 A 19890227 1989.
[30] Soda K. Biotransformation of oleic acid to ricinoleic acid. Proc - World Conf Biotechnol Fats Oils Ind 1988:178-179.
[31] E. Mercade MR, M. J. Espuny, M. P. Bosch, M. A. Manresa, J. L. Parra and J. Guinea. New surfactant isolated from *Pseudomonas* 42A2. Journal of American Oil Chemists' Society 1988;65:1915-1916.
[32] Ohsugi M, Inoue Y. Formation of pimelic and azelaic acids, biotin intermediates, derived from oleic acid by Micrococcus sp. Agr Biol Chem 1981;45:2355-2356.
[33] Yi ZH, Rehm HJ. Bioconversion of elaidic acid to Δ9-*trans*-1,18-octadecenedioic acid by *Candida tropicalis* Appl Biochem Biotechnol 1988;29:305-309.
[34] Z.H. Yi, Rehm HJ. Identification and production of Δ9-cis-1,18-octadecenedioic acid by Candida tropicalis Appl Biochem Biotechnol 1989;30:327-331.
[35] Hill RJ, Prescott DJ, Spence SL, Conner RL. Characterization of an unsaturated fatty acid auxotroph of Tetrahymena thermophila. BBA-Lipid Lipid Met 1983;754:150-158.
[36] Blank W, Takayanagi H, Kido T, Meussdoerffer F, Esaki N, Soda K. Transformation of oleic acid and its esters by *Sarcina lutea*. Agr Biol Chem 1991;55:2651-2652.
[37] Yang W, Dostal L, Rosazza JP. Stereospecificity of microbial hydrations of oleic Acid to 10-hydroxystearic Acid. App Environ Microb 1993;59:281-284.
[38] Kaneshiro T, Huang J-K, Weisleder D, Bagby MO. 10(R)-Hydroxystearic acid production by a novel microbe, NRRL B-14797, isolated from compost. J Ind Microbiol 1994;13:351-355.
[39] Hudson JA, MacKenzie CA, Joblin KN. Conversion of oleic acid to 10-hydroxystearic acid by two species of ruminal bacteria. Appl Microbiol Biotechnol 1995;44:1-6.
[40] Chai W, Li Z. Hydroxylation of oleic acid by *Nocardia sp.* Shengwu Gongcheng Xuebao 1995;11:356-360.
[41] El-Sharkawy SH, Rosazza JPN. Microbial transformation of lipids: Selective hydration of oleic acid. Bulletin of Pharmaceutical Sciences, Assiut University 1995;18:103-106.
[42] Hudson JA, Mackenzie CA, Joblin KN. Factors affecting the formation of 10-hydroxystearic acid from oleic acid by a ruminal strain of *Enterococcus faecalis*. Appl Microbiol Biotechnol 1996;45:404-407.
[43] Latrasse A, Paitier S, Lachot B, Bonnarme P, Feron G, Durand A, Quere JLL. Conversion of oleic acid to 10-hydroxystearic acid by *Nocardia paraffinae*. Biotechnol Lett 1997;19:715-718.
[44] Morvan B, Joblin KN. Hydration of oleic acid by *Enterococcus gallinarum*, *Pediococcus acidilactici* and *Lactobacillus sp.* isolated from the rumen. Anaerobe 1999;5:605-611.
[45] El-Sharkawy SH, Yang W, Dostal L, Rosazza JP. Microbial oxidation of oleic acid. App Environ Microb 1992;58:2116-2122.
[46] Lanser AC. Conversion of oleic acid to 10-ketostearic acid by a *Staphylococcus* species. JAOCS 1993;70:543-545.
[47] Hou CT. Production of 10-ketostearic acid from oleic acid by *Flavobacterium sp.* strain DS5 (NRRL B-14859). App Environ Microb 1994;60:3760-3763.
[48] Iwate M. Production of 10-ketostearic acid from oleic acid by a strain of *Flavobacterium sp.* 12-4A. Biotechnol Lett 1995;17:493-496.
[49] Lanser AC, Nakamura LK. Identification of a *Staphylococcus warneri* species that converts oleic acid to 10-ketostearic acid. Curr Microbiol 1996;32:260-263.
[50] Kuo TM, Lanser AC, Kaneshiro T, Hou CT. Conversion of oleic acid to 10-ketostearic acid by *Sphingobacterium sp.* Strain 022. JAOCS 1999;76:709-712.
[51] Gotouda H. Production of hydroxy and oxo fatty acids by microorganisms as a model of adipocere formation. The Hokkaido journal of medical science 1991;66:142-150.
[52] Takatori T. Investigations on the mechanism of adipocere formation and its relation to other biochemical reactions. Forensic Sci Int 1996;80:49-61.

[53] Picataggio S, Rohrer T, Eirich LD. Method for increasing the w-hydroxylase activity of *Candida tropicalis* in the manufacture of a,w-dicarboxylic acids. WO 9114781 A1 19911003 1991.

[54] Fabritius D, Schaefer HJ, Steinbuechel A. Identification and production of *cis*-3-hydroxy-1,18-octadec-9-enedioic acid by mutants of *Candida tropicalis*. Appl Microbiol Biotechnol 1996;45:342-348.

[55] Fabritius D, Schafer HJ, Steinbuchel A. Microbial production of 3-hydroxydicarboxylic acids by *Candida tropicalis* M25. Schriftenreihe "Nachwachsende Rohstoffe" 1998;10:231-237.

[56] Farbood MI, Morris JA, McLean LB. Fermentation process for preparing 10-hydroxy-C18-carboxylic acid and gamma-dodecalactone derivatives. EP 578388 A2 19940112 1994.

[57] Gocho S, Tabogami N, Inagaki M, Kawabata C, Komai T. Biotransformation of oleic acid to optically active g-dodecalactone. Biosci Biotech Bioch 1995;59:1571-1572.

[58] Hosoi K, Ookawa T. Microbial manufacture of g-dodecalactone from oleic acid. JP 07274986 A 19951024 1995.

[59] Haffner T, Tressl R. Biosynthesis of (R)-g-decanolactone in the yeast *Sporobolomyces odorus*. J Agr Food Chem 1996;44:1218-1223.

[60] Kaneshiro T, Vesonder RF, Peterson RE, Weisleder D, Bagby MO. 9(Z)-Octadecenamide and fatty amides by *Bacillus megaterium* (B-3437) conversion of oleic acid. JAOCS 1994;71:491-494.

[61] Kaneshiro T, Nakamura LK, Bagby MO. Oleic acid transformations by selected strains of *Sphingobacterium thalpophilum* and *Bacillus cereus* from composted manure. Curr Microbiol 1995;31:62-67.

[62] Rau U, Manzke C, Wagner F. Influence of substrate supply on the production of sophorose lipids by *Candida bombicola* ATCC 22214. Biotechnol Lett 1996;18:149-154.

[63] Vollbrecht E, Rau U, Lang S. Microbial conversion of vegetable oils into surface-active di-, tri-, and tetrasaccharide lipids (biosurfactants) by the bacterial strain *Tsukamurella* spec. Fett/Lipid 1998;101:389-394.

[64] Eggink G, Wal Hvd, Huijberts G, Gern NM, Waard Pd. Oleic acid as a substrate for poly-3-hydroxyalkanoate formation in *Alcaligenes eutrophus* and *Pseudomonas putida*. Ind Crop Prod 1992;1:157-163.

[65] Waard Pd, Wal Hvd, Huijberts GN, Eggink G. Heteronuclear NMR analysis of unsaturated fatty acids in poly(3-hydroxyalkanoates). Study of beta-oxidation in *Pseudomonas putida*. The Journal of Biological Chemistry 1993;268:315-319.

[66] Tan IKP, Kumar KS, Theanmalar M, Gan SN, Gordon B. Saponified palm kernel oil and its major free fatty acids as carbon substrates for the production of polyhydroxyalkanoates in *Pseudomonas putida* PGA1. Appl Microbiol Biotechnol 1997;47:207-211.

[67] Zhang G, Wu Q, Tian W, Hong K, Sun S, Zhang R, Chen G. Production of medium chain length polyhydroxyalkanoates by *Pseudomonas mendocina* 0806 from related and unrelated carbon sources. Tsinghua Science and Technology 1999;4:1535-1538.

[68] Majid MIA, Hori K, Akiyama M, Doi Y. Production of poly(3-hydroxybutyrate) from plant oils by *Alcaligenes sp.* Studies in Polymer Science 1994;12:417-424.

[69] Lee SY, Chang HN. Production of poly(3-hydroxybutyric acid) by recombinant *Escherichia coli* strains: genetic and fermentation studies. Canadian Journal of Microbiology 1995;41:1207-1215.

[70] Lee SY, Lee YK, Chang HH. Stimulatory effects of amino acids and oleic acid on poly(3-hydroxybutyric acid) synthesis by recombinant *Escherichia coli*. J Ferment Bioeng 1995;79:177-180.

[71] Lee Y, Lee SH, Lee SY. Fed-batch culture of *Aeromonas hydrophila* for the production of poly(3-hydroxybutyrate-co-3-hydroxyhexanoate) using two carbon sources. Biotechnology and Bioprocess Engineering 1999;4:195-198.

[72] Lanser AC, Plattner RD, Bagby MO. Production of 15-, 16- and 17-hydroxy-9-octadecenoic acids by bioconversion of oleic acid with *Bacillus pumilus*. JAOCS 1992;69:363-366.

[73] Esaki N, Ito S, Blank W, Soda K. Biotransformation of oleic acid by *Alcaligenes sp.* 5-18, a bacterium tolerant to high concentrations of oleic acid. J Ferment Bioeng 1994;77:148-151.

[74] Esaki N, Ito S, Blank W, Soda K. Biotransformation of oleic acid by *Micrococcus luteus* cells. Biosci Biotech Bioch 1994;58:319-321.

[75] Lanser AC. Bioconversion of oleic acid to a series of keto-hydroxy and dihydroxy acids by *Bacillus* species NRRL BD-447: identification of 7-hydroxy-16-oxo-9-cis-octadecenoic acid. JAOCS 1998;75:1809-1813.
[76] Lanser AC, Manthey LK. Bioconversion of oleic acid by *Bacillus* strain NRRL BD-447: identification of 7-hydroxy-17-oxo-9-cis-octadecenoic acid. JAOCS 1999;76:1023-1026.
[77] Rozes N, Marques JF, Peres C. Fermentation of olive mill wastewater by *Lactobacillus plantarum*. Acta Horticulturae 1999;474:735-740.
[78] Thomas T, Reddy A, Nuccio M, Freyssinet G. D-6-desaturase of *Synechocystis*, and cloning and expression of its gene for manufacture of g-linolenic acid. WO 9306712 A1 19930415 1993.
[79] Cripps C, Borgeson C, Blomquist GJ, Renobales MD. The D12-desaturase from the house cricket, *Acheta domesticus* (*Orthoptera: Gryllidae*): characterization and form of the substrate. Arch Biochem Biophys 1990;278:46-51.
[80] Lomascolo A, Dubreucq E, Galzy P. Study of the D12-desaturase system of *Lipomyces starkeyi*. Lipids 1996;31:253-259.
[81] Pinot F, Salaun JP, Bosch H, Lesot A, Mioskowski C, Durst F. w-Hydroxylation of Z-9-octadecenoic, Z-9,10-epoxystearic and 9,10-dihydroxystearic acids by microsomal cytochrome P450 systems from *Vicia sativa*. Biochem Bioph Res Co 1992;184:183-193.
[82] Pinot F, Bosch H, Alayrac C, Mioskowski C, Vendais A, Durst F, Salaun JP. w-Hydroxylation of oleic acid in Vicia sativa microsomes. Inhibition by substrate analogs and inactivation by terminal acetylenes. Plant Physiol 1993;102:1313-1318.
[83] Blee E, Schuber F. Efficient epoxidation of unsaturated fatty acids by a hydroperoxide-dependent oxygenase. The Journal of Biological Chemistry 1990;265:12887-12894.
[84] Hamberg M, Hamberg G. Hydroperoxide-dependent epoxidation of unsaturated fatty acids in the broad bean (*Vicia faba L.*). Arch Biochem Biophys 1990;283:409-416.
[85] Hamberg M, Hamberg G. Peroxygenase-catalyzed fatty acid epoxidation in cereal seeds. Sequential oxidation of linoleic acid into 9(S),12(S),13(S)-trihydroxy-10(E)-octadecenoic acid. Plant Physiol 1996;110:807-815.
[86] Certik M, Nakahara T, Kamisaka Y. Oleate 6-hydroxylase activity in the membrane fraction from an oleaginous fungus, *Mortierella ramanniana var. angulispora*. Biochim Biophys Acta 1996;1304:56-64.
[87] Pei M, Huo R. Study on kinetics of oxidation of oleic acid catalyzed with soybean lipoxygenase. Huanan Ligong Daxue Xuebao, Ziran Kexueban 1996;24:15-20.
[88] Hou CT, Bagby MO, Plattner RD, Koritala S. A novel compound, 7,10-dihydroxy-8(E)-octadecenoic acid from oleic acid by bioconversion. JAOCS 1991;68:99-101.
[89] Hou CT, Bagby MO. 10-Hydroxy-8(*Z*)-octadecenoic acid, an intermediate in the bioconversion of oleic acid to 7,10-dihydroxy-8(*E*)-octadecenoic acid. J Ind Microbiol 1992;9:103-107.
[90] Gardner HW, Hou CT. All (*S*) stereoconfiguration of 7,10-dihydroxy-8(*E*)-octadecenoic acid from bioconversion of oleic acid by *Pseudomonas aeruginosa*. JAOCS 1999;76:1151-1156.
[91] Adam P, Hannemann K, Reiner J, Spiteller G. 10-hydroxystearic acid - identified after homogenization of tissue - is derived from bacteria. Zeitschrift fuer Naturforschung, C: Journal of Biosciences 2000;55:965-970.
[92] Jenkins TC, AbuGhazaleh AA, Freeman S, Thies EJ. The production of 10-hydroxystearic and 10-ketostearic acids is an alternative route of oleic acid transformation by the ruminal microbiota in cattle. J Nutr 2006;136:926-931.
[93] Yu I-S, Yeom S-J, Kim H-J, Lee J-K, Kim Y-H, Oh D-K. Substrate specificity of Stenotrophomonas nitritireducens in the hydroxylation of unsaturated fatty acids. Appl Microbiol Biotechnol 2008;78:157-163.
[94] Kuo TS, Nakamura LK. Diversity of oleic acid, ricinoleic acid and linoleic acid conversions among *Pseudomonas aeruginosa* strains. Curr Microbiol 2004;49:261-266.
[95] Kuo TM, Lanser AC, Nakamura LK, Hou CT. Production of 10-ketostearic acid and 10-hydroxystearic acid by strains of *Sphingobacterium thalpophilum* isolated from composted manure. Curr Microbiol 2000;40:105-109.
[96] Kuo TM, Kaneshiro T. Selection of saprophytic bacteria and characterization of their fatty acid bioconversions during compost formation. ACS Symposium Series 2001;776:55-64.
[97] Kuo TM. Conversion of unsaturated fatty acids by compost bacteria. Abstracts of Papers, 225th ACS National Meeting, New Orleans, LA, United States 2003;March 23-27.

[98] Kim B-N, Yeom S-J, Oh D-K. Conversion of oleic acid to 10-hydroxystearic acid by whole cells of *Stenotrophomonas nitritireducens*. Biotechnol Lett 2011;33:993-997.
[99] Oh DG, Kim BN. Fermentative preparation of 1-hydroxy-stearic acid from oleic by *Stenotrophomonas nitritireducens*. Repub Korean Kongkae Taeho Kongbo 2012;KR 2012029905 A 20120327.
[100] Heo S-H, Kim BS. Production and recovery of oxygenated fatty acids from oleic acid by *Flavobacterium sp.* strain DS5. Hwahak Konghak 2009;47:620-623.
[101] Kim MH, Park MS, Chung C-H, Kim CT, Kim YS, Kyung KH. Conversion of unsaturated food fatty acids into hydroxy fatty acids by lactic acid bacteria. J Microbiol Biotechn 2003;13:360-365.
[102] Jeon E-Y, Lee J-H, Yang K-M, Joo Y-C, Oh D-K, Park J-B. Bioprocess engineering to produce 10-hydroxystearic acid from oleic acid by recombinant *Escherichia coli* expressing the oleate hydratase gene of *Stenotrophomonas maltophilia*. Process Biochem 2012;47:941-947.
[103] Joo Y-C, Seo E-S, Kim Y-S, Kim K-R, Park J-B, Oh D-K. Production of 10-hydroxystearic acid from oleic acid by whole cells of recombinant *Escherichia coli* containing oleate hydratase from *Stenotrophomonas maltophilia*. J Biotechnol 2012;158:17-23.
[104] Kim B-N, Joo Y-C, Kim Y-S, Kim K-R, Oh D-K. Production of 10-hydroxystearic acid from oleic acid and olive oil hydrolyzate by an oleate hydratase from *Lysinibacillus fusiformis*. Appl Microbiol Biotechnol 2012;95:929-937.
[105] Oh DG, Kim BN, Park JB. Oleate hydratase and method using recombined microorganism containing the same for manufacturing 10-hydroxystearic acid. Repub Korean Kongkae Taeho Kongbo 2013;KR 2013001039 A 20130103.
[106] Volkov A, Liavonchanka A, Kamneva O, Fiedler T, Goebel C, Kreikemeyer B, Feussner I. Myosin cross-reactive antigen of *Streptococcus pyogenes* M49 encodes a fatty acid double bond hydratase that plays a role in oleic acid detoxification and bacterial virulence. JBiol Chem 2010;285:10353-10361.
[107] Yang B, Chen H, Song Y, Chen YQ, Zhang H, Chen W. Myosin-cross-reactive antigens from four different lactic acid bacteria are fatty acid hydratases. Biotechnol Lett 2013;35:75-81.
[108] Tressl R, Garbe L-A, Lange H. Biosynthesis of optically active lactones by lipoxygenase/peroxygenase catalyzed pathways in yeast. Frontiers of Flavour Science, [Proceedings of the Weurman Flavour Research Symposium], 9th, Freising, Germany 2000:383-388.
[109] Okamoto K, Chimori M, Iwanaga F, Hattori T, Yanase H. Production of gamma-lactones by the brown-rot basidiomycete *Piptoporus soloniensis*. J Biosci Bioeng 2002;94:182-185.
[110] Komai T. Production of aroma chemicals by biochemical methods. Koryo 2010;247:83-89.
[111] Wanikawa A, Shoji H, Hosoi K, Nakagawa K-I. Stereospecificity of 10-Hydroxystearic acid and formation of 10-Ketostearic acid by lactic acid bacteria. J Am Soc Brew Chem 2002;60:14-20.
[112] Li H. Method for producing natural perfume g-dodecalactone with microbial transformation. Faming Zhuanli Shenqing 2011;CN 101967503 A 20110209.
[113] Wanikawa A, Hosoi K, Kato T. Conversion of unsaturated fatty acids to precursors of g-lactones by lactic acid bacteria during the production of malt whisky. J Am Soc Brew Chem 2000;58:51-56.
[114] Alkyl-g-lactones fungicides. Fr Demande 2000;FR 2780972 A1 20000114.
[115] Hudson JA, Cai Y, Corner RJ, Morvan B, Joblin KN. Identification and enumeration of oleic acid and linoleic acid hydrating bacteria in the rumen of sheep and cows. J Appl Microbiol 2000;88:286-292.
[116] Vossenberg JLCMvd, Joblin KN. Biohydrogenation of C18 unsaturated fatty acids to stearic acid by a strain of *Butyrivibrio hungatei* from the bovine rumen. Lett Appl Microbiol 2003;37:424-428.
[117] Mosley EE, Powell GL, Riley MB, Jenkins TC. Microbial biohydrogenation of oleic acid to *trans* isomers in vitro. J Lipid Res 2002;43:290-296.
[118] AbuGhazaleh AA, Riley MB, Thies EE, Jenkins TC. Dilution rate and pH effects on the conversion of oleic acid to *trans* C18:1 Positional isomers in continuous culture. J Diary Sci 2005;88:4334-4341.

[119] Mosley EE, Nudda A, Corato A, Rossi E, Jenkins T, McGuire MA. Differential biohydrogenation and isomerization of [U-(13)C]oleic and [1-(13)C]oleic acids by mixed ruminal microbes. Lipids 2006;41:513-517.

[120] Wiechers JW, Groenhof FJ, Wortelncent VAL, Miller RM, Hindle NA, Drewitt-Barlow A. Octadecenedioic acid for a more even skin tone. Cosmet Toiletries 2002;117:55-68.

[121] Eschenfeldt WH, Zhang Y, Samaha H, Stols L, Eirich LD, Wilson CR, Donnelly MI. Transformation of fatty acids catalyzed by cytochrome P450 monooxygenase enzymes of *Candida tropicalis*. App Environ Microb 2003;69:5992-5999.

[122] Zibek S, Wagner W, Hirth T, Rupp S, Huf S. Fermentative manufacture of the a,w-dicarboxylic acid 1,18-octadecenedicarboxylic acid as a starting material for bio-based plastics. Chemie Ingenieur Technik 2009;81:1797-1808.

[123] Levinson WE, Kuo TM, Kurtzman CP. Production of Fatty Amides via Biocatalysis - A Brief Overview. Abstracts, 36th Great Lakes Regional Meeting of the American Chemical Society, Peoria, IL, United States, 2004.

[124] Kuo TM, Levinson WE. Biocatalytic production of 10-hydroxystearic acid, 10-ketostearic acid, and their primary fatty amides. JAOCS 2006;83:671-675.

[125] Gumienna M, Lasik M, Roszyk H, Czarnecki Z. Oleic acid as a hydrophobic carbon source in biosynthesis of surface active compounds by *Candida bombicola* yeast. Zywnosc 2002;9:43-53.

[126] Solaiman DKY, Ashby RD, Nunez A, Foglia TA. Production of sophorolipids by *Candida bombicola* grown on soy molasses as substrate. Biotechnol Lett 2004;26:1241-1245.

[127] Solaiman DKY, Ashby RD, Zerkowski JA, Foglia TA. Simplified soy molasses-based medium for reduced-cost production of sophorolipids by *Candida bombicol*a. Biotechnol Lett 2007;29:1341-1347.

[128] Fukuoka T, Morita T, Konishi M, Imura T, Kitamoto D. Characterization of new glycolipid biosurfactants, tri-acylated mannosylerythritol lipids, produced by *Pseudozyma* yeasts. Biotechnol Lett 2007;29:1111-1118.

[129] Fukuoka T, Kawamura M, Morita T, Imura T, Sakai H, Abe M, Kitamoto D. A basidiomycetous yeast, *Pseudozyma crassa*, produces novel diastereomers of conventional mannosylerythritol lipids as glycolipid biosurfactants. Carbohyd Res 2008;343:2947-2955.

[130] Kim HS, Cho DH, Kim BH, Oh HM, Kim GN, Ahn CY, Hwang GY. Cost-effective method for preparing glycolipid surfactant using *Pseudozyma sp.* Repub Korean Kongkae Taeho Kongbo 2012;KR 2012130965 A 20121204.

[131] Song J-W, Jeon E-Y, Song D-H, Jang H-Y, Bornscheuer UT, Oh D-K, Park J-B. Multistep Enzymatic Synthesis of Long-Chain a,w-Dicarboxylic and w-Hydroxycarboxylic Acids from Renewable Fatty Acids and Plant Oils. Angewandte Chemie, International Edition 2013;52:2534-2537.

[132] Wu Z, Weng P, Bajpai RK. Metabolic characteristic and product analysis for bioconversion of oleic acid by *Bacillus pumilus*. Zhongguo Liangyou Xuebao 2007;22:87-90.

[133] Wu Z-F, Bajpai RK, Yan W. Screening for w-1-hydroxy fatty acid over-producing mutants for bioconversion of oleic acid by combining general mutagenesis and specific selection. Biocatal Biotransfor 2008;26:444-449.

[134] Lu W, Yang Y, Zhang X, Xie W, Cai M, Gross RA. Fatty acid biotransformations: W-hydroxy- and W-carboxy fatty acid building blocks using a engineered yeast biocatalyst. Polymer Preprints (American Chemical Society, Division of Polymer Chemistry) 2009;50.

[135] Budde M, Maurer SC, Schmid RD, Urlacher VB. Cloning, expression and characterisation of CYP102A2, a self-sufficient P450 monooxygenase from *Bacillus subtilis*. Appl Microbiol Biotechnol 2004;66:180-186.

[136] Akakabe Y, Matsui K, Kajiwara T. a-Oxidation of long-chain unsaturated fatty acids in the marine green alga *Ulva pertusa*. Biosci Biotech Bioch 2000;64:2680-2681.

[137] Huang J-K, Sershon VC, Wells KD, Gessner RV, Keudell KC, Wen L. Bioconversion of oleic acid to 7-hydroxy-8-octadecenoic and 7,10-dihydroxy-8-octadecenoic acids by *Pseudomonas aeruginosa* was enhanced in the presence of a yeast. Abstracts of Papers, 222nd ACS National Meeting, Chicago, IL, United States 2001.

[138] Huang J-K, Wen L, Gessner RV, Keudell KC. Conversion of oleic acid to 7-hydroxy-8-octadecenoic acid by lipoxygenase from *Pseudomonas aeruginosa* 2HS. Abstracts, 38th Midwest Regional Meeting of the American Chemical Society, Columbia, MO, United States, 2003;114.

[139] Rodriguez E, Espuny MJ, Manresa A, Guerrero A. Identification of (E)-11-hydroxy-9-octadecenoic acid and (E)-9-hydroxy-10-octadecenoic acid by biotransformation of oleic acid by *Pseudomonas sp.* 32T3. JAOCS 2001;78:593-597.

[140] Weil K, Gruber P, Heckel F, Harmsen D, Schreier P. Selective (R)-3-hydroxylation of FA by *Stenotrophomonas maltophilia*. Lipids 2002;37:317-323.

[141] Wallbrunn Av, Richnow HH, Neumann G, Meinhardt F, Heipieper HJ. Mechanism of *cis-trans* isomerization of unsaturated fatty acids in *Pseudomonas putida*. J Bacteriol 2003;185:1730-1733.

[142] Oh DG, Yoo IS, Kim HJ, Kim YH. Method for producing fatty acid with hydroxy group by using *Stenotrophomonas acidaminiphila*. Repub Korean 2008;KR 824969 B1 20080428.

[143] Orellana-Coca C, Toernvall U, Adlercreutz D, Mattiasson B, Hatti-Kaul R. Chemo-enzymatic epoxidation of oleic acid and methyl oleate in solvent-free medium. Biocatal Biotransfor 2005;23:431-437.

[144] Miao S, Zhang S, Su Z, Wang P. Chemoenzymatic synthesis of oleic acid-based polyesters for use as highly stable biomaterials. J Polym Sci Pol Chem 2008;46:4243-4248.

[145] Gross RA, Lu W, Yang Y. Methods for preparing long-chain hydroxyacids, diacids and oligomers and polymers. US Pat Appl Publ 2009;US 20090054610 A1 20090226.

[146] Umidjon I, Khozin-Goldberg I, Hacohen Z. Identification and characterization of D12, D6 and D5 desaturases from green microalga *Parietochloris incisa*, and use for production of very long-chain polyunsaturated fatty acids. PCT Int Appl 2011;WO 2011083463 A2 20110714.

[147] Wang B, Li Y, Qin G, Li X, Cao X. Identification of fatty acid composition and D5-unsaturated fatty acids in *Pinus armandii* kernel. Shipin Kexue 2011;32:164-166.

[148] Jung JH, Kim H, Go YS, Lee SB, Hur C-G, Kim HU, Suh MC. Identification of functional BrFAD2-1 gene encoding microsomal D-12 fatty acid desaturase from *Brassica rapa* and development of *Brassica napus* containing high oleic acid contents. Plant Cell Reports 2011;30:1881-1892.

[149] Matsuda T, Sakaguchi K, Kobayashi T, Abe E, Kurano N, Sato A, Okita Y, Sugimoto S, Hama Y, Hayashi M. Molecular cloning of a *Pinguiochrysis pyriformis* oleate-specific microsomal D12-fatty acid desaturase and functional analysis in yeasts and thraustochytrids. J Biochem-Tokio 2011;150:375-383.

[150] Matsuda T, Sakaguchi K, Hamaguchi R, Kobayashi T, Abe E, Hama Y, Hayashi M, Honda D, Okita Y, Sugimoto S. Analysis of D12-fatty acid desaturase function revealed that two distinct pathways are active for the synthesis of PUFAs in *T. aureum* ATCC 34304. J Lipid Res 2012;53:1210-1222.

[151] Okada S, Zhou X-R, Damcevski K, Gibb N, Wood C, Hamberg M, Haritos VS. Diversity of D12 Fatty Acid desaturases in santalaceae and their role in production of seed oil acetylenic Fatty acids. J Biol Chem 2013;288:32405-32413.

[152] Zhu QQ, Pollak DMW. Production of g-linolenic acid in oleaginous yeast transformed with D12 and D6 desaturases. US Pat Appl Publ 2006;US 20060035351 A1 20060216.

[153] Chuang L-T, Chen D-C, Nicaud J-M, Madzak C, Chen Y-H, Huang Y-S. Co-expression of heterologous desaturase genes in *Yarrowia lipolytica*. New biotechnology 2010;27:277-282.

[154] Bauer J, Qiu X, Vrinten P. Use of *Limonomyces roseipellis* D15 desaturase and other elongases and desaturases for producing long chain polyunsaturated fatty acids such as arachidonic acid, eicosapentaenoic acid and docosahexaenoic acid in yeast and plants. PCT Int Appl 2011;WO 2011064181 A1 20110603.

[155] Yan Z, Zhuo L, Mulan J, Xia W, Yangmin G, Yinbo Z, Fenghong H. Clone and identification of bifunctional D12/D15 fatty acid desaturase LKFAD15 from *Lipomyces kononenkoae*. Food Sci Technol 2013;22:573-576.

[156] Tian W, Hong K, Chen G-Q, Wu Q, Zhang R-Q, Huang W. Production of polyesters consisting of medium chain length 3-hydroxyalkanoic acids by *Pseudomonas mendocina* 0806 from various carbon sources. Antonie van Leeuwenhoek 2000;77:31-36.

[157] Kellerhals MB, Kessler B, Witholt B, Tchouboukov A, Brandl H. Renewable Long-Chain Fatty Acids for Production of Biodegradable Medium-Chain-Length Polyhydroxyalkanoates (mcl-PHAs) at Laboratory and Pilot Plant Scales. Macromolecules 2000;33:4690-4698.

[158] Jiang M, Shang L-A, Yun Z. Preparation of medium-chain-length polyhydroxyalkanoates by high cell density culture of *Pseudomonas putida* KT2442. Nanjing Gongye Daxue Xuebao, Ziran Kexueban 2003;25:25-28.

[159] Sin MC, Gan SN, Annuar M, Suffian M, Tan IKP. Thermodegradation of medium-chain-length poly(3-hydroxyalkanoates) produced by *Pseudomonas putida* from oleic acid. Polym Degrad Stabil 2010;95:2334-2342.

[160] Gumel AM, Mohamad A, Mohamad S, Heidelberg T. Biosynthesis and characterization of polyhydroxyalkanoates copolymers produced by *Pseudomonas putida* Bet001 isolated from palm oil mill effluent. PLoS One 2012;7:e45214.

[161] Ballistreri A, Giuffrida M, Guglielmino SPP, Carnazza S, Ferreri A, Impallomeni G. Biosynthesis and structural characterization of medium-chain-length poly(3-hydroxyalkanoates) produced by *Pseudomonas aeruginosa* from fatty acids. Int J Biol Macromol 2001;29:107-114.

[162] Dalal J, Sarmayangshu PM, Mandal AK, Lal B. Response surface optimization of poly (3-hydroxyalkanoic acid) production using oleic acid as an alternative carbon source by *Pseudomonas aeruginosa*. Biomass Bioenerg 2013;54:67-76.

[163] Solaiman DKY, Ashby RD, Foglia TA. Physiological characterization and genetic engineering of *Pseudomonas corrugata* for medium-chain-length polyhydroxyalkanoates synthesis from triacylglycerols. Curr Microbiol 2002;44:189-195.

[164] Choi J-I, Lee SH, Lee SY. Isolation and characteristics of polyhydroxyalkanoate producing *Pseudomonas sp.* MBEL21. Han'guk Misaengmul-Saengmyongkong Hakhoechi 2004;32:123-127.

[165] Ciesielski S, Mozejko J, Przybylek G. The influence of nitrogen limitation on mcl-PHA synthesis by two newly isolated strains of *Pseudomonas sp*. J Ind Microbiol Biot 2010;37:511-520.

[166] Fernandez D, Rodriguez E, Bassas M, Vinas M, Solanas AM, Llorens J, Marques AM, Manresa A. Agro-industrial oily wastes as substrates for PHA production by the new strain *Pseudomonas aeruginosa* NCIB 40045: Effect of culture conditions. Biochem Eng J 2005;26:159-167.

[167] Simon-Colin C, Raguenes G, Costa B, Guezennec J. Biosynthesis of medium chain length poly-3-hydroxyalkanoates by *Pseudomonas guezennei* from various carbon sources. React Funct Polym 2008;68:1534-1541.

[168] Chee J-Y, Tan Y, Samian M-R, Sudesh K. Isolation and characterization of a *Burkholderia sp.* USM (JCM15050) capable of producing polyhydroxyalkanoate (PHA) from triglycerides, fatty acids and glycerols. Journal of Polymers and the Environment 2010;18:584-592.

[169] Poirier Y, Erard N, Petetot JM-C. Synthesis of polyhydroxyalkanoate in the peroxisome of *Pichia pastoris*. FEMS Microbiology Letters 2002;207:97-102.

[170] Djamaan A, Abdul M, Mohammed I, Noor M, Azizan M. Fed-batch fermentation on production of a biodegradable plastic poly(3-hydroxybutyrate) from oleic acid. Majalah Farmasi Indonesia 2003;14:256-264.

[171] Lo KW, Chua H, Lawford H, Lo WH, Yu PHF. Effects of fatty acids on growth and poly-3-hydroxybutyrate production in bacteria. App Biochem Biotech 2005;121-124:575-580.

[172] Grigull VH, Silva DDd, Garcia MCF, Furlan SA, Pezzin APT, Schneider ALS, Aragao GF. Production and characterization of poly(3-hydroxybutyrate) from oleic acid by *Ralstonia eutropha*. Food Technol Biotech 2008;46:223-228.

[173] Ng K-S, Ooi W-Y, Goh L-K, Shenbagarathai R, Sudesh K. Evaluation of jatropha oil to produce poly(3-hydroxybutyrate) by *Cupriavidus necator* H16. Polym Degrad Stabil 2010;95:1365-1369.

[174] Marangoni C, Furigo AJ, Aragao GMFD. Oleic acid improves poly(3-hydroxybutyrate-co-3-hydroxyvalerate) production by *Ralstonia eutropha* in inverted sugar and propionic acid. Biotechnol Lett 2000;22:1635-1638.

[175] Pavaranggoon K, Kulpreecha S, Shioya S. Production of poly(3-hydroxybutyrate-co-3-hydroxyvalerate) with high 3HV mole fraction by *Bacillus sp*. BA-019. Biotechnology for Sustainable Utilization of Biological Resources in the Tropics 2003;16:73-80.

[176] Lee SH, Oh DH, Ahn WS, Lee Y, Choi JI, Lee SY. Production of poly(3-hydroxybutyrate-co-3-hydroxyhexanoate) by high-cell-density cultivation of *Aeromonas hydrophila*. Biotechnol Bioeng 2000;67:240-244.

[177] Aziz NA, Sipaut CS, Abdullah AA-A. Improvement of the production of poly(3-hydroxybutyrate-co-3-hydroxyvalerate-co-4-hydroxybutyrate) terpolyester by manipulating the culture condition. J Chem Technol Biot 2012;87:1607-1614.

[178] Ashby RD, Solaiman DKY, Foglia TA. The synthesis of short- and medium-chain-length poly(hydroxyalkanoate) mixtures from glucose- or alkanoic acidgrown *Pseudomonas oleovorans*. J Ind Microbiol Biot 2002;28:147-153.

[179] Kuo TM, Lanser AC. Factors influencing the production of a novel compound, 7,10-dihydroxy-8(E)-octadecenoic acid, by *Pseudomonas aeruginosa* PR3 (NRRL B-18602) in batch cultures. Curr Microbiol 2003;47:186-191.

[180] Kuo TM, Ray KJ, Manthey LK. A facile reactor process for producing 7,10-dihydroxy-8(E)-octadecenoic acid from oleic acid conversion by *Pseudomonas aeruginosa*. Biotechnol Lett 2003;25:29-33.

[181] Kuo TM, Huang J-K, Labeda D, Wen L, Knothe G. Production of 10-Hydroxy-8(E)-Octadecenoic Acid from Oleic Acid Conversion by Strains of *Pseudomonas aeruginosa*. Curr Microbiol 2008;57:437-441.

[182] Bae J-H, Suh M-J, Lee N-Y, Hou CT, Kim H-R. Production of a value-added hydroxy fatty acid, 7,10-dihydroxy-8(E)-octadecenoic acid, from high oleic safflower oil by *Pseudomonas aeruginosa* PR3. Biotechnology and Bioprocess Engineering 2010;15:953-958.

[183] W. Kim, Tengra FK, Young Z, Shong J, Marchand N, Chan HK, Pangule RC, Parra M, Dordick JS, Plawsky JL, Collins CH. Spaceflight Promotes Biofilm Formation by *Pseudomonas aeruginosa*. PLoS ONE 2013;8:e62437.

[184] Todar K. Todar's Online Textbook of Bacteriology. . http://textbookofbacteriologynet/pseudomonashtml retrieved on 2013-11-13:1.

[185] Joo Y-C, Oh D-K. Lipoxygenases: Potential starting biocatalysts for the synthesis of signaling compounds. Biotechnol Adv 2012;30:1524-1532.

[186] Imbs AB. Prostaglandins and Oxylipins of Corals. Russian Journal of Marine Biology 2011;37:325-334.

[187] Hansen J, Garreta A, Benincasa M, Fusté MC, Busquets M, Manresa A. Bacterial lipoxygenases, a new subfamily of enzymes? A phylogenetic approach. Appl Microbiol Biotechnol 2013;97:4737-4747.

[188] Huang F-C, Schwab W. Cloning and characterization of a 9-lipoxygenase gene induced by pathogen attack from *Nicotiana benthamiana* for biotechnological application. BMC Biotechnology 2011;11:1-15.

[189] Andres CD, Mercade E, Guinea J, Manresa A. 7,10-Dihydroxy-8(E)-octadecenoic acid produced by *Pseudomonas* 42A2: evaluation of different cultural parameters of the fermentation. World Journal of Microbiology & Biotechnology 1994;10:106-109.

[190] Hou CT, Bagby MO, Plattner RD, Koritala S. A novel compound 7,10-dihydroxy-8(E)-octadecenoic acid from oleic acid by bioconversion. JAOCS 1991;68:99-101.

[191] Guerrero A, Casals I, Busquets M, León Y, Manresa A. Oxidation of oleic acid to (E)-10-hydroperoxy-8-octadecenoic acid and (E)-10-hydroxy-8-octadecenoic acid by *Pseudomonas sp*. 42A2. Biochimica et Biophysica Acta 1997;1347:75-81.

[192] Bastida J, Andres CD, Cullere J, Busquets M, Manresa A. Biotransformation of oleic acid into 10-hydroxy-8E-octadecenoic acid by Pseudomonas sp. 42A2. Biotechnol Lett 1999;21:1031-1035.

[193] Cullere J, Durany O, Busquets M, Manresa A. Biotransformation of oleic acid into (E)-10-hydroxy-8-octadecenoic acid and (E)-7,10-dihydroxy-8-octadecenoic acid by *Pseudomonas sp*. 42A2 in an immobilized system. Biotechnol Lett 2001;23:215-219.

[194] Bodalo A, Bastida J, Maximo MF, Hidalgo AM, Murcia MD. Production of (E) 10-hydroxy-8-octadecenoic acid with lyophilized microbial cells. American Journal of Biochemistry and Biotechnology 2005;1:1-4.

[195] Busquets M, Deroncele V, Vidal-Mas J, Rodriguez E, Guerrero A, Manresa A. Isolation and characterization of a lipoxygenase from *Pseudomonas* 42A2 responsible for the biotransformation of oleic acid into (S)-(E)-10-hydroxy-8-octadecenoic acid. Antonie van Leeuwenhoek 2004;85:129-139.

[196] Vidal-Mas J, Busquets M, Manresa A. Cloning and expression of a lipoxygenase from *Pseudomonas aeruginosa* 42A2. Antonie van Leeuwenhoek 2005;87:245-251.

[197] Bassas M, Rodriguez E, Llorens J, Manresa A. Poly(3-hydroxyalkanoate) produced from *Pseudomonas aeruginosa* 42A2 (NCBIM 40045): Effect of fatty acid nature as nutrient. 2006;352:2259-2263.

[198] Bassas M, Marques AM, Manresa A. Study of the crosslinking reaction (natural and UV induced) in polyunsaturated PHA from linseed oil. Biochem Eng J 2008;40:275-283.
[199] Bassas M, Diaz J, Rodriguez E, Espuny MJ, Prieto MJ, Manresa A. Microscopic examination in vivo and in vitro of natural and cross-linked polyunsaturated mclPHA. Appl Microbiol Biotechnol 2008;78:587-596.
[200] E. Martinez MH, M. Busquets, P. Diaz, A. Manresa and E. H. Oliw. Biochemical Characterization of the Oxygenation of Unsaturated Fatty Acids by the Dioxygenase and Hydroperoxide Isomerase of *Pseudomonas aeruginosa* 42A2. The Journal of Biological Chemistry 2010;285:9339-9345.
[201] Garreta A, Val-Moraes SP, García-Fernández Q, Busquets M, Juan C, Oliver A, Ortiz A, Gaffney BJ, Fita I, Manresa A, Carpena X. Structure and interaction with phospholipids of a prokaryotic lipoxygenase from *Pseudomonas aeruginosa*. FASEB journal : official publication of the Federation of American Societies for Experimental Biology 2013.
[202] Martin-Arjol I, Bassas-Galia M, Bermudo E, Garcia F, Manresa A. Identification of oxylipins with antifungal activity by LC-MS/MS from the supernatant of *Pseudomonas* 42A2. Chem Phys Lipids 2010;163:341-346.
[203] Peláez M, Orellana C, Marqués A, Busquets M, Guerrero A, Manresa A. Natural Estolides Produced by *Pseudomonas sp*. 42A2 Grown on Oleic Acid: Production and Characterization. JAOCS 2003;80:859-866.
[204] Kapoor M, Gupta MN. Lipase promiscuity and its biochemical applications. Process Biochem 2012;47:555-569.
[205] Houde A, Kademi A, Leblanc D. Lipases and their industrial applications - An overview. Appl Biochem Biotechnol 2004;118:155-170.
[206] Rekha KSS, Chandana-Lakshmi MVV, Sridevi V, Manasa M. An Overview of Microbial Lipases. Journal of Chemical, Biological and Physical Sciences 2012;2:1379-1389.
[207] Cesarini S. Improvement and evaluation of new microbial lipases for biodiesel synthesis Universitat de Barcelona 2013;Barcelona:Doctoral thesis.
[208] Gupta R, Gupta N, Rathi P. Bacterial lipases: an overview of production, purification and biochemical properties. Applied Microbiololgy and Biotechnology 2004;64:763-781.
[209] Bofill C, Prim N, Mormeneo M, Manresa A, Pastor J, Diaz P. Differential behaviour of *Pseudomonas sp*. 42A2 LipC, a lipase showing greater versatility than its counterpart LipA. Biochemie 2010;92:307-316.
[210] S.Cesarini, Bofill C, Pastor J, Reetz MT, Diaz P. A thermostable variant of *P. aeruginosa* cold-adapted LipC obtained by rational design and saturation mutagenesis. Process Biochem 2012;47:2064-2071.
[211] Williams JA. Keys to bioreactor selection. CEP Magazine 2002;March:34-41.
[212] Julien C, Whitford W. Bioreactor Monitoring, Modeling, and Simulation. BioProcess International 2007;January:10-17.
[213] Calam CT. The culture of microorganisms in liquid medium. 1969.
[214] Berovic M, Enfors S-O. Comprehensive bioprocess engineering. European Federation on Biotechnology Working Group on Bioreactor Performance University of Ljubljana 2010.
[215] Fyferling M, Uribelarrea J-L, Goma G, Molina-Jouve C. Oxygen transfer in intensive microbial culture. Bioprocess Biosyst Eng 2008;31:595-604.
[216] Czermak P, Weber C, Nehring D. A ceramic microsparging aeration system for cell culture reactors. Publication Series of IBPT 2005;University of Applied Sciences Giessen-Friedberg:1-6.
[217] Vardar-Sukan F. Foaming and its control in bioprocesses. Recent AdVances in Biotechnology 1992;Kluwer Academic Publishers: Netherlands:113-146.
[218] Tasseff RA, Varner JD. Comprehensive Biotechnology. Chapter: Mathematical models in biotechnology 2011.
[219] Andrews SS, Bray D. Stochastic simulation of chemical reactions with spatial resolution and single molecule detail. Phys Biol 2004;1:137-151.
[220] Fakruddin M, Mazumder RM, Mannan KSB. Predictive microbiology: Modeling microbial responses in food. Ceylon Journal of Science (Bio Sci) 2011;40:121-131.
[221] Sin G, Woodley JM, Gernaey KV. Application of Modeling and Simulation Tools for the Evaluation of Biocatalytic Processes: A Future Perspective. Biotechnol Prog - AICHE 2009;25:1529-1538.
[222] Carcano S. A Model for Cell Growth in Batch Bioreactors. Politecnico di Milano Facoltà di Ingegneria dei Sistemi 2010;Corso di Laurea Specialistica in Ingegneria Matematica.

[223] Tanase C, Caramihai M, Muntean O. Study of the Growth Kinetic Models of a Bacterium for a Human Use Therapeutic Product. Rev Chim (Bucharest) 2013;64:182-185.
[224] Mata-Alvarez J, Mitchell DA. Mathematical Modeling in Biotechnology. Biotechnology - Encyclodedia of Life Support Systems;II.
[225] Roberts TA. Combinations of antimicrobials and processing methods. Food Technol 1989;43:156-163.
[226] Roels JA, Kossen NWF. On the modeling of microbial metabolism. Prog Ind Microbiol 1978;14:95-203.
[227] Whiting RC, Buchanan RL. A classification of models for predictive microbiology. Food Microbiol 1993;10:175-177.
[228] Dunn IJ, Heinzle E, Ingham J, Prenosil JE. Biological reaction engineering. Wiley-VCH Verlag 2003.
[229] Grund A, Ulbrich E, Wirth T. The oxidation of paraffin. Georg Schicht A-G, Aussig a d E Ber 1920;53B:987-996.
[230] Grund A. Interesterification of glycerides and their technical applications. Chemische Umschau auf dem Gebiete der Fette, Oele, Wachse und Harze 1925;32:225.
[231] Bauer KH. Polymerization and oxidation of unsaturated fatty Acids. Chemische Umschau auf dem Gebiete der Fette, Oele, Wachse und Harze 1926;33:198-199.
[232] Bauer KH. Rearrangement and transformation of oleic acid. Chemisch-Metallurgische Zeitschrift 1930;20:1912-1913.
[233] Bauer KH, Eberle A. The behavior of polyhydroxy acids upon heating. Angewandte Chemie 1930;43:902-904.
[234] Organic acids. GB 368552 19320310 1931.
[235] Groote MD, Keiser B. Breaking petroleum emulsions of the water-in-oil type. US 2079762 19370511 1937.
[236] Resinous compositions. GB 492965 19380926 1938.
[237] Esafov VI, Shpadi AV. The products of thermal treatment of ricinoleic acid and its mixture with oxalic acid. Zhurnal Prikladnoi Khimii (Sankt-Peterburg, Russian Federation) 1940;13:1040-1044.
[238] Petrov NA. Lubricant. SU 65870 19460228 1946.
[239] Meade EM. Acylation of ricinoleic esters. GB 590386 19470716 1947.
[240] Parry EG. Hydroxy fatty acid estolide ester-ethers. GB 640464 19500719 1950.
[241] Cunningham OD, Orville OL. Esters of a-hydroxy acids and their estolides. US 2652410 19530915 1953.
[242] Willibrord JF, Unilever NV. Emulsifiers consisting of partial ester-ethers. NL 82891 19561015 1956.
[243] Gracht WJFvd. Surface-active compounds. US 2785978 19570319 1957.
[244] Dilworth JP, Culnane CH, Nelson RF. Greases containing anhydrous calcium 12-hydroxystearate and estolides. US 2862884 19581202 1958.
[245] Roach JR, Crook-Shank FT. Lubricating greases. US 3068175 19621211 1962.
[246] Lyons JF, Jackson JW, Thomas PR. Power steering lubricant. US 3429820 A 19690225 1969.
[247] Stein W, Heins A. Polyurethane foam from polyisocyanates and polyesters. DE 1282947 B 19681114 1968.
[248] Smith MK. Effect of heat on 12-hydroxystearic acid. NLGI Spokesman 1959;23:271-273.
[249] Hawke F, Kohll EA. Autoreactions of ricinoleic acid. I. Reaction at 180°, 147°, 122-3°, and room temperature. Journal of the South African Chemical Institute 1959;12:1-16.
[250] Hawke F, Kohll EA. Autoreactions of ricinoleic acid. II. Catalyzed dehydration of ricinoleic acid. Journal of the South African Chemical Institute 1959;12:17-25.
[251] Modak SN, Kane JG. Estolides. I. Kinetics of estolide formation and decomposition. JAOCS 1965;42:428-432.
[252] Venkatesan TK, Subrahmanyam VVR, Kane JG. Estolides. II. Kinetics of decomposition of hydrogenated estolides. Journal of the Oil Technologists' Association of India 1969;1:30-33.
[253] Teupel M, Pollerberg J. Analysis of ricinoleic acid monoglycerides by column chromatography and nuclear magnetic resonance spectroscopy. Tenside 1968;5:275-278.
[254] Syroezhko AM, Potekhin VM, Proskuryakov VA. Bifunctional compounds in products of the liquid-phase oxidation of n-decane. Zhurnal Prikladnoi Khimii (Sankt-Peterburg, Russian Federation) 1973;46:2694-2698.

[255] Ottaviani P, Graille J, Biasini S, Perfetti P, Naudet M. Study of the nonvolatile fraction of compounds formed in thermal oxidation of heated soybean oil. Actes Congr Mond - Soc Int Etude Corps Gras, 13th 1976;Sect. A:43-50.
[256] Verburg CC, Rek JHM. Soft margarine. DE 2156121 A 19720518 1972.
[257] Crawford WC, Godfrey AW. Lubricating oil composition. US 3909425 A 19750930 1975.
[258] Tilik VT, Avramenko IN, Movshovich VS, Garazhai AP, Tselovalnikov VM, Vyazovskaya SS, Simonov AI, Sterkhova LN, Terekhova GF. Lubricant for cold working of metals by pressure. SU 810767 A1 19810307 1981.
[259] Jong FD, Vermeule J. Lubricating-oil compositions. EP 194718 A2 19860917 1986.
[260] Kusenko AG. Study of the effect of chemically active additives on the antiwear properties of cable grease. Neftepererabotka i Neftekhimiya (Moscow, Russian Federation) 1978;5:24-26.
[261] Venkatesan TK. Studies in estolides. Part III. Plasticizer for polyvinyl chloride. JAOCS 1979;56:569-570.
[262] Fujita A, Yoshikawa T. Plant wax. I. Constituents of the wax of Juniperus rigida. Yakugaku Zasshi 1951;71:913-916.
[263] Tulloch AP, Bergter L. Epicuticular wax of Juniperus scopulorum. Phytochemistry 1981;20:2711-2716.
[264] Herbin GA, Sharma K. Plant cuticular waxes. V. Wax coatings of pine needles: a taxonomic survey. Phytochemistry 1969;8:151-160.
[265] Franich RA, Wells LG, Holland PT. Epicuticular wax of Pinus radiata needles. Phytochemistry 1978;17:1617-1623.
[266] Guenthardt-Goerg MS. Epicuticular wax of needles of Pinus cembra, Pinus sylvestris and Picea abies. European Journal of Forest Pathology 1986;16:400-408.
[267] Franich RA, Kroese HW, Jakobsson E, Jensen S, Kylin H. Trace constituents of natural and anthropogenic origin from New Zealand Pinus radiata needle epicuticular wax. New Zealand Journal of Forestry Science 1993;23:101-109.
[268] Gordon DC, Percy KE, Riding RT. Effects of u.v.-B radiation on epicuticular wax production and chemical composition of four *Picea* species. New Phytologist 1998;138:441-449.
[269] Schulten HR, Simmleit N, Rump HH. Field desorption mass spectrometry of lipids. III. Soft ionization mass spectrometry of epicuticular waxes isolated from coniferous needles. Chemistry and Physics of Lipids 1986;41:209-224.
[270] Isoi K. Leaf-waxes of deciduous conifers. Yakugaku Zasshi 1958;78:814.
[271] Kariyone T, Takahashi M, Isoi K, Yoshikura M. Chemical constituents of the plants of *Coniferae* and allied order. XXXIV. Waxes from the plants of *Casuarina* and *Picea* and constituents of the grafted plants of *Taxodiaceae*. Yakugaku Zasshi 1959;79:1340-1342.
[272] Brieskorn CH. Surface lipids and lipid polymers of plants. Fette, Seifen, Anstrichmittel 1978;80:15-20.
[273] Moreau RA, Doehlert DC, Welti R, Isaac G, Roth M, Tamura P, Nunez A. The identification of mono-, di-, tri-, and tetragalactosyl-diacylglycerols and their natural estolides in oat kernels. Lipids 2008;43:533-548.
[274] Zhang H, Olson DJH, Van D, Purves RW, Smith MA. Rapid identification of triacylglycerol-estolides in plant and fungal oils. Industrial Crops and Products 2012;37:186-194.
[275] Vakar AB, Sosedov NI, Shvetsova VA, Drozdova ZB, Naymova AT. A study on the rancidity of stored wheat flour. Biokhim Zerna, Sbornik 1958;4:206-228.
[276] Noble WR, Eisner A, Scanlan JT. Isolation of a hydroxy acid concentrate from wool wax acids. JAOCS 1960;37:14-16.
[277] Gunawan ER, Basri M, Rahman MBA, Salleh AB, Rahman RNZA. Lipase-Catalyzed Synthesis of Palm-Based Wax Esters. Journal of Oleo Science 2004;53:471-477.
[278] Smedley SR, Schroeder FC, Weibel DB, Meinwald J, Lafleur KA, Renwick JA, Rutowski R, Eisner T. Mayolenes: Labile defensive lipids from the glandular hairs of a caterpillar (*Pieris rapae*). PNAS 2002;99:6822-6827.
[279] Butovich IA. Cholesteryl esters as a depot for very long chain fatty acids in human meibum. Journal of Lipid Research 2009;50:501-513.
[280] Wojtowicz JC, Uchiyama E, Pascuale MAD, Aronowicz JD, McCulley JP. Ojo Seco: Efecto de la Capa Lipídica de la Película Lagrimal. Vision Pan-America 2008;VII:48-51.

[281] Martin-Arjol I, Busquets M, Manresa A. Production of 10(*S*)-hydroxy-8(E)-octadecenoic acid mono-estolides by lipases in non-aqueous media. Process Biochemistry 2013;48:224-230.
[282] Cermak SC, Isbell TA, Evangelista RL, Johnson BL. Synthesis and physical properties of petroselinic based estolide esters. Industrial Crops and Products 2011;33:132-139.
[283] Burg DA, Kleiman R, Erhan SM. Production of hydroxy fatty acids and estolide intermediates. US 662606 A0 19910901 1991.
[284] Isbell TA, Kleiman R, Erhan SM. Characterization of Monomers Produced from Thermal High-Pressure Conversion of Meadowfoam and Oleic Acids into Estolides. JAOCS 1992;69:1177-1183.
[285] Erhan SM, Kleiman R, Isbell TA. Methods for Increasing Estolide Yields in a Batch Reactor. JAOCS 1995;72:671-674.
[286] Isbell TA, Frykman HB, Abbott TP, Lohr JE, Drozd JC. Optimization of the Sulfuric Acid.Catalyzed Estolide Synthesis from Oleic Acid. JAOCS 1997;74:473-476.
[287] Isbell TA, Edgcomb MR, Lowery BA. Physical properties of estolides and their ester derivatives. Industrial Crops and Products 2001;13.
[288] Cermak SC, Isbell TA. Synthesis of Estolides from Oleic and Saturated Fatty Acids. JAOCS 2001;78:557-565.
[289] Cermak SC, Isbell TA. Physical properties of saturated estolides and their 2-ethylhexyl esters. Industrial Crops and Products 2002;16:119-127.
[290] Isbell TA, Cermak SC. Synthesis of Triglyceride Estolides from Lesquerella and Castor Oils. JAOCS 2002;79:1227-1233.
[291] Cermak SC, Isbell TA. Synthesis and physical properties of estolide-based functional fluids. Industrial Crops and Products 2003;18:183-196.
[292] Cermak SC, Isbell TA. Synthesis and Physical Properties of Cuphea-Oleic Estolides and Esters. JAOCS 2004;81:297-303.
[293] Cermak SC, Skender AL, Deppe AB, Isbell TA. Synthesis and Physical Properties of Tallow-Oleic Estolide 2-Ethylhexyl Esters. JAOCS 2007;84:449-456.
[294] Bernhardt RJ, Dado GP, Murphy DS, Alonso L, Gariepy CA, Filipovic EI. Sulfonated estolides and other derivatives of fatty acids, methods of making them, and compositions and processes employing them. WO 2009094336 A2 20090730 2009.
[295] Allen DR, Bernhardt RJ, Brown A, Masters RA, Wolfe PS. Hard surface cleaners based on compositions derived from natural oil metathesis. WO 2012061103 A2 20120510 2012.
[296] Mikusch JDV. Fast-drying binder based on dehydrated, epoxidized linseed oil in theory and practice. Farbe + Lack 1971;77:1173-1178.
[297] Bredsguard J, Forest J. Epoxidized estolides, sulfurized estolides, and methods of making the same. WO 2012173666 A1 20121220 2012.
[298] Meng DM, Liu JK, Li ZJ. Microwave assisted condensation of oleic acid catalyzed by perchloric acid-ionic liquids. Jiangnan Daxue Xuebao, Ziran Kexueban 2011;10:319-322.
[299] Allen DR, Bernhardt RJ, Brown A, Luebke G, Luka R, Malec A, Masters R, Skelton P, Sook B, Weitgenant JA. Sulfonates from natural oil metathesis. WO 2012061101 A1 20120510 2012.
[300] Thompson T, Parson K, Bredsguard J, Forest J. Processes for preparing estolide base oils and oligomeric compounds that include cross metathesis. US 20130158277 A1 20130620 2013.
[301] Okumura S, Iwai M, Tsujisaka Y. Synthesis of estolides during hydrolysis of castor oil by Geotrichum candidum lipase. Yukagaku 1983;32:271-273.
[302] Yamaguchi C, Akita M, Asaoka S, Osada F. Enzymic manufacture of castor-oil fatty acid estolides. Japanese Kokai Tokkyo Koho 1989:JP 01016591 A 19890120.
[303] Yoshida Y, Kawase M, Yamaguchi C. Manufacture of estolide from ricinoleic acid with immobilized lipase. Japanese Kokai Tokkyo Koho 1993:JP 05211878 A 19930824.
[304] Yamaguchi C, Yoshida Y, Kawase M. Manufacture of estolide with immobilized lipase. Japanese Kokai Tokkyo Koho 1993:JP 05304966 A 19931119.
[305] Yoshida Y, Kawase M, Yamaguchi C, Yamane T. Synthesis of estolides with immobilized lipase. Yukagaku 1995;44:328-333.
[306] Goto M, Hatanaka C, Haraguchi T. Formation of ricinoleic acid by lipase immobilized within isopropylacrylamide gel beads. Kitakyushu Kogyo Koto Senmon Gakko Kenkyu Hokoku 1999;32:161-164.

[307] Hayes DG, Kleiman R, Phillips BS. The triglyceride composition, structure, and presence of estolides in the oils of Lesquerella and related species. JAOCS 1995;72:559-569.
[308] Bódalo A, Bastida J, Máximo MF, Montiel MC, Murcia MD, Ortega S. Influence of the operating conditions on lipase-catalysed synthesis of ricinoleic acid estolides in solvent-free systems. Biochemical Engineering Journal 2009;44:214-219.
[309] Yoshida Y, Kawase M, Yamaguchi C, Yamane T. Enzymic synthesis of estolides by a bioreactor. JAOCS 1997;74:261-267.
[310] Bódalo-Santoyo A, Bastida-Rodríguez J, Máximo-Martín MF, Montiel-Morte MC, Murcia-Almagro MD. Enzymatic biosynthesis of ricinoleic acid estolides. Biochem Eng J 2005;26:155-158.
[311] Bódalo A, Bastida J, Máximo MF, Montiel MC, Gómez M, Murcia MD. Production of ricinoleic acid estolide with free and immobilized lipase from *Candida rugosa*. Biochem Eng J 2008;39:450-456.
[312] Horchani H, Bouaziz A, Gargouri Y, Sayari A. Immobilized *Staphylococcus xylosus* lipase-catalysed synthesis of ricinoleic acid esters. J Mol Catal B: Enzym 2012;75:35-42.
[313] Ye R, Hayes DG. Optimization of the Solvent-Free Lipase-Catalyzed Synthesis of Fructose-Oleic Acid Ester Through Programming of Water Removal. JAOCS 2011;88:1351-1359.
[314] Klibanov AM. Improving enzymes by using them in organic solvents. Nature 2001;409:241-246.
[315] Santos JC, Bueno T, Rós PCMd, Castro HFd. Lipase-catalyzed synthesis of butyl esters by direct esterification in solvent-free system. Journal of Chemical Technology and Biotechnology 2007;82:956-961.
[316] Hills MJ, Kiewitt I, Mukherjee KD. Lipase from Brassica napus L. discriminates against cis-4 and cis-6 unsaturated fatty acids and secondary and tertiary alcohols. Biochimica et Biophysica Acta-Lipids and Lipid Metabolism 1990;1042:237-240.
[317] Mukherjee K, Kiewitt I. Specificity of Carica papaya Latex as Biocatalyst in the Esterification of Fatty Acids with 1-Butanol. Journal of Agricultural and Food Chemistry 1996;44:1948-1952.
[318] Mukherjee K, Kiewitt I. Substrate Specificity of Lipases in Protease Preparations. Journal of Agricultural and Food Chemistry 1998;46:2427-2432.
[319] Borgdorf SWaR. Substrate selectivity of lipases in the esterification of *cis/trans*-isomers and positional isomers of conjugated linoleic acid. Biotechnology Letters 2000;22:1151-1155.
[320] Pedersen S, Holmer G. Studies of the fatty acid speci®city of the lipases from Rhizomucor miehei toward 20:1n-9, 20:5n-3, 22:1n-9 and 22:6n-3. JAOCS 1995;72:239-243.
[321] Warwel S, Borgdorf R, Brühl L. Substrate selectivity of lipases in the esterification of oleic acid, linoleic acid, linolenic acid and their all-trans-isomers and in the transesterification of *cis*/*trans*-isomers of linoleic acid methyl ester. Biotechnol Lett 1999;21.
[322] Brockerhoff H. Substrate specificity of pancreatic lipase: Influence of the structure of fatty acids on the reactivity of esters. Biochimica et Biophysica Acta-Enzymology 1970;212:92-101.
[323] Kleiman R, Earle FR, Tallent WH, Wolff IA. Retarded hydrolysis by pancreatic lipase of seed oils with *trans*-3 unsaturation. Lipids 1970;5:513-518.
[324] Warwel S, Borgdorf R. Substrate selectivity of lipases in the esterification of cis/trans-isomers and positional isomers of conjugated linoleic acid (CLA). Biotechnology Letters 2000;22:1151-1155.
[325] Lange LG, Bergmann SR, Sobel BE. Identification of fatty acid ethyl esters as products of rabbit myocardial ethanol metabolism. The Journal of biological chemistry 1981;256:12968-12973.
[326] Hu C, Ge F, Hyodo E, Arai K, Iwata S, Lobdell H, Walewski JL, Zhou S, Clugston RD, Jiang H. Chronic ethanol consumption increases cardiomyocyte fatty acid uptake and decreases ventricular contractile function in C57BL/6J mice. Journal of molecular and cellular cardiology 2013:5930-5940.
[327] Elamin EE, Masclee AA, Dekker J, Jonkers DM. Ethanol metabolism and its effects on the intestinal epithelial barrier. Nutrition Reviews 2013;71:483-499.
[328] Petersen OH, Gerasimenko OV, Tepikin AV, Gerasimenko JV. Aberrant Ca(2+) signalling through acidic calcium stores in pancreatic acinar cells. Cell Calcium 2011;50:193-199.
[329] Waszkiewicz N, Zalewska A, Szulc A, Kepka A, Konarzewska B, Zalewska-Szajda B, Chojnowska S, Waszkiel D, Zwierz K. The influence of alcohol on the oral cavity,

salivary glands and saliva. Polski merkuriusz lekarski: organ Polskiego Towarzystwa Lekarskiego 2011;30:69-74.
[330] Waszkiewicz N, Szulc A. Immunity defects in acute and chronic alcohol intoxication. Polski merkuriusz lekarski: organ Polskiego Towarzystwa Lekarskiego 2010;29:269-273.
[331] Alhomsi K, Selig M, Sustic T, Katrangi E, Weissig V, Laposata M. Induction of apoptosis and necrosis in human peripheral blood mononuclear cells by fatty acid ethyl esters. Alcoholism: Clinical & Experimental Research 2008;32:534-543.
[332] Ren J, Wold LE. Mechanisms of alcoholic heart disease. Therapeutic advances in cardiovascular disease 2008;2:497-506.
[333] Salem RO, Laposata M. Activation and impairment of platelet function in vitro by fatty acid ethyl ester, a nonoxidative ethanol metabolite: effect of fatty acid ethyl esters on human platelets. Alcoholism, clinical and experimental research 2006;30:2079-2088.
[334] Wu H, Cai P, Clemens DL, Jerrells TR, Ansari GAS, Kaphalia BS. Metabolic basis of ethanol-induced cytotoxicity in recombinant HepG2 cells: role of nonoxidative metabolism. Toxicology and applied pharmacology 2006;216:238-247.
[335] Salem RO, Laposata M, Rajendram R, Cluette-Brown JE, Preedy VR. The total body mass of fatty acid ethyl esters in skeletal muscles following ethanol exposures greatly exceeds that found in the liver and the heart. Alcohol and Alcoholism (Oxford, United Kingdom) 2006;41:598-603.
[336] Hannuksela ML, Ramet ME, Nissinen AET, Liisanantti MK, Savolainen MJ. Effects of ethanol on lipids and atherosclerosis. Pathophysiology: the official journal of the International Society for Pathophysiology 2004;10:93-103.
[337] Tyulina OV, Prokopieva VD, Dodd RD, Hawkins JR, Clay SW, Wilson DO, Boldyrev AA, Johnson P. In vitro effects of ethanol, acetaldehyde and fatty acid ethyl esters on human erythrocytes. Alcohol and alcoholism (Oxford, Oxfordshire) 2002;37:179-186.
[338] Bora PS, Lange LG. Molecular mechanism of ethanol metabolism by human brain to fatty acid ethyl esters. Alcoholism, clinical and experimental research 1993;17:28-30.
[339] Hastedt M, Buchner M, Rothe M, Gapert R, Herre S, Krumbiegel F, Tsokos M, Kienast T, Heinz A, Hartwig S. Detecting alcohol abuse: traditional blood alcohol markers compared to ethyl glucuronide (EtG) and fatty acid ethyl esters (FAEEs) measurement in hair. Forensic science, medicine, and pathology 2013;DOI 10.1007/s12024-013-9416-8.
[340] Gonzalez-Illan F, Ojeda-Torres G, Diaz-Vazquez LM, Rosario O. Detection of fatty acid ethyl esters in skin surface lipids as biomarkers of ethanol consumption in alcoholics, social drinkers, light drinkers, and teetotalers using a methodology based on microwave-assisted extraction followed by solidphase microextraction and gas chromatography-mass spectrometry. Journal of analytical toxicology 2011;35:232-237.
[341] Albermann ME, Musshoff F, Madea B. Comparison of ethyl glucuronide (EtG) and fatty acid ethyl esters (FAEEs) concentrations in hair for testing abstinence. Analytical and Bioanalytical Chemistry 2011;400:175-181.
[342] Pragst F. Interpretation problems in a forensic case of abstinence determination using alcohol markers in hair. Forensic Science International 2012;217:e4-7.
[343] Hastedt M, Krumbiegel F, Gapert R, Tsokos M, Hartwig S. Fatty acid ethyl esters (FAEEs) as markers for alcohol in meconium: method validation and implementation of a screening program for prenatal drug exposure. Forensic science, medicine, and pathology 2013;9:287-295.
[344] Ugliano M, Travis B, Francis IL, Henschke PA. Volatile Composition and Sensory Properties of Shiraz Wines As Affected by Nitrogen Supplementation and Yeast Species: Rationalizing Nitrogen Modulation of Wine Aroma. Journal of agricultural and food chemistry 2010;58:12417-12425.
[345] Aznar M, Lopez R, Cacho JF, Ferreira V. Identification and quantification of impact odorants of aged red wines from Rioja. GC-olfactometry, quantitative GCMS, and odor evaluation of HPLC fractions. Journal of agricultural and food chemistry 2001;49:2924-2929.
[346] Madrera RR, Valles BS, Lobo AP. Chemical and sensory changes in fresh cider spirits during maturation in inert containers. Journal of the science of food and agriculture 2011;91:797-804.
[347] Shpritsman EM. Accelerated technology of whisky production. Novye Metody Tekhnol Kontr Konserv Vinodel Proizvod 1972:105-111.

[348] Kayahara K, Aoyagi N, Kawasaki I, Miyachi N. Flavor components of whisky. XIII. Higher fatty acid ethyl esters contained in commercial whiskies. Hakko Kogaku Zasshi 1968;46:362-366.
[349] Pino J, Marti MP, Mestres M, Perez J, Busto O, Guasch J. Headspace solid-phase microextraction of higher fatty acid ethyl esters in white rum aroma. Journal of chromatography A 2002;954:51-57.
[350] Ziolkowska A, Henryk HJ. Differentiation of raw spirits of rye, corn and potato using chromatographic profiles of volatile compounds. Journal of the science of food and agriculture 2012;92:2630-2637.
[351] Halcox JP. Cardiovascular risk and lipid management beyond statin therapy: the potential role of omega-3 polyunsaturated fatty acid ethyl esters. Clinical Lipidology 2013;8:329-344.
[352] Mason CM, Long J, Conroy C. Prescription omega-3s: an overview for nurse practitioners. The Journal of cardiovascular nursing 2011;26:290-297.
[353] Mickleborough TD. Treating hypertriglyceridemia with prescription omega-3 fatty acid ethyl esters. The Physician and sportsmedicine 2009;37:160-162.
[354] Bhatnagar D, Hussain F. Omega-3 fatty acid ethyl esters (Omacor) for the treatment of hypertriglyceridemia. Future Lipidology 2007;2:263-270.
[355] Cawood AL, Ding R, Napper FL, Young RH, Williams JA, Ward JAM, Gudmundsen O, Vige R, Payne PKS, Ye S. Eicosapentaenoic acid (EPA) from highly concentrated n-3 fatty acid ethyl esters is incorporated into advanced atherosclerotic plaques and higher plaque EPA is associated with decreased plaque inflammation and increased stability. Atherosclerosis 2010;212:252-259.
[356] Wong TYA, Chan DC, Barrett PHR, Adams LA, Watts GF. Supplementation with n3 fatty acid ethyl esters increases large and small artery elasticity in obese adults on a weight loss diet. The Journal of nutrition 2013;143:437-441.
[357] Hajjaji N, Bougnoux P. Selective sensitization of tumors to chemotherapy by marine-derived lipids: A review. Cancer Treatment Reviews 2013;39:473-488.
[358] Burns CP, Halabi S, Clamon GH, Hars V, Wagner BA, Hohl RJ, Lester E, Kirshner JJ, Vinciguerra V, Paskett E. Phase I clinical study of fish oil fatty acid capsules for patients with cancer cachexia: cancer and leukemia group B study 9473. Clinical cancer research: an official journal of the American Association for Cancer Research 1999;5:3942-3947.
[359] Gerber M. Omega-3 fatty acids and cancers: a systematic update review of epidemiological studies. British Journal of Nutrition 2012;107:228-239.
[360] Patterson RE, Flatt SW, Newman VA, Natarajan L, Rock CL, Thomson CA, Caan BJ, Parker BA, Pierce JP. Marine Fatty Acid Intake Is Associated with Breast Cancer Prognosis. The Journal of Nutrition Nutrition and Disease 2011;141:201-206.
[361] Lorgeril M, Salen P. New insights into the health effects of dietary saturated and omega-6 and omega-3 polyunsaturated fatty acids. BMC Medicine 2012;10.
[362] Chajès V, Torres-Mejía G, Biessy C, Ortega-Olvera C, Angeles-Llerenas A, Ferrari P, Lazcano-Ponce E, Romieu I. ω-3 and ω-6 Polyunsaturated Fatty Acid Intakes and the Risk of Breast Cancer in Mexican Women: Impact of Obesity Status. Cancer Epidemiology, Biomarkers & Prevention 2011;21:319-326.
[363] Giros A, Grzybowski M, Sohn VR, Pons E, J.Fernandez-Morales, Xicola RM, Sethi P, Grzybowski J, Goel A, Boland CR, Gassull MA, Llor X. Regulation of Colorectal Cancer Cell Apoptosis by the n-3 Polyunsaturated Fatty Acids Docosahexaenoic and Eicosapentaenoic. Cancer Prevention Research 2009;2:732-742.
[364] Habermann N, Schön A, Lund EK, Glei M. Fish fatty acids alter markers of apoptosis in colorectal adenoma and adenocarcinoma cell lines but fish consumption has no impact on apoptosis-induction ex vivo. Apoptosis 2010;15:621-630.
[365] Cockbain AJ, Toogood GJ, Hull MA. Omega-3 polyunsaturated fatty acids for the treatment and prevention of colorectal cancer. GUT 2012;61:135-149.
[366] Orcharda TS, Pana X, Cheeka F, Inga SW, Jackson RD. A systematic review of omega-3 fatty acids and osteoporosis. British Journal of Nutrition 2012;107:253-260.
[367] Milesa EA, Calder PC. Influence of marine n-3 polyunsaturated fatty acids on immune function and a systematic review of their effects on clinical outcomes in rheumatoid arthritis. British Journal of Nutrition 2012;107:171-184.
[368] Freemantle E, Vandal M, J.Tremblay-Mercier, Tremblay S, Blache JC, Bégin ME, Brenna JT, Windust A, Cunnane SC. Omega-3 fatty acids, energy substrates, and brain

function during aging. Prostaglandins, Leukotrienes and Essential Fatty Acids 2006;75:213-220.
[369] Moyad MA, M.D., M.P.H. An introduction to dietary/supplemental omega-3 fatty acids for general health and prevention: Part II. Urologic Oncology: Seminars and Original Investigations 2005;23:36-48.
[370] Ortega RM, Rodríguez-Rodríguez E, López-Sobaler AM. Effects of omega 3 fatty acids supplementation in behavior and non-neurodegenerative neuropsychiatric disorders. British Journal of Nutrition 2012;107:261-270.
[371] Tur JA, Bibiloni MM, Sureda A, Pons A. Dietary sources of omega 3 fatty acids: public health risks and benefits. British Journal of Nutrition 2012;107:23-52.
[372] Cheong LZ, Guo Z, Yang Z, Chua SC, Xu X. Extraction and enrichment of n-3 polyunsaturated fatty acids and ethyl esters through reversible p-p complexation with aromatic rings containing ionic liquids. Journal of agricultural and food chemistry 2011;59:8961-8967.
[373] Rossi PC, Pramparo MC, Gaich MC, Grosso NR, Nepote V. Optimization of molecular distillation to concentrate ethyl esters of eicosapentaenoic (20:5 w-3) and docosahexaenoic acids (22:6 w-3) using simplified phenomenological modeling. Journal of the science of food and agriculture 2011;91:1452-1458.
[374] Perretti G, Motori A, Bravi E, Favati F, Montanari L, Fantozzi P. Supercritical carbon dioxide fractionation of fish oil fatty acid ethyl esters. Journal of Supercritical Fluids 2007;40:349-353.
[375] Borch-Jensen C, Staby A, Mollerup JM. Phase Equilibria of Urea-Fractionated Fish Oil Fatty Acid Ethyl Esters and Supercritical Carbon Dioxide. Industrial & Engineering Chemistry Research 1994;33:1574-1579.
[376] Ozawa I, Kim M, Saito K, Sugita K, Baba T, Moriyama S, Sugo T. Purification of docosahexaenoic acid ethyl ester using a silver-ion-immobilized porous hollow-fiber membrane module. Biotechnology progress 2001;17:893-896.
[377] Suzuki T, Tanaka Y, Kato S, Nagahama K. Extraction polyunsaturated fatty acid ethyl esters from aqueous silver nitrate solution using supercritical ethane and ethylene and modeling of the extraction process. Kagaku Kogaku Ronbunshu 1994;20:97-104.
[378] Huang CB, Ebersole JL. A novel bioactivity of omega-3 polyunsaturated fatty acids and their ester derivatives. Molecular oral microbiology 2010;25:75-80.
[379] Huang CB, George B, Ebersole JL. Antimicrobial activity of n-6, n-7 and n-9 fatty acids and their esters for oral microorganisms. Archives of oral biology 2010;55:555-560.
[380] Knothe G. Dependence of biodiesel fuel properties on the structure of fatty acid alkyl esters. Fuel Processing Technology 2005;86:1059-1070.
[381] Rodrigues RC, Volpato G, Wada K, Ayub MAZ. Enzymatic synthesis of biodiesel from transesterification reactions of vegetable oils and short chain alcohols. JAOCS 2008;85:925-930.
[382] Narwal SK, Gupta R. Biodiesel production by transesterification using immobilized lipase. Biotechnology Letters 2013;35:479-490.
[383] Veras IC, Silva FAL, Ferrão-Gonzales AD, Moreau VH. One-step enzymatic production of fatty acid ethyl ester from high-acidity waste feedstocks in solvent-free media. Bioresource Technology 2011;102:9653-9658.
[384] Hama S, Kondo A. Enzymatic biodiesel production: An overview of potential feedstocks and process development. Bioresource Technology 2013;135.
[385] Du W, Li W, Sun T, Chen X, Liu D. Comparative study on lipase-catalyzed transformation of soybean oil for biodiesel production with different acyl acceptors. J Mol Catal B: Enzym 2004;30:125-129.
[386] Talukder MMR, Beatrice KLM, Song OP, Puah S, Wu JC, Won CJ, Chow Y. Improved method for efficient production of biodiesel from palm oil. Energy Fuels 2008;22:141-144.
[387] Lee JH, Kwon CH, Kang JW, Park C, Tae B, Kim SW. Biodiesel production from various oils under supercritical fluid conditions by *Candida antarctica* lipase B using a stepwise reaction method. Appl Biochem Biotechnol 2009;156:454-464.
[388] Fernandez D, Rodriguez E, Bassas M, Vinas M, Solanas AM, Llorens J, Marques AM, Manresa A. Agro-industrial oily wastes as substrates for PHA production by the new strain *Pseudomonas aeruginosa* NCIB 40045: Effect of culture conditions. Biochem Eng J 2005;26:159-167.

[389] Higbie R. Rate of absorption of a pure gas into still liquid during short periods of exposure. Transactions of the American Institute of Chemical Engineers 1935;35:365-389.
[390] Poling BE, Prausnitz JM, O'Connell JP. The properties of gases and liquids. Chapter 11. 5th Edition McGraw-Hill 2001.
[391] Llorens J, Mans C, Costa J. Discrimination of the effects of surfactants in gas absorption. Chem Eng Sci 1988;43:443-450.
[392] Mercade E, Robert M, Espuny MJ, Bosch MP, Manresa MA, Parra JL, Guinea J. New surfactant isolated from *Pseudomonas* 42A2. Journal of American Oil Chemists' Society 1988;65:1915-1916.
[393] Vazquez G, Chenlo F, Navaza JM, Alvarez E, Antorrena G. Determinación de propiedades gas-líquido en una columna de pared mojada. Afinidad 1991;48:97-100.
[394] Berovic M, Enfors S-O. Comprehensive bioprocess engineering. European Federation on Biotechnology Working Group on Bioreactor Performance University of Ljubljana 2010.
[395] Vrkoslav V, Míková R, Cvacka J. Characterization of natural wax esters by MALDI-TOF mass spectrometry. Journal of Mass Spectrometry 2008;44:101-110.
[396] Williams JA. Keys to bioreactor selection. CEP Magazine 2002;March:34-41.
[397] Cermak SC, Biresaw G, Isbell TA, Evangelista RL, Vaughn SF, Murray R. New crop oils—Properties as potential lubricants. Industrial Crops and Products 2013;44:232-239.
[398] Bastida J, Andres CD, Cullere J, Busquets M, Manresa A. Biotransformation of oleic acid into 10-hydroxy-8E-octadecenoic acid by Pseudomonas sp. 42A2. Biotechnol Lett 1999;21:1031-1035.
[399] Price NPJ, Manitchotpisit P, Vermillion KE, Bowmanc MJ, Leathers TD. Structural characterization of novel extracellular liamocins (mannitol oils) produced by *Aureobasidium pullulans* strain NRRL 50380. Carbohyd Res 2013;370:24-32.
[400] Martin-Arjol I, Busquets M, Isbell TA, Manresa A. Production of 10(*S*)-hydroxy-8(*E*)-octadecenoic and 7,10(*S*,*S*)-dihydroxy-8(*E*)-octadecenoic ethyl esters by Novozym 435 in solvent-free media. Appl Microbiol Biotechnol 2013;97:8041-8048.
[401] Higbie R. Rate of absorption of a pure gas into still liquid during short periods of exposure. Transactions of the American Institute of Chemical Engineers 1935;35:365-389.
[402] Mercade E, Robert M, Espuny MJ, Bosch MP, Manresa MA, Parra JL, Guinea J. New surfactant isolated from *Pseudomonas* 42A2. Journal of American Oil Chemists' Society 1988;65:1915-1916.
[403] The Engineering Toolbox. http://wwwengineeringtoolboxcom/oxygen-solubility-water-d_841html April, 2013.
[404] Ferreira BS, Keulen Fv, Fonseca MMRd. Novel calibration method for mass spectrometers for on-line gas analysis. Set-up for the monitoring of a bacterial fermentation. Bioprocess Eng 1998;19:289-296.
[405] C D DeMoyer ELS, J S Gulliver, S C Wilhelms. Impact of bubble and free surface oxygen transfer on diffused aeration systems. Water Research 2003;37:1890-1904.
[406] Atkinson B, Mavituna F. Biochemical Engineering and Biotechnology Handbook 2nd Edition. Stockton Press, New York 1991.
[407] Guerrero A, Casals I, Busquets M, León Y, Manresa A. Oxidation of oleic acid to (E)-10-hydroperoxy-8-octadecenoic acid and (E)-10-hydroxy-8-octadecenoic acid by *Pseudomonas sp*. 42A2. Biochimica et Biophysica Acta 1997;1347:75-81.
[408] Martinez E, Hamberg M, Busquets M, Diaz P, Manresa A, Oliw EH. Biochemical Characterization of the Oxygenation of Unsaturated Fatty Acids by the Dioxygenase and Hydroperoxide Isomerase of *Pseudomonas aeruginosa* 42A2. The Journal of Biological Chemistry 2010;285:9339-9345.
[409] Hanefeld U, Gardossib L, Magnerc E. Understanding enzyme immobilisation. Chem Soc Rev 2008;38:453-468.
[410] Chisti Y, M-Young M. Fermentation Technology, Bioprocessing, Scale-Up and Manufacture. Biotechnology: The Science and the Business 1999;Cap. 13:177-222.
[411] Kuo TM, Lanser AC. Factors influencing the production of a novel compound, 7,10-dihydroxy-8(E)-octadecenoic acid, by *Pseudomonas aeruginosa* PR3 (NRRL B-18602) in batch cultures. Curr Microbiol 2003;47:186-191.
[412] Berovic M, Enfors S-O. Comprehensive bioprocess engineering. European Federation on Biotechnology Working Group on Bioreactor Performance University of Ljubljana 2010.
[413] Kronemberger FA, Anna LMMS, Fernandes AC, Menezes RR, Borges CP, Freire DM. Oxygen-controlled biosurfactant production in a bench scale bioreactor. App Biochem Biotech 2007;147:33-45.

[414] Gomez E, Santos VE, Alcon A, Martin AB, Garcia-Ochoa F. Oxygen-Uptake and Mass-Transfer Rates on the Growth of *Pseudomonas putida* CECT5279: Influence on Biodesulfurization (BDS) Capability. Energy & Fuels 2006;20:1565-1571.
[415] Carragher JM, McClean WS, Woodley JM, Hack CJ. The use of oxygen uptake rate measurements to control the supply of toxic substrate: toluene hydroxylation by *Pseudomonas putida* UV4. Enzyme Microb Tech 2001;28:183-188.
[416] Cermak SC, Isbell TA. Physical properties of saturated estolides and their 2-ethylhexyl esters. Industrial Crops and Products 2002;16:119-127.
[417] Borgdorf R, Warwel S. Substrate selectivity of various lipases in the esterification of *cis*- and *trans*-9-octadecenoic acid. Appl Microbiol Biotechnol 1999;51:480-485.
[418] Laane C, Boeren S, Vos K, Veeger C. Rules for optimization of biocatalysis in organic solvents Biotechnol Bioeng 1986;30:81-87.
[419] Aguieiras ECG, Veloso CO, Bevilaqua JV, Rosas DO, Silva MAPd, Langone MAP. Estolides Synthesis Catalyzed by Immobilized Lipases. Enzyme Research 2011:1-7.
[420] Horchani H, Bouaziz A, Gargouri Y, Sayari A. Immobilized *Staphylococcus xylosus* lipase-catalysed synthesis of ricinoleic acid esters. J Mol Catal B: Enzym 2012;75:35-42.
[421] Bódalo A, Bastida J, Máximo MF, Montiel MC, Gómez M, Murcia MD. Production of ricinoleic acid estolide with free and immobilized lipase from *Candida rugosa*. Biochem Eng J 2008;39:450-456.
[422] Radzi SM, Basri M, Salleh AB, Ariff A, Mohammad R, Rahman MBA, Rahman RNZRA. High performance enzymatic synthesis of oleyl oleate using immobilised lipase from *Candida antarctica*. Electron J Biotechnol 2005;8:291-298.
[423] Bayer E, Gfrörer P, Rentel C. Coordination-Ionspray-MS (CIS-MS), a Universal Detection and Characterization Method for Direct Coupling with Separation Techniques. Angew Chem Int Ed 1999;38:992-995.
[424] Nielen MWF. Maldi time-of-flight mass spectrometry of synthetic polymers. Mass Spectrom Rev 1999;18:309-344.
[425] Vrkoslav V, Míková R, Cvacka J. Characterization of natural wax esters by MALDI-TOF mass spectrometry. Journal of Mass Spectrometry 2008;44:101-110.
[426] Bódalo-Santoyo A, Bastida-Rodríguez J, Máximo-Martín MF, Montiel-Morte MC, Murcia-Almagro MD. Enzymatic biosynthesis of ricinoleic acid estolides. Biochem Eng J 2005;26:155-158.
[427] Kelly AR, Hayes DG. Lipase-Catalyzed Synthesis of Polyhidryc Alcohol-Poly(ricinoleic acid) Ester Star Polymers. Journal of Applied Polymer Science 2006;101:1646-1656.
[428] Cermak SC, Isbell TA. Synthesis and physical properties of mono-estolides with varying chain lengths. Ind Crops Prod 2009;29:205-213.
[429] Santos JC, Bueno T, Rós PCMd, Castro HFd. Lipase-catalyzed synthesis of butyl esters by direct esterification in solvent-free system. Journal of Chemical Technology and Biotechnology 2007;82:956-961.
[430] Martin-Arjol I, Busquets M, Manresa A. Production of 10(*S*)-hydroxy-8(E)-octadecenoic acid mono-estolides by lipases in non-aqueous media. Process Biochemistry 2013;48:224-230.
[431] Isbell TA, Kleiman R. Characterization of Estolides Produced from the Acid-Catalyzed Condensation of Oleic Acid. JAOCS 1994;71:379-383.
[432] Kleiman TAIaR. Mineral Acid-Catalyzed Condensation of Meadowfoam Fatty Acids into Estolides. JAOCS 1996;73:1097-1107.
[433] Cermak SC, Isbell TA. Synthesis of Estolides from Oleic and Saturated Fatty Acids. JAOCS 2001;78:557-565.
[434] Isbell TA, Edgcomb MR, Lowery BA. Physical properties of estolides and their ester derivatives. Industrial Crops and Products 2001;13.
[435] Isbell TA, Lowery BA, DeKeyser SS, Winchell ML, Cermak SC. Physical properties of triglyceride estolides from lesquerella and castor oils. Industrial Crops and Products 2006;23:256-263.
[436] Ortega S. Síntesis biocatalítica de polirricinoleato de poliglicerol. Universidad de Murcia, Departamento de Ingeniería Química 2011.
[437] García-Zapateiro LA, Franco JM, Valencia C, Delgado MA, Gallegos C, Ruiz-Méndez MV. Chemical, thermal and viscous characterization of high-oleic sunflower and olive pomace acid oils and derived estolides. Grasas y Aceites 2013;64:497-508.
[438] Giap SGE. The Hidden Property of Arrhenius-type Relationship: Viscosity as a Function of Temperature. Journal of Physical Science 2010;21:29-39.

[439] Quinchia LA, Delgado MA, Valencia C, Franco JM, Gallegos C. Viscosity modification of different vegetable oils with EVA copolymer for lubricant applications. Ind Crop Prod 2010;32:607-612.
[440] Valeri D, Meirelles AJA. Viscosities of Fatty Acids, Triglycerides,and Their Binary Mixtures. JAOCS 1997;74:1221-1226.
[441] Cermak SC, Brandon KB, Isbell TA. Synthesis and physical properties of estolides from lesquerella and castor fatty acid esters. Industrial Crops and Products 2006;23:54-64.
[442] Lide DR. CRC Handbook of Chemistry and Physics. Internet Version 2007;87th Edition:16-41.
[443] Oliveira D, Luccio MD, Faccio C, Rosa CD, Bender JP, Lipke N, Menoncin S, Amroginski C, Oliveira JVd. Optimization of Enzymatic Production of Biodiesel from Castor Oil in Organic Solvent Medium. Applied Biochemistry and Biotechnology 2004;113-116:771-780.
[444] Ghesti GF, Macedo JLd, Resck IS, Dias JA, Dias SCL. FT-Raman Spectroscopy Quantification of Biodiesel in a Progressive Soybean Oil Transesterification Reaction and Its Correlation with ^{1}H NMR Spectroscopy Methods. Energy & Fuels 2007;21:2475-2480.
[445] Zagonel GF, Peralta-Zamora P, Ramos LP. Multivariate monitoring of soybean oil ethanolysis by FTIR. Talanta 2004;63:1021-1025.
[446] R.Guzatto, Defferrari D, Reiznautt QB, Cadore IR, Samios D. Transesterification double step process modification for ethyl ester biodiesel production from vegetable and waste oils. Fuel 2012;92:197-203.
[447] Isbell TA, Kleiman R, Plattner BA. Acid-Catalyzed Condensation of Oleic Acid into Estolides and Polyestolides. JAOCS 1994;71:169-174.
[448] Watanabe Y, Shimada Y, Sugihara A, Noda H, Fukuda H, Tominaga Y. Continuous Production of Biodiesel Fuel from Vegetable Oil Using Immobilized *Candida antarctica* Lipase. JAOCS 2000;77:355-360.
[449] Wang Y, Cao X. Enzymatic synthesis of fatty acid ethyl esters by utilizing camellia oil soapstocks and diethyl carbonate. Bioresource Technology 2011;102:10173-10179.
[450] Veras IC, Silva FAL, Ferrão-Gonzales AD, Moreau VH. One-step enzymatic production of fatty acid ethyl ester from high-acidity waste feedstocks in solvent-free media. Bioresource Technology 2011;102:9653-9658.
[451] P.Sreenivas, Mamilla VR, Sekhar KC. Development of Biodiesel from Castor Oil. IJES 2011;1:192-197.
[452] Okullo A, Temu AK, Ogwok P, Ntalikwa JW. Physico-Chemical Properties of Biodiesel from Jatropha and Castor Oils. International Journal of Renewable Energy Research 2012;2:2012.

7. Appendix

Table A.1. Experimental sets of data from OA oxidation in bioreactor experiments by *P. aeruginosa* 42A2.

	Concentration ($g \cdot l^{-1}$)					
Time (h)	**OA**	**(10*S*)-HPOME**	**(10*S*)-HOME**	**(7*S*,10*S*)-DiHOME**	**X**	**NO_3^-**
0.0	9.57	0.00	1.10	2.10	0.24	2.55
1.5	8.09	0.27	1.20	2.20	0.30	2.50
3.0	6.80	0.32	1.27	2.30	1.00	1.75
4.5	5.80	0.61	1.26	2.47	2.00	1.00
6.0	4.56	1.06	1.30	2.80	3.04	0.75
7.5	4.14	1.98	1.44	3.17	3.74	0.50
10.5	2.24	4.74	1.78	4.28	3.64	0.18
13.5	0.00	5.58	2.16	5.16	3.98	0.10
16.5	0.00	3.28	2.82	6.45	3.60	0.05
19.5	0.00	1.84	2.85	6.60	3.86	0.05
22.5	0.00	1.15	2.51	6.25	3.68	0.00
0	15.20	0.00	1.08	2.05	0.24	2.55
0.5	15.30	0.50	0.55	1.72	0.30	2.50
1	15.40	0.59	0.62	1.92	0.40	2.50
2	15.43	0.71	0.67	2.02	0.50	2.50
4	13.16	1.17	0.50	1.97	0.60	1.00
6	12.41	2.23	0.62	2.18	1.00	0.75
8	9.67	3.73	0.57	2.43	2.50	0.50
10.5	7.81	4.95	0.91	2.60	3.64	0.38
13.5	4.34	6.82	1.11	3.19	4.62	0.25
16.5	0.77	7.82	2.43	4.36	5.14	0.05
20.5	0.00	2.65	4.46	5.45	5.22	0.00
23.5	0.00	0.00	5.53	6.11	5.17	0.00
25.5	0.00	0.00	5.24	6.32	5.23	0.00
0	19.65	0.00	1.54	1.15	0.24	2.55
2	19.50	1.38	1.28	1.22	0.30	1.00
4	17.50	2.49	0.87	1.19	0.50	0.50
6	15.05	5.00	0.93	1.81	1.70	0.50
8	9.82	7.00	1.06	2.07	3.24	0.25
12	2.86	9.11	2.28	3.05	6.36	0.05
15	0.70	8.03	4.73	4.10	5.86	0.00
18	0.00	6.18	7.17	5.65	5.96	0.00
21	0.00	3.33	7.19	6.49	5.84	0.00
23	0.00	2.18	7.52	7.64	6.64	0.00
25	0.00	0.00	8.62	8.02	6.36	0.00
28	0.00	0.00	7.37	8.03	5.90	0.00
30	0.00	0.00	8.60	9.18	6.06	0.00

OA: Oleic acid. **(10*S*)-HPOME**: 10(*S*)-hydroperoxy-8(*E*)-octadecenoic acid. **(10*S*)-HOME**: 10(*S*)-hydroxy-8(*E*)-octadecenoic acid. **(7*S*,10*S*)-DiHOME**: 7,10(*S*,*S*)-hydroxy-8(*E*)-octadecenoic acid. **X**: biomass. **NO_3^-**: nitrates.

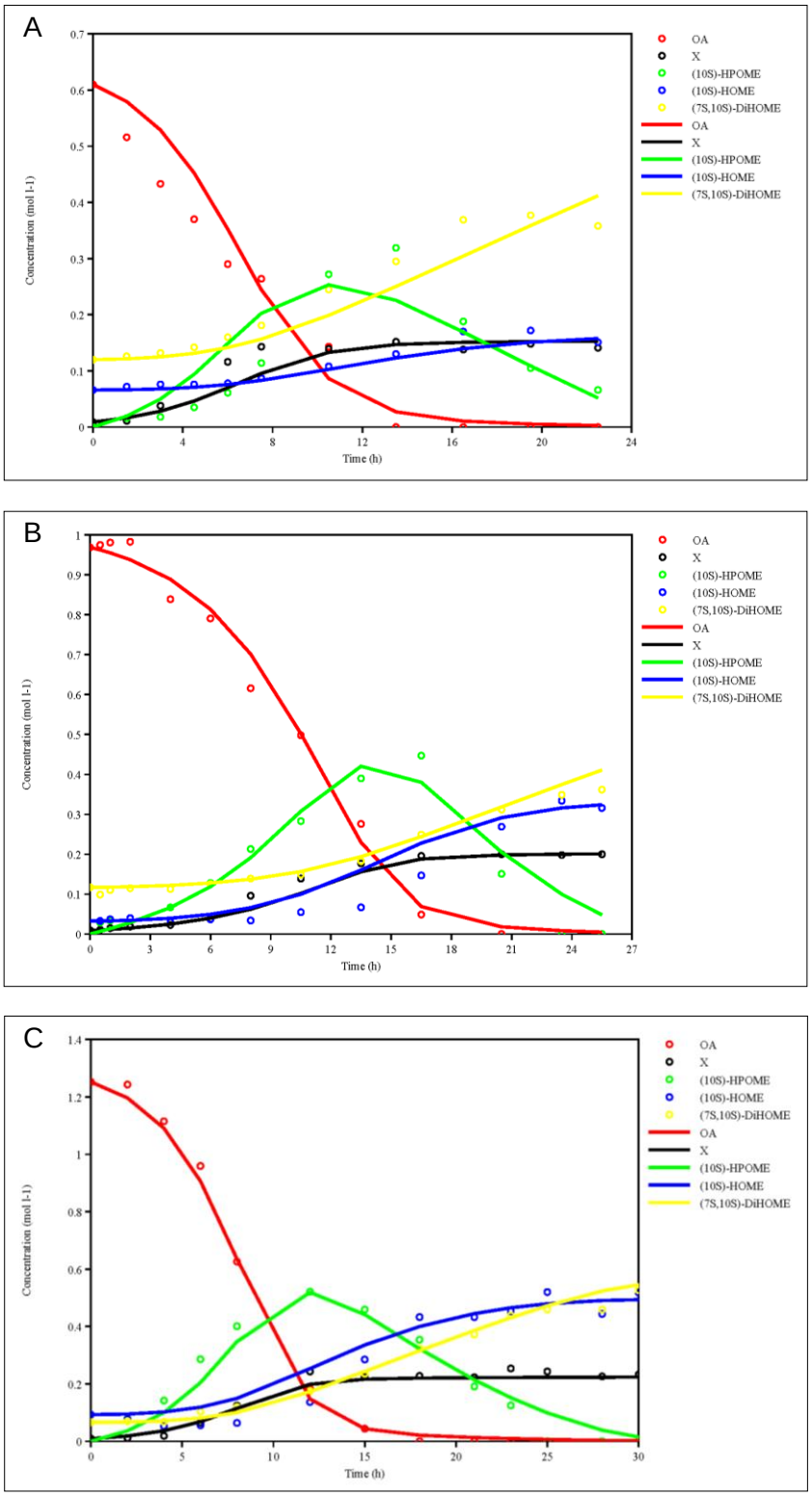

Figure A.1. Resulted simulations of the experimental data when Monod equation was introducted in the mathematical model. **A**: Oleic acid initial concentration of 10 $g \cdot l^{-1}$. **B**: Oleic acid initial concentration of 15 $g \cdot l^{-1}$. **C**: Oleic acid initial concentration 20 $g \cdot l^{-1}$. Dots: experimental data. Lines: simulated data. Units in $mol \cdot l^{-1}$.

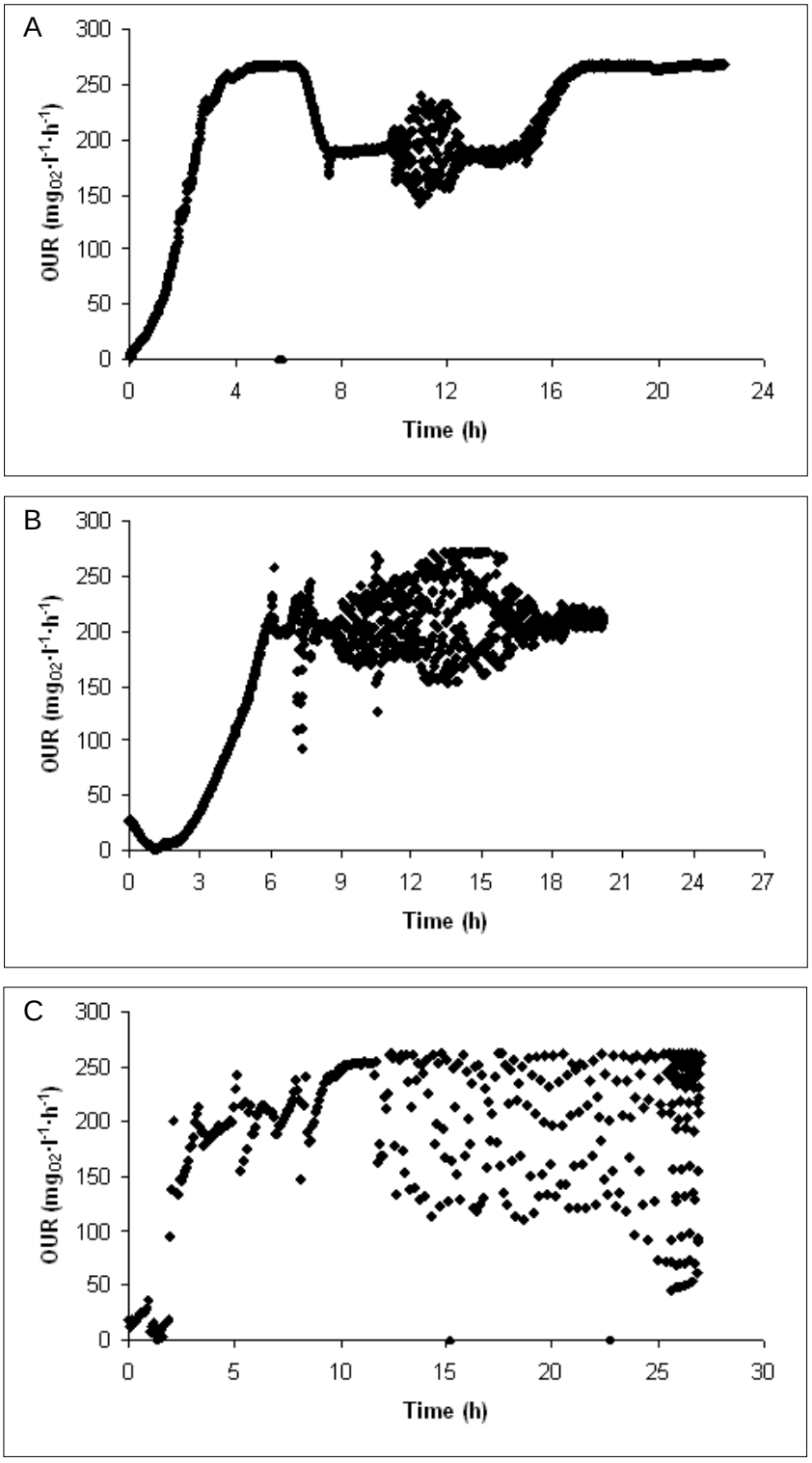

Figure A.2. Oxygen uptake rate (OUR) during OA oxidation by *P. aeruginosa* 42A2. **A**: OA initial concentration of 10 $g·l^{-1}$. **B**: OA initial concentration of 15 $g·l^{-1}$. **C**: OA initial concentration of 20 $g·l^{-1}$

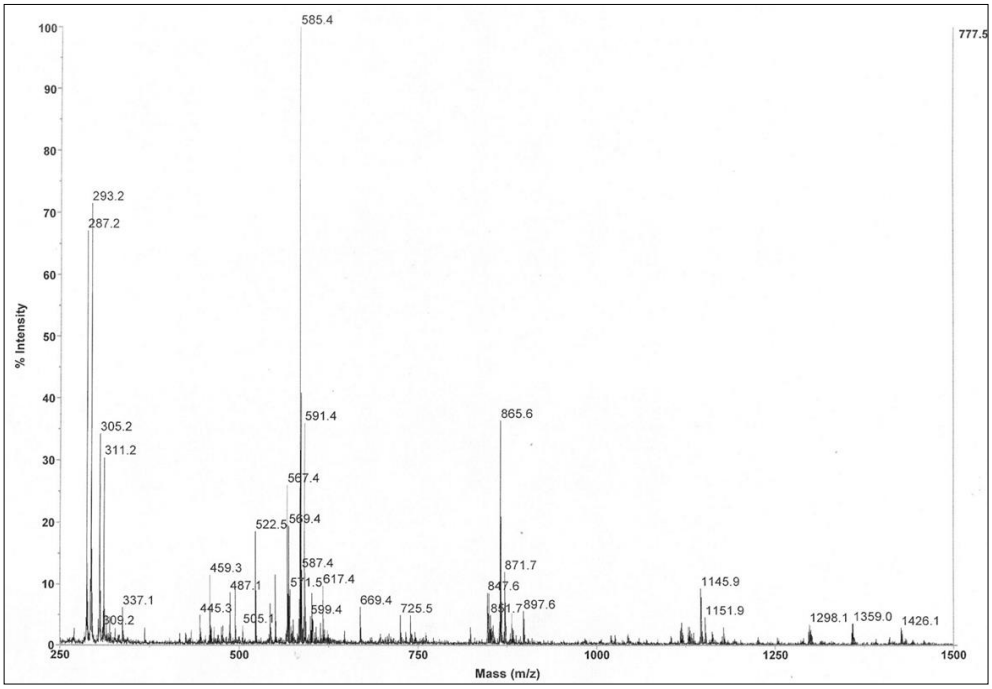

Figure A.3. MALDI TOF mass spectrum of estolides from RA of a sample with an AV of 68 $mg_{KOH} \cdot g_{sample}^{-1}$. DHB matrix was neutralized with LiOH.

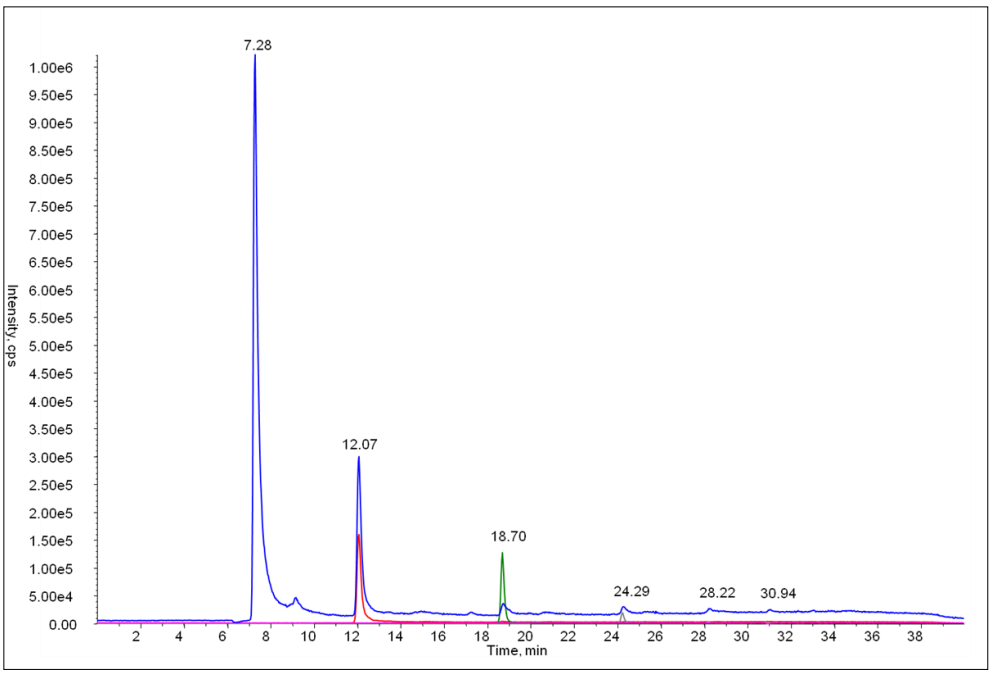

Figure A.4. Six extracted ion chromatogram. Ions *m/z* 298 (blue) (7.28, 12.07, 18.70, 24.29, 28.22, 30.94 min), 578 (red) (12.07 min), 858 (green) (18.70 min), 1138 (grey) (24.29 min), 1419 (28.22 min) and 1699 (30.94 min) of the estolides from RA, AV of 68 $mg_{KOH} \cdot g_{sample}^{-1}$.

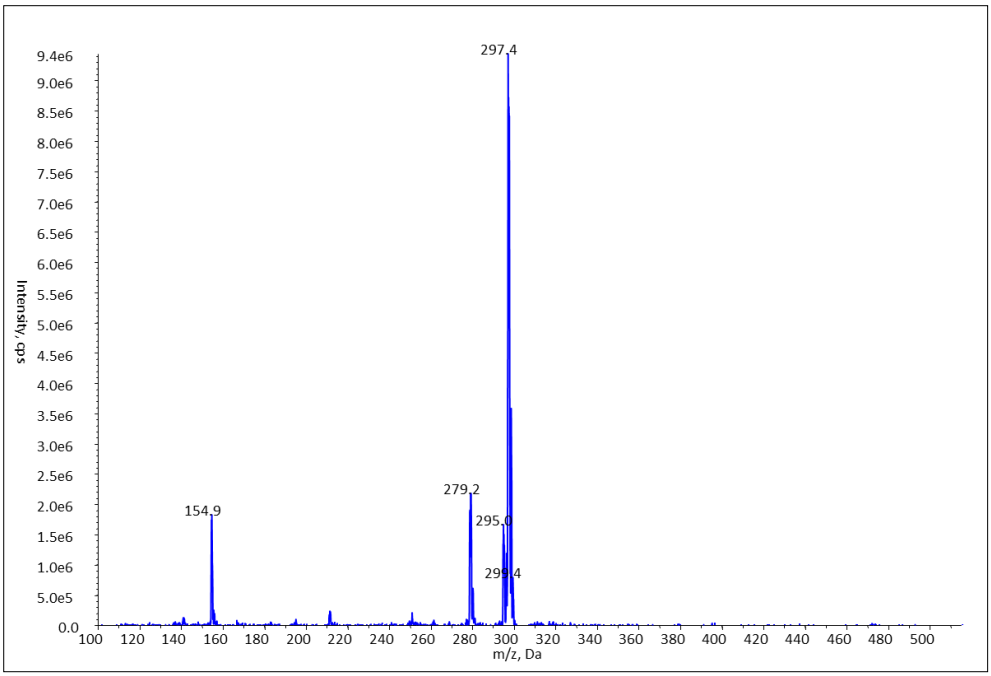

Figure A.5. Mass spectrum of the peak of 7.25 min: (10*S*)-HOME.

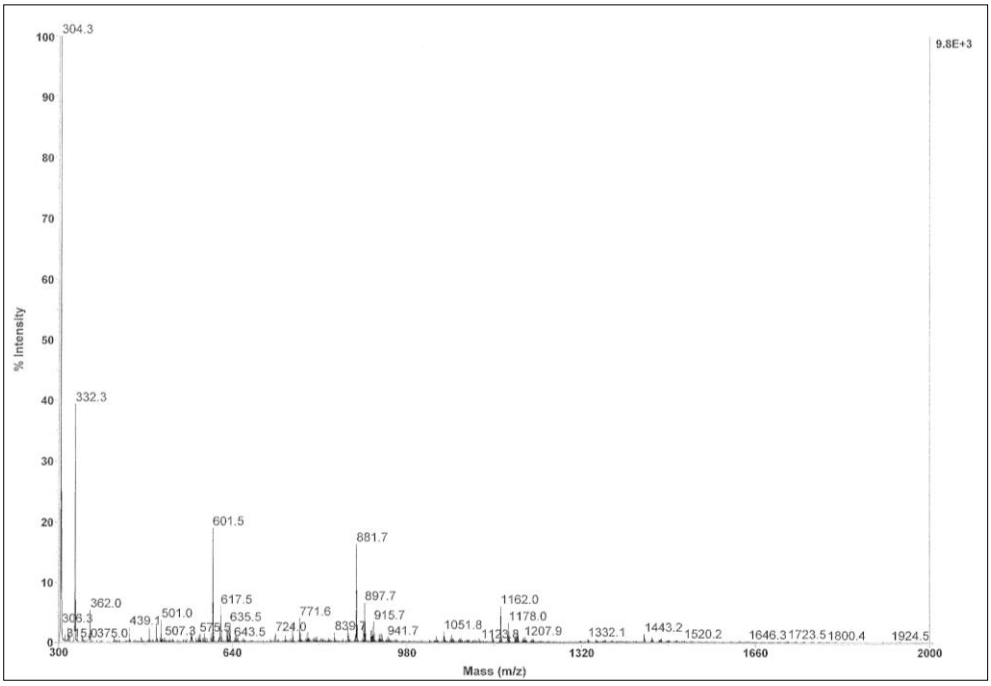

Figure A.6. MALDI TOF mass spectrum of estolides from RA of a sample with an AV of 68 $mg_{KOH} \cdot g_{sample}^{-1}$. DHB matrix was saturated in acetonitrile.

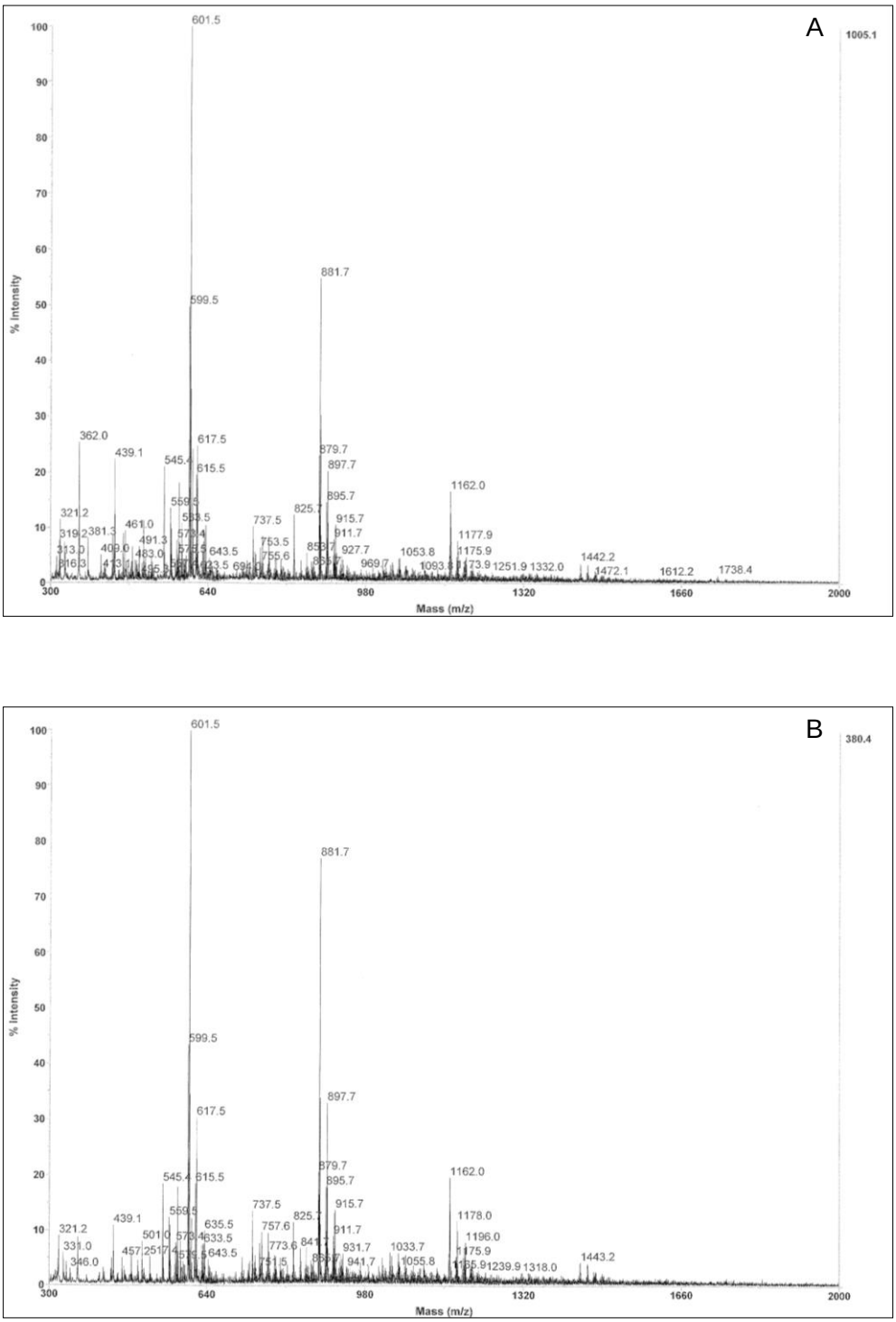

Figure A.7. MALDI TOF mass spectra with DHB saturated in acetonitrile, (10*S*)-HOME. **A**: (10*S*)-HOME polymerized with Lipozyme RM IM (12% *w/w*) at 80ºC during 168 h and vacuum (total preassure of 1.6 kPa). **B**: (10*S*)-HOME polymerized with Lipozyme TL IM (12% *w/w*) at 80ºC during 168 h and vacuum (total preassure of 1.6 kPa).

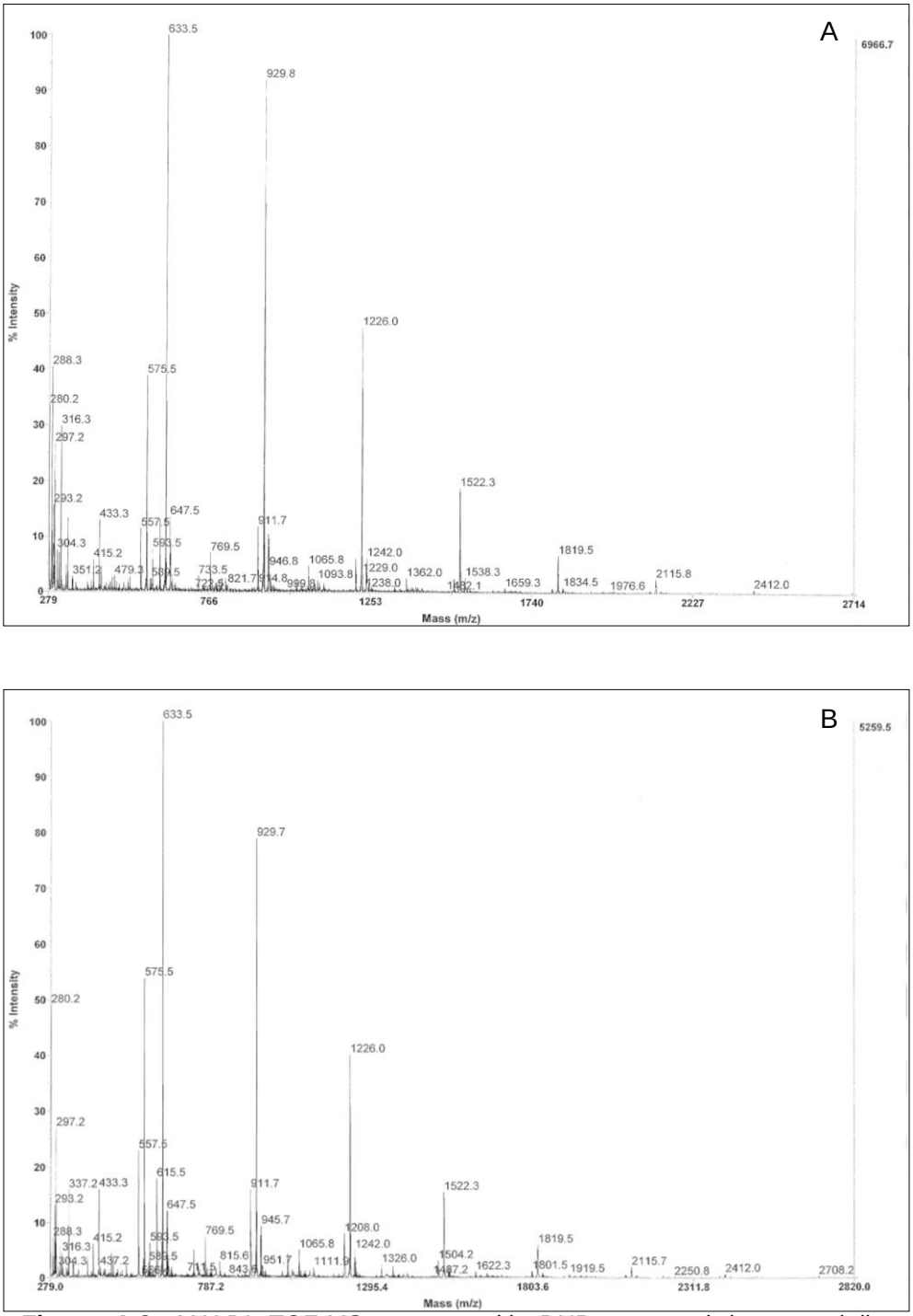

Figure A.8. MALDI TOF-MS spectra with DHB saturated in acetonitrile, (7*S*,10*S*)-DiHOME. **A**: (7*S*,10*S*)-DiHOME polymerized with Lipozyme RM IM (12% *w/w*) at 80ºC during 168 h and vacuum (total preassure of 1.6 kPa). **B**: (7*S*,10*S*)-DiHOME polymerized with Lipozyme TL IM (12% *w/w*) at 80ºC during 168 h and vacuum (total preassure of 1.6 kPa).

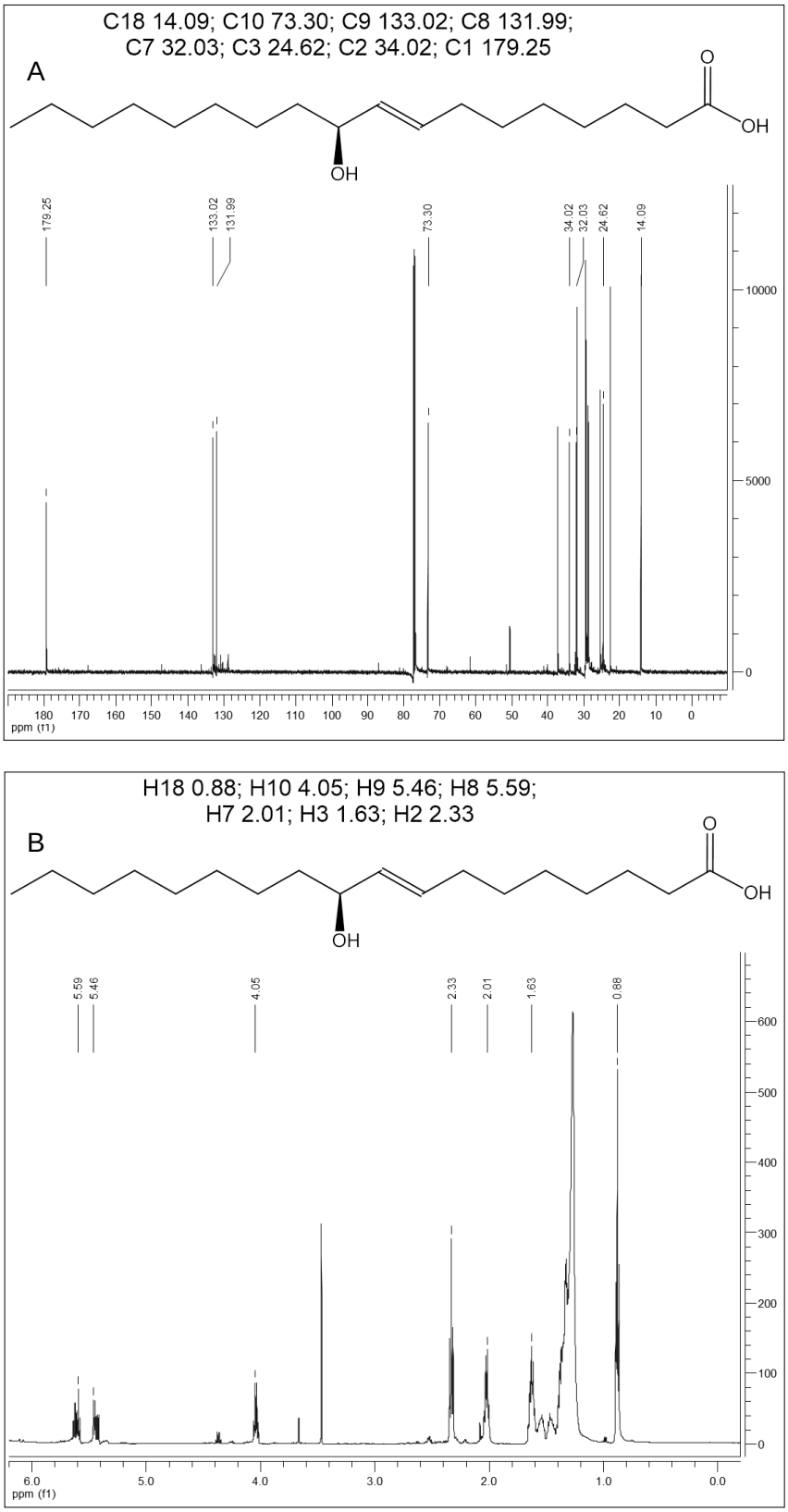

Figure A.9. (10*S*)-HOME NMR spectra. **A**: ^{13}C NMR spectrum. **B**: ^{1}H NMR spectrum. (10*S*)-HOME was 91% pure. Chemical shifts are expressed in parts per million.

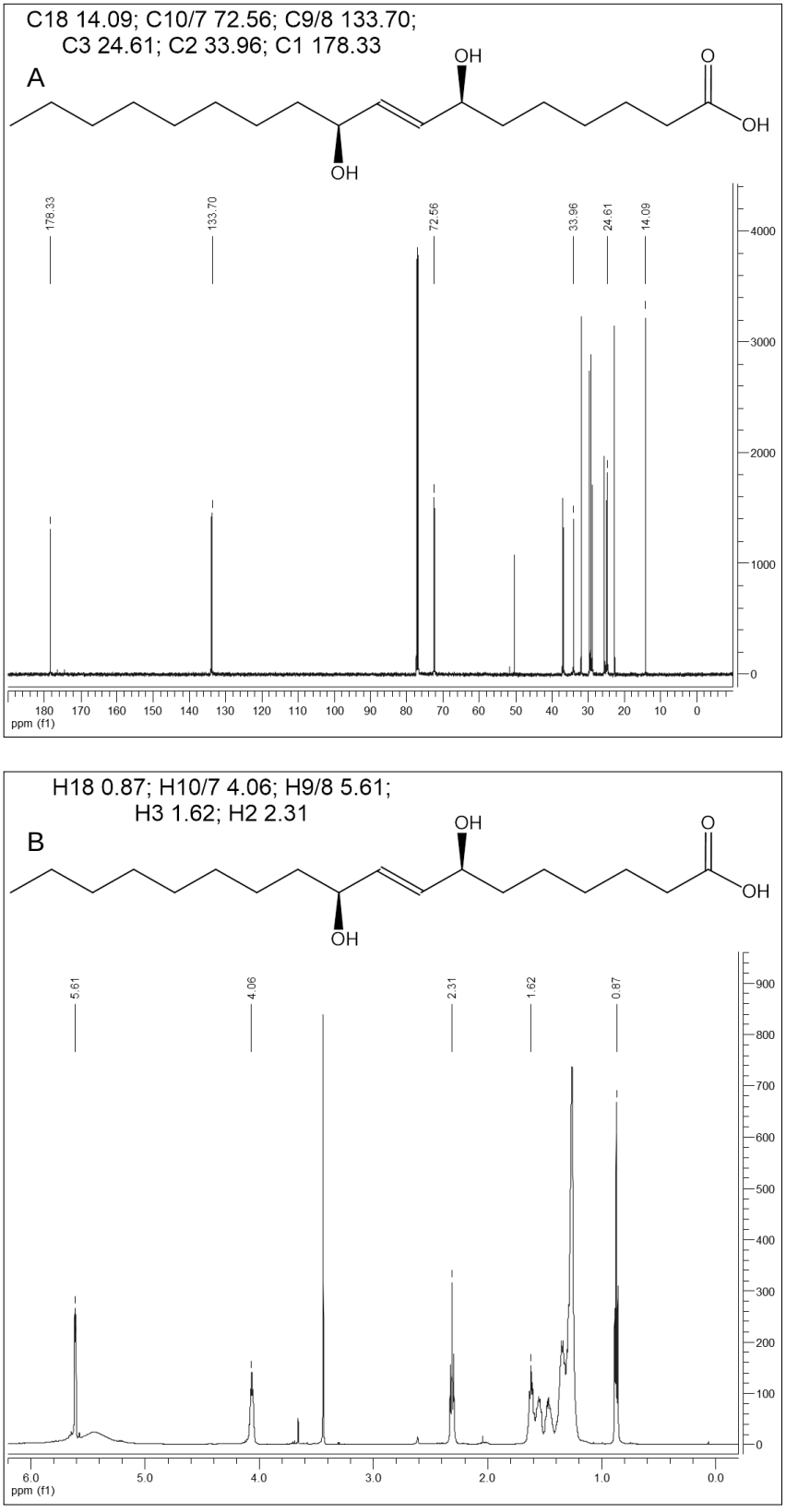

Figure A.10. (7*S*,10*S*)-DiHOME NMR spectra. **A**: ^{13}C NMR spectrum of (7*S*,10*S*)-HOME. **B**: ^{1}H NMR spectrum of (7*S*,10*S*)-HOME. (7*S*,10*S*)-HOME was 96% pure. Chemical shifts are expressed in parts per million.

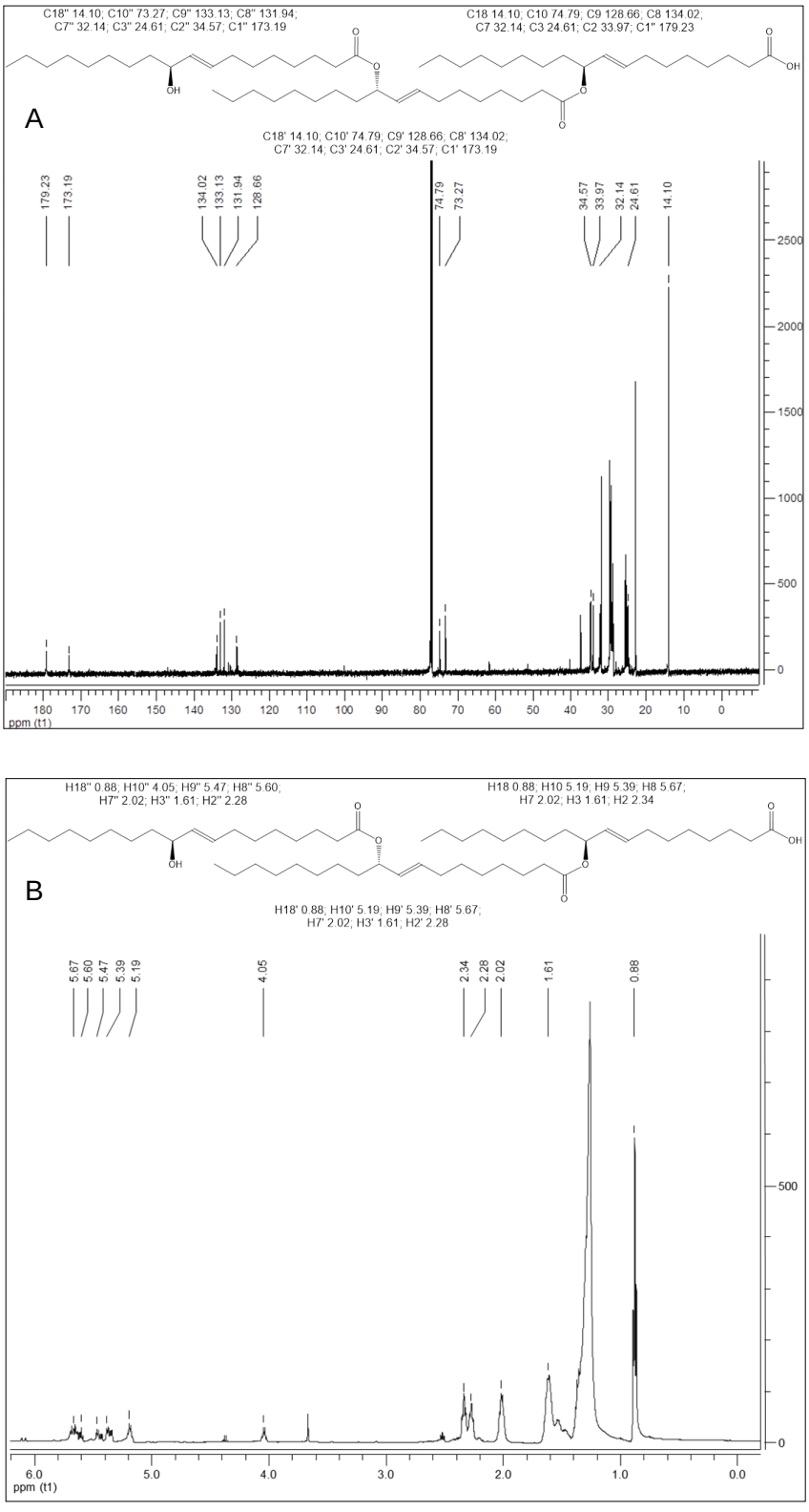

Figure A.11. NMR spectra of (10*S*)-HOME estolides synthesized by Lipozyme RM IM. **A**: ^{13}C NMR spectrum. **B**: ^{1}H NMR spectrum. Estolides were synthetized by Lipozyme RM IM (12% *w/w*) at 80ºC during 168 h and vacuum (total preassure of 1.6 kPa) in a solvent-free medium. Chemical shifts are expressed in parts per million. Depicted molecules in the figures are a guide to understand the different types of atoms present in the polyesters.

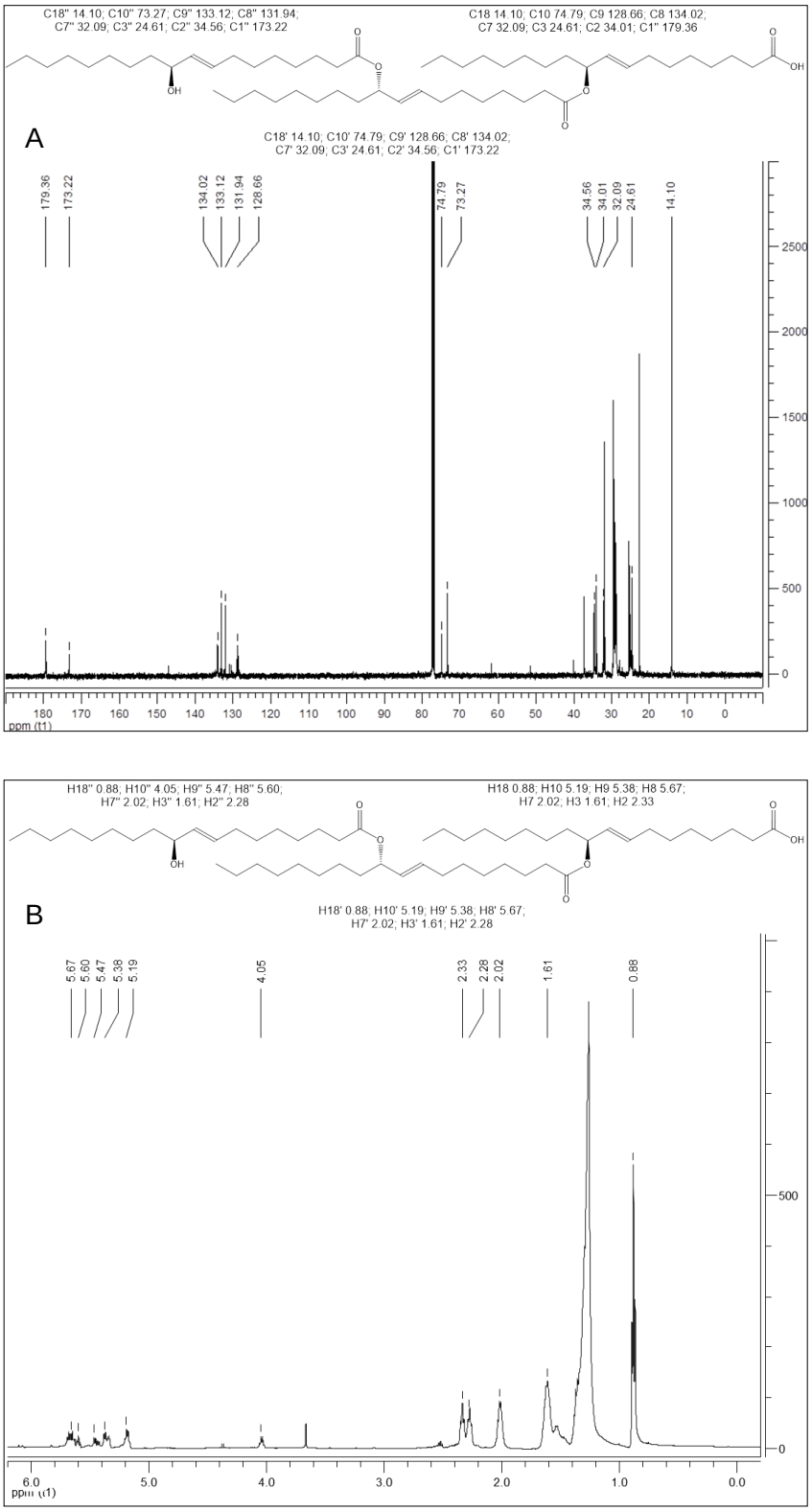

Figure A.12. NMR spectra of (10*S*)-HOME estolides synthesized by Lipozyme TL IM. **A**: ^{13}C NMR spectrum. **B**: ^{1}H NMR spectrum. Estolides were produced by Lipozyme TL IM (12% *w/w*) at 80ºC during 168 h and vacuum (total preassure of 1.6 kPa) in a solvent-free medium. Chemical shifts are expressed in parts per million. Depicted molecules in the figures are a guide to understand the different types of atoms present in the polyesters.

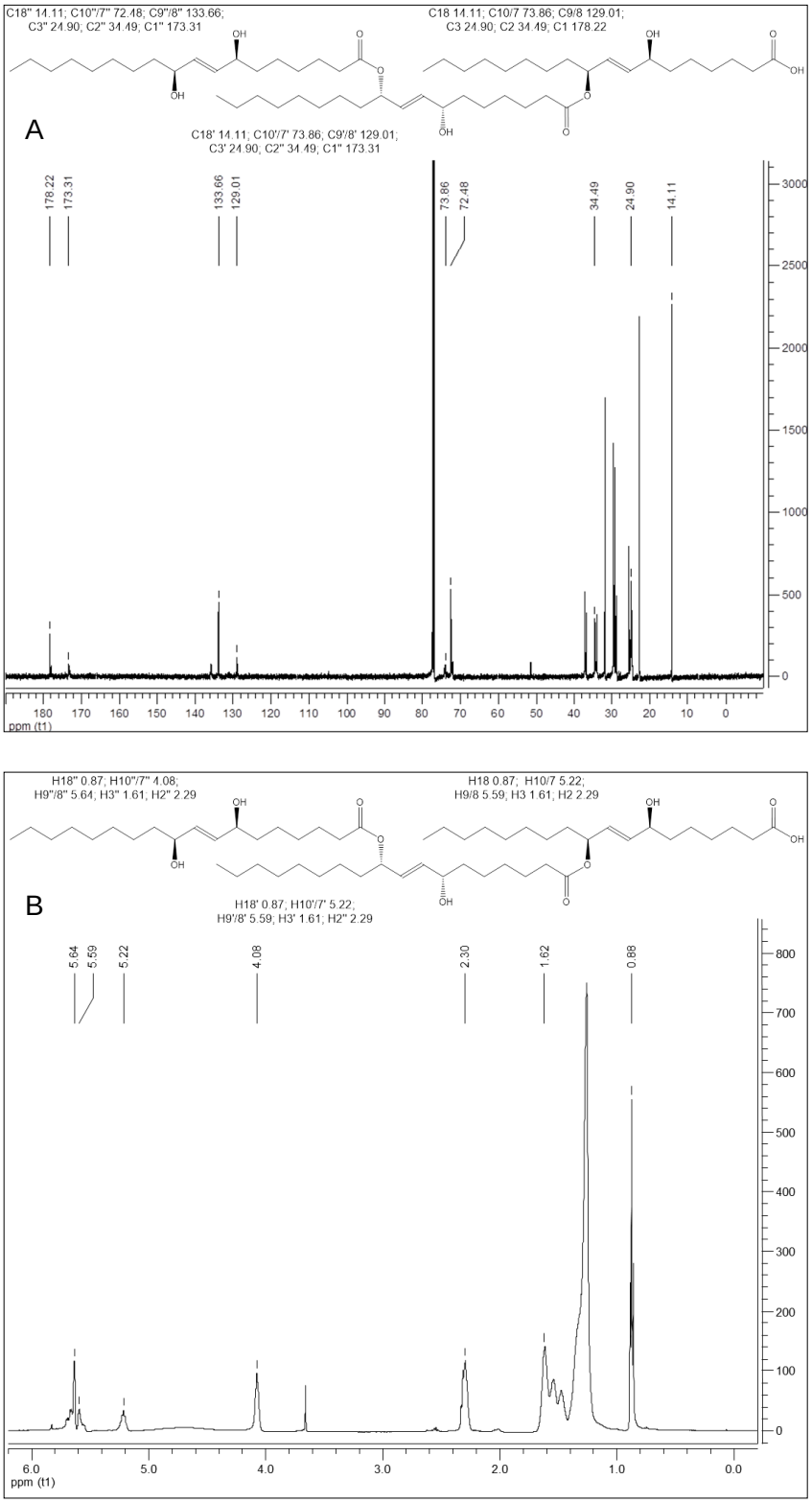

Figure A.13. NMR spectra of (7*S*,10*S*)-DiHOME estolides synthesized by Lipozyme RM IM. **A**: ^{13}C NMR spectrum. **B**: ^{1}H NMR spectrum. Estolides were produced by Lipozyme RM IM (12% *w/w*) at 80ºC during 168 h and vacuum (total preassure of 1.6 kPa) in a solvent-free medium. Chemical shifts are expressed in parts per million. Depicted molecules in the figures are a guide to understand the different types of atoms present in the polyesters.

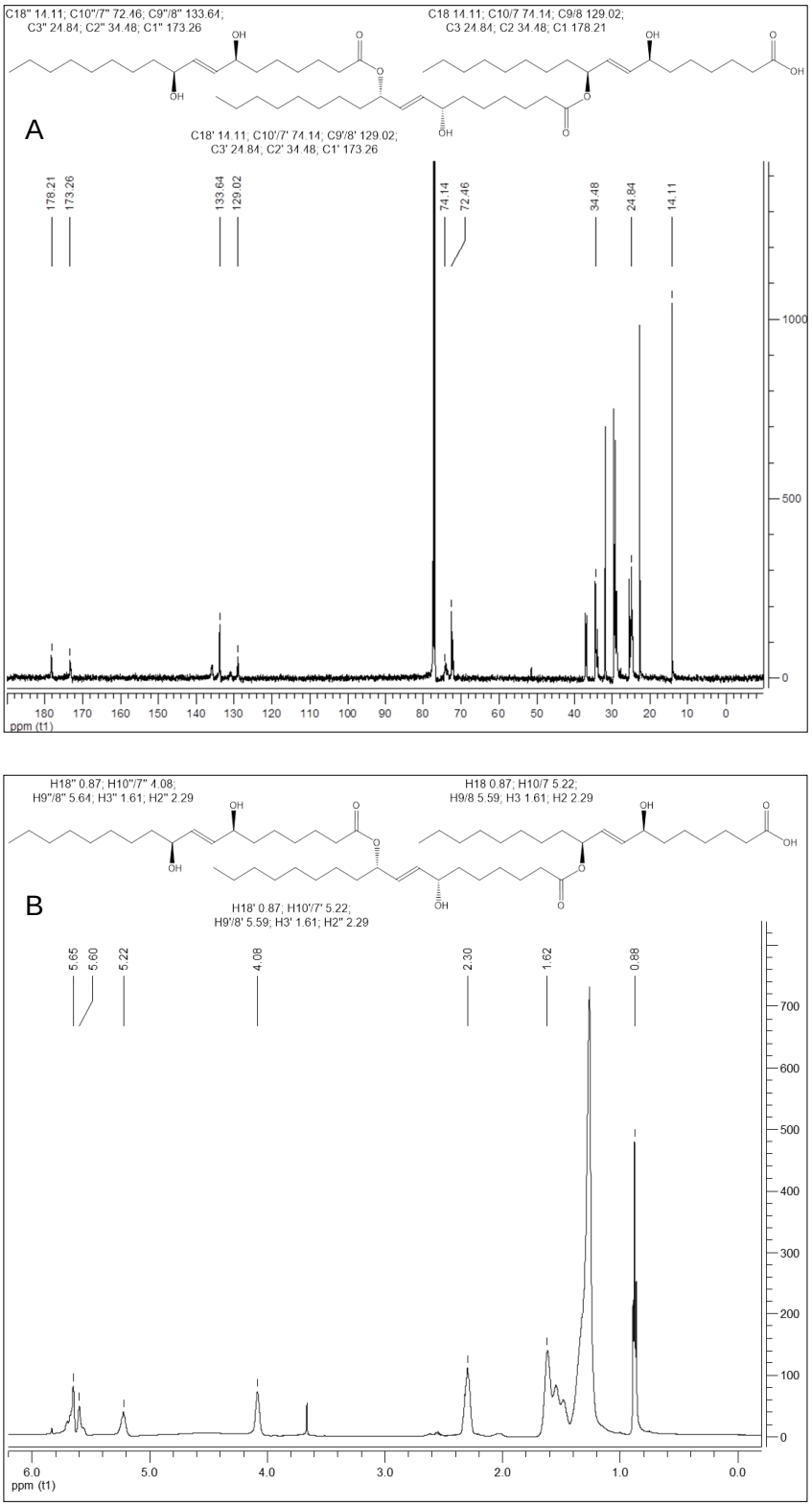

Figure A.14. NMR spectra of (7*S*,10*S*)-DiHOME estolides synthesized by Lipozyme TL IM. **A**: ^{13}C NMR spectrum. **B**: ^{1}H NMR spectrum. Estolides were produced by Lipozyme TL IM (12% *w/w*) at 80ºC during 168 h and vacuum (total preassure of 1.6 kPa) in a solvent-free medium. Chemical shifts are expressed in parts per million. Depicted molecules in the figures are a guide to understand the different types of atoms present in the polyesters.

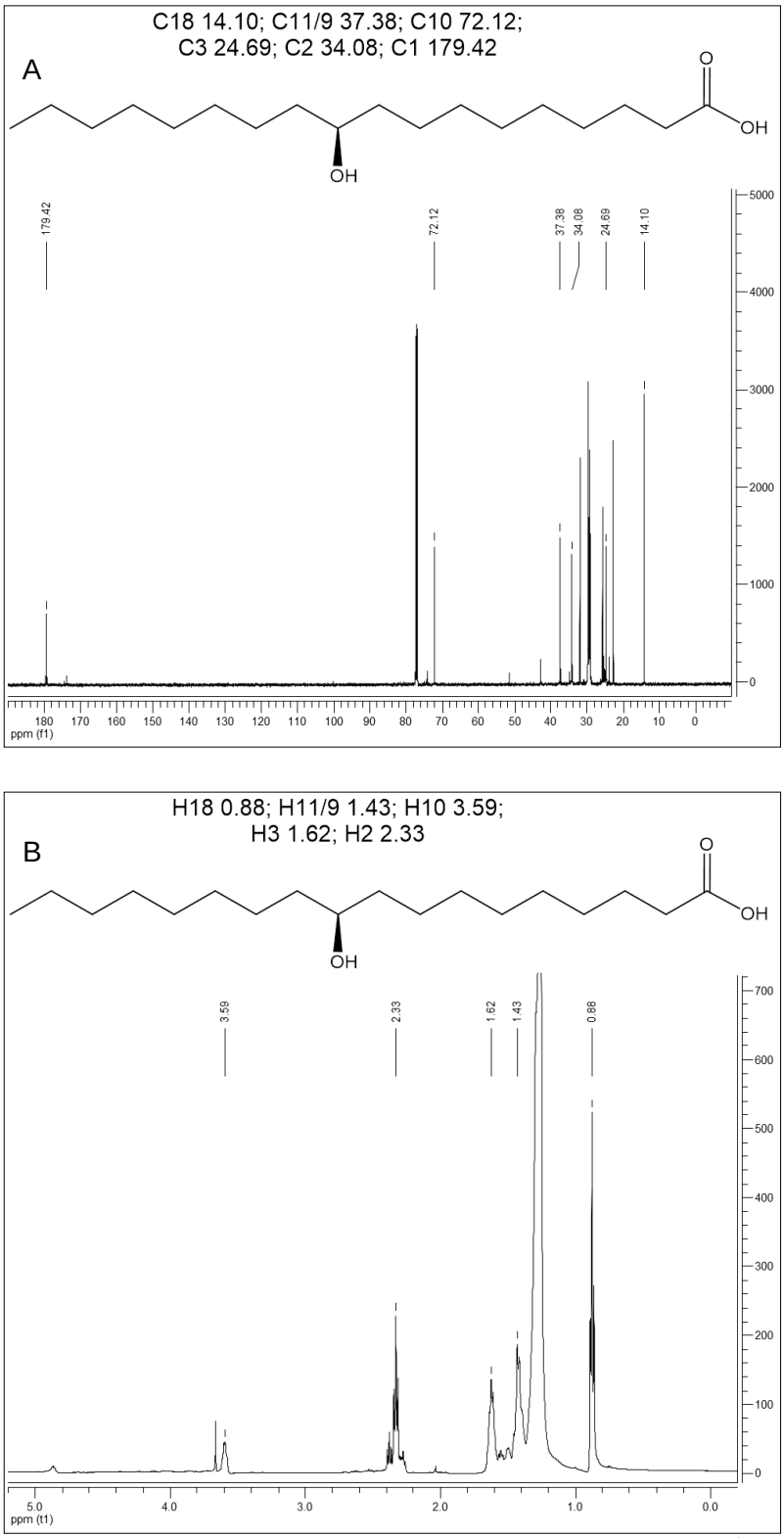

Figure A.15. NMR spectra of saturated (10*S*)-HOME. **A**: ^{13}C NMR spectrum. **B**: ^{1}H NMR spectrum. Chemical shifts are expressed in parts per million.

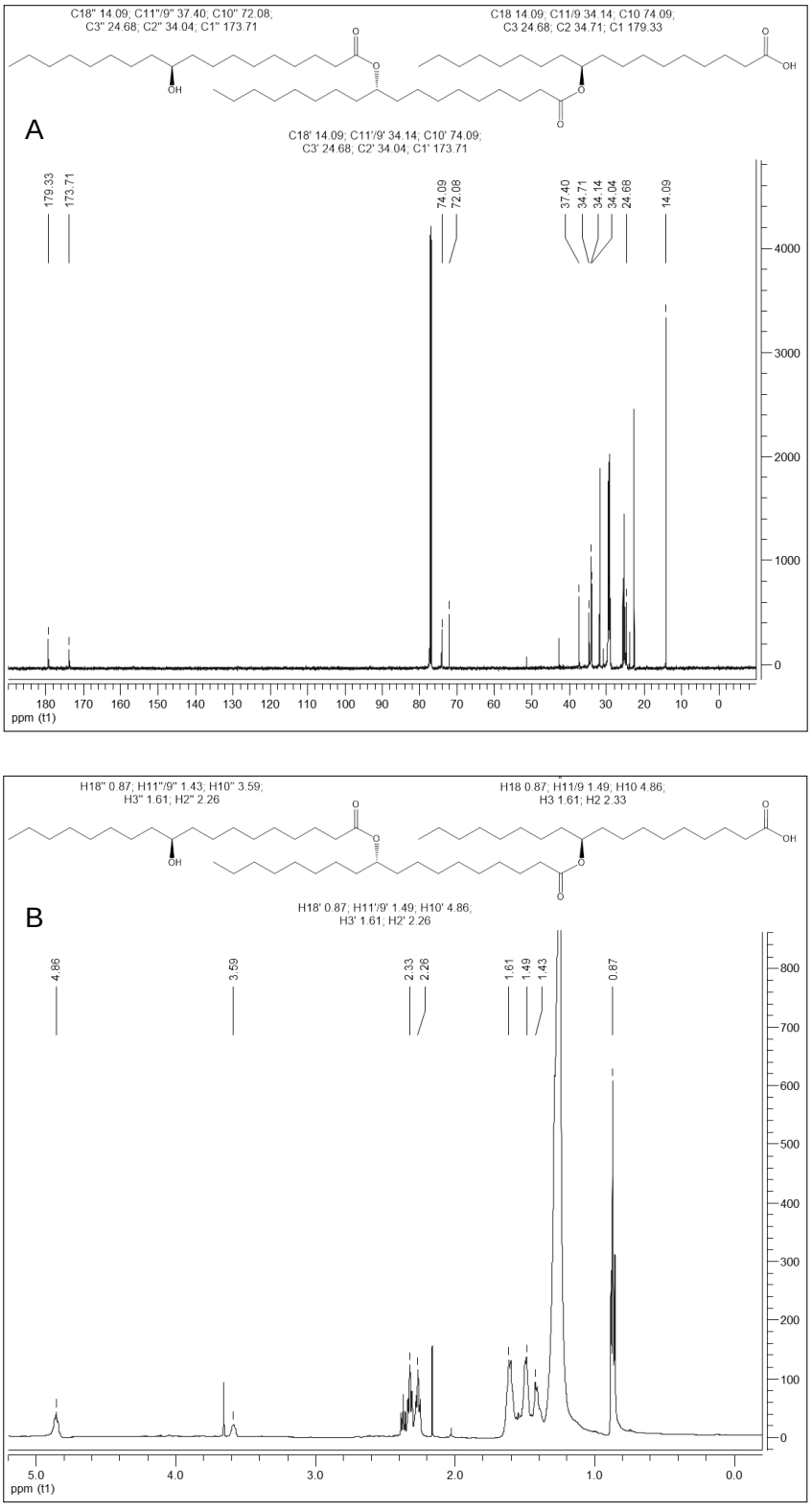

Figure A.16. NMR spectra of saturated (10*S*)-HOME estolides chemically produced. **A**: ^{13}C NMR spectrum. **B**: ^{1}H NMR spectrum. Reaction conditions were: 80ºC during 168 h and vacuum (total preassure of 1.6 kPa) in a solvent-free medium. Chemical shifts are expressed in parts per million. Depicted molecules in the figures are a guide to understand the different types of atoms present in the polyesters.

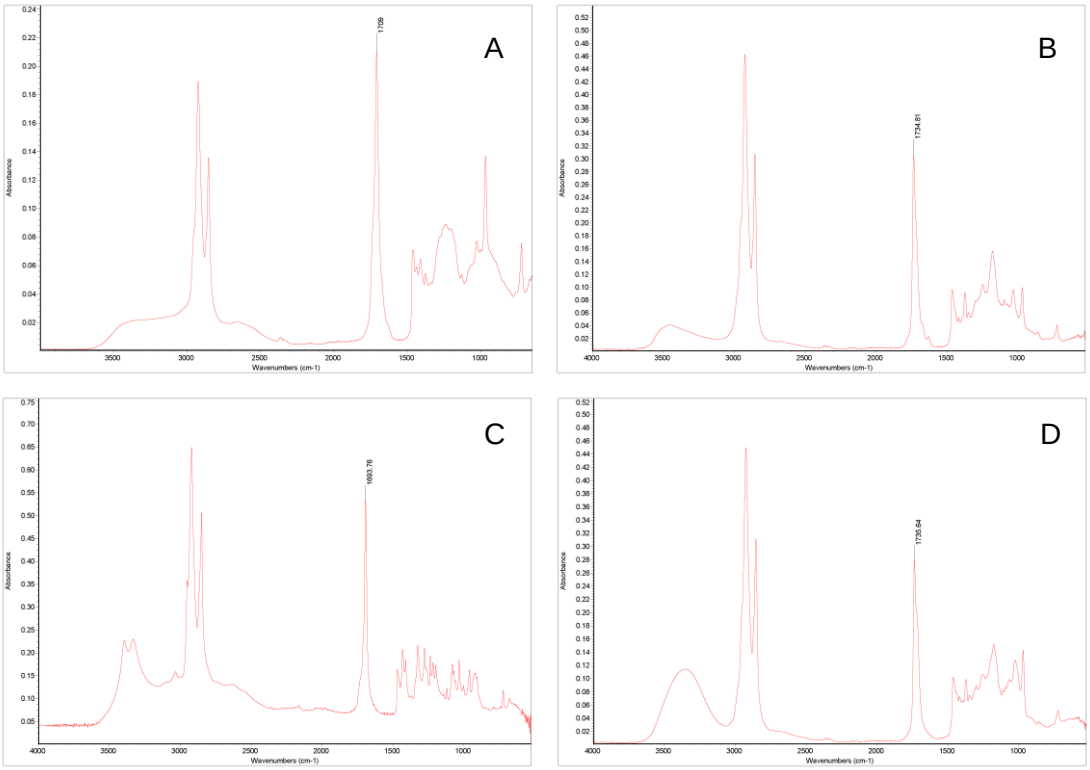

Figure A.17. Fourier transformed infrared spectroscopy spectra of *trans*-HFA ethyl esters. **A**: (10*S*)-HOME; **B**: (10*S*)-HOME ethyl ester; **C**: (7*S*,10*S*)-DiHOME; and, **D**: (7*S*,10*S*)-DiHOME ethyl ester.

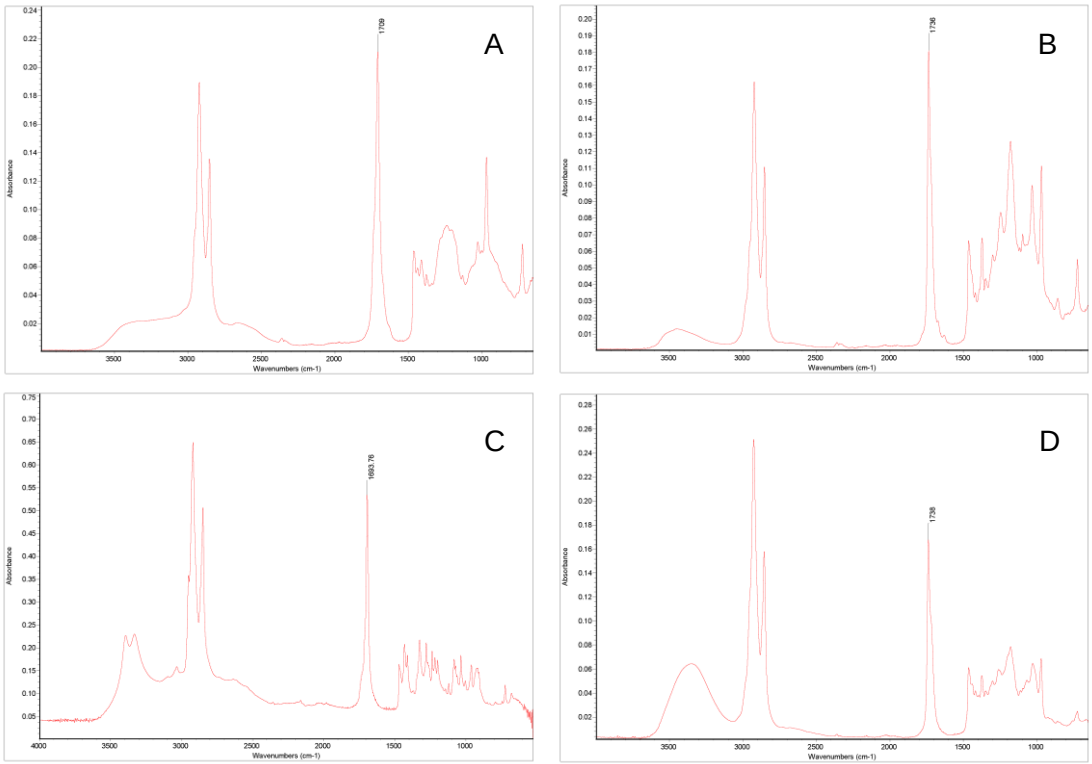

Figure A.18. Fourier transformed infrared spectroscopy spectra of *trans*-HFA estolide ethyl esters. **A**: (10*S*)-HOME; **B**: (10*S*)-HOME estolides ethyl ester; **C**: (7*S*,10*S*)-DiHOME; and, **D**: (7*S*,10*S*)-DiHOME estolides ethyl ester.

8. Publications

Appl Microbiol Biotechnol (2012) 93:2551–2561
DOI 10.1007/s00253-011-3646-z

Hydroxy-fatty acid production in a *Pseudomonas aeruginosa* 42A2 PHA synthase mutant generated by directed mutagenesis

Noelia Torrego-Solana · Ignacio Martin-Arjol · Mònica Bassas-Galia · Pilar Diaz · Angeles Manresa

Received: 8 September 2011 / Revised: 26 September 2011 / Accepted: 13 October 2011 / Published online: 15 November 2011

Abstract *Pseudomonas aeruginosa* 42A2 growing on waste frying oils is capable to synthesize polyhydroxyalkanoic acids (PHAs) and hydroxy-fatty acids as a result of several enzymatic conversions. In order to study the physiological role of PHA biosynthesis in *P. aeruginosa* with respect to the synthesis of hydroxy-fatty acids, an unmarked deletion mutant deficient for PHA biosynthesis was generated in *P. aeruginosa* 42A2. A combination of the *sac*B-based negative selection system with a *cre-lox* antibiotic marker recycling method was used for mutant isolation. Electron microscopy, nuclear magnetic resonance analysis, and transmission electron microscopy confirmed that PHA accumulation was completely abolished in the mutant strain. Interestingly, the new mutant strain showed higher carbon and oxygen uptake rate than the wild-type strain and higher efficiency in the conversion of oleic acid into (E)-10-hydroxy-8-octadecenic acid-octadecenoic acid.

N. Torrego-Solana · P. Diaz (✉)
Department of Microbiology, Faculty of Biology,
University of Barcelona,
Av. Diagonal 645,
08028 Barcelona, Spain
e-mail: pdiaz@ub.edu

N. Torrego-Solana · I. Martin-Arjol · A. Manresa (✉)
Laboratory of Microbiology, Faculty of Pharmacy,
University of Barcelona,
Joan XXIII s/n,
08028 Barcelona, Spain
e-mail: amanresa@ub.edu

M. Bassas-Galia
Environmental Microbiology Laboratory,
Helmholtz Center for Infection Research,
Inhoffenstraße 7,
38124 Braunschweig, Germany

Keywords *Pseudomonas aeruginosa* · PHA-negative mutant · *sac*B-based negative selection · *cre-lox* antibiotic recycling · Hydroxy-fatty acids

Introduction

A large number of microorganisms synthesize polyhydroxyalkanoic acids (PHAs), which are accumulated as intracellular, water-insoluble inclusions (Rehm and Steinbuchel 1999) in the cytoplasm. This occurs under stress situations for cell populations, like a relative excess of carbon source and a nitrogen, magnesium, or phosphorous depletion (Lee 1996; Luengo et al. 2003; Prieto et al. 2007). The genus *Pseudomonas* can synthesize and accumulate large amounts of medium chain length PHAs constituted by various 3-hydroxy-fatty acids with carbon chain lengths ranging from 6 to 14 carbon atoms. The production and composition of PHAs depend on the microorganism itself as well as on its PHA synthases (PhaC) specificities, on the nature of the carbon source, and on the metabolic routes involved (Rehm and Steinbuchel 1999; Witholt and Kessler 1999; Rehm 2003).

Pseudomonas aeruginosa 42A2 (NCIMB 40045) was isolated from a waste oil-contaminated water sample. When growing on waste oils, *P. aeruginosa* 42A2 produces intracellular PHAs and various extracellular products: (E)-7,10-dihydroxy-8-octadecenoic [(7*S*,10*S*)-DiHOME]; (E)-10-hydroperoxy-8E-octadecenoic acid [(10S)-HPOME], and (E)-10-hydroxy-8-octadecenoic [(10S)-HOME] (Guerrero et al. 1997). Several enzymes are involved in the hydroxylated fatty acid production (Busquets et al. 2004; Martinez et al. 2010). These compounds can be further polymerized into estolides by means of one or more secreted lipases (Erhan and Isbell 1997; Pelaez et al. 2003; Bofill et al. 2010).

With the aim to improve the production yield of secreted hydroxy-fatty acids, a *P. aeruginosa* 42A2 negative PHA mutant was generated. The resulting mutant was evaluated for the production of HOME and DiHOME.

Materials and methods

Bacterial strains, plasmids, and growth conditions

Escherichia coli and *P. aeruginosa* strains and the plasmids used in this work are listed in Table 1. *E. coli* DH5α or S17.1 were used as recipient strains for recombinant plasmids and were grown in Luria–Bertani medium (LB) (Panreac, Spain) at 37°C (supplemented with 10 μg gentamicin/ml or 100 μg ampicillin/ml, when necessary). *P. aeruginosa* 42A2 (NCIMB 40045) was routinely grown in LB medium at 30°C. Cultures were incubated on a reciprocal rotary shaker (150 rpm), and the required antibiotics added at appropriate concentrations: 350 μg carbenicillin/ml, 350 μg gentamicin/ml, 350 μg tetracycline/ml, and 300 μg kanamycin/ml. Electroporated *P. aeruginosa* cells were grown in SOC medium at 30°C (Hanahan 1983). For kinetics of product formation (PHA and hydroxy-fatty acid), growth was performed in a 2-l bioreactor saline medium composed of the following salts (in grams per liter): $CaCl_2$ (0.01), $NaNO_3$ (3.5), K_2HPO_4 (2.0), KH_2PO_4 (1.0), KCl (0.1), $MgSO_4{\cdot}7H_2O$ (0.5), $FeSO_4{\cdot}7H2O$ (0.012), and 0.05 ml/l of trace elements solution. The trace element solution was as follows (in milligrams per 100 milliliter): H_3BO_3 (148), $CuSO_4{\cdot}5H_2O$ (196), $MnSO_4{\cdot}H_2O$ (154), $Na_2MoO_4{\cdot}2H_2O$ (15), and $ZnSO_4{\cdot}7H_2O$ (307). This medium was supplemented with 2% waste frying oil (WFO) (olive:sunflower oil, 50:50 *v*/*v*) containing oleic acid as the major component (41. 65%) (Fernandez et al. 2005).

Table 1 Bacterial strains, plasmids, and primers used in this work

Strains	Relevant traits	Reference
Pseudomonas aeruginosa		
42A2	NCIMB 40045a	Bassas et al. 2006
42A2 ΔAGmD	42A2 containing chromosomal deletion of *phaC1-Z-C2* genes and an insertion of a Gm resistance cassette	This study
42A2 ΔAD	42A2 containing chromosomal deletion of *phaC1-Z-C2* genes	This study
Escherichia coli		
DH5a	F^-, *gyr*A96, *rec*A1, *rel*A1, *end*A1 *thi*-1, hsdR17 (r_k^- m_k^+), glnV44, deorD(lacZYA-argF)u169, [f80dD(lacZ)M15]	Hanahan 1983
S17-1	*recA*; harbors the t*ra* genes of plasmid RP4 in the chromosome; *proA thi*-	Simon et al. 1983
Plasmids	Relevant traits	Reference
pGEM®-T	Ap^R, *lacZ, lacI*	Promega, Spain
pGEM-TAD	Ap^R, pGEM-T vector containing AD amplified insert	This study
pUCGmlox	Ap^R, Gm^R, pUC18-based vector containing the *lox* flanked *aac*C1 (Gm resistance cassette) gene	Quénée et al. 2005
pEx100Tlink	Ap^R, pEX100T with a MCS	Quénée et al. 2005
pEx100TAD	Ap^R, pEX100T*link* vector containing AD	This study
pEx100TAGmD	Ap^R, Gm^R, pEX100TAD vector containing the *lox* flanked *aac*C1 gene (Gm*lox*) inside the AD amplified insert	This study
pCM157	Tc^R, *cre* expression vector	Marx et al. 2002
Name	Sequence (5′→3′)	Reference
(A) U58	5′ GCGAATTCGATGAGTCAGAAGAAC 3′	This study
(B) L555 *Bam*HI[a]	5′ C**GGATCC**TGTCTACAGTAGCTCGTTGTTCACCAGGTCCTTG 3′	This study
(C) U3973 *Bam*HI[a]	5′ ACCAACTGTAGACA**GGATCC**GGCCGGCAACTGCGCAAGGTCAG 3′	This study
(D) L4730	5′ GGCCGAAGCTTTCAGCGTATATGC 3′	This study
(E) U 11	5′ CTTCGTCTTCCGGACCATC 3′	This study
(F) l 823	5′ GGAACGGACGAGGGTGCAT 3′	This study

[a] *Bam*HI restriction site in bold

Inoculum preparation and bioreactor cultivation

The bioreactor was inoculated with 200 ml of an overnight culture in a saline medium containing 20 g/l of WFO as carbon substrate. Incubation was carried out on an orbital shaker for 18 h at 150 rpm rotational speed and 30°C. Cells were harvested by centrifugation and resuspended at 2% (*v*/*v*) to an optical density of 2 at 540 nm prior to inoculation into the bioreactor.

Cultures were carried out at a working volume of 2 l in a 3-l benchtop bioreactor (Biostat B. Braun Biotech International GmbH, Melsungen, Germany), using the mineral salts medium described above. During the culture, dissolved oxygen was monitored continuously with an O_2 electrode (Ingold 12/200 B. Braun Biotech. International GmbH, Melsungen, Germany) and maintained at 30% oxygen saturation by cascade automatic control of the stirrer speed, 500–700 rpm, with an air flow between 2.5 and 7.5 l/min. Air flow was enriched with industrial oxygen (Carburos Metálicos, Barcelona, Spain) when needed. CO_2 was measured by titration of the air flow exhaust from the bioreactor at time intervals. Temperature was maintained at 30°C with a temperature sensor Pt-100/200-4 (B. Braun Biotech. International GmbH, Melsungen, Germany). The pH was kept at 7 automatically using two solutions of HCl (2 M) and NaOH (2 M). Data were registered in an external computer connected to the control unit of the bioreactor. The software used was MFCS/win 2.0 (B. Braun Biotech International, Sartorius, Mesulgen, Germany).

Molecular manipulation procedures

Standard nucleic acid manipulation techniques were employed as described (Sambrook 2001). Plasmid DNA was purified using commercial kits (Illustra_PlasmidPrep, GE Healthcare, UK). Restriction nucleases (Roche, Suisse) and *taq* or *pfu* polymerases (Biotools, Spain) were used according to the manufacturer's instructions. To obtain the nucleotide sequences of DNA, the PCR-amplified fragments were analyzed as described (Sanger et al. 1977). Competent *E. coli* cells were routinely transformed following the standard procedures (Sambrook 2001), and conjugation between *E. coli* S17.1 and *P. aeruginosa* 42A2 was performed following the protocol described (Quenee et al. 2005). Electroporation of *P. aeruginosa* was performed as previously described (Smith and Iglewski 1989), using competent cells obtained after centrifuging an overnight culture of cells resuspended in cold sucrose (0.3 M) and six washing steps in half volume of a cold 0.3 M sucrose solution (Solaiman 1998). Competent cells (50 μl) were mixed with 0.5–3 μl plasmid DNA and electroporated using a Bio-Rad Gene Pulser II electroporator equipped with a Pulse Controller Plus module. The variables of the electroporation system were set at 129 Ω, 5 ms, and 2 kV.

Construction of a *P. aeruginosa* 42A2 PHA negative mutant

An isogenic *phaC1-phaZ-phaC2* knockout mutant of *P. aeruginosa* 42A2 was obtained by replacement of the 3′ end of *phaC1*, the whole *phaZ*, and the 5′ end of *phaC2* genes, using a gentamicin resistance cassette (Quenee et al. 2005). PCR amplification of the truncated *pha* cluster and further cloning of the released fragment into the suicide vector pEX100T (Table 1; Quenee et al. 2005) were used to obtain the desired construct. Primers A and B (Table 1) were used for the amplification of the *phaC1* 5′ segment, whereas primers C and D (Table 1) allowed the amplification of the *phaC2* 3′ fragment. The gentamicin resistance cassette inserted between the two amplified DNA fragments was extracted from *Bam*HI-digested pUCGm*lox* (Quenee et al. 2005).

Allele exchange was performed in two steps involving homologous recombination, as described before (Quenee et al. 2005). Initially, a single-crossover event allowed integration of the suicide plasmid in the strain's genome resulting in an insertional mutant containing the wild-type and mutant alleles. In the second step, a double recombinant was obtained by *sac*B-mediated sucrose counter-selection in the presence of gentamicin. As a result, the desired *P. aeruginosa* 42A2 chromosomal deletion mutant for PHA synthase was obtained (Fig. 1).

The isogenic mutant obtained—*P. aeruginosa* 42A2 ΔAGmD—was verified by PCR amplification employing either primers E and F (Table 1), which bind to the 5′- and 3′-ends of the *phaZ* gene, or using primers A and D, binding upstream the *phaC1* start codon and close to the *phaC2* stop codon, respectively. The amplified products were analyzed by gel electrophoresis and DNA sequencing for confirmation.

Gentamicin resistance extraction from *P. aeruginosa* 42A2 ΔAGmD

Plasmid pCM157 coding for recombinase Cre was electroporated into *P. aeruginosa* 42A2 ΔAGmD to remove the gentamicin cassette. The pCM157 IncP origin of replication (oriV) and a tetracycline resistance marker allows this plasmid to be maintained and selected in *P. aeruginosa*. A tetracycline-resistant (Tc^R) transconjugant clone from mutant *P. aeruginosa* 42A2 ΔAGmD was grown overnight in LB supplemented with tetracycline in order to allow the expression of Cre recombinase, used to remove the Gm resistance cassette (Quenee et al. 2005) (Fig. 2).

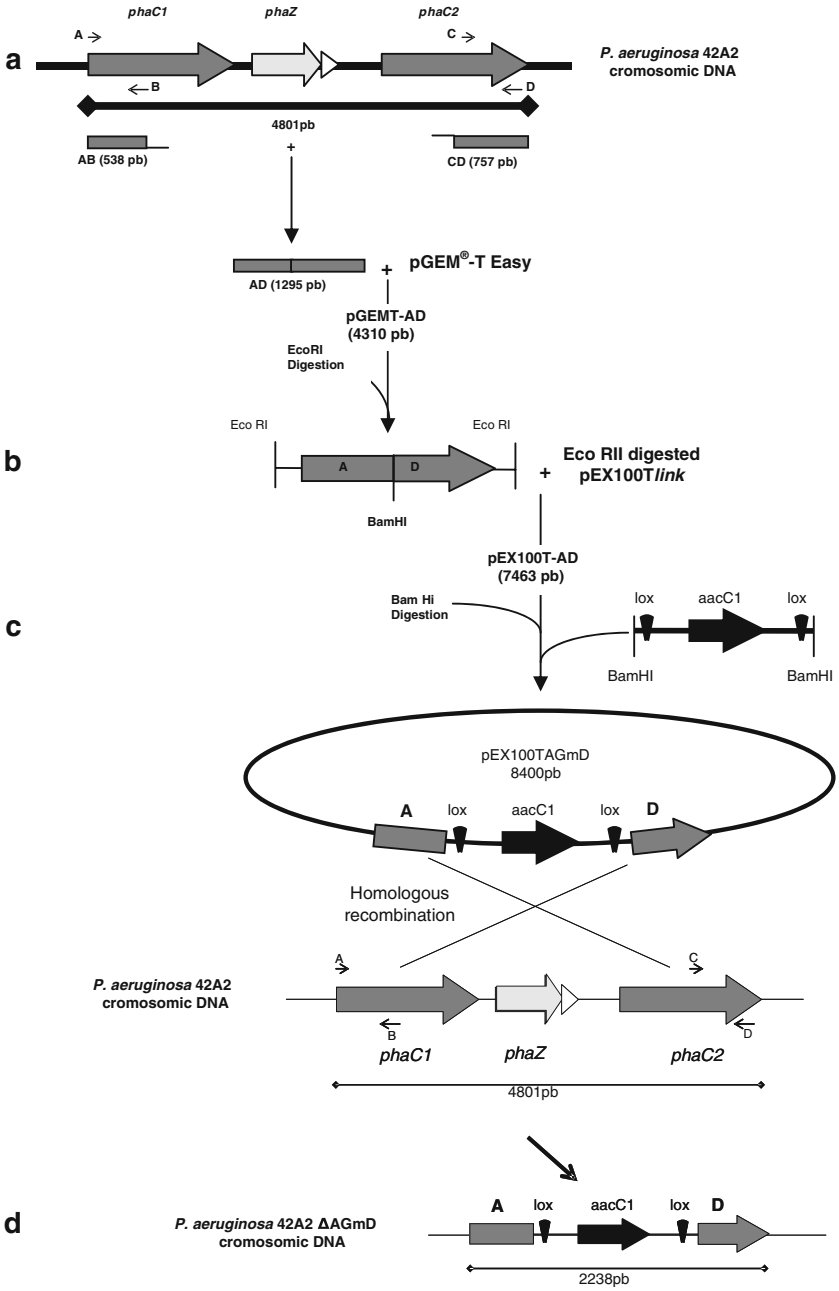

Fig. 1 Schematic representation of the construction of *P. aeruginosa* mutants with PHA synthase genes knocked out. *A* generation of the mutant fragment by overlapping extension PCR; *B* cloning of the new mutant DNA fragment into pEX100T*link*, an allelic exchange vector allowing *sac*B-based negative selection; *C* insertion of lox-flanked *aaC1* gen (gentamicin resistance) from pUCGmlox at a unique site inside the insert, resulting in the suicide vector pEX100TAGmD. The latter was transferred to *P. aeruginosa* 42A2 and exchanged with the chromosome to generate the desired deletion mutant. *D* Upon transformation and allelic exchange, and given that the allelic exchange vector cannot replicate, positive GmR, sucrose-resistant, and Cb^S colonies were selected

Plasmid pCM157 was then cured from the strain by three successive growth cycles in LB without tetracycline. The selected mutant clone, *P. aeruginosa* 42A2 ΔAD, was thus sensitive to both gentamicin and tetracycline.

Nile Red staining and fluorescence microscopy

For PHA granule visualization, cells from parental and mutant *P. aeruginosa* 42A2 strains were stained with Nile Red and analyzed by fluorescence microscopy. Stock solutions of Nile Red (Sigma, 0.25 mg/ml) in DMSO were prepared and stored protected from light. Staining was carried out on unfixed cells suspended in Ringer ¼ (Sharlau, Spain), using a l:100 dye dilution. Fluorescence microscopy studies were carried out with a BX-40 Olympus Photomicroscope equipped for epi-illumination. Nile Red fluorescence was detected at red spectral setting, using a 515–560-nm band pass exciter filter, a 580-nm center wavelength chromatic beam splitter, and a 590-nm long pass barrier filter (Spiekermann et al. 1999).

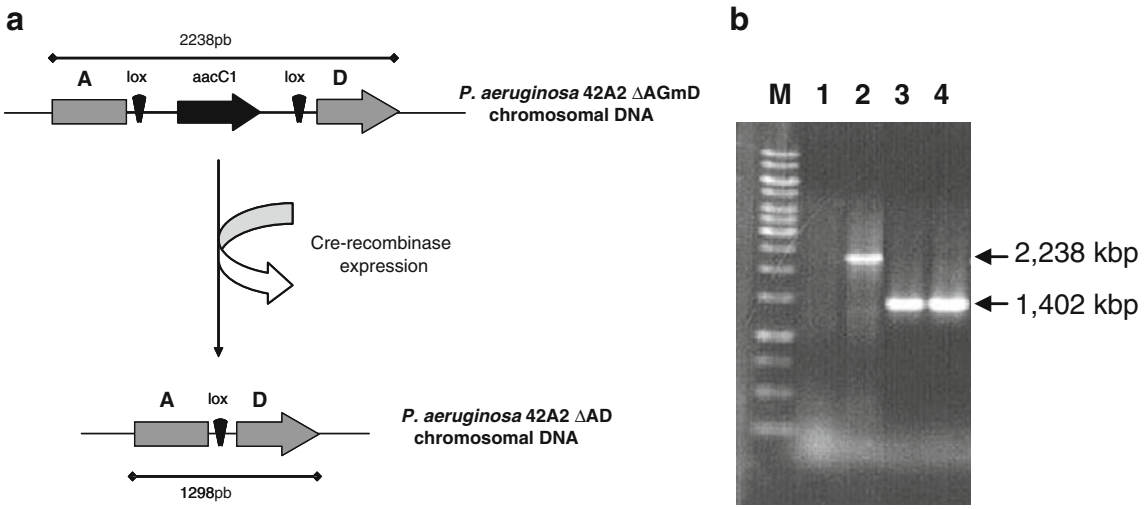

Fig. 2 **a** Isolation of an unmarked mutant after Cre-recombinase-mediated excision of the Gm marker. **b** PCR analysis of the allelic exchange and subsequent marker removal. Primers forward and reverse flanking the *phaC1-phaZ-phaC2* genes were used to amplify across the entire three genes. The molecular weight standard in the first lane is a 1-kb DNA Ladder (Promega, Spain), the subsequent lines are: *1* → colonial PCR of *P. aeruginosa* 42A2, *2* → colonial PCR of *P. aeruginosa* 42A2 ΔAGmD (2,238 kb), *3* → colonial PCR of *P. aeruginosa* 47T2 AD (1,402 kb), *4* → colonial PCR of *P. aeruginosa* 42A2 ΔAD (1,402 kb)

Transmission electron microscopy

Transmission electron microscopy (TEM) of parental and mutant strains was carried out by embedding glutaraldehyde fixed and OsO_4, $K_3Fe(CN)_6$-stained cells in 2.5% agar. Samples were then dehydrated, included in Spurr resin, and left to polymerize for 48 h at 60°C (Spurr 1969). Ultrathin sections (30–90 nm thick) were deposited on a copper grid, stained with 2% uranyl acetate for 30 min, and viewed with a Phillips EM 301 microscope, with accelerating voltages of 60 kV. Images were acquired with a Megaview III camera using the software SoftImaging (Olympus, Germany).

Isocitrate liase activity assay

Isocitrate liase activity was assayed using crude extracts of *P. aeruginosa* strains harvested by centrifugation in the middle of the exponential growth phase (15 h). It was measured as millimolar of glyoxylate produced by milligrams of protein (in millimolar Gly/mg prot). Cells were suspended in 50 mM Tris–HCl (pH 7.3) with a protease inhibitor cocktail tablet (Complete Mini, EDTA-free, Roche, USA). Then they were disrupted by freezing and thawing and by sonication. Finally cell debris was removed by 15 min centrifugation at 4°C and 14,000×*g* (Centrikon T-124, Kontron, Italy) and the clear supernatant was used as protein extract. The protein concentration was determined by Thermo Scientific NanoDrop 1,000 Spectrophotometer (Thermo, USA).

Enzyme activity was spectrophotometrically determined by monitoring the production of glyoxylate with 2,4-dinitrophenylhydrazine (2,4-DNPH) at 450 nm and using glyoxylate as standard (Katsuki et al. 1971; Romanov et al. 1999). Protein extracts (15 μg) were mixed in 25 mM Tris–HCl (pH 7.3) containing 5 mM $MgCl_2$, 2 mM isocitrate, and 600 μl of this reaction mixture were incubated for 15 min at room temperature. The reaction was stopped by adding 100 μl of 2,4-DNPH solution (5 mM in 2 N HCl, stable up to 2 weeks stored in darkness) followed by incubation at room temperature for 15 min. The samples were diluted adding 1 ml of water and 1 ml of freshly prepared alkaline solution (1 M sodium phosphate adjusted to pH 12.5 with NaOH). After 15-min incubation at room temperature, the absorbance at 450 nm was measured in a Shimadzu UV-1700 spectrophotometer (Shimadzu, Kyoto, Japan).

Determination of biomass and growth parameters

Cell dry weight (CDW) was determined gravimetrically. An aliquot (15 ml) of the culture was withdrawn aseptically and centrifuged at 20,000×*g* for 20 min at 4°C (Kontron, Italy). The supernatant was discarded, and the cell pellet was washed twice with deionized water/hexane solution (10:1) to remove contaminating residual carbon source and residual culture medium, and then washed twice with deionized water. The washed cells were dried at 100°C for 24 h in a hot air oven to a constant weight in preweighed tubes and then cooled in a desiccator and weighed. All measurements were made in triplicate. Cell concentration was expressed as gram CDW/l. Residual biomass (RB) was defined as CDW minus PHA weight and expressed as gram of RB/l. Cell growth (×, grams per liter) was also monitored

by measuring the protein content of the culture, following Lowry's method (Lowry et al. 1951). All measures were carried out in triplicate. Nitrate concentration was determined by the nitrate test (Merck 111170, Germany).

PHA extraction, purification, and determination

Cells were harvested at time intervals after centrifugation at 20,000×*g* for 20 min, washed, centrifuged, resuspended in distilled water, and finally lyophylized in a Cryodos-50 system (Telstar, Spain) at −56°C and 10^{-2} mbar. Lyophilized biomass was extracted with hot chloroform for 3 h at 80°C. The chloroform solution was filtered to remove any remaining cell debris and concentrated by rotary evaporation (Bücchi, Switzerland). PHAs were then purified by precipitation of the chloroform solution through dropwise addition to cold methanol. The methanol–chloroform mixture was decanted, and the pure polymer was washed with ice-cold methanol. Purified PHAs were then dissolved in chloroform, concentrated to dryness under vacuum (Bücchi, Switzerland), and weighed prior to storage under N_2 at −20°C (Bassas et al. 2008).

NMR analysis

The ^{1}H- analysis of the PHA samples was carried out on a Mercury-400F system (Varian VNMRS-400, Inc., CA). The 400 MHz ^{1}H-NMR spectra were recorded at 25°C using an acquisition time of 2.55 s, spectral width of 6,410 Hz, and pulses of 2 s. The samples were diluted in $CDCl_3$. Chemical shifts in parts per million were relative to TMS at 0 ppm as internal standard.

Hydroxy-fatty acid extraction and analysis

Culture samples were removed from the bioreactor at time intervals, centrifuged, and the cells discarded. The supernatant samples were acidified to pH 3 with 2 M HCl and extracted twice with chloroform/methanol (2:1 *v*/*v*). The resulting extracts were dried over anhydrous sodium sulfate, filtered, and the solvent removed with a rotary evaporator. The corresponding organic extracts were then analyzed by a thin-layer chromatography (TLC, Macherey-Nagel, Germany) (Christie 2003; Joh et al. 1995) and liquid chromatography.

Liquid chromatography

Quantitative analysis of the hydroxylated fatty acids (10*S*)-HOME, (7*S*,10*S*)-DiHOME, and oleic acid as a measure of the remaining WFO was carried out by liquid chromatography in a Shimadzu LC-9A Chromatograph. (Shimadzu, Japan). Samples were injected in the HPLC with a light-scattering detector, Sedex 55 (SEDERE, France), equipped with a Tracer Excel 120 C8 column (5 μ, 150× 4.6 mm) (Teknokroma, Spain). Optimal separation was achieved with an elution gradient using A, acetonitrile (0.1% *v*/*v* acetic acid) and B, water (0.1% *v*/*v* acetic acid) at a flow rate of 1 ml/min. The gradient (time, percent solution B) used was as follows: (0, 70); (10, 0); (15, 0); (20, 70); and (25, 70). Injection volume was 50 μl. A known home-made standard of each hydroxylated fatty acid and oleic acid was used for the identification of the retention times and quantification of the samples.

Results

Generation of a *P. aeruginosa* 42A2 negative mutant for PHA production

In order to study the interaction of PHA biosynthesis in *P. aeruginosa* with respect to the production of (10*S*)-HOME and (7*S*,10*S*)-DiHOME, an isogenic *phaC1-phaZ-phaC2* knockout mutant was generated by insertional inactivation of the chromosomal *phaC1-phaZ-phaC2* gene region (Fig. 1). For this purpose, plasmid pEX100TAGmD (Table 1), containing a gentamicin resistance cassette replacing most of the two synthase genes (*phaC1* and *phaC2*) plus the entire *phaZ* gene, was constructed. This construction was transferred by conjugation into *P. aeruginosa* 42A2, and gentamicin/sucrose-resistant transformants, which were putative double recombinant clones carrying an interrupted *phaC1-phaZ-phaC2* gene region, were selected (Quenee et al. 2005). A selected mutant clone was analyzed by PCR amplification, using primers E and F (Table 1), which bind to the 5′- and to the 3′-ends of the *phaZ* gene, respectively. As expected, no PCR product was obtained from mutant genomic DNA, whereas the predicted PCR product of about 0.8 kb was obtained from wild-type strain genomic DNA (not shown), indicating that the mutation was indeed the result of a double recombination event in which the *phaC1-phaZ-phaC2* gene region was interrupted by the gentamicin resistance cassette (Fig. 1). This was further confirmed by PCR amplification using primers A and D (Table 1) binding to the 5′-end of *phaC1* (A) and to the 3′-end of *phaC2* (D), respectively. In this occasion, the expected 2.3 kb DNA product was obtained after amplification of mutant chromosomal DNA (not shown). Finally, confirmation of the correct disposition of the knockout isogenic chromosomal mutant was performed by DNA sequencing, showing that the gentamicin resistance cassette was indeed inserted in the *phaC1-phaZ-phaC2* gene region. Thus, mutant *P. aeruginosa* 42A2 ΔAGmD, with the *pha*C1 and C2 synthase genes abolished, was obtained.

Antibiotic marker removal

For the generation of an unmarked *P. aeruginosa* 42A2 mutant, the gentamicin-resistant (Gm^R) antibiotic cassette was removed from the previous construction (Quenee et al. 2005). For this purpose, plasmid pCM157 (Table 1), carrying a Tc^R and an IncP origin of replication (oriV) that allows replication in *P. aeruginosa* was introduced by electroporation into *P. aeruginosa* 42A2 ΔAGmD (Fig. 2). Transconjugant clones were grown overnight in LB supplemented with tetracycline to allow expression of Cre recombinase, responsible for the removal of the resistance cassette *aacC1 lox*. Plasmid pCM157 was then cured from the mutant strain resulting in an unmarked mutant clone—*P. aeruginosa* 42A2 ΔAD—that was sensitive to both, gentamicin and tetracycline, as a result of Cre recombinase-mediated excision of the Gm marker (Fig. 2a). The presence of the desired deletion in the unmarked mutant was verified by DNA sequencing and colony PCR, using primers A and D (Fig. 2b).

Synthesis of PHA by the *phaC1-phaZ-phaC2* deletion mutant *P. aeruginosa* 42A2 ΔAD

For PHA biosynthesis analysis, cells of parental and mutant *P. aeruginosa* 42A2 strains were cultured under PHA-accumulating conditions on mineral medium containing 2% (*v*/*v*) WFO. Four different assays [fluorescence microscopy (not shown), transmission electron microscopy, NMR analysis, and PHA content determination] were carried out in parallel to assess the PHA production in the PHA-negative mutant obtained, using the parental strain as a control (Fig. 3). Fluorescence microscopy and TEM images showed no PHA granule accumulation in *P. aeruginosa* 42A2 ΔAD mutant (Fig. 3e, f), whereas abundant PHA granules appeared inside *P. aeruginosa* 42A2 parental strain cells (Fig. 3c, d).

The cell extracts of both strains (*P. aeruginosa* 42A2 and the PHA mutant) were analyzed by NMR (Fig. 3a). ^{1}H-NMR spectra of the biopolymer obtained with the wild-type *P. aeruginosa* 42A2 strain displayed the most relevant signals corresponding to PHA polymer. The peaks at 0.8 and at 1.2 ppm were assigned to the methyl and methylene groups in the side chain, respectively. The peaks at 2.5 and 5.2 ppm represent the methylene groups at α-position and the methine group at β-position of the ester, respectively. The signal of the olefinic protons in the side chain appeared in the expected region between 5.25 and 5.35 ppm. The signals at 2.0 and 2.35 ppm belong to protons adjacent to the double bonds. These peaks were not found in *P. aeruginosa* 42A2 ΔAD, indicating a complete lack of PHA in the mutant strain (Fig. 3b). The NMR spectra showed PHA production only in the wild-type strain, while in the impaired mutant, only signals related to fatty acids, probably belonging to the cell membrane, were observed. Therefore, we can conclude that the newly constructed 42A2 ΔAD cannot synthesize PHA.

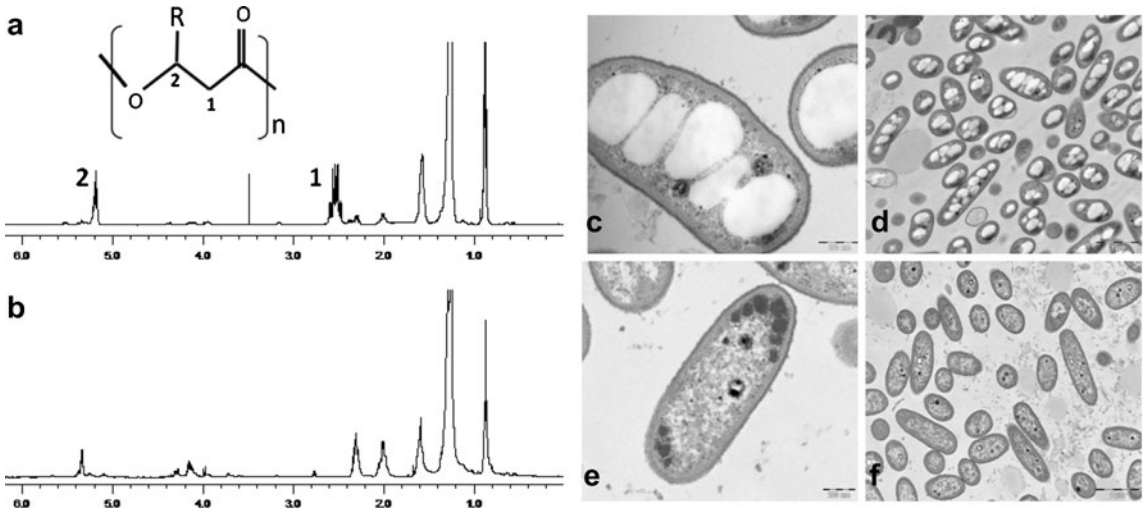

Fig. 3 Analysis of PHA production in *P. aeruginosa* 42A2 parental and mutant strains. *Left* ^{1}H-NMR spectra monitored on mercury-400F (400 MHz) of purified PHAs obtained from *P. aeruginosa* 42A2 (**a**) and the PHA negative mutant 42A2 ΔAD (**b**). On the wild-type strain spectra A, the peaks at 0.8 and 1.2 ppm were assigned to the methyl and methylene groups in the side chain, respectively. The peaks at 2.5 ppm (*1*) and 5.2 ppm (*2*) correspond to the methylene groups at α-position and the methine group at β-position of the ester, respectively. The signal of the olefinic protons in the side chain appeared in the expected region between 5.25 and 5.35 ppm. The signals at 2.0 and 2.35 ppm belong to protons adjacent to the double bonds. *Right* Transmission electron microphotographs of cells obtained from cultures of *P. aeruginosa* 42A2 (**c** and **d**) and the PHA-negative mutant 42A2 ΔAD (**e** and **f**) grown on minimal medium supplemented with waste frying oils at 30°C. *Scale bars* are 200 nm in **c** and **e** and 1 μm in **d** and **f**

Synthesis of hydroxylated fatty acids by the *phaC1-phaZ-phaC2* deletion mutant

Once confirmed that mutant *P. aeruginosa* 42A2 ΔAD was not able to synthesize PHA, the production of the exo-products (7*S*,10*S*)-DiHOME and (10*S*)-HOME was investigated. The LC chromatograms of the supernatant of organic extracts indicated that no other hydroxy-fatty acids than (7*S*,10*S*)-DiHOME or (10*S*)-HOME was produced by both strains. The absence of unpolymerized 3-hydroxyalkanoic acids is remarkable, that is, the building blocks for PHA synthesis did not accumulate in the supernatant of any strain.

Kinetics of the exo-product accumulation of the wild type and mutant strain is shown in Fig. 4. The mutant strain displayed a growth rate of μ=0.09 h^{-1}, whereas for the wild-type strain was μ=0.14 h^{-1}. The growth yields of the mutant strain on carbon and nitrogen ($Y_{X/C}$ and $Y_{X/N}$) for protein, calculated at the end of the culture, were 0.08 and 0.47, respectively, lower than those of wild-type strain ($Y_{X/C}$ 0.1 and $Y_{X/N}$ 0.74). The carbon consumption rate in the mutant strain was q_c=0.46 gC/gX·h, higher than that calculated for the wild type strain, q_c=0.38 gC/gX·h.

Interestingly, the production yield ($Y_{P/X}$) was 12.8 g/g in the case of the mutant strain, higher than that obtained for the wild-type strain (8.7 g/g). However, the product volumetric production rate (q_p) was similar for both strains, being q_p=0.41 gP/l·h and q_p=0.46 gP/l·h for the mutant and the wild-type strains, respectively.

Differences were observed in the accumulation profile of the exoproducts between both strains. In cultures of the mutant strain, (10*S*)-HOME steadily increased along the incubation time, achieving at the end of the culture a volumetric productivity of 0.37 g of (10*S*)-HOME/l·h, whereas in the case of the wild-type strain, maximum (10*S*)-HOME was achieved after 18 h of incubation, resulting in a volumetric productivity of 0.66 g (10*S*)-HOME/l·h. The carbon conversion yield in the mutant strain was $Y_{HOME/C}$ 0.84 g/g, being $Y_{HOME/C}$ 0.68 g/g for the wild-type strain. Higher cellular yield, $Y_{HOME/X}$ 11.6 g/g, was found in the mutant compared with the wild-type strain, $Y_{HOME/X}$ 3.4 g/g.

With regard to the accumulation of (7*S*,10*S*)-DiHOME, it is noticeable that a negligible amount of product was accumulated in the case of the mutant strain (only 1.31 g/l at the end of the incubation time), that is a production rate of $q_{DiHOME/C}$ of 0.04 gDiHOME/l·h. The overall conversion yield in the mutant strain was $Y_{DiHOME/C}$ 0.09 g/g. These values were much lower than those calculated for the wild-type strain, $q_{DiHOME/C}$ 0.26 g DiHOME/l·h, and $Y_{DiHOME/C}$= 0.41 g/g. The cellular yield for (7*S*,10*S*)-DiHOME production in the mutant strain was $Y_{DiHOME/X}$=1.1 g/g, whereas it was higher for the wild-type strain, $Y_{DiHOME/X}$=4.2 g/g.

The specific oxygen consumption rate (sOUR) calculated for the process was sOUR=214 mgO_2/mgX·h for mutant 42A2 ΔAD. This value is critically different than that observed for the wild-type strain, sOUR=163 mgO_2/mgX·h. In order to better understand the consumption of oxygen and the production of carbon dioxide (being in the mutant and wild-type strains 1.53 $molCO_2$/molX and 0.78 $molCO_2$/molX, respectively), the carbon flow through the central metabolism was checked by measuring the level of isocitrate liase. The enzyme activity accounted was 15.14 mM Gly/mg prot in the case of the mutant strain, while the isocitrate liase activity found for the wild-type strain was 7.57 mM Gly/mg prot, suggesting that the carbon flow was driven through the glyoxylate pathway in the mutant strain.

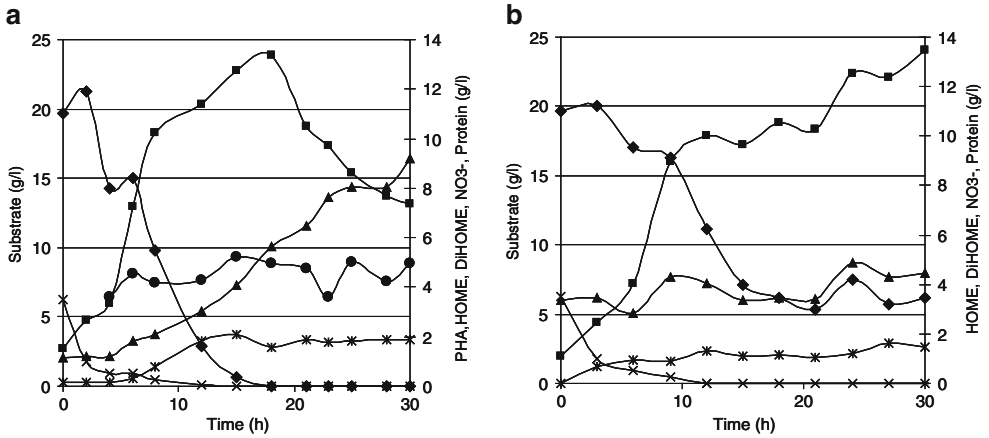

Fig. 4 Time course of growth and product formation of *P. aeruginosa* 42A2 wild type (**a**) and *P. aeruginosa* 42A2 ΔAD mutant (**b**) when cultivated in a mineral medium in a 3 l Braun Biotech reactor (see text for conditions). Polyhydroxyalkanoic acids (PHAs) (*filled circle*); Carbon substrate (*diamond*); Sodium nitrate (*multiplication sign*); Protein (*asterisk*); (E)-10-hydroxy-8-octadecenoic acid, (HOME) (*filled square*); (E)-7,10-dihydroxy-8-octadecenoic acid, (DiHOME) (*triangle*)

Discussion

A knockout mutant deficient for PHA biosynthesis was constructed in *P. aeruginosa* 42A2. This was done in order to evaluate the putative relationship of PHA biosynthesis and the production of hydroxylated fatty acids, considering the wild-type strain for comparative purposes. The isogenic knockout mutant *P. aeruginosa* 42A2 ΔAD was generated by means of insertional inactivation of the *phaC1-phaZ-phaC2* gene region encoding the two PHA synthases and the intracellular PHA depolymerase. This mutant was generated by combining efficient negative selection against single-crossover ex-conjugants, due to the *sac*B presence, with the antibiotic marker recycling *cre-lox* strategy (Quenee et al. 2005). This methodology allows allelic exchange between a target gene and a gentamicin cassette flanked by the two *lox* sequences. A tetracycline plasmid expressing Cre recombinase was then introduced in the mutant strain to catalyze excision of the *lox*-flanked resistance marker. This functional *cre-lox* recycling antibiotic marker system allows the creation of *P. aeruginosa* strains with multiple mutations, without modifying the antibiotic resistance profile when compared to the parental strain *P. aeruginosa* 42A2.

Effective DNA exchange and recycling of the resistance marker were monitored by PCR amplification and sequencing, and the phenotypic effect of the deletion was confirmed by examining the PHA accumulation profiles of the mutant strain with respect to those of the wild type. As it is well known, PHA accumulation occurs in discrete inclusions inside the cell (Fernandez et al. 2005; Steinbuchel and Valentin 1995). A thin section of wild-type *P. aeruginosa* 42A2 containing PHA inclusions is shown in Fig. 3, where PHA granules appear in TEM micrographs as light intracellular inclusions with a diameter of 200–400 nm, depending on the granule. As expected, TEM and epifluorescence microscopy (not shown), together with NMR analysis (Fig. 3) revealed that the mutant *P. aeruginosa* 42A2 ΔAD, deleted for the *phaC1-phaZ-phaC2* genes, was impared for PHA production. NMR analysis confirmed PHA accumulation in the case of *P. aeruginosa* 42A2, whereas for the mutant *P. aeruginosa* 42A2 ΔAD, the NMR showed only the presence of few free fatty acids, probably belonging to the cell membrane. These results were further corroborated by the lack of accumulation of PHA in the mutant strain, whereas accumulation in the wild-type strain was 23% w/w.

Strain *P. aeruginosa* 42A2 also produces hydroxy-fatty acids as extracellular products (Fernandez et al. 2005). The influence of PHA synthesis in hydroxy-fatty acid production by *P. aeruginosa* was investigated for the first time with regard to the carbon balance influencing the synthesis of hydroxylated fatty acids. In addition, having such a specific mutation in the *phaC1-phaZ-phaC2* region, any effect on other gene expression could be expected (Ouyang et al. 2007), since *Pha*C encodes for a PHA synthase using the substrate (R)-3-hydroxyacyl-CoA, and *Pha*Z encodes for a PHA depolymerase (Rehm et al. 2001; de Eugenio et al. 2007).

The new mutant *P. aeruginosa* 42A2 ΔAD grew slower than the parental strain. A stoichiometric approach of the kinetics of the culture was undertaken on the basis of the volumetric production rate, the specific production rates, the cellular yield, the conversion, and the oxygen uptake.

Two noticeable features were observed: (1) the carbon consumption rate for the mutant strain was higher than of the wild-type strain. This fact was reflected in the cellular yield for carbon as well as the cellular yield for nitrogen, the mutant strain being less efficient in nitrogen assimilation; (2) the specific yield of carbon dioxide formation in the mutant strain was twofold compared to the wild-type strain, which was consistent with the specific oxygen uptake found in the case of the mutant (214 $mgO_2/mgX{\cdot}h$), compared to the wild-type strain (163 $mgO_2/mgX{\cdot}h$).

These data led us to focus on the central metabolism of carbon. It is well known that bacterial populations can cope with a variety of stress situations, such as high amounts of alkylic carbon substrates like those used in this study, where medium/long chain length fatty acids are contained in the waste frying oils. The uptake of fatty acids in *Pseudomonas* to produce PHA occurs through different mechanisms (Rehm et al. 1998; Sudesh et al. 2000), being the β-oxidation pathway one of the main routes leading to the increase of acetyl-CoA within the cell. High concentrations of this metabolic intermediate produce a metabolic stress. The cellular strategy to release the accumulated intracellular acetyl-CoA is to activate the glyoxylate pathway to shorten the tricarboxylic acid cycle. Similar situations occur with PHA mutants of other *Pseudomonas* strains (A. Prieto, personal communication). The critical increase in the isocitrate liase activity found in this work for the mutant strain is consistent with the physiological role of PHA as an electron sink for excess reducing power, developed when bacteria grow under an excess of carbon substrate (Hocking and Marcessault 1998).

It is noteworthy to remark the poor accumulation of DiHOME by the mutant strain. The wild-type strain is 3.5-fold more efficient, on basis of cellular yield, than the mutant strain. This might be a consequence of the oxygen being driven towards the energy metabolism of cells, since the two oxygens in the hydroxyl group derive from the same molecule of O_2, as previously reported (Martinez et al. 2010). Significantly, the cellular yield of the mutant strain for HOME synthesis was 3.6-fold higher than for the wild-type strain.

In this work, a mutant on PHA production was obtained. The new mutant was a highly efficient strain for the production of (E)-10-hydroxy-8-octadecenoic acid when incubated with a rich oleic acid substrate. Some interesting effects due to the lack of PHA synthesis were observed, especially on the specific oxygen uptake and the increase of carbon dioxide production.

Acknowledgments We thank Dra. MA Prieto for her assessment in the enzymatic determination for the study of the carbon flow. This work was financed by the Scientific and Technological Research Council (CICYT, Spain), grant CTQ2010-21183-C02-01/02/PPQ, by the IV Pla de Recerca de Catalunya (Generalitat de Catalunya), grant 2009SGR-819, and by the Generalitat de Catalunya to the "Xarxa de Referència en Biotecnologia" (XRB). Dra. N Torrego-Solana was a recipient of a BRD fellowship and postdoctoral contract from the University of Barcelona. I Martin-Arjol is a recipient of an APIF fellowship from the Universisty of Barcelona.

References

Bassas M, Rodríguez E, Llorens J, Manresa A (2006) Poly (3-hydroxyalkanoate) produced from *Pseudomonas aeruginosa* 42A2 (NCBIM 40045): effect of fatty acid nature as nutrient. J Non-Cryst Solids 352:2259–2263

Bassas M, Diaz J, Rodriguez E, Espuny MJ, Prieto MJ, Manresa A (2008) Microscopic examination in vivo and in vitro of natural and cross-linked polyunsaturated mclPHA. Appl Microbiol Biotechnol 78:587–596

Bofill C, Prim N, Mormeneo M, Manresa A, Pastor FIJ, Diaz P (2010) Differential behaviour of *Pseudomonas* sp 42A2 LipC, a lipase showing greater versatility than its counterpart LipA. Biochimie 92:307–316

Busquets M, Deroncele V, Vidal-Mas J, Rodriguez E, Guerrero A, Manresa A (2004) Isolation and characterization of a lipoxygenase from *Pseudomonas* 42A2 responsible for the biotransformation of oleic acid into (S)-(E)-10-hydroxy-8-octadecenoic acid. Antonie Leeuwenhoek 85:129–139

Christie W (ed) (2003) Lipid analysis. Oily, Bridgewater

de Eugenio LI, Garcia P, Luengo JM, Sanz JM, San Roman J, Garcia JL, Prieto MA (2007) Biochemical evidence that phaZ gene encodes a specific intracellular medium chain length polyhydroxyalkanoate depolymerase in *Pseudomonas putida* KT2442. Characterization of a paradigmatic enzyme. J Biol Chem 282:4951–4962

Erhan SM, Isbell TA (1997) Estolide production with modified clay catalysts and process conditions. JAOCS 74:249–254

Fernandez D, Rodriguez E, Bassas M, Viñas M, Solanas AM, Llorens J, Marqués AM, Manresa A (2005) Agro-industrial oily wastes as substrates for PHA production by the new strain *Pseudomonas aeruginosa* NCBB 40045: effect of culture conditions. Biochem Eng J 26:159–167

Guerrero A, Casals I, Busquets M, León Y, Manresa A (1997) Oxidation of oleic acid to (E)-10-hydroperoxy-8-octadecenoic acid and (E)-10-hydroxy-8-ocatadecenoic acids by *Pseudomonas* sp. 42A2. Biochim Biophys Acta 1347:75–81

Hanahan D (1983) Studies on transformation of *Escherichia coli* with plasmids. J Mol Biol 166:557–580

Hocking PJ, Marcessault RH (1998) Polyhydroxyalkanoates. In: Kaplan DL (ed) Biopolymers from renewable resources. Springer, Berlin

Joh YG, Brechany EY, Christie WW (1995) Characterization of wax esters in the roe oil of amber fish, *Seriola aureovittata*. JAOCS 72:707–713

Katsuki H, Yoshida T, Tanegashima C, Takaka T (1971) Improved direct method for determination of keto acids by 2,4-dinitrophenylhydrazine. Anal Biochem 43:349–356

Lee SY (1996) Bacterial polyhydroxyalkanoates. Biotechnol Bioeng 49:1–14

Lowry OH, Rosebrough N, Farr AL, Randall AL (1951) Protein measurement with the Folin phenol reagent. J Biol Chem 193:265–257

Luengo JM, García B, Sandoval A, Naharro G, Oliveira ER (2003) Bioplastics from microorganisms. Curr Op Microbiol 6:1–10

Martinez E, Hamberg M, Busquets M, Diaz P, Manresa A, Oliw EH (2010) Biochemical characterization of the oxygenation of unsaturated fatty acids by the dioxygenase and hydroperoxide isomerase of *Pseudomonas aeruginosa* 42A2. J Biol Chem 285:9339–9345

Marx CJ, Lidstrom ME (2002) Broad-Host-Range cre-lox System for Antibiotic Marker Recycling in Gram-Negative Bacteria. Bio-Tech 33:1062–1067

Ouyang SP, Liu Q, Fang L, Chen GQ (2007) Construction of pha-operon-defined knockout mutants of *Pseudomonas putida* KT2442 and their applications in poly(hydroxyalkanoate) production. Macromol Biosci 7:227–233

Pelaez M, Orellana C, Marques A, Busquets M, Guerrero A, Manresa A (2003) Natural estolides produced by *Pseudomonas* sp 42A2 grown on oleic acid: production and characterization. JAOCS 80:859–866

Prieto MA, de Eugenio LI, Galán B, Luengo JM, Witholt B (2007) Synthesis and degradation of polyhydroxyalkanoates. In: Ramos JL, Filloux A (eds) *Pseudomonas*: a model system in biology. *Pseudomonas*, vol. V. Springer, Berlin, pp 397–428

Quenee L, Lamotte D, Polack B (2005) Combined sacB-based negative selection and cre-lox antibiotic marker recycling for efficient gene deletion in *Pseudomonas aeruginosa*. Biotech 38:63–67

Rehm BHA (2003) Polyester synthases: natural catalysts for plastics. Biochem J 376:15–33

Rehm BHA, Steinbuchel A (1999) Biochemical and genetic analysis of PHA synthases and other proteins required for PHA synthesis. Int J Biol Macromol 25:3–19

Rehm B, Krüger N, Steinbüchel A (1998) A new metabolic link between fatty acid de novo synthesis and polyhydroxyalkanoic acid synthesis. J Biol Chem 273(37):24044–24051

Rehm B, Mitsky TA, Steinbüchel A (2001) Role of fatty acid de novo biosynthesis in polyhydroxyalkanoic acid (PHA) and Rhamnolipid synthesis by Pseudomonads: establishment of the transacylase (PhaG)-mediated pathway for PHA biosynthesis in *Escherichia coli*. Appl Environ Microbiol 67(7):3102–3109

Romanov V, Merski MT, Hausinger RP (1999) Assays for allantoinase. Anal Biochem 268(1):49–53

Sambrook JRD (ed) (2001) Molecular cloning: a laboratory manual. Cold Spring Harbor Laboratory, New York

Sanger F, Nicklen S, Coulson AR (1977) DNA sequencing with chain-terminating inhibitors. Proceed Nat Acad Sci USA 74:5463–5467

Simon R, Priefer U, Pühler A (1983) A broad host range mobilization system for in vivo genetic engineering: transposon mutagénesis in Gram-negative bacteria. BioTechnology 1:784–791

Smith AW, Iglewski BH (1989) Transformation of *Pseudomonas aeruginosa* by electroporation. Nucl Acids Res 17:10509–10509

Solaiman DKY (1998) Genetic transformation of *Pseudomonas oleovorans* by electroporation. Biotech Tech 12:829–832

Spiekermann P, Rehm BHA, Kalscheuer R, Baumeister D, Steinbüchel A (1999) A sensitive, viable-colony count staining using Nile red for direct screening of bacteria that accumulate polyhydroxyalkaonic acids and other lipid storage compounds. Arch Microbiol 171:73–80

Spurr AR (1969) A low-viscosity epoxy resin embedding medium for electron microscopy. J Ultrastruct Res 26:31–34

Steinbuchel A, Valentin HE (1995) Diversity of bacterial polyhydroxyalkanoic acids. FEMS Microbiol Lett 128:219–228

Sudesh K, Abe H, Doi Y (2000) Synthesis, structure and properties of polyhydroxyalkanoates: biological polyesters. J Non-Cryst Solids 325:1503–1555

Witholt B, Kessler B (1999) Perspectives of medium chain length poly (hydroxyalkanoates), a versatile set of bacterial bioplastics. Curr Op Biotechnol 10:279–285

Process Biochemistry 48 (2013) 224–230

Contents lists available at SciVerse ScienceDirect

Process Biochemistry

journal homepage: www.elsevier.com/locate/procbio

Production of 10(*S*)-hydroxy-8(E)-octadecenoic acid mono-estolides by lipases in non-aqueous media

I. Martin-Arjol[a], M. Busquets[b], A. Manresa[a,*]

[a] *Departament de Microbiologia i Parasitologia Sanitàries, Facultat de Farmàcia, Universitat de Barcelona, Av. Joan XXIII s/n, 08028 Barcelona, Spain*
[b] *Departament de Bioquímica i Biologia Molecular, Universitat de Barcelona, Av. Diagonal 643, 08028 Barcelona, Spain*

ARTICLE INFO

Article history:
Received 5 July 2012
Received in revised form
10 December 2012
Accepted 11 December 2012
Available online 20 December 2012

Keywords:
Lipase
Novozym 435
trans-hydroxy-fatty acids
Estolides
MALDI-TOF

ABSTRACT

In this study, Novozym 435, a lipase B from *Candida antarctica*, was used for fatty acid polymerization. For the first time, an apolar reaction media, *n*-hexane, was used to synthesize *in vitro* estolides from *trans*-hydroxy-fatty acids derived from the biotransformation of oleic acid by *Pseudomonas aeruginosa* 42A2 NCIMB 40045. We studied the effects of the substrate, the enzyme ratio, the enzyme stability and the reusability of the biocatalyst. To determine the structure of the oligomers formed, both liquid chromatography mass spectrometry and MALDI-TOF mass spectrometry, with a DHB matrix neutralized with lithium hydroxide, were used to obtain simpler mass spectra. Estolides composed of two units of (10*S*)-HOME were synthesized with a reaction yield of 30%. Finally, various lipases were screened, and another apolar organic solvent, *iso*-octane, was assayed to try to increase the reaction yield.

1. Introduction

Estolides, a class of polymeric molecules containing an unsaturated bond or hydroxy-fatty acids bonded to a carboxyl moiety of another acyl group [1], have been detected in the seed oil of several plants: *Euphorbiaceae*, *Brasicaceae*, *Cruciferae*, *Limmanthaceae*, *Compositae* and, most notably, the genus *Lesquerella* [1–3]. Estolides have also been found in secretions from the glandular hairs of a caterpillar, *Pieris rapae* [4], and in human meibum as a wax ester (WE) [5]. Finally, it should be noted that estolides were also detected in cultures of *Pseudomonas aeruginosa* 42A2 when cultivated with oleic acid [6].

There is great interest in producing estolides and their derivatives as biodegradable lubricants, functional fluids, cosmetics, inks or coatings [7]. To this end, the first attempt to produce estolides relied on the polymerization of ricinoleic acid from castor oil [8] or oleic acid in a reaction that required a temperature of 250 °C under pressure [9]. Currently, estolides are produced chemically from vegetable oils (soybean, meadow foam, lesquerella, castor, coconut or palm kernel oils) composed of unsaturated fatty acids of ten or more carbon atoms [9–11]. To overcome these extreme conditions and to prevent side effects due to the use of an inorganic catalyst, a biocatalytic method with random lipases from *Candida rugosa* [12], *Candida antarctica* or *Rhizomucor miehei* [13,14] was developed. The starting materials of this method were ricinoleic acid (RA), 12(*R*)-hydroxy-9(Z)-octadecenoic acid, or lesquerolic acid, 14(*R*)-hydroxy-11(Z)-icosenoic acid [1,15].

Although there are a large number of reports about the biotransformation of lipids with lipases, there are few studies on the polymerization of hydroxy-fatty acids by lipases. In 1989, Yamaguchi et al. were the first to report the esterification of castor oil in a two-step enzymatic reaction to obtain estolides with a high yield [16]. Later, they reported the importance of controlling the amount of water present in the reaction media and showed the advantage of immobilizing the lipases; the reaction yield was improved, and the product obtained reached acid values (AV) of 40 [17–19]. With estolides from ricinoleic acid applications arising, different strategies have been tested: (i) improving the immobilizing carriers [19,20]; (ii) encapsulating lipases in a reverse micelle [1]; and (iii) from 1997 to 2009, optimized reaction conditions in a bioreactor to increase the quality and quantity of estolides production were reported [12,21–23]. More recently, organic apolar solvents have started to be used as part of the reaction media [24] and to introduce new applications of ricinoleic acid estolides in the food industry [12]. Likewise, molecular sieves have been employed to adsorb water released during polycondensation in order to shift thermodynamic balance [25]. Several other methods, such as air drying [12], nitrogen bubbling, vacuum pressure, or a combination of these two, have also been employed [26].

Little has been documented about the polymerization of *trans*-hydroxy-acids with specific lipases toward *trans*-monomers. The studies by Borgdorf and Warwel, in which thirty-nine

* Corresponding author.
E-mail address: amanresa@ub.edu (A. Manresa).

1359-5113/$ – see front matter © 2012 Elsevier Ltd. All rights reserved.
http://dx.doi.org/10.1016/j.procbio.2012.12.006

commercial lipases were classified according to a ratio competitive factor (RCF), are very helpful in determining substrate selectivity toward isomeric 9-octadecenoic acids in *n*-hexane [27].

It is a difficult to both detect and characterize estolides. Gas chromatography coupled with mass spectrometry has proven useless due to the high boiling point of estolides [28–30]. In recent years, matrix-assisted laser desorption/ionization time-of-flight mass spectrometry (MALDI-TOF-MS) has emerged as a powerful technique to analyze synthetic polymers. Cvacka and co-workers analyzed WE using the MALDI-TOF-MS technique with a matrix of lithium salt of 2,5-dihydroxybenzoic acid (DBH) to increase the intensity of the signal for obtaining a good reproducibility [31]. They were able to characterize natural samples of WE with great accuracy.

The primary goal of this research is to develop new bio-based materials from agroindustrial wastes. To this end, oleic acid, which is present to a high degree in residual oily wastes, was used as a substrate for the production of 10(*S*)-hydroxy-8(E)-octadecenoic and 7,10(*S*,*S*)-dihydroxy-8(E)-octadecenoic acids ((10*S*)-HOME and (7*S*,10*S*)-DiHOME, respectively) by *P. aeruginosa* 42A2. Next, the monomer (10*S*)-HOME was used to synthesize estolides *in vitro* with Novozym 435. MALDI-TOF-MS and LC–MS techniques were used to determine the estolides' structure. Finally, lipases were screened in an organic medium to improve the reaction yield of the catalytic synthesis of estolides.

2. Materials and methods

2.1. Materials

P. aeruginosa 42A2 NCIMB 40045 was maintained on TSA (Trypticase soy agar; Difco, Franklin lakes, IL, USA) slants at 30 °C and after an incubation period of 24 h was kept at 4 °C and subcultured every two weeks. The strain was preserved frozen (−80 °C) in cryobilles (AES CHEMUNEX S.A., Terrassa, Spain). A lipase from *C. rugosa* (1104 units/mg solid) was purchased from Sigma–Aldrich (Madrid, Spain). Novozym 435, immobilized lipase B from *C. antarctica* (10,000 propyl laureate units/g solid), Lipozyme RM IM (an immobilized lipase from *R. miehei*, 275 interestification units/g solid) and Lipozyme TL IM (a lipase from *Thermomyces lanuginosus*, 250 interestification units/g solid) were generous gifts from Novozym A/S (Bagsvaerd, Denmark). Lipase A from *Rhizopus oryzae* was donated by Prof. Francisco Valero (Chem Eng Dept UAB, Cerdanyola del Vallès, Spain). Analytical grade *n*-hexane, methanol and diethyl ether were purchased from Carlo-Erba Reagents-SdS (Sabadell, Spain). Analytical grade *iso*-octane for spectroscopy UV–IR and potassium hydroxide (KOH) 85% were purchased from Panreac (Castellar del Vallès, Spain). Ricinoleic acid (RA) 80% was supplied by Fluka (Madrid, Spain) and oleic acid (OA) technical grade 90% was purchased from Sigma–Aldrich (Madrid, Spain).

2.2. Production and quantification of monomers

P. aeruginosa 42A2 NCIMB 40045 was cultured in the following saline medium (in $g\,l^{-1}$): $CaCl_2$ (0.01), $NaNO_3$ (3.5), K_2HPO_4 (2.0), KH_2PO_4 (1.0), KCl (0.1), $MgSO_4{\cdot}7H_2O$ (0.5), $FeSO_4{\cdot}7H_2O$ (0.012) and 0.05 ml l^{-1} trace elements solution. The trace elements solution was as follows (in mg 100 ml^{-1}): H_3BO_3 (148), $CuSO_4{\cdot}5H_2O$ (196), $MnSO_4{\cdot}H_2O$ (154), $Na_2MoO_4{\cdot}2H_2O$ (15) and $ZnSO_4{\cdot}7H_2O$ (307). This medium was supplemented with OA at 2% (v/v).

The bioreactor was inoculated with 200 ml of a 24 h culture in a saline medium containing 20 g l^{-1} OA as a carbon source. The inoculum-culture was carried out on an orbital shaker for 18 h at 150 rpm rotational speed and 30 °C. Cells were harvested by centrifugation (14,700 × *g* for 30 min at 4 °C) and resuspended with NaCl 0.9% (w/v) at 2% (v/v) to an optical density of 2.0 at 540 nm prior to inoculation into the bioreactor. The cultures were cultivated at a working volume of 2 l in a 3-L bench top bioreactor (Biostat B. Braun Biotech International GmbH, Melsungen, Germany) using the mineral salts medium described above. During the culture, dissolved oxygen was monitored continuously with an O_2 electrode (Ingold 12/200 B. Braun Biotech. International GmbH, Melsungen, Germany) and maintained at 30% oxygen saturation by automatic cascade control of the stirrer speed, 500–700 rpm, with an air flow between 2.5 and 7.5 l min^{-1}. The air flow was enriched with oxygen (Carburos Metálicos, Spain) when needed. The temperature was measured at 30 °C by a Pt-100/200-4 temperature sensor (B. Braun Biotech. International GmbH, Melsungen, Germany). The pH was automatically kept at 7.0 using 2 M HCl and 2 M NaOH solutions. The data were recorded using an external computer connected to the control unit of the bioreactor. The software used was MFCS/win 2.0 (B. Braun Biotech International, Sartorius, Mesulgen, Germany). The culture was maintained until all 10(*S*)-hydroperoxy-8(E)-octadecenoic acid ((10*S*)-HPOME) was converted to (10*S*)-HOME and (7*S*,10*S*)-DiHOME.

Quantitative analysis of OA, (10*S*)-HPOME, (10*S*)-HOME and (7*S*,10*S*)-DiHOME was carried out by liquid chromatography in a Shimadzu LC-9A Chromatograph (Kyoto, Japan). Samples were injected into the HPLC with a Sedex 55 light-scattering detector (Sedere, Alfortville Cedex, France) equipped with a Tracer Excel 120 C8 column (5 μm, 150 mm × 4.6 mm) (Teknokroma, Sant Cugat del Vallès, Spain). Optimal separation was achieved with an elution gradient using A, acetonitrile (Fischer Scientific, Madrid, Spain) (0.1%, v/v acetic acid), and B, water (0.1%, v/v acetic acid), at a flow rate of 1 ml min^{-1}. The gradient (time (min), %B) used was as follows: (0, 70), (10, 0), (15, 0), (20, 70), and (25, 70). The injection volume was 20 μl. A known homemade standard of each hydroxy-fatty acid and substrate was used to identify the retention times and to quantify the samples. Cell growth was calculated as dry cell weight. The biomass of the samples was placed in an oven at 100 °C for 24 h. The nitrate concentration was determined using QUANTOFIX® nitrate/nitrite test strips (Macherey-Nagel, Düren, Germany). All concentrations are expressed in g l^{-1}.

2.3. Purification of trans-hydroxy-fatty acids

At the end of cultivation, the culture was centrifuged (14,700 × *g* for 30 min at 4 °C), the supernatant was acidified to pH 2.0 with 37% HCl (Panreac, Castellar del Vallès, Spain), and two extractions were performed with a half volume of ethyl acetate (Carlo-Erba Reagents-SdS, Sabadell, Spain). The organic phase was dried over an anhydrous sodium sulfate filter (Panreac, Castellar del Vallès, Spain), and the solvent of the combined extracts was evaporated with a rotary evaporator (Bücchi, Postfach, Switzerland), resulting in a yellow oil. Organic extracts were kept in vials at 4 °C under nitrogen to prevent further oxidation. The (10*S*)-HOME and (7*S*,10*S*)-DiHOME were purified by flash-chromatography in a glass column (50 cm long and with 3 cm inner diameter) filled with silica gel 60 (0.040–0.063 mm, Merck, Madrid, Spain). The mobile phase used was formed by *n*-hexane:diethyl ether:methanol (80:20:7, v:v:v) and a stream of nitrogen (Carburos Metálicos, Barcelona, Spain) was applied to obtain the purified products. The purified products were kept at 4 °C under nitrogen, as stated above.

2.4. Product yields and productivity of monomers

The whole specific product yield ($Y_{P/X}$ (Eq. (1))) and specific (10*S*)-HOME and (7*S*,10*S*)-DiHOME yields ($Y_{(10S)\text{-HOME}/X}$ and $Y_{(7S,10S)\text{-HOME}/X}$ (Eq. (2))), were calculated over the entire process as the productivity of each hydroxy-fatty acid, $q_{(10S)\text{-HOME}}$, $q_{(7S,10S)\text{-DiHOME}}$, instead of the OA consumption rate, q_{OA}, which was calculated over the first 15 h of cultivation (Eq. (3)).

$$Y_{P/X\,(g\,g^{-1})} = \frac{\Delta C((10S)\text{-HOME}) + \Delta C(7S,\,10S)\text{-DiHOME})}{\Delta C(X)} \tag{1}$$

$$Y_{(10S)\text{-HOME}/X\,(g\,g^{-1})} = \frac{\Delta C(10S)\text{-HOME}}{\Delta C(X)};$$

$$Y_{(7S,10S)\text{-DiHOME}/X\,(g\,g^{-1})} = \frac{\Delta C(7S,\,10S)\text{-DiHOME}}{\Delta C(X)} \tag{2}$$

$$q_{(7S,10S)\text{-DiHOME}}\,(g\,l^{-1}\,h^{-1}) = \frac{\Delta C((7S,\,10S)\text{-DiHOME})}{\Delta t}; \qquad q_{OA}\,(g\,l^{-1}\,h^{-1}) = \frac{\Delta C(OA)}{\Delta t} \tag{3}$$

2.5. Measurement of the reaction yield of estolides synthesis

The reactions were monitored by titration to determine the acid value (AV) [23] of the samples. After evaporating the organic solvent, a 30 mg aliquot of the reaction mixture was titrated with 0.05 M KOH using phenolphthalein as indicator. All samples were analyzed in triplicate. The AV and the yield of the reaction were calculated as follows (Eq. (4)):

$$\eta\,(\%) = \frac{AV_{substrate} - AV_{product}}{AV_{substrate}} \cdot 100 \tag{4}$$

2.6. Effect of enzyme concentration

Different quantities of Novozym 435 (0.3–1.5 g) were assayed to obtain the optimal amount of enzyme for a reaction with 0.6 g of (10*S*)-HOME in 20 ml of *n*-hexane in a 100 ml Erlenmeyer flask for 48 h at 50 °C. A rotary evaporator system was used to achieve an efficient degree of contact between the enzyme and the substrate and to maintain the required temperature. All reactions were carried out at atmospheric pressure. The reaction extension was calculated using Eq. (4), as shown above. A control was assayed to confirm that this reaction does not occur spontaneously.

2.7. Effect of substrate/enzyme ratio with Novozym 435

An aliquot of 0.5 g of Novozym 435 was used to study polymerization with different amounts of (10*S*)-HOME (0.25–1.0 g). The enzymatic reaction was performed under the same conditions described above and included a control. The yield of the reaction was calculated with Eq. (4).

2.8. Reusability of the Novozym 435 biocatalyst

The biocatalytic reaction was performed with 0.5 g of organic substrate (10*S*)-HOME, which was added to 0.5 g of enzyme. The reaction conditions were the same as described above. After each cycle, the enzyme was removed from the reaction medium by filtration and then rinsed with *n*-hexane several times. Finally, the solvent was evaporated under a stream of air at room temperature. The product was analyzed, and the stability of the enzyme was determined as the reaction yield.

2.9. Screening of other lipases for estolides formation

An aliquot of 100 mg of *C. rugosa* lipase, lipase A from *R. oryzae*, Lipozyme RM IM, Lipozyme TL IM and Novozym 435 were assayed with 0.6 g of (10*S*)-HOME in 20 ml of *n*-hexane or *iso*-octane in a 100 ml Erlenmeyer flask for 48 h at 50 °C. A rotary evaporator was used to attain a high mixing degree and to control the necessary temperature. The polymerization reactions were carried out at atmospheric pressure, and the reaction extension was calculated with Eq. (4).

2.10. Liquid chromatography coupled to mass spectrometry (LC–MS)

Chromatographic separation was carried out in a Perkin-Elmer (Whaltham, MA, USA) Series 200 liquid chromatographer coupled to a PE SCIEX API 150 EX single-quadrupole mass spectrometer (Applied Biosystems, Carlsbad, CA, USA). A Tracer Kromasil 100 C8 column (250 mm × 46 mm, 5 μm) (Teknokroma, Sant Cugat del Vallès, Spain) was used. Separation was achieved with a gradient elution using A: acetonitrile (0.1%, v/v acetic acid); B: acetone (0.1%, v/v acetic acid) at a flow rate of 0.5 ml min^{-1}. Gradient (time (min), %B): (0, 35), (25, 100), (30, 100), (35, 35), (40, 35). All reported data were acquired with an APCI ionization source in negative mode using the following parameters: vaporizer temperature of 400 °C, 3 mA nebulizer current, −25 V declustering potential, −110 V focusing potential, −10 V entrance potential and nitrogen as a nebulizer and curtain gas with 10 and 12 arbitrary units. The scan data were obtained by scanning from *m*/*z* 100–2000 amu. For the analysis of estolides from ricinoleic acid, the selected ion monitoring (SIM) technique was used to detect high molecular mass oligomers with a better signal. The ions selected were those corresponding to the different oligomers synthesized. All data were recorded using Analyst Software v. 1.4.2 (Applied Biosystems, Carlsbad, CA, USA).

2.11. MALDI-time-of-flight mass spectrometry (TOF-MS) structural determination

MALDI-TOF-MS experiments were performed on a 4800 Plus MALDI-TOF/TOF Analyzer (ABSciex – 2010, Framingham, MA, USA). The samples were analyzed in MS Reflector mode using positive ion detection. Desorption and ionization were achieved with an Nd-YAG laser (355 nm, 3–7 ns pulse, 200 Hz). The data were recorded using 4000 Series Explorer software (ABSciex – 2010, Framingham, MA, USA). A 2,5-dihydroxybenzoic acid matrix was neutralized with lithium hydroxide (Sigma–Aldrich, Madrid, Spain), as Cvacka and co-workers established [31]. Lithium salt matrix, 10 mg ml^{-1}, was dissolved in a mixture of acetone:trichloromethane (2:1, v:v). An aliquot of 1 μl of the matrix solution was spotted on the target plate until the organic solvent evaporated completely. Then, 1 μl of the samples diluted in 2.5 mg ml^{-1} trichloromethane was deposited over the matrix spot and allowed to dry before analysis.

3. Results and discussion

3.1. Production of trans-hydroxy-fatty acids by submerged fermentation

P. aeruginosa 42A2 NCIMB 40045 was isolated from an olive oil-contaminated site. This strain catalyzes the conversion of oleic acid (OA) into new derivatives of the *trans*-configuration: 10(*S*)-hydroxy-8(E)-octadecenoic acid ((10*S*)-HOME)) and 7,10(*S*,*S*)-dihydroxy-8(E)-octadecenoic acid ((7*S*,10*S*)-DiHOME)) [32]. As Fig. 1 shows, the maximum production of (10*S*)-HOME and (7*S*,10S)-DiHOME was achieved at the end of the incubation (8.6 and 9.2 g l^{-1}, respectively), *i.e.*, 89% of substrate conversion. The entire specific product yield, $Y_{P/X}$, was 2.62 g g^{-1}, and the OA consumption rate, q_{OA}, was 1.267 g l^{-1} h^{-1}. The productivity of (10*S*)-HOME, $q_{(10S)\text{-HOME}}$, was 0.237 g l^{-1} h^{-1} with a cell yield, $Y_{(10S)\text{-HOME/X}}$, of 1.23 g g^{-1}. The (7*S*,10*S*)-DiHOME productivity, $q_{(7S,10S)\text{-DiHOME}}$, was 0.267 g l^{-1} h^{-1}, and its cell yield, $Y_{(7S,10S)\text{-DiHOME/X}}$, was 1.39 g g^{-1}. After organic extraction (10*S*)-HOME was purified up to 91% purity, and (7*S*,10*S*)-DiHOME was purified to 96%. Table 1 summarizes the calculations of *trans*-hydroxy-fatty acid production from OA by *P. aeruginosa* 42A2 in the bioreactor.

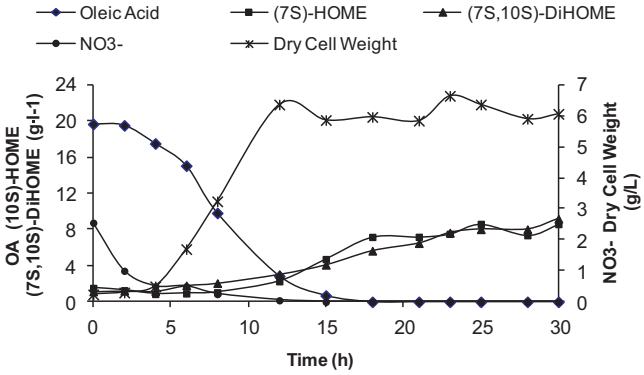

Fig. 1. Time course of growth and product formation of *P. aeruginosa* 42A2 when cultivated in a mineral medium in a 3-L B. Braun Biotech reactor (see text for conditions). OA: (♦); (10*S*)-HOME: (■); (7*S*,10*S*)-DiHOME: (▲); NO_3^-: (●); dry cell weight: (*).

3.2. Novozym 435 for trans-hydroxy-fatty acid isomer esterification: enzyme amount and substrate/enzyme ratio

In terms of selectivity to a *cis*/*trans* configuration of the double bond in 9-octadecenoic acid isomers, the lipases were classified according to a ratio competitive factor (RCF) [27]. This factor describes the selectivity of one single lipase toward two substrates with the same leaving group and to two different acyl groups. Thus, in this study, Novozym 435, with an RCF of 0.7, was chosen because it is slightly more active with *trans*-9-octadecenoic isomers, it exhibits versatility, and its optimal temperature of enzyme activity is 40–60 °C. To generate compatible new compounds in cosmetic or food applications, *n*-hexane with a log *P* of 3.5 [33] was chosen. Log *P* is a measurement of solvent polarity. Along with the partition coefficient and the enzyme/solvent interaction, log *P* may determine biocatalytic activity; this activity is low in solvents at log *P* < 2, moderate at log *P* between 2 and 4 and high in a polar solvent with log *P* > 4 [34].

Different amounts of enzyme were tested to establish the optimal amount of biocatalyst for 0.6 g of (10*S*)-HOME. The results are given in Fig. 2. It could be observed that the reaction yield increased with the amount of enzyme. At values near 0.5 g of enzyme, this yield was 35%, and it increased slightly to 42% at a substrate/enzyme ratio of 1.2 g g^{-1}. Thus, the thermodynamic limit for yield was very similar to this latter value. There are no data in the literature about polymerization with *trans* monomers, although this value is lower than the 58% obtained by Horchani et al. when using ricinoleic acid to produce estolides in *n*-hexane for 55 h at 55 °C [25]. Bódalo et al. obtained a 72% reaction yield when *C. rugosa* was immobilized in Lewatit Monoplus MP64, an anion exchange resin, for 150 h at 40 °C in a solvent-free system [23].

Various substrate/enzyme ratios were tested to establish the optimal concentration of substrate to be used. As Fig. 3 shows, the yield increased up to a ratio of 1, after which the yield remained

Table 1
Experimental data of the production process of (10*S*)-HOME. i: OA, (10*S*)-HOME, (7*S*,10*S*)-DiHOME and products.

Compound	$Y_{i/X}$ (g g^{-1})	q_i (g l^{-1} h^{-1})	Purity (%)	Purification recovery (%)
OA	3.42	1.267	–	–
(10*S*)-HOME	1.23	0.237	91	43
(7*S*,10*S*)-DiHOME	1.39	0.267	96	29
Products	2.62	0.504	–	–

OA: oleic acid; (10*S*)-HOME: 10(*S*)-hydroxy-8(E)-octadecenoic acid; (7*S*,10*S*)-DiHOME: 7,10(*S*,*S*)-dihydroxy-8(E)-octadecenoic acid; products: (10*S*)-HOME and (7*S*,10*S*)-DiHOME. Data are the average of three replicates.

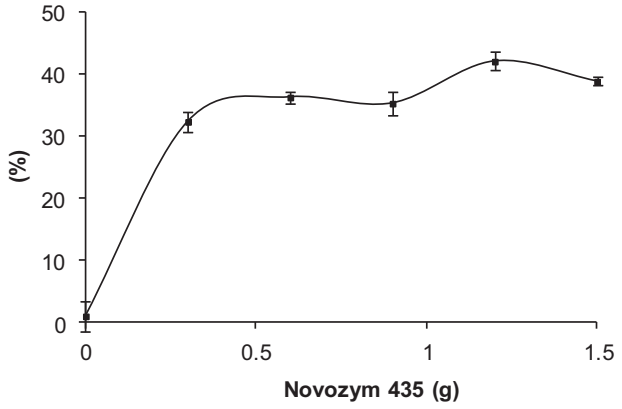

Fig. 2. Yield of the polymerization with different amounts of enzyme, Novozyme 435, in 0.6 g of (10*S*)-HOME at 50 °C during 48 h in *n*-hexane, 20 ml. Yield is calculated as percentage of the reduction of AV.

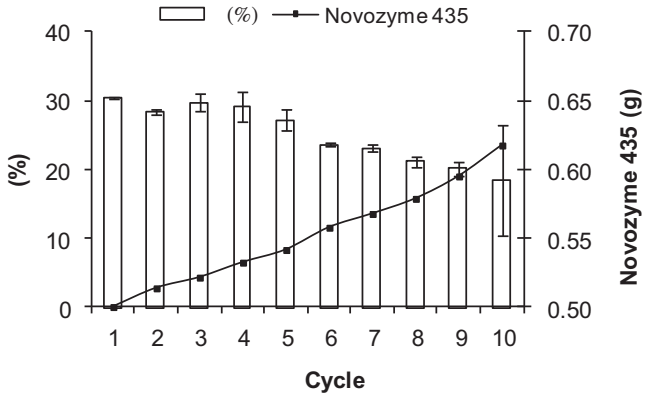

Fig. 4. Yield of the polymerization and enzyme weight at each cycle. In all experiments 0.5 g of Novozyme 435 and 0.5 g of (10*S*)-HOME were dissolved in 20 ml of *n*-hexane during 48 h at 50 °C. Yield is calculated as percentage of the reduction of AV. Novozyme 435: (■); bars: yield.

constant at 30%, indicating that an excess substrate concentration is not effective in enhancing the AV decrease. A similar ratio was found by Langone and co-workers after the conversion of oleic acid/methyl ricinoleate to estolides using Novozym 435 as a biocatalyst in a solvent-free system for 48 h at 80 °C [34].

3.3. Effect of enzyme stability

The use of enzymes or immobilized enzymes for repeated use may help decrease product cost and make the enzymatic process economically viable. The ability of lipase B of *C. antarctica*, Novozym 435, to retain its stability during recycling by using fatty acids as substrate was studied by several researchers [34,35].

Fig. 4 shows the profile of the polymerization yield during different cycles. As observed, the synthetic stability of the enzyme decreased throughout the cycles assayed. The yield decreased by 53.3% after ten cycles, from 30.4% to 18.5%, whereas the enzyme weight increased. Although the biocatalyst was rinsed several times with *n*-hexane, a portion of the substrate remained adsorbed on the support due to the poor solubility of the (10*S*)-HOME in *n*-hexane. Langone and co-workers observed a similar reduction in enzyme stability (55%) in the production of estolides from oleic acid and methyl ricinoleate with Novozym 435 in four batches [34]. In contrast, Radzi et al. [35] observed great synthetic stability even after nine cycles (91.9%) during the production of oleyl oleate in *n*-hexane for 1 h, indicating a negligible effect on enzyme stability. This indicates that using an appropriate apolar organic solvent may help maintain enzyme stability and solubilizing the substrate may help so as not to affect enzyme activity.

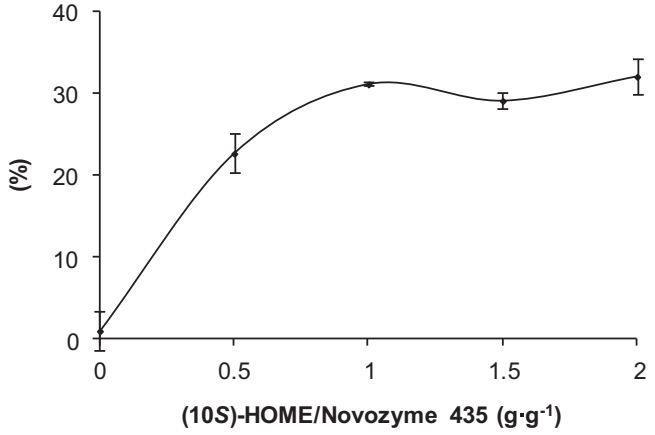

Fig. 3. Yield of the polymerization with different amounts of (10*S*)-HOME/Novozyme 435 ratio. 0.5 g of Novozyme 435 were used in all experiments in 20 ml of *n*-hexane as organic solvent at 50 °C during 48 h. Yield is calculated as percentage of the reduction of AV.

3.4. Structural determination of (10*S*)-HOME estolides

A gel-permeation analysis of the polymers has certain difficulties that we tried to overcome, such as the difficulty of separating different degrees of polymerization properly, especially when the molecular mass of the oligomers analyzed does not differ enough. At this juncture, more than one gel permeation column is needed to achieve a good separation, which increases the analysis time and makes this technique tedious and expensive. Alternatively, Bayer et al. introduced coordination-ion-spray mass-spectrometry (CIS-MS), in which non-polar compounds or substances with weakly basic or acidic groups are detected, but with poor sensitivity [36]. MALDI-TOF is ideally suited for polymer analysis because of the simplicity of the mass spectra [37], which show mainly single-charged quasi-molecular ions with little fragmentation when cationization salts are used. To this end, lipase-formed estolides from (10*S*)-HOME were analyzed using ricinoleic acid estolides that were enzymatically produced as a control to confirm the validity of the following structural techniques: liquid chromatography–mass spectrometry and MALDI-time-of-flight mass spectrometry.

3.4.1. Liquid chromatography–mass spectrometry (LC–MS) structural determination

Estolides from RA were enzymatically produced using the method described by Bódalo et al. [22]. Thus, RA estolides, with an AV of 68 $mg_{KOH}\ g^{-1}_{sample}$, were used to confirm the validity of the LC–MS techniques applied in order to determine the structure of the apolar polymers as polyesters of C18-hydroxyl-fatty acids. In addition, selected ion monitoring (SIM) was used to detect high molecular mass oligomers with greater intensity. Six ions were selected, *m*/*z* 298, 578, 858, 1138, 1419 and 1699, that correspond to RA and its oligomers [2RA-H_2O], [3RA-2H_2O], [4RA-3H_2O], [5RA-4H_2O] and [6RA-5H_2O], respectively. The six-extracted ion-superimposed chromatogram (Fig. S1, Supporting Information) gives the retention times at which various selected ions are detected. As can be observed, the ion with *m*/*z* 298 appears at 7.28 min peak is unreacted RA; and at the peaks (min) 12.07, 18.70, 24.29, 28.22 and 30.94, an ion with *m*/*z* 298 appears as a marker of the cleavage of one of the ester bonds in the oligomers synthesized. However, ions with *m*/*z* 578 (red), 858 (green) and 1138 (gray) are

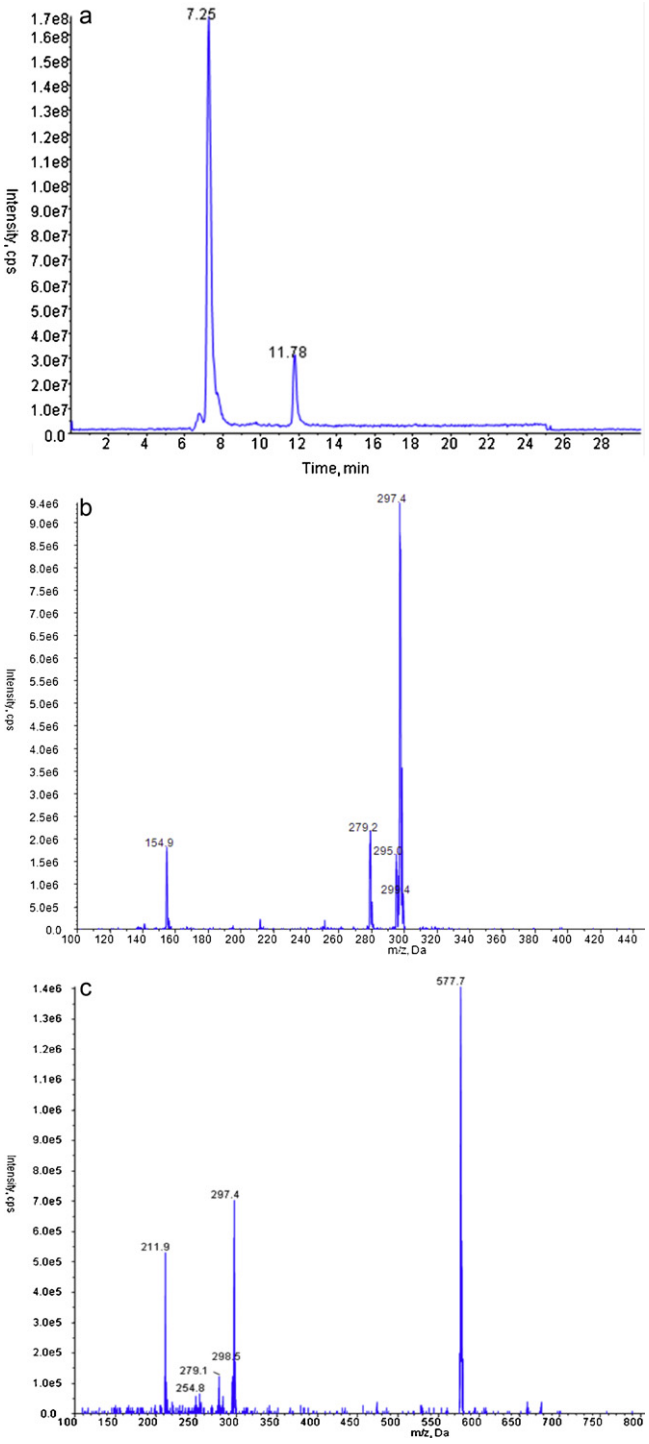

Fig. 5. (a) Full scan chromatogram of (10*S*)-HOME polymerized with Novozyme 435 at 50 °C during 48 h; AV of the sample of 127.8 $mg_{KOH}\ g^{-1}_{sample}$. (b) Mass spectra of the peak of 7.25 min retention time: (10*S*)-HOME. (c) Mass spectra of the peak of 11.78 min retention time: dimmer of (10*S*)-HOME.

only observed at retention times of 12.07, 18.70 and 24.29 min, respectively. Finally, ions with *m*/*z* 1419 and 1699 (not in the figure) are only detected at retention times of 28.22 and 30.94 min, respectively.

A sample of (10*S*)-HOME polymerized in *n*-hexane with Novozym 435 was analyzed, with an AV of 127.8 $mg_{KOH}\ g^{-1}_{sample}$. As seen from Fig. 5a, two noticeable peaks at 7.25 and 11.78 min were detected in the full scan chromatogram. The mass spectrum

Table 2
Reaction yield, η (%), in the lipase screening with different apolar solvents.

Lipase	RCF[a]	*n*-hexane	*Iso*-octane	Specificity
Novozyme 435	0.7	11.7	16.0	Non specific
Lipozyme RM IM	1.3	26.4	23.6	sn-1,3
Candida rugosa	2.9	16.8	12.5	Non specific
Rhizopus oryzae lip A	3.7–4.1[b]	15.1	13.8	sn-1,3
Lipozyme TL IM	–	36.4	32.7	sn-1,3

Data are the average of two replicates.
[a] Ratio competitive factor $(1/\alpha)_{cis}/(1/\alpha)_{trans}$.
[b] From *Rhizopus arrhizus* and *Rhizopus delemar* (Borgdorf and Warwel [27]).

of the 7.25 min peak is shown in Fig. 5b, and an ion with *m*/*z* 297.3 corresponding to the $[M-H]^-$ ion of (10*S*)-HOME can be detected. Likewise, the mass spectrum of the 11.78 min peak shows two main ions (Fig. 5c), *m*/*z* 577.8 and 297.5. The first ion indicates the presence of an oligomer of two units of (10*S*)-HOME, $[2M\text{-}H_2O\text{-}H]^-$, and the second one represents the cleavage of the ester bond of the same compound.

3.4.2. MALDI-time-of-flight mass spectrometry (TOF-MS) structural determination

Selecting an appropriate MALDI matrix, cationization salts and sample preparation techniques are critical success factors for obtaining a reliable mass spectrum from which to infer structural information [31]. A 2,5-dihydroxybenzoic acid (DHB) matrix, neutralized with lithium hydroxide, was used to analyze RA estolides using the method developed by Cvacka and co-workers in order to analyze wax esters, esters from a fatty acid and a fatty alcohol. As can be observed (Fig. S2, Supporting Information), a relatively low-intensity peak of *m*/*z* 305.19 corresponded to the lithium molecular adduct of RA $[RA+Li^7]^+$; a peak of *m*/*z* 287.19 appeared due to the loss of water from the RA lithium adduct. Three peaks in the central part of the spectra (585.53, 865.65 and 1145.87 *m*/*z*) stand out, and these peaks correspond to molecular adducts with lithium: $[2RA\text{-}H_2O+Li^7]^+$, $[3RA\text{-}2H_2O+Li^7]^+$ and $[4RA\text{-}3H_2O+Li^7]^+$. Finally, a very low-intensity peak, which coincides with the mass of the $[5RA\text{-}4H_2O+Li^7]^+$ oligomer, appears in the high-mass field of the spectra, at *m*/*z* 1426. In contrast to the findings of Hayes and Kelly [38], who used a *trans*-3-indoleacrylic acid matrix with a sodium chloride solution to analyze polyhydric alcohol-poly (ricinoleic acid) species, lithium DHB salt matrix could be used to detect quasi-molecular ions with a molecular weight lower than 500 Da. Other matrices, DHB and α-cyano-4-hydroxycinnamic acid, without cationization salts were tested to detect ricinoleic acid estolides, but highly fragmented mass spectra were obtained, making it tedious and difficult to identify the quasi-molecular ions.

When a sample of (10*S*)-HOME polymerized with Novozym 435 in *n*-hexane was analyzed with an AV of 127.8 $mg_{KOH}\ g^{-1}_{sample}$ (Fig. 6), two groups of peaks were found. In the first group, the lithium molecular adduct of the monomer $[M+Li^7]^+$ with *m*/*z* 305.2 was observed. In the second group, a peak of *m*/*z* 585.4 was observed, which corresponds to the lithium adduct of the oligomer formed by two units of (10*S*)-HOME $[2M\text{-}H_2O+Li^7]^+$, thus confirming the results found by liquid chromatography.

3.5. Screening of other lipases for estolides formation

Finally, some other lipases were tested to improve the conversion rate of estolide production. An aliquot of 0.6 g of (10*S*)-HOME was assayed with 100 mg of different lipases in both apolar organic solvents, *n*-hexane and *iso*-octane (log *P* = 4.5 [33]), for 48 h at 50 °C. Table 2 summarizes the reaction yields, and the lipases are listed according to their ratio competitive factors (RCF). It is notable that there is no relationship between the RCF and the yield of the reaction when the reaction proceeds in an aqueous-free solvent. It was

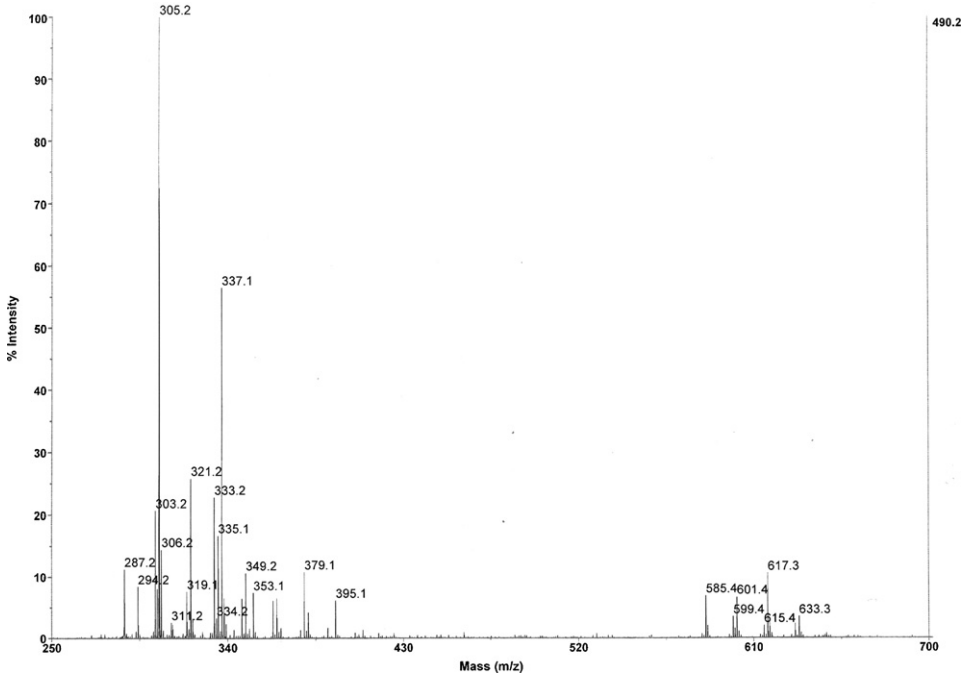

Fig. 6. MALDI-TOF mass spectra of (10*S*)-HOME polymerized with Novozyme 435 at 50 °C during 48 h using a matrix of DHB neutralized with LiOH; AV of the sample of 127.8 $mg_{KOH}\ g^{-1}_{sample}$.

expected that higher reaction yields would be found with Novozym 435 (11.7%) due to its low RCF (0.7), but the observed values were similar to those of *C. rugosa* and *R. oryzae* lipases (16.8% and 15.1%, respectively), which both have an RCF higher than 1. On the other hand, Lipozyme RM IM and Lipozyme TL IM had RCF values of 26.4% and 36.4%, respectively. Although the specificity of the assayed lipases was listed with the aim of establishing a correlation with the yield observed, it seems that the non-specific lipases (Novozym 435 and *C. rugosa*) had lower reaction yields than did the sn-1,3-specific lipases (Lipozyme RM IM, Lipozyme TL IM and *R. oryzae* lip A) with the exception of lip A from *R. oryzae*. However, Bódalo found that 1,3-selective lipases are unable to attack secondary alcohols [22]; perhaps, the configuration of the double bond and its relative position to the secondary alcohol had an important effect.

In addition, *iso*-octane, another apolar organic solvent with a higher log *P* value was tested (4.5). Unlike *n*-hexane, *iso*-octane is not a compatible solvent in food applications. However, estolides produced with this apolar solvent can be used as lubricants in cosmetics, inks or coatings [7]. *Iso*-octane was selected to increase the solubility of the substrate (10*S*)-HOME and, thus, the reaction yield, but no significant differences were observed. Given these results, a future study of the production of estolides with Lipozyme RM IM or Lipozyme TL IM and an apolar organic solvent that enhances the solubility of (10*S*)-HOME is needed. In such a study, there would be an increase in the polymerization conversion to test the physical properties of this new family of *trans*-estolides.

4. Conclusions

For the first time, estolides from a *trans*-hydroxy fatty acid (10*S*)-HOME, have been synthesized *in vitro* using Novozym 435, lipase B of *C. antarctica*, in an apolar organic medium and *n*-hexane. The reaction media were optimized to achieve a 30% reaction yield, at which point two structural techniques were used to determine the nature of the synthesized products: MALDI-TOF-MS and LC–MS. By adapting the analysis conditions, especially using a lithium-DHB-salt matrix for the MALDI experiments, simpler mass spectra were obtained and the identity of the quasi-molecular ions of the products became clear. Estolides of two units of (10*S*)-HOME were detected. Because the results show no high conversion yields, a new array of reaction media with diverse apolar solvents and lipases is possible.

Acknowledgments

This work was supported by the Ministerio de Economía y Competitividad (CICYT, project CTQ2010-21183-C02-01), Spain, and by the IV Pla de Recerca de Catalunya (Generalitat de Catalunya) grant 2009SGR819. I. Martin-Arjol is a grateful recipient of an APIF-fellowship from the University of Barcelona. We also thank Novozyms for kindly providing the lipase samples and Dr. F. Valero (Dept. Ingenyeria Química, Universitat Autònoma Barcelona, Spain) for the *R. oryzae* lipase samples, Dr. I. Ferández-Vidal and Dr. A. Adeva from the Centres Científics i Tecnològics (CCiT) of the University of Barcelona who performed the spectrometric analysis of the samples.

Appendix A. Nomenclature

(10*S*)-HOME 10(*S*)-hydroxy-8(E)-octadecenoic acid
(7*S*,10*S*)-DiHOME 7,10(*S*,*S*)-dihydroxy-8(E)-octadecenoic acid
amu atomic mass units [Da]
AV acid value [$mg_{KOH}\ g^{-1}_{sample}$]
C((10*S*)-HOME) concentration of (10*S*)-HOME [$g\ l^{-1}$]
C((7*S*,10*S*)-DiHOME) concentration of (7*S*,10*S*)-DiHOME [$g\ l^{-1}$]
C(X) concentration of biomass as dry cell weight [$g\ l^{-1}$]
CIS coordination-ion-spray
C_{KOH} concentration of potassium hydroxide [M]
Da Daltons
DHB 2,5-dihydroxybenzoic acid
LC liquid chromatography
log *P* partition coefficient [–]
M (10*S*)-HOME

MALDI matrix-assisted laser desorption/ionization
MM_{KOH} molecular mass of potassium hydroxide [g mol^{-1}]
MS mass spectrometry
OA oleic acid, 9(Z)-octadecenoic acid
$q_{(10S)\text{-HOME}}$ (10*S*)-HOME productivity [g l^{-1} h^{-1}]
$q_{(7S,10S)\text{-DiHOME}}$ (7*S*,10*S*)-DiHOME productivity [g l^{-1} h^{-1}]
q_{OA} OA consumption rate [g l^{-1} h^{-1}]
RA ricinoleic acid, 12(*R*)-hydroxy-9(Z)-octadecenoic acid
RCF ratio competitive factor $(1/\alpha)_{cis}/(1/\alpha)_{trans}$ [–]
t time [h]
TOF time-of-flight
V_{KOH} volume of potassium hydroxide [ml]
WE wax esters
W_{sample} sample weight [g]
X dry cell weight [g l^{-1}]
$Y_{(10S)\text{-HOME/X}}$ specific (10*S*)-HOME yield [g g^{-1}]
$Y_{(7S,10S)\text{-HOME/X}}$ specific (7*S*,10*S*)-DiHOME yield [g g^{-1}]
$Y_{P/X}$ whole specific product yield [g g^{-1}]
Δ increment [–]
α competitive factor [–]
η reaction yield [%]

Appendix B. Supplementary data

Supplementary data associated with this article can be found, in the online version, at http://dx.doi.org/10.1016/j.procbio.2012.12.006.

References

[1] Hayes DG, Kleiman R, Phillips BS. The triglyceride composition, structure, and presence of estolides in the oils of *Lesquerella* and related species. JAOCS 1995;72:559–69.
[2] Burg DA, Kleiman R. Preparation of meadowfoam dimer acids and dimer esters, and their use as lubricants. JAOCS 1991;68:600–3.
[3] Kleiman R, Spencer GF, Earle FR, Nieschlang HJ. Tetra-acid triglycerides containing new hydroxy eicosadienoyl moiety in *Lesquerella auriculata* seed oil. Lipids 1972;7:660–5.
[4] Smedley SR, Schroeder FC, Weibel DB, Meinwald J, Lafleur KA, Renwick JA, et al. Labile defensive lipids from the glandular hairs of a caterpillar (*Pieris rapae*). PNAS 2002;99:6822–7.
[5] Butovich IA. Cholesteryl esters as a depot for very long chain fatty acids in human meibum. J Lipid Res 2009;50:501–13.
[6] Peláez M, Orellana C, Marqués A, Busquets M, Guerrero A, Manresa A. Natural estolides produced by *Pseudomonas sp.* 42A2 grown on oleic acid: production and characterization. JAOCS 2003;80:859–66.
[7] Cermak SC, Isbell TA. Synthesis and physical properties of mono-estolides with varying chain lengths. Ind Crops Prod 2009;29:205–13.
[8] Achaya KT. Chemical derivatives of castor oil. JAOCS 1971;48:758–63.
[9] Cermak SC, Isbell TA. Synthesis of estolides from oleic and saturated fatty acids. JAOCS 2001;78:557–65.
[10] Isbell TA. Chemistry and physical properties of estolides. Grasas Aceites 2011;62:8–20.
[11] Cermak SC, Skender AL, Deppe AB, Isbell TA. Synthesis, physical properties of tallow-oleic estolide 2-ethylhexyl esters. JAOCS 2007;84:449–56.
[12] Bódalo A, Bastida J, Máximo MF, Montiel MC, Murcia MD, Ortega S. Influence of the operating conditions on lipase-catalysed synthesis of ricinoleic acid estolides in solvent-free systems. Biochem Eng J 2009;44: 214–9.
[13] Awang R, Basri M, Ahmad S, Salleh AB. Enzymatic esterification of dihydroxystearic acid. JAOCS 2000;77:609–12.
[14] Gosh M, Bhattacharyya DK. Lipase-catalyzed synthesis of hydroxy stearates and their properties. JAOCS 1998;75:1057–9.
[15] Hayes DG. The catalytic activity of lipases toward hydroxy fatty acids – a review. JAOCS 1996;73:543–9.
[16] Yamaguchi C, Akita M, Asaoka S, Osada F. Enzymic manufacture of castor-oil fatty acid estolides. Japanese Kokai Tokkyo Koho 1989, JP 01016591 A 19890120.
[17] Yoshida Y, Kawase K, Yamaguchi C. Manufacture of estolide from ricinoleic acid with immobilized lipase. Japanese Kokai Tokkyo Koho 1993, JP 05211878 A 19930824.
[18] Yamaguchi C, Yoshida Y, Kawase M. Manufacture of estolide with immobilized lipase. Japanese Kokai Tokkyo Koho 1993, JP 05304966 A 19931119.
[19] Yoshida Y, Kawase M, Yamaguchi C, Yamane T. Synthesis of estolides with immobilized lipase. Yukagaku 1995;44:328–33.
[20] Goto M, Hatanaka C, Haraguchi T. Formation of ricinoleic acid by lipase immobilized within isopropylacrylamide gel beads. Res Rep Kitakyushu Tech Coll 1999;32:161–4.
[21] Yoshida Y, Kawase M, Yamaguchi C, Yamane T. Enzymic synthesis of estolides by a bioreactor. JAOCS 1997;74:261–7.
[22] Bódalo-Santoyo A, Bastida-Rodriguez J, Máximo-Martín MF, Montiel-Morte MC, Murcia-Almagro MD. Enzymatic biosynthesis of ricinoleic acid estolides. Biochem Eng J 2005;26:155–8.
[23] Bódalo A, Bastida J, Máximo MF, Montiel MC, Gómez M, Murcia MD. Production of ricinoleic acid estolide with free and immobilized lipase from *Candida rugosa*. Biochem Eng J 2008;39:450–6.
[24] Klibanov AM. Improving enzymes by using them in organic solvents. Nature 2001;409:241–6.
[25] Horchani H, Bouaziz A, Gargouri Y, Sayari A. Immobilized *Staphylococcus xylosus* lipase-catalysed synthesis of ricinoleic acid esters. J Mol Catal B: Enzym 2012;75:35–42.
[26] Hayes DG, Ye R. Optimization of the solvent-free lipase-catalyzed synthesis of fructose-oleic acid ester through programming of water removal. JAOCS 2011;88:1351–9.
[27] Borgdorf R, Warwel S. Substrate selectivity of various lipases in the esterification of *cis* and *trans*-9-octadecenoic acid. Appl Microbiol Biotechnol 1999;51:480–5.
[28] Stránský K, Zarevúcka M, Valterová I, Wimmer Z. Gas chromatographic retention data of wax ester. J Chromatogr A 2006;1128:208–19.
[29] Tachi M, Iwamori M. Mass spectrometric characterization of cholesterol esters and wax esters in epidermis of fetal, adult and keloidal human skin. Exp Dermatol 2007;17:318–23.
[30] Rijpstra WIC, Reneerkens J, Piermas T, Damsté JS. Structural identification of the b-hydroxy fatty acid-based diester preen gland waxes of shorebirds. J Nat Prod 2007;70:1804–7.
[31] Vrkoslav V, Míková R, Cvacka J. Characterization of natural wax esters by MALDI-TOF mass spectrometry. J Mass Spectrom 2008;44:101–10.
[32] Martinez E, Hamberg M, Busquets M, Díaz P, Manresa A, Oliw E. Biochemical characterization of the oxygenation of unsaturated fatty acids by the diogenase and hydroperoxide isomerase of *Pseudomonas aeruginosa* 42A2. J Biol Chem 2010;285:9339–45.
[33] Laane C, Boeren S, Vos K, Veeger C. Rules for optimization of biocatalysis in organic solvents. Biotechnol Bioeng 1986;30:81–7.
[34] Aguieiras ECG, Veloso CO, Bevilaqua JV, Rosas DO, da Silva MAP, Langone MAP. Estolides synthesis catalyzed by immobilized lipases. Enzyme Res 2011;2011:1–7.
[35] Radzi SM, Basri M, Salleh AB, Ariff A, Mohammad R, Rahman MBA, et al. High performance enzymatic synthesis of oleyl oleate using immobilised lipase from *Candida antarctica*. Electron J Biotechnol 2005;8:291–8.
[36] Bayer E, Gfrörer P, Rentel C. Coordination-ionspray-MS (CIS-MS), a universal detection and characterization method for direct coupling with separation techniques. Angew Chem Int Ed 1999;38:992–5.
[37] Nielen MWF. Maldi time-of-flight mass spectrometry of synthetic polymers. Mass Spectrom Rev 1999;18:309–44.
[38] Kelly AR, Hayes DG. Lipase-catalyzed synthesis of polyhydric alcohol-poly(ricinoleic acid) ester star polymers. J Appl Polym Sci 2006;101:1646–56.

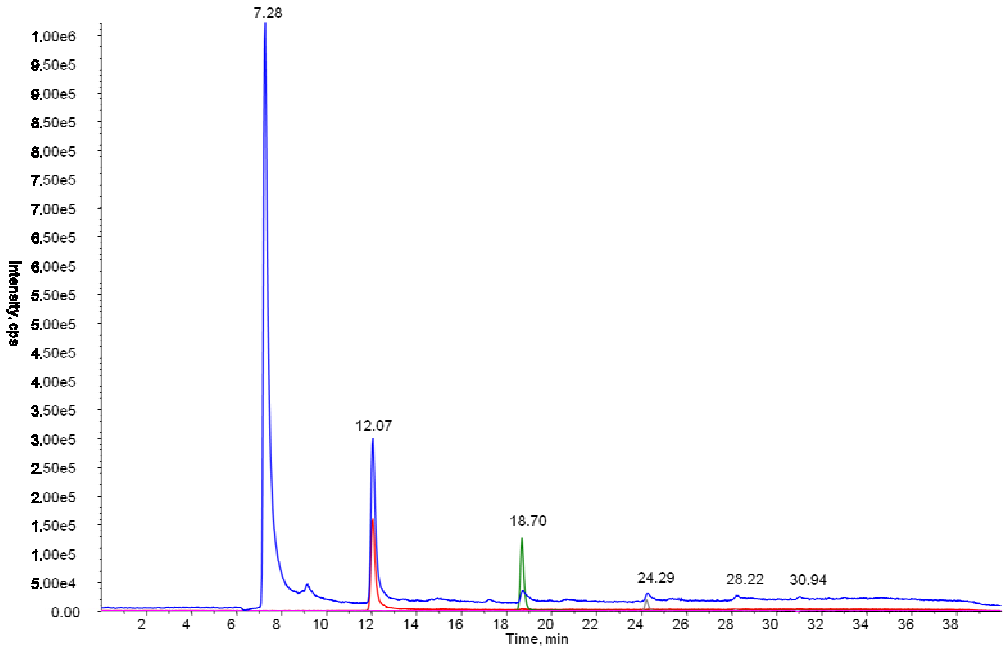

Figure S1. Six extracted ion chromatogram of ions *m/z* 298 (blue) (7.28, 12.07, 18.70, 24.29, 28.22, 30.94 min), 578 (red) (12.07 min), 858 (green) (18.70 min), 1138 (gray) (24.29 min), 1419 (28.22 min) and 1699 (30.94 min) of the estolides from ricinoleic acid, AV of 68 $mg_{KOH} \cdot g_{sample}^{-1}$.

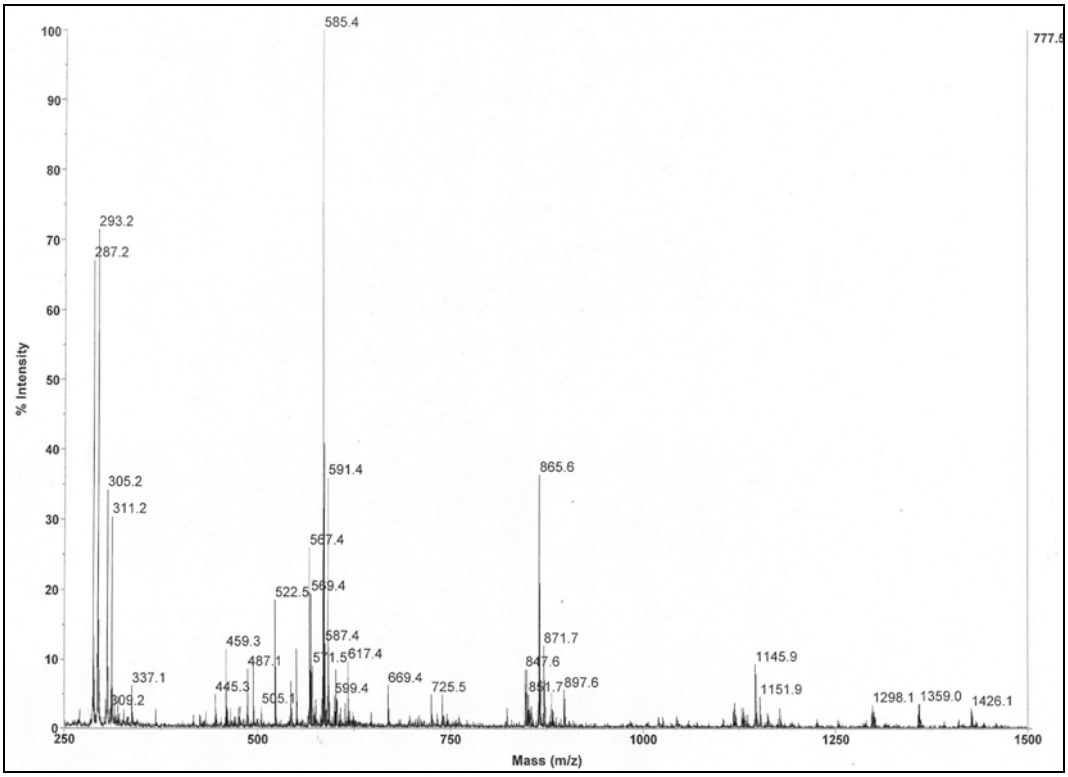

Figure S2. MALDI-TOF mass spectra of estolides from ricinoleic acid of a sample of an AV of 68 $mg_{KOH} \cdot g_{sample}^{-1}$ using a DHB matrix neutralised with LiOH.

Appl Microbiol Biotechnol (2013) 97:8041–8048
DOI 10.1007/s00253-013-5059-7

Production of 10(*S*)-hydroxy-8(*E*)-octadecenoic and 7,10(*S*,*S*)-hydroxy-8(*E*)-octadecenoic ethyl esters by Novozym 435 in solvent-free media

Ignacio Martin-Arjol · Montse Busquets · Terry A. Isbell · Angels Manresa

Received: 9 May 2013 / Revised: 12 June 2013 / Accepted: 13 June 2013 / Published online: 29 June 2013

Abstract Novozym 435, lipase B from *Candida antarctica*, was used in this study for the production of ethyl esters. For the first time, *trans*-hydroxy-fatty acid ethyl esters were synthesized in vitro in solvent-free media. We studied the effects of the substrate–ethanol molar ratio and enzyme synthetic stability of the biocatalyst. To determine the structure of the formed compounds, Fourier transformed infrared spectroscopy, nuclear magnetic resonance, and matrix-assisted laser desorption/ionization–time-of-flight mass spectrometry were used, three less time-consuming structural techniques. *trans*-Hydroxy-fatty acid ethyl esters were synthesized with a reaction yield of 90 % or higher with optimal reaction conditions.

Keywords Lipase · Novozym 435 · *trans*-Hydroxy-fatty acids · Ethyl esters · Solvent-free media

Electronic supplementary material The online version of this article (doi:10.1007/s00253-013-5059-7) contains supplementary material, which is available to authorized users.

M. Busquets
Departament de Bioquímica i Biologia Molecular, Facultat de Biologia, Universitat de Barcelona, Av Diagonal 643, 08028 Barcelona, Spain

T. A. Isbell
Bio-Oils Research, National Center for Agricultural Utililization Research, Agricultural Research Service, USDA, 1815 North University Street, Peoria, IL, USA

I. Martin-Arjol · A. Manresa (✉)
Departament de Microbiologia i Parasitologia Sanitàries, Facultat de Farmàcia, Universitat de Barcelona, Av. Joan XXIII s/n, 08028 Barcelona, Spain
e-mail: amanresa@ub.edu

Introduction

Hydroxy fatty acids (HFA) are known as functional oxylipins containing hydroxyl groups on fatty acid backbones. HFA are common in nature, especially in mammals, plant systems, and in microorganisms (Hou 2008). HFA are important industrial materials because the hydroxyl group confers special properties such as higher viscosity and reactivity. HFA are used in a wide range of industrial products as resins, waxes, nylons, plastics, lubricants, cosmetics, and additives in coatings and paints (Kim et al. 2000). Moreover, HFA could be used as intermediates in the production of biodegradable plastics, cyclic lactones, and pharmaceutical agents (Wang et al. 2012). Given that HFAs have great commercial potential, many efforts have been made to produce them in a chemical or biological manner.

In 1988, Mercadé and co-workers reported the production of a new HFA, 7,10(*S*,*S*)-hydroxy-8(*E*)-octadecenoic acid, by *Pseudomonas aeruginosa* 42A2 when cultivated in a mineral salt medium using oleic acid as carbon source; it was shown to have surfactant properties (Mercade et al. 1988). Later, in 1997, *P. aeruginosa* 42A2 was shown to also produce 10(*S*)-hydroperoxy-8(*E*)-octadecenoic ((10*S*)-HPOME)[1] and 10(*S*)-hydroxy-8(*E*)-octadecenoic ((10*S*)-HOME) acids (Guerrero et al. 1997) after 24 h using the same reaction conditions. Recently, Martinez and collaborators proved that (10*S*)-HPOME is the intermediate in the enzymatic oxidation of oleic acid to (7*S*,10*S*)-DiHOME whereas (10*S*)-HOME is produced as a chemical reduction of the (10*S*)-HPOME. The reaction is performed by a hydroperoxide isomerase also located in the periplasm (Martinez et al. 2010). These two

[1] In the acronyms HPOME, HOME, or DiHOME, M stands for monoenoic (acid).

enzymatic reactions are known as diol synthase activity. Further studies are being carried out to understand the (10*S*)-HOME production.

Though there are a huge number of reports about the biotransformation of fatty acids with lipases, there are few about the esterification of hydroxy-fatty acids with ethanol by lipases. Biodiesel is known as a mixture of fatty acid esters, preferentially methyl and ethyl esters, which is obtained from edible, nonedible, waste oils, and/or animal fats (Aguieiras et al. 2011; Su et al. 2011; Véras et al. 2011; Soumanou et al. 2012; Raitaa et al. 2011). Attention is focused on enzymatic transesterifications of triglycerides or free fatty acids with methanol or ethanol to produce biodiesel; however, *trans*-HFA as raw materials have not been taken into account to produce biodiesel; only a few works focused on esterification of ricinoleic acid are published (de Oliveira et al. 2004).

This work was undertaken to evaluate the suitability of producing *trans*-HFA ethyl esters with Novozym 435 in solvent-free media. An optimization of the reaction media was carried out, and different structural techniques were used to determine structural properties of the synthesized compounds: Fourier transformed infrared spectroscopy (IR), magnetic nuclear resonance (NMR), and matrix-assisted laser desorption/ionization–time-of-flight mass spectrometry (MALDI-TOF-MS).

Material and methods

Material

Novozym 435 (immobilized lipase B of *Candida antarctica*) was a generous gift from Novozym A/S (Bagsvaerd, Denmark). Absolute ethanol (EtOH) was supplied by Decon Laboratories Inc. (King of Prussia, PA, USA). Experimental conditions for the production and purification of *trans*-HFA, (10*S*)-HOME, and (7*S*,10*S*)-DiHOME were the same as reported before (Martin-Arjol et al. 2013).

Measurement of the reaction yield

The reaction yield was calculated as the consumption of the substrate by normal-phase high-pressure liquid chromatography (HPLC). Normal-phase HPLC analyses were performed on a Thermo Separations Spectra System AS1000 autosampler/injector (Fremont, USA) with a P2000 binary gradient pump from Thermo Separation Products (Fremont, USA) coupled to an Alltech ELSD 500 evaporative light scattering detector (Alltech Associates, Deerfield, USA). The chromatographic separation was carried out using a Dynamax Microsorb 60-8Si (250 mm×4.6 mm, 8 μm particle size) from Rainin Instrument Co. (Woburn, MA, USA). A 15-min run time was used to determine the conversion of the reaction. The mobile phase was composed of *n*-hexane/acetone (50:50) at a flow rate of 1 ml min^{-1}. The ELSD drift tube was set at 56 °C with the nebulizer set at 20 psi N_2, providing a flowrate of 2.0 standard liters per minute. The yield of the reaction was calculated using Eq. 1.

$$\eta(\%) = \frac{(A_{substrate\ 0} - A_{substrate\ t})}{A_{substrate\ 0}} \cdot 100 \quad (1)$$

Effect of ethanol on *trans*-HFA molar ratio

Esterification reactions took place in a 15-ml batch reactor magnetically stirred, 200 rpm. The reaction medium temperature, 50 °C, was kept constant using a J-Kem Scientific temperature controller (St. Louis, MO, USA). Different molar ratios of pure EtOH and 1 mol of each *trans*-HFA were tested separately; 1 g of (10*S*)-HOME or (7*S*,10*S*)-DiHOME, with 0.12 g of Novozym 435 during 24 h. All the reactions were carried out at atmospheric pressure. The extent of product formation for the reaction was calculated using Eq. 1 as stated above.

Effect of lipase concentration

Different quantities of Novozym 435, 0.001 to 0.18 g, were assayed in order to obtain the optimal enzyme amount in the esterification reactions with a molar ratio of each *trans*-HFA to ethanol of 1:3. Esterifications were carried out under the same conditions as stated above. The reaction yield was calculated with Eq. 1. All the reactions were carried out at atmospheric pressure. A control without enzyme was assayed in order to confirm that this reaction does not occur spontaneously.

Reusability of the Novozym 435

Reusability of the biocatalyst was carried out using the optimal conditions found in the previous set of experiments: a molar ratio of *trans*-HFA to ethanol of 1:3 and 0.06 g of Novozym 435 when (10*S*)-HOME was used as cosubstrate and 0.10 g with (7*S*,10*S*)-DiHOME. Reaction conditions were the same as described above. After each cycle, the enzyme was removed from the reaction medium by filtration and rinsed with *n*-hexane several times. In the set of experiments with (7*S*,10*S*)-DiHOME, after the fifth cycle, the enzyme was rinsed with pure ethanol. Finally, the solvent was evaporated under a stream of air at room temperature until the enzyme reached a stable weight. The product was analyzed, and the stability of the enzyme was determined based on reaction yield (Eq. 1).

Fourier transformed infrared spectroscopy

Infrared spectra were obtained using a Nicolet iZ10 FTIR module with a smart endurance single-bounce diamond ATR

cell. Spectra over the 4,000–650 cm^{-1} range were obtained by the co-addition of 32 scans with a resolution of 4 cm^{-1}. Spectral manipulation such as baseline adjustment, smoothing, and normalization was performed using OMNIC (Thermo Scientific, USA) software package.

Nuclear magnetic resonance

^{1}H and ^{13}C NMR experiments were recorded on a Bruker (Karlsruhe, Germany) Avance 500 spectrometer using a 5-mm BBI probe with an absolute frequency of 500.11 MHz for ^{1}H and 125.76 MHz for ^{13}C. Correlation spectroscopy, heteronuclear single quantum correlation, and heteronuclear multiple bond correlation two-dimensional spectra were also collected. Fifty milligrams of each sample was dissolved in 5 ml of 99.8 % $CDCl_3$ (Cambridge Isotope Laboratories Inc. Andover, MA, USA). Chemical shifts are expressed in parts per million using the same organic solvent as internal standard. Sixteen scans were used in ^{1}H experiments, whereas 1,024 scans were used in ^{13}C experiments.

MALDI-TOF-MS

MALDI-TOF-MS experiments were performed on a 4800 Plus MALDI-TOF/TOF Analyzer (ABSciex—2010, Framingham, MA, USA). The samples were analyzed in MS Reflector mode using positive ion detection. Desorption and ionization were achieved with an Nd–YAG laser (355 nm, 3–7 ns pulse, 200 Hz). The data were recorded using 4000 Series Explorer software (ABSciex—2010, Framingham, MA, USA). A 2,5-dihydroxybenzoic acid matrix was neutralized with lithium hydroxide (Sigma-Aldrich, Madrid, Spain), as Vrkoslav and co-workers established (Vrkoslav et al. 2008). Lithium salt matrix, 10 $mg \cdot ml^{-1}$, was dissolved in a mixture of acetone/chloroform (2:1 *v*/*v*). An aliquot of 1 μl of the matrix solution was spotted on the target plate until the organic solvent evaporated completely. Then, 1 μl of the samples diluted in 2.5 mg ml^{-1} trichloromethane was deposited over the matrix spot and allowed to dry before analysis.

Results

Effect of *trans*-HFA on ethanol molar ratio

Different molar ratios of *trans*-HFA to EtOH were assayed to determine the optimal molar ratio to maximize reaction yield with 0.12 g of Novozym 435 at 50 °C during 24 h (Fig. 1). It could be observed that both *trans*-HFA presented the same pattern, reaction yield increased from molar ratio 1:1 to 1:3, and afterwards, conversion remained practically constant. The optimal molar ratio was 1:3 (*trans*-HFA/EtOH) considering both the reaction yield and the future production costs.

Effect of lipase concentration

Different amounts of enzyme were tested to establish the optimal amount of biocatalyst for a *trans*-HFA to EtOH molar ratio of 1:3 (Fig. 2). As observed, higher yields were achieved when (7*S*,10*S*)-DiHOME was used as a substrate (98 %) instead of using the monohydroxylated compound (90 %). However, less quantity of Novozym 435 was needed to reach higher yields when (10*S*)-HOME, 0.06 g, than using the dihydroxylated fatty acid, 0.10 g.

Reusability of the Novozym 435

The synthetic stability of Novozym 435 was studied under the optimal reaction conditions as well as the enzyme weight after each cycle (Fig. 3). When (10*S*)-HOME was used as substrate, the enzyme synthetic stability remained constant around 79 % even after ten reaction cycles; and, enzyme weight never exceeded a value of 0.07 g. In contrast, when (7*S*,10*S*)-DiHOME was used, enzyme stability dropped abruptly after the fifth cycle, reaching a yield of 16.3 %. An enzyme stability reduction of 81.4 % was detected after five cycles, which occurred with an increase on enzyme weight. After these five trials, the enzyme was rinsed with EtOH to dessorb the (7*S*,10*S*)-DiHOME from the carrier of Novozym 435. As a consequence, the enzymatic stability was partially recovered, 37.4 %, and within the next five cycles diminished slowly to 19.8 %; and, the enzyme weight did not increase as seen in the first five cycles.

Fourier transformed infrared spectroscopy

One sample of each starting substrate and *trans*-HFA ethyl ester synthesized under optimal reaction conditions was analyzed to determine the functional groups present (Fig. S1). In both cases, FTIR spectra from substrates to their corresponding ethyl esters showed one main difference: the movement of a carbonyl stretch corresponding to the free fatty acid to a carbonyl stretch of an ester bond. In the case of the monohydroxylated compound, a frequency of 1709 cm^{-1} corresponding to the stretching of the carbonyl ($\upsilon_{C=O}$) in a acid moiety moved to a frequency of 1736 cm^{-1} corresponding to the stretching of carbonyl in an ester compound. In the case of the dihydroxy-fatty acid, the movement of the carbonyl band shifted from 1693 cm^{-1} to 1738 cm^{-1}.

Nuclear magnetic resonance structural determination

As could be observed in (10*S*)-HOME and (7*S*,10*S*)-DiHOME ethyl ester ^{13}C NMR spectra (Fig. 4) a signal for an ester carbonyl appears at 173.76 ppm (C1); moreover, no signal of an acid carbonyl group, 179.15 ppm, is appreciable in the spectra, indicating a total conversion under the optimal reaction

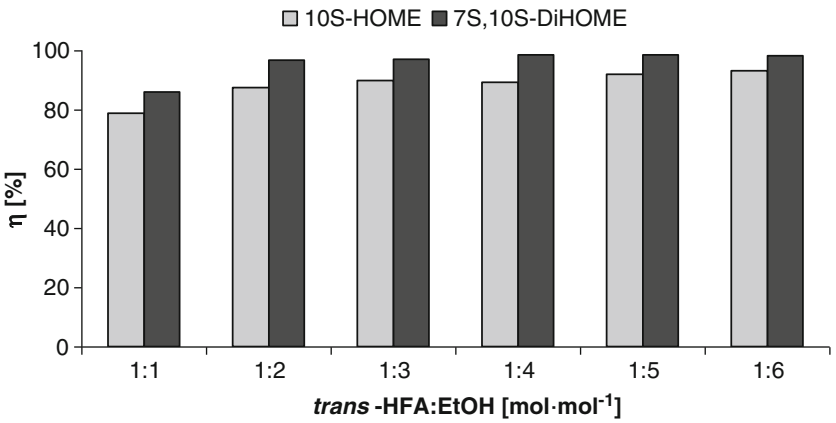

Fig. 1 Effect of the molar ratio of *trans*-HFA to EtOH on the yield of ethyl ester synthesis with Novozym 435, 0.12 g, at 50 °C during 24 h. Yield was calculated using Eq. 1

conditions described previously. A double signal of the terminal methyl carbons appeared at 14.00 and 14.15 ppm. The signal of 14.15 ppm corresponds to the methyl carbon of the ethyl ester side chain (C20) and the one at 14.00 ppm to the methyl carbon of the *trans*-HFA side (C18). The signal at 60.10 ppm is due to the methylene carbon of the ethyl ester side (C19); the ones at 72–73 ppm indicate the methine carbons in which the hydroxy groups are bonded (C10 and C7 in the case of dihydroxylated ethyl ester); and the signals at 131–134 ppm represent the olefinic carbons of the *trans*-double bond (C8 and C9). Finally, the signals at 34 ppm correspond to the methylene carbon next to the carbonyl moiety in the *trans*-HFA side chain (C2) and the signal of 24 ppm is another methylene on carbon C3.

In (10*S*)-HOME and (7*S*,10*S*)-DiHOME ethyl ester ^{1}H NMR spectra (Fig S2) the signal of the terminal methyl hydrogens are at 0.86 and 1.23 ppm. The downfield signal corresponds to the methyl hydrogens of the ethyl ester side chain (H20) and the other one to the methyl hydrogens of the *trans*-HFA chain (H1). 4.10 ppm represents a downfield methylene hydrogen signal next to ester moiety in the ethyl ester side (H19). The methine hydrogens, which are bounded to the same carbon as hydroxyl moiety, have a chemical shift of 4.03 ppm (H10 and H7 in the case of dihydroxylated ethyl ester). In the case of the (10*S*)-HOME ethyl ester, the methylenic hydrogens next to the double bond (H7) appear at 2.00 ppm. Ultimately, the methylene hydrogens H2 and H3 have a chemical shift of 2.26 and 1.60 ppm, respectively.

Finally, there is a signal in both ^{1}H NMR spectra which are important. There is a low-intensity quadruplet, 5.16 ppm, in the ^{1}H NMR from the monohydroxylated ethyl ester which corresponds to a methine signal. This methine signal reveals the formation of estolides and is downfield of saturated estolides caused by the effect of the *trans*-double bond. The integration of the estolide (HE) and H7/10 signals provided a ratio for the number of estolide-ester bonds, estolides number (EN), calculated as:

$$EN = HE/H10 \text{ or } H7/10 \tag{2}$$

giving a value of 0.29. This value indicates that the average formation of an estolide ethyl ester is a small part of the sample since and EN value of 1.00 would represent that 100 % of the sample is a monoestolide. In the case of the dihydroxylated ethyl ester ^{1}H NMR spectrum, this estolide signal has a chemical shift of 5.20 ppm and an EN value of 0.13, which reveals that the average formation of one monoestolide ethyl ester, is minimal.

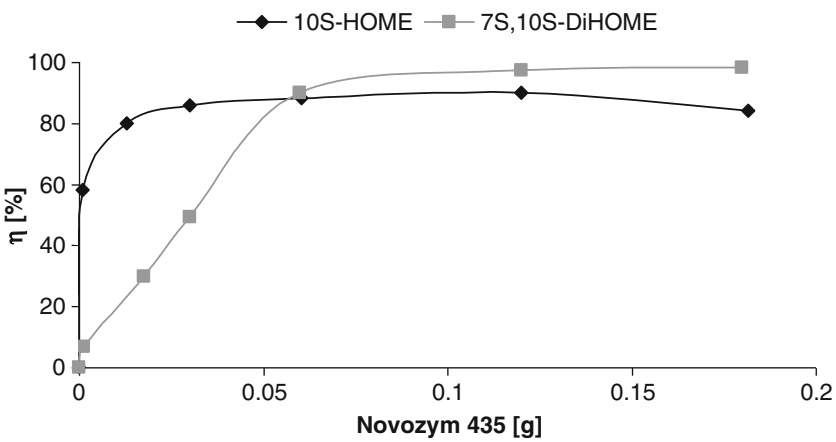

Fig. 2 Effect of Novozym 435 on the yield of ethyl esters synthesis with a molar ratio of *trans*-HFA to EtOH of 1:3 at 50 °C during 24 h. Yield was calculated using Eq. 1

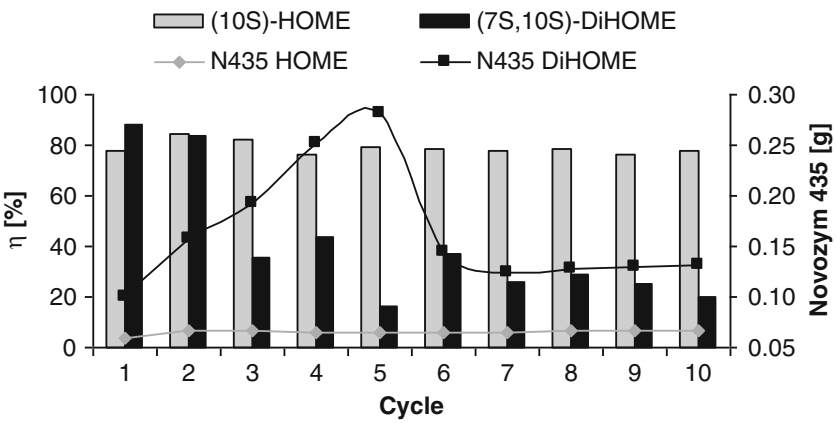

Fig. 3 Yield of the *trans*-hydroxy-fatty ethyl esters synthesis and Novozym 435 weight at each cycle. Optimal reaction conditions were used in all experiments. Yield was calculated with Eq. 1. *HOME*, (10*S*)-HOME; *DiHOME*, (7*S*,10*S*)-DiHOME; *N435 HOME*, Novozym 435 weight when (10*S*)-HOME was used as substrate; and *N435 DiHOME*, Novozym 435 weight when (7*S*,10*S*)-HOME was used as substrate

MALDI-TOF-MS

trans-HFA esters synthesized in optimal reaction conditions were analyzed by MALDI-TOF-MS to determine the molecular mass of these compounds (Fig. 5). In the spectrum of (10*S*)-HOME ethyl ester (M), two groups of ions are noticeable. In the low-mass ion group, an ion of *m*/*z* 333.2 stands out. This ion corresponds to molecular adduct of M with lithium, $[M+^{7}Li]^{+}$. The two low-intensity ions of *m*/*z* 349.2 and 365.2 are important. These are the molecular adducts of M with sodium and potassium, respectively: $[M+^{23}Na]^{+}$ and $[M+^{39}K]^{+}$. These three adducts give a molecular mass of M of 326.2 Da. In the second group, there is a high-intensity ion of *m*/*z* 613.5. This ion is the molecular lithium adduct of a monoestolide ethyl ester (M_1), $[M_1+^{7}Li]^{+}$. Next to this ion, there is a lower-intensity signal of *m*/*z* 629.5 which corresponds to the sodium molecular adduct of M_1, $[M_1+^{23}Na]^{+}$. The molecular mass obtained for the monoestolide ethyl ester from these two adducts is 606.5 Da. Finally, a very low-intensity ion, *m*/*z* 893.7, is noticeable. This ion is the lithium adduct of a diestolide ethyl ester (M2), $[M_2+^{7}Li]^{+}$, with a mass of 886.7 Da.

The (7*S*,10*S*)-DiHOME ethyl ester (M′) spectrum shows one main ion of *m*/*z* 349.2 which corresponds to molecular adduct of M′ with lithium, $[M'+^{7}Li]^{+}$. Next to it, there are two low-intensity ions of *m*/*z* 365.2 and 381.2. These two ions represent the molecular adducts of M′ with sodium and potassium, respectively; $[M'+^{23}Na]^{+}$ and $[M'+^{39}K]^{+}$. These three adducts give a mass of 342.2 Da for M′. Then, there is another important group of ions in which an *m*/*z* 645.5 ion stands out. This ion is the molecular adduct of a monoestolide ethyl ester with lithium, $[M'_1+^{7}Li]^{+}$, and the potassium molecular adduct of M'_1, $[M'_1+^{23}Na]^{+}$, is also noticeable with a mass of 677.5 Da. These two adducts reveal a mass for M'_1 of 638.5 Da. Ultimately, a low-intensity ion of *m*/*z* 941.7 reveals the formation of a diestolide ethyl ester, $[M'_2+^{7}Li]^{+}$, with a molecular mass of 934.7 Da.

Discussion

This is the first time in which hydroxy-fatty acids, positionally different from ricinoleic acid, were used to synthesize their corresponding ethyl esters in solvent-free media. The *trans*-HFA to EtOH molar ratio and the amount of enzyme, Novozym 435, were studied to find the reaction conditions that maximize the in vitro conversion yield. There are no data in the literature about the production of *trans*-HFA ethyl esters, although this molar ratio value, *trans*-HFA to EtOH of 1:3, agrees with the one found in the production of methyl esters from a vegetable oil (a soybean and rapeseed oil mixture) in a solvent-free system for 36 h at 30 °C (Watanabe et al. 2000) and with the one in the production of fatty acid ethyl esters from camellia oil soapstocks and diethyl carbonate, instead of a short-chain alcohol, for 24 h at 50 °C (Wang and Cao 2011), both using Novozym 435. The amounts of enzyme needed in each reaction system, 0.06 and 0.10 g, when (10*S*)-HOME and (7*S*,10*S*)-DiHOME were used as substrate, respectively, which represent 8.6 and 14.3 % (*w*/*v*), respectively, were in the same range of Novozym 435 concentration, 10–15 % (*w*/*v*), used in the production of fatty acid ethyl esters from palm oil fatty acids in a solvent-free medium (Véras et al. 2011). The reusability or synthetic stability of Novozym 435 was tested during ten cycles with no appreciable loss of activity when (10*S*)-HOME was used as substrate; however, with (7*S*,10*S*)-DiHOME, the enzyme stability was reduced dramatically after the second batch. After the fifth cycle, the biocatalyst was rinsed several times with EtOH, and synthetic stability was recovered immediately and reduced at a slower rate during the subsequent cycles. Likewise, the weight of the enzyme was notably affected by the rinses with EtOH. EtOH removed more quantity of (7*S*,10*S*)-DiHOME than *n*-hexane from the enzyme carrier improving the stability of Novozym 435. This fact indicated that (7*S*,10*S*)-DiHOME was adsorbed on the enzyme carrier compromising the synthetic performance of Novozym 435 under the reaction conditions tested, as it was already

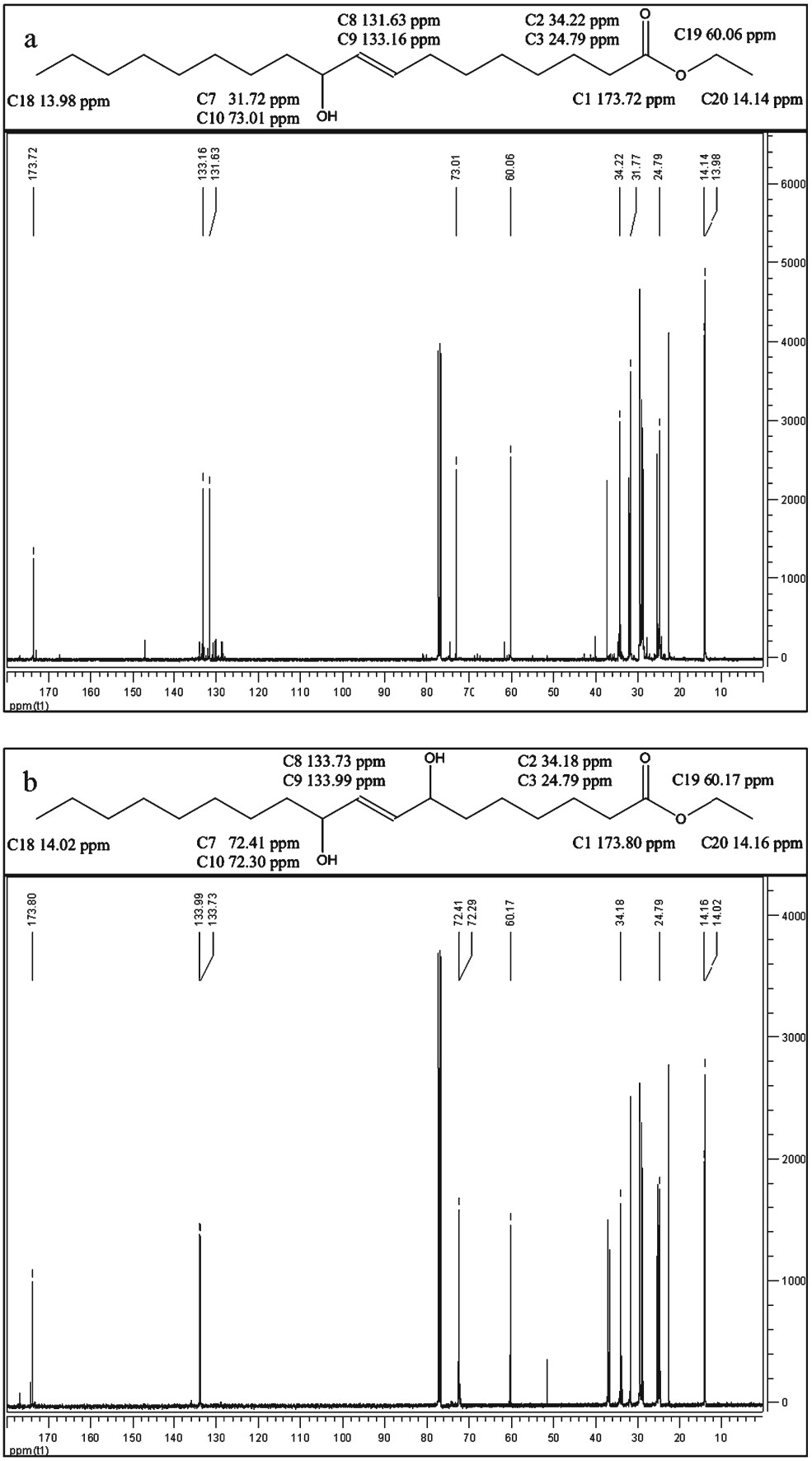

Fig. 4 ^{13}C spectra of (10*S*)-HOME ethyl ester (**a**) and (7*S*,10*S*)-DiHOME ethyl ester (**b**). Chemical shifts are expressed in parts per million

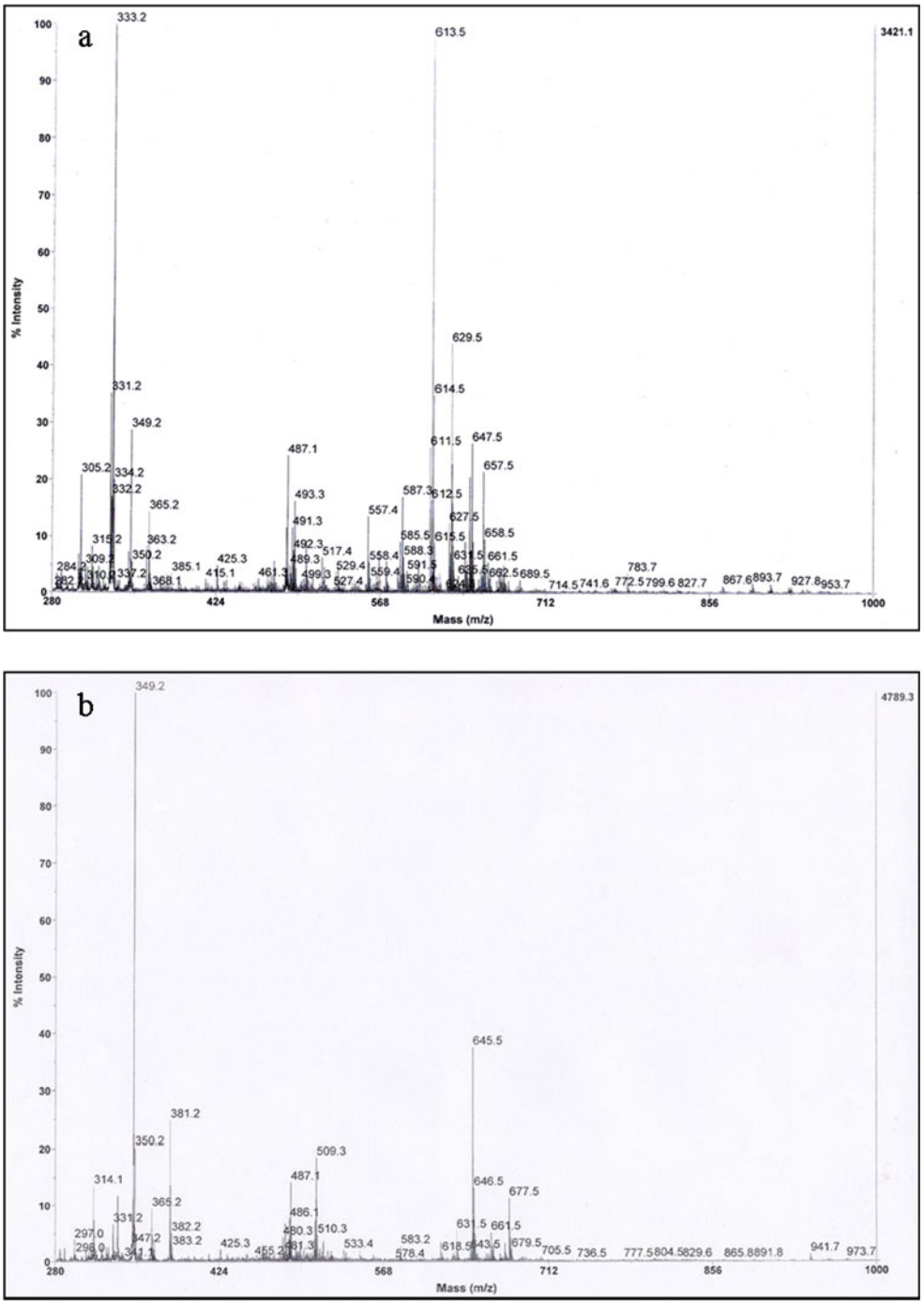

Fig. 5 MALDI-TOF-MS spectra of (10*S*)-HOME ethyl ester (**a**) and (7*S*,10*S*)-DiHOME ethyl ester (**b**)

demonstrated in the production of estolides from (10*S*)-HOME in *n*-hexane with the same commercial lipase (Martin-Arjol et al. 2013).

Different non-time-consuming structural techniques (Ghesti et al. 2007) were used to determine the nature of the compounds synthesized. FTIR revealed the presence of ester bonds by the identification of the stretching band of a carbonyl present in an ester group (Zagonel et al. 2004). NMR experiments exposed the same conclusion by the identification of a signal of 173.80 ppm corresponding to a carbonyl ester moiety in ^{13}C analyses (Isbell and Kleiman 1994). On the other hand, the absence of acid carbonyl signal on ^{13}C analyses emphasizes the total conversion of *trans*-HFA in their corresponding ethyl ester when they were produced under the optimal reaction conditions. Moreover, ^{1}H NMR analyses showed the synthesis of monoestolide ethyl esters of each *trans*-HFA. We previously reported the capability of Novozym 435 to synthesize (10*S*)-HOME monoestolides in apolar organic media (Martin-Arjol et al. 2013). Furthermore, the average oligomeric distribution of estolide ethyl esters is calculated based on the integration of

HE and H10 or H7/10 proton signals (Isbell et al. 1994). Finally, a 2,5-dihydroxybenzoic acid matrix neutralized with lithium hydroxide was used to obtain less fragmented spectra in MALDI-TOF-MS analyses (Vrkoslav et al. 2008). This structural technique was used to determine the molecular mass of the *trans*-HFA ethyl esters produced, confirming the synthesis of monoestolide ethyl esters as well as paralleling the results obtained by NMR analyses.

Acknowledgments This work was supported by the Ministerio de Economía y Competitividad (CICYT, project CTQ2010-21183-C02-01), Spain, and by the IV Pla de Recerca de Catalunya (Generalitat de Catalunya) grant 2009SGR819. I. Martin-Arjol is a grateful recipient of an APIF fellowship from the University of Barcelona. We also thank Novozymes for kindly providing the lipase sample, Dra. I. Fernández and Dra N. Ferrer-Felis from the Centres Científics i Tecnològics (CCiT) of the University of Barcelona who performed the spectrometric analysis of the samples, and Karl E. Vermilion who performed the NMR experiments in the National Center for Agricultural Utililization Research, USDA, Peoria IL, USA.

References

Aguieiras ECG, Veloso CO, Bevilaqua JV, Rosas DO, da Silva MAP, Langone MAP (2011) Estolides synthesis catalyzed by immobilized lipases. Enzyme Research 2011:1–7

de Oliveira D, Luccio MD, Faccio C, Rosa CD, Bender JP, Lipke N, Menoncin S, Amroginski C, de Oliveira JV (2004) Optimization of enzymatic production of biodiesel from castor oil in organic solvent medium. Appl Biochem Biotechnol 113–116:771–780

Ghesti GF, de Macedo JL, Resck IS, Dias JA, Dias SCL (2007) FT-Raman spectroscopy quantification of biodiesel in a progressive soybean oil transesterification reaction and its correlation with ^{1}H NMR spectroscopy methods. Energy Fuel 21(5):2475–2480

Guerrero A, Casals I, Busquets M, León Y, Manresa A (1997) Oxidation of oleic acid to (E)-10-hydroperoxy-8-octadecenoic acid and (E)-10-hydroxy-8-octadecenoic acid by *Pseudomonas* sp. 42A2. Biochim Biophys Acta 1347:75–81

Hou CT (2008) New bioactive fatty acids. Asia Pac J Clin Nutr 17(S1): 192–195

Isbell TA, Kleiman R (1994) Characterization of estolides produced from the acid-catalyzed condensation of oleic acid. JAOCS 71(4):379–383

Isbell TA, Kleiman R, Pattner BA (1994) Acid-catalyzed condensation of oleic acid into estolides and polyestolides. JAOCS 71(2): 169–174

Kim H, Gardner HW, Hou CT (2000) Production of isomeric 9,10,13 (9,12,13)-tryhidroxy-11*E* (10*E*)-octadecenoic acid from linoleic acid by *Pseudomonas aeruginosa* PR3. J Ind Microbiol Biotechnol 25:109–115

Martin-Arjol I, Busquets M, Manresa A (2013) Production of 10(*S*)-hydroxy-8(E)-octadecenoic acid mono-estolides by lipases in non-aqueous media. Process Biochem 48:224–230

Martinez E, Hamberg M, Busquets M, Diaz P, Manresa A, Oliw EH (2010) Biochemical characterization of the oxygenation of unsaturated fatty acids by the dioxygenase and hydroperoxide isomerase of *Pseudomonas aeruginosa* 42A2. J Biol Chem 285(13): 9339–9345

Mercade E, Robert M, Espuny MJ, Bosch MP, Manresa MA, Parra JL, Guinea J (1988) New surfactant isolated from *Pseudomonas* 42A2. J Am Oil Chem Soc 65(12):1915–1916

Raitaa M, Laothanachareon T, Champredab V, Laosiripojanaa N (2011) Biocatalytic esterification of palm oil fatty acids for biodiesel production using glycine-based cross-linked protein coated microcrystalline lipase. J Mol Catal B Enzym 73:73–79

Soumanou MM, Djenontin ST, Tchobo FP, Sohounhloue DCK, Bornscheuer UT (2012) Lipase-catalysed biodiesel production from *Jatropha curcas* oil. Lipid Technol 24(7):158–160

Su E, Du L, Gong X, Wang P (2011) Lipase-catalyzed irreversible transesterification of *Jatropha curcas* L. seed oil to fatty acid esters: an optimization study. JAOCS 88:793–800

Véras IC, Silva FAL, Ferrao-Gonzales AD, Moreau VH (2011) One-step enzymatic production of fatty acid ethyl ester from high-acidity waste feedstocks in solvent-free media. Bioresour Technol 102(20):9653–9658

Vrkoslav V, Mikova R, Cvacka J (2008) Characterization of natural wax esters by MALDI-TOF mass spectrometry. J Mass Spectrom 44:101–110

Wang Y, Cao X (2011) Enzymatic synthesis of fatty acid ethyl esters by utilizing camellia oil soapstocks and diethyl carbonate. Bioresour Technol 102:10173–10179

Wang X, Li L, Zheng Y, Zou H, Cao Y, Liu H, Liu W, Xian M (2012) Biosynthesis of long chain hydroxyfatty acids from glucose by engineered *Escherichia coli*. Bioresour Technol 114:561–566

Watanabe Y, Shimada Y, Sugihara A, Noda H, Fukuda H, Tominaga Y (2000) Continuous production of biodiesel fuel from vegetable oil using immobilized *Candida antarctica* lipase. JAOCS 77(4): 355–360

Zagonel GF, Peralta-Zamora P, Ramos LP (2004) Multivariate monitoring of soybean oil ethanolysis by FTIR. Talanta 63(5): 1021–1025